

A ‘constant Lagrangian’ fit of the galaxy rotation curves of the complete SPARC database of 175 galaxies.

E.P.J. de Haas^{1, a)}

Nijmegen, The Netherlands

(Dated: May 18, 2018)

In this paper I apply the ‘constant Lagrangian’ model for galactic dynamics to the complete SPARC database of 175 galaxies. For twenty five percent, 43 out of 175, of the galaxies of the series, a single fit model already remains nicely within the error margins. Fifteen galaxies are more complicated and clearly need a threefold fit. One exceptional galaxy justified five fits. So 116 galaxies, 66 percent, have a dual fit. The multiple fit appears to follow the mass composition of galaxies as composed of a bulge, possibly a disk and mostly extended gas clouds. As in previous papers, I will first repeat a presentation of the ‘constant Lagrangian’ approach. The original part of this paper is the fit of the complete set of the SPARC database and a first categorization of the result in single, dual, triple or multiple fit galaxies. Through the extensive database fit, the ‘constant Lagrangian’ approach can be inverted from a deductive to an inductive result: huge stretches of all galaxies can be fitted on a constant Lagrangian curve, while remaining within the empirical margin of errors. This paper’s galaxy fits prove this restricted claim beyond doubt. The issue then becomes to explain this empirical, inductive result.

PACS numbers: 95.30.Sf, 95.35.+d

Keywords: Dark Matter, MOND, Schwarzschild, Galactic rotation curves

^{a)}Electronic mail: haas2u@gmail.com

CONTENTS

I. Introduction	3
II. The ‘constant Lagrangian’ model for galactic dynamics	3
III. The dual fit approach towards rotation curves	9
IV. Conclusion	15
References	16
A. The fit of the 175 SPARC database galaxies.	18

I. INTRODUCTION

In a previous paper I introduced the ‘constant Lagrangian’ model for galactic dynamics (de Haas, 2018b). In two sub-sequential papers I made a first qualitative attempt at fitting real rotational velocity curves using the proposed model (de Haas, 2018d,c). In (de Haas, 2018e) paper I gave a more quantitative analysis by including the error bars of the measured velocity. This approach was applied to a subset of 25 galaxies of the [SPARC database](#), including the error margins, as provided by (Lelli et al., 2016). In that subset, non of the F-series galaxies were included. In a subsequent paper the ‘constant Lagrangian’ fit of the F-series was presented (de Haas, 2018a). In this paper, I present the full quantitative fit of the SPARC database of 175 galaxy rotation curves.

But as with the previous papers, I start by introducing the ‘constant Lagrangian’ model of galactic dynamics. Then I include the dual fit approach that proved to be the best way to model most galaxies. After that, the fit of the F series is presented. The introduction of the model is mostly a copy of the previous three papers and the presentation of the dual fit approach is copied from the previous ones, (de Haas, 2018a). The reason to include these two paragraphs again in this paper is to make this paper as more or less stand alone. The original part of this paper, its justification, is the fit of all the galaxies from the SPARC database.

II. THE ‘CONSTANT LAGRANGIAN’ MODEL FOR GALACTIC DYNAMICS

I start by repeating the essentials of this model, which I then apply to the rotation curve of galaxy NGC 1560. The Lagrangian equation of motion reads

$$\frac{d}{dt} \left(\frac{\partial L}{\partial \dot{q}} \right) - \frac{\partial L}{\partial q} = 0. \quad (1)$$

In classical gravitational dynamics I assume circular orbits with $\dot{q} = v$ and $q = r$. The Lagrangian itself is then given by $L = K - V$, with V the Newtonian potential gravitational energy and K the kinetic energy. One then gets

$$\frac{d}{dt} \left(\frac{\partial L}{\partial \dot{q}} \right) = \frac{dp}{dt} = F. \quad (2)$$

The other part gives

$$\frac{\partial L}{\partial q} = -\frac{dV}{dr}, \quad (3)$$

so one gets Newton's equation of motion in a central field of gravity

$$F_g = -\frac{dV}{dr}. \quad (4)$$

Further analysis of the context results in the identification of the Hamiltonian of the system, $H = K + V$, as being a constant of the orbital motion and the virial theorem as describing a relation between K and V in one single orbit but also between different orbits, $2K + V = 0$.

The previous analysis is problematic relative to the notion of geodetic motion in General Relativity. The problem can best be described in a semi-relativistic approach using the classical Lagrangian equation of motion for geodetic orbits. The most important aspect of geodetic motion in GR is that it requires no force to move on a geodetic. This has important implications for the Lagrangian equation of motion, because $F = 0$ on a geodetic. One gets

$$\frac{d}{dt} \left(\frac{\partial L}{\partial \dot{q}} \right) = F_g = 0 \quad (5)$$

and as a consequence also

$$\frac{\partial L}{\partial q} = -\frac{dL}{dr} = 0. \quad (6)$$

As a result, one gets the crucial

$$L = K - V = \text{constant} \quad (7)$$

on geodetic orbits.

This result, the Lagrangian of the system as being the constant of the geodetic motion, is used on a daily basis by many of us because it is used by GNSS systems for the relativistic correction of atomic clocks in their satellites. Let's elaborate this a bit further. If we apply the Schwarzschild metric in polar coordinates, we have (Ruggiero et al., 2008)

$$ds^2 = \left(1 + \frac{2\Phi}{c^2}\right) c^2 dt^2 - \left(1 + \frac{2\Phi}{c^2}\right)^{-1} dr^2 - r^2 d\theta^2 - r^2 \sin^2 \theta d\phi^2. \quad (8)$$

In case of a clock on a circular geodesic on the equator of a central non-rotating mass M we have $\frac{dr}{dt} = 0$, $\frac{d\theta}{dt} = 0$, $\sin\theta = 1$ and $\frac{d\phi}{dt} = \omega$. We thus get, with $v_{\text{orbit}} = r\omega$, the GR result

$$\frac{d\tau}{dt} = \sqrt{1 + \frac{2\Phi}{c^2} - \frac{v_{\text{orbit}}^2}{c^2}} \quad (9)$$

with $d\tau$ as the clock-rate of a standard clock A in a geodetic orbit and dt as the ‘universal’ clock-rate G of a standard clock at rest in infinity, the only condition for which $d\tau = dt$. The result of Eqn. (9) is the basic relativistic correction used in GNSS clock frequencies, with the first as the gravity effect or gravitational potential correction and the second as the velocity effect or the correction due to Special Relativity (Ashby, 2002; Hećimović, 2013; Delva and Lodewyck, 2013).

Given the classical definitions of $K = \frac{mv_{\text{orbit}}^2}{2}$ and $V = m\Phi$, we get

$$\frac{d\tau}{dt} = \sqrt{1 - \frac{2L}{U_0}}. \quad (10)$$

All the satellites of a GNSS system are being installed on a similar orbit and thus syntonized relative to one another because they share the same high and velocity and have constant L and $\frac{d\tau}{dt}$ on those orbits. But different GNSS systems, as for example GPS compared to GALILEO, are functioning on different orbits with different velocities and those systems aren’t syntonized relative to one another. This non-syntonization between satellites on orbits with different heights and virial theorem connected velocities is very annoying for the effort towards realizing an integration of the different GNSS systems into one single global network.

Fundamental in the approach of this paper is to analyze gravity using relative frequency shifts, and thus $\frac{d\tau}{dt}$, as one of the basic experimental inputs. Such a method is also looming in today’s geodesy. In modern gravitational geodesy scientists are investigating the relativistic frequency shift as a new observable type for gravity field recovery (Mayrhofer and Pail, 2012). Driven by this development, modern geodesy is about to go through a change from the Newtonian paradigm to Einstein’s theory of general relativity (Kopeikin et al., 2017). A new generation of atomic clock is the game changer for this new domain of chronometric geodesy, and requires additional new techniques to be developed in the field of frequency transfer and comparison (Delva and Lodewyck, 2013). The paradigm shift towards gravitational divergence recovery is based on the principle of frequency comparison between two clocks on different space-time locations in order to measure the frequency shift between them (Delva and Lodewyck, 2013). The knowledge of the Earth’s gravitational field has often been used to predict frequency shifts between distant clocks. In relativistic geodesy, the problem is reversed and the measurement of frequency shifts between distant clocks now provides knowledge of the gravitational field (Delva and Lodewyck, 2013). This reversal also looms

in my postulate of the ‘constant Lagrangian’ model. A constant Lagrangian implies a zero divergence in the syntonization of atomic oscillators and thus an absence of gravitational stress. A divergence in the Lagrangian implies a divergence in the time dilation factor $\frac{d\tau}{dt}$ and thus a non-zero gravitational stress.

The ‘constant Lagrangian’ model for galactic dynamics starts with the postulate that the geodetic Lagrangian $L = K - V$ is a galactic constant, not just an orbital constant. In this ‘time bubble halo’ model the classical Newtonian potential is assumed valid. This potential in the case of a model galaxy with a perfect quasi-solid bulge and a perfect Schwarzschild emptiness around it is given in Fig.(1). My model galaxy is build of a model bulge with mass M and radius R and a Schwarzschild metric emptiness around it. The model bulge has constant density $\rho_0 = \frac{M}{V} = \frac{3M}{4\pi R^3}$ and its composing stars rotate on geodetics in a quasi-solid way. So all those stars in the bulge have equal angular velocity on their geodetic orbits, with $v = \omega r$. On the boundary between the quasi solid spherical bulge and the emptiness outside of it, the orbital velocities are behaving smoothly. So the last star in the bulge and the first star in the Schwarzschild region have equal velocities and potentials. I also assume that the Newtonian potential itself is unchanged and unchallenged, remains classical in the whole galaxy and its surroundings. Such a model galaxy doesn’t have a SMBH in the center of its bulge and it only has some very lonely stars in the space outside the bulge.

The ‘constant Lagrangian model postulates $L = K - V = \text{constant}$ in the entire galaxy, without changing the Newtonian potential. As a result, in such a model bulge, L is a constant of the motion, not only in one orbit but also between orbits.

$$\frac{L}{m} = \frac{v_{\text{orbit}}^2}{2} + \frac{GM}{r} = \frac{3GM}{2R} = \text{constant}. \quad (11)$$

For the region $0 \leq r \leq R$ we get

$$v_{\text{orbit}}^2 = \frac{GM}{R} \cdot \frac{r^2}{R^2} \quad (12)$$

and outside the model bulge, where $R \leq r \leq \infty$, we have

$$v_{\text{orbit}}^2 = \frac{3GM}{R} - \frac{GM}{r}. \quad (13)$$

From the perspective of a free fall Einstein elevator observer, the free fall on a radial geodetic from infinity towards the center of the bulge, the other free fall tangential geodetics seem to abide the law of conservation of energy, because the escape kinetic energy plus the orbital kinetic energy is a constant on my model galaxy with galactic constant L . An

Point	Relation	Expression
Outside the bulge	$r > R$	$-\frac{GM}{r}$
On the Surface	$r = R$	$-\frac{GM}{R}$
Inside the bulge	$r < R$	$-GM \left[\frac{3R^2 - r^2}{2R^3} \right]$
At the centre	$r = 0$	$-\frac{3}{2} \left(\frac{GM}{R} \right)$

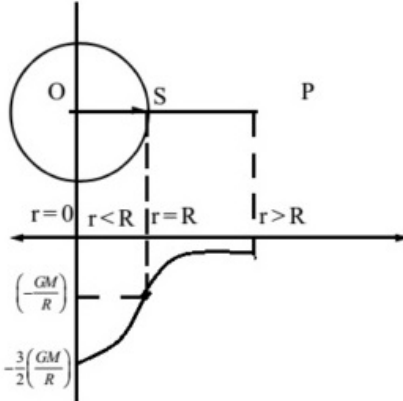


FIG. 1. The potential inside and out of a model bulge

Einstein elevator system with test mass m that would be put in an orbital collapse situation, magically descending from orbit to orbit in a process in thermodynamic equilibrium, would have constant total kinetic energy, from the radial free fall perspective. This can be expressed as $L = K_{orbit} - V = K_{orbit} + K_{escape} = K_{final}$. In Fig.(2) I sketched the result, with $-V = +K_{escape}$.

Such a model galaxy would also be a GNSS engineer's dream come true because the whole model galaxy is in one single syntonized time-bubble.

$$\frac{d\tau}{dt} = \sqrt{1 - \frac{2L}{U_0}}. \quad (14)$$

Given the Baryonic Tully-Fisher relation in Milgrom's version $v_{final}^4 = Ga_0 M$ with $2\pi a_0 \approx cH_0$, with a_0 as Milgrom's galactic minimum acceleration and H_0 as the Hubble constant

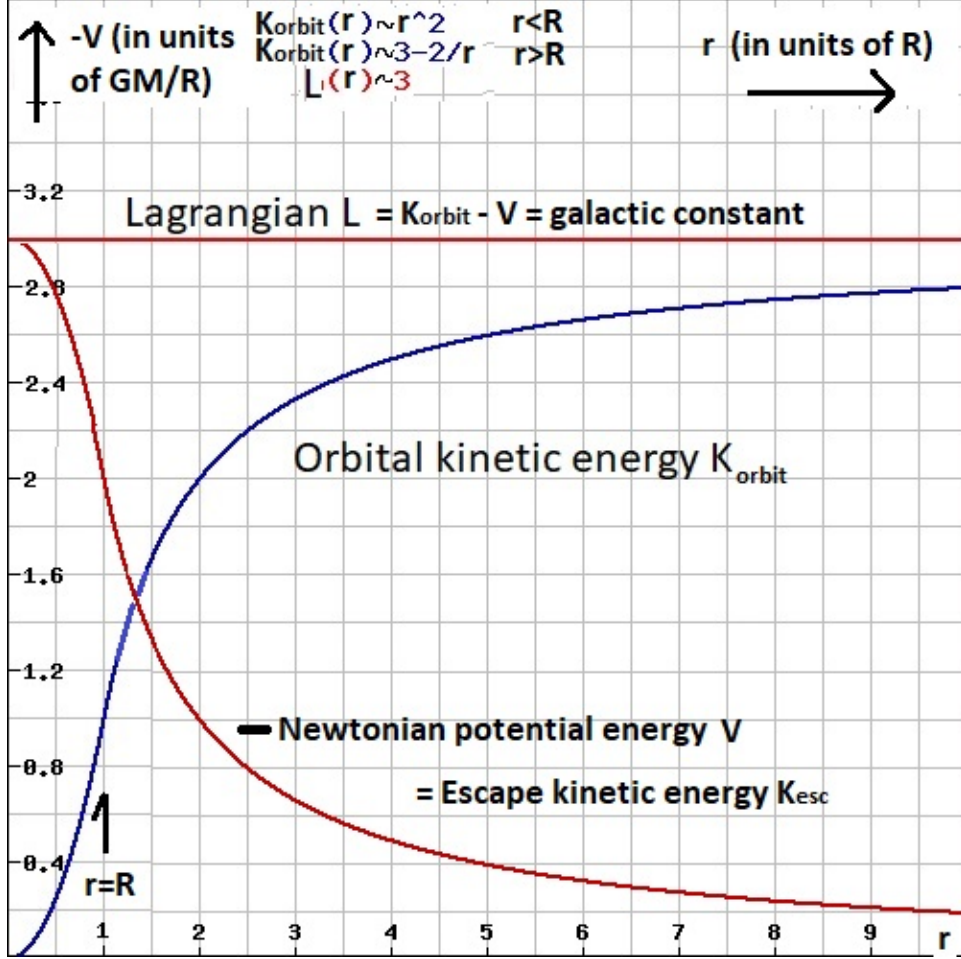


FIG. 2. The square of the orbital velocity profile in the model galaxy with $L = \text{constant}$.

(Milgrom, 1983; McGaugh, 2005), we get as a galactic time bubble fix

$$\frac{d\tau}{dt} = \sqrt{1 - \frac{2L}{U_0}} = \sqrt{1 - \frac{v_{final}^2}{c^2}} = \sqrt{1 - \sqrt{\frac{v_{final}^4}{c^4}}} = \quad (15)$$

$$\sqrt{1 - \sqrt{\frac{Ga_0 M}{c^4}}} = \sqrt{1 - \sqrt{\frac{GH_0 M}{2\pi c^3}}} = \sqrt{1 - \sqrt{\frac{M}{2\pi M_U}}}, \quad (16)$$

in which I used $L = 3GM/R = K_{final} = \frac{1}{2}mv_{final}^2$ and $M_U = \frac{c^3}{GH_0}$. This last constant can be referred to as an apparent mass of the Universe, a purely theoretical number constant, see (Mercier, 2015).

In a model Universe, this would imply that my model galaxy would be in a proper time bubble with clock-rate $d\tau$ relative to the universal clock-rate dt in proportion to the masses of galaxy M and Universe M_U . In my model galaxy theoretical environment the Baryonic Tully-Fisher relationship implies that the galactic time bubble is fixed through the mass of

my model galaxy and that this fix is a cosmological one. So what is a universal acceleration minimum a_0 in MOND can be interpreted as a universally correlated (through M_U) but still local (through M) time bubble fix in my model galaxy geodetic environment. In such a model Universe, the time bubble of a galaxy immediately functions as a gravitational lens, because $\frac{d\tau}{dt}$, as measuring the curvature of the metric, also determines the gravitational index of refraction of the time bubble relative to Cosmic space where $dt = d\tau$. In my model, the Dark Matter halo is above all present as a time bubble halo, determined by the factor $\frac{d\tau}{dt}$.

III. THE DUAL FIT APPROACH TOWARDS ROTATION CURVES

Having determined the model galactic velocity rotation curve based on the Lagrangian as a galactic constant of orbital motion, the question is to what extend real galaxies can be modeled in this way. In my Lagrangian approach I analyze the plot of v_{orb}^2 , in $(km/s)^2$ against r , in kpc . This in contrast to the usual rotation curves where v_{orb} , in (km/s) against r , in kpc . In the Lagrangian approach, the energies, not the velocities, are primary. In each plot the experimental values in red stars with vertical error bars and the theoretical values in black circles and black triangles. The fitting plot is with one single fit for M , in units of $10^{10}Msolar$, and R , in units of kpc . The most important cut in the model is the change from the model bulge to the model empty space around it. In the model bulge, $V_{orb}^2 \propto r^2$, outside the model bulge $V_{orb}^2 \propto -r^{-1}$. In the dual approach, another important part is the shift from the first (M_1, R_1) -fit to the second (M_2, R_2) -fit.

This shift from a first fit to a second fit for the rotation curve of one single galaxy grew out of the analysis of the data. The justification of this dual approach is situated in the difference between the pure model with a perfect bulge and an emptiness around it with only some spare stars and some H1-gas. In reality, galaxies are way more complicated, as being composed of an inner bulge, a disk and H1 gas clouds. The constant Lagrangian' model includes the classical Newtonian potential and that allows for the use of inner and outer shells in the model approach. A shell of H1-gas that is treated as a perfect outside shell can be ignored for the inner shell dynamics. A shell of H1-gas that is an inner shell can be treated as part of the bulge. Going through a shell means leaving the inner model curve and progressing to the outer model curve.

This experimentally driven extension of the pure model with a perfect bulge and a perfect

Schwarzschild empty metric around it appeared first while analyzing the rotation curve of NGC 1560. The velocity rotation curve data of NGC 1560 come from (Broeils, 1992). The comparison with other fitting models came from (Gentile et al., 2010). The rotation curve of NGC 1560 has a peculiar “wiggle”. This “wiggle” in the graph of NGC is described in the following quote.

In the rotation curve of NGC 1560, as derived by B92, there is a clear “wiggle” in the total rotation velocity, which corresponds very closely to a similar wiggle in the gas contribution to the rotation curve. Mass models such as MOND naturally reproduce the feature, whereas models that include a dominant spherical (or triaxial) halo are too smooth to do so. (Gentile et al., 2010)

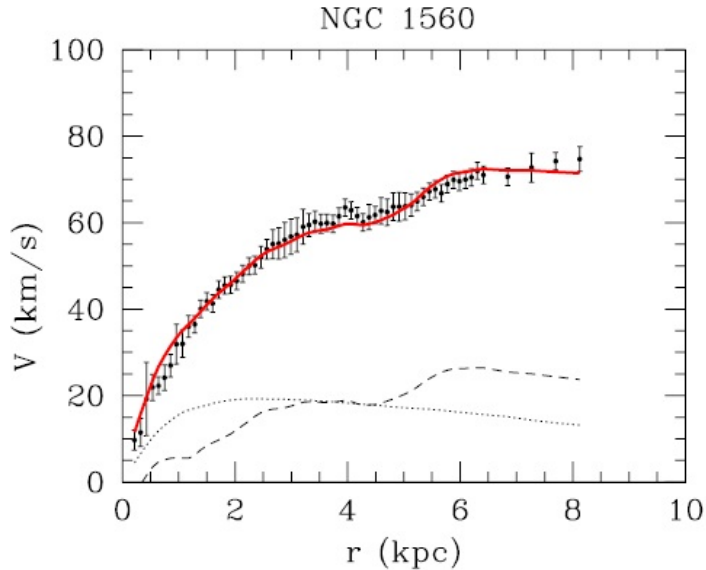


Figure 12. Rotation curve fit using MOND. The best-fit distance is 2.94 Mpc. Lines and symbols are like those in Fig. 10.

FIG. 3. (Gentile et al., 2010) fit of NGC 1560, using MOND. In this graph, the “wiggle” occurs where the stars, represented by the dotted line, give in to the H₁ gas clouds, represented by the barred line, around 4 – 5 kpc.

In my approach, I first have to determine the model galaxy curve that fits best, using the parameters M and R , and then I can use M as a free parameter in order to create a perfect time bubble. In case of NGC 1560 however, it seems that in phase 1 two models partially fit the rotation curve. The first pure model fits NGC 1560 before the “wiggle” the second pure model fits NGC 1560 after the “wiggle”, see Fig.(4). Thus in my approach, the ‘constant Lagrangian’ model, the modeling indicates the underlying dynamics and the real world of unpredictable but observable mass distributions of stars and H1 gas clouds. The “wiggle” divides NGC 1560 in two regions, which both follow their respective pure model relatively smoothly without being disturbed by that other part of the galaxy. The baryonic matter further away from the center than the H1 gas of producing “wiggle” just behaves as if the bulge end where the “wiggle” ends. The baryonic matter closer to the center than the H1 gas of producing “wiggle” just behaves as if the H1 gas of the “wiggle” is a perfect shell which doesn’t gravitate inside that shell. So the fact that two pure models can be made to partially fit the rotation curve actually reveals a lot of the underlying dynamics, reproducing known baryonic behavior under the influence of a Newtonian potential.

This fact, that one can only reasonably fit NGC 1560 by using two model fits, appeared to be the case for most galaxies. The shift from one model fit to the other model fit mostly follows the shift from stars dominated mass distribution to H1 gas dominated mass distribution. Sometimes however it follows the shift from bulge to disk.

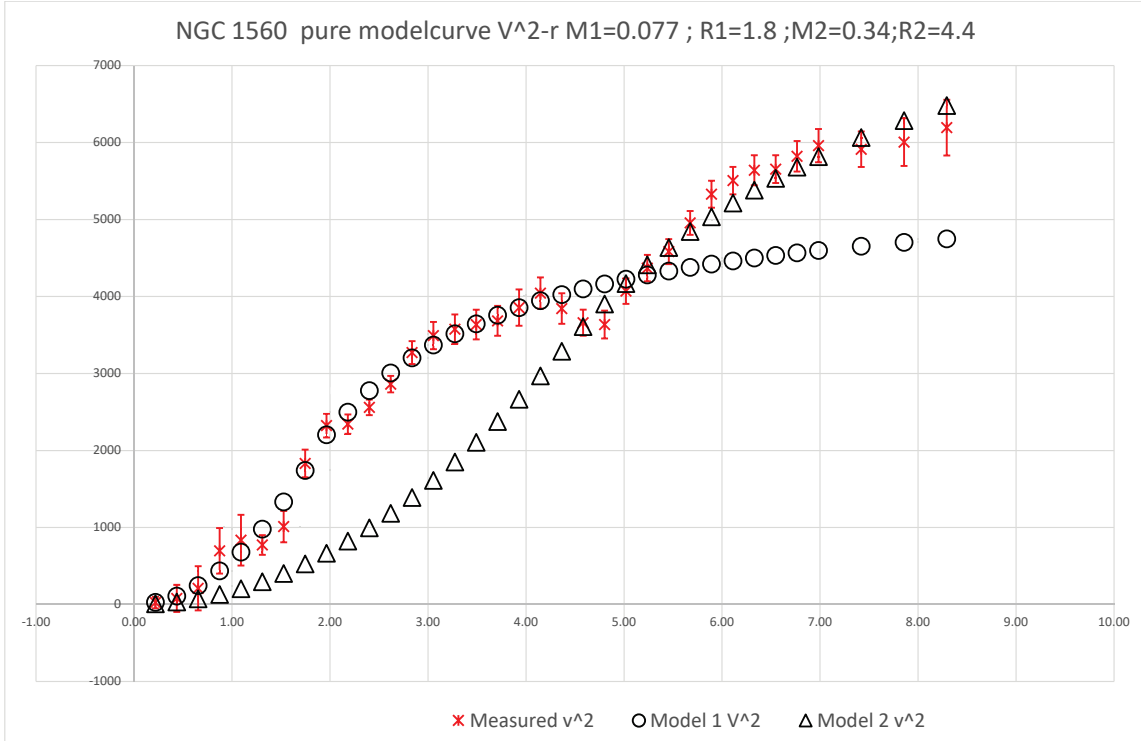


FIG. 4. Dual fit of NGC1560, V_{orb}^2 against r .

While analyzing the SPARC database, this shift proved quite general. In the following I will give one example of such a shift, with galaxy DDO161. First I give the dual plot of the rotation curve, then I compare the result against the mass distribution made available by SPARC (from the [MassModels-LTG.zip](#) file).

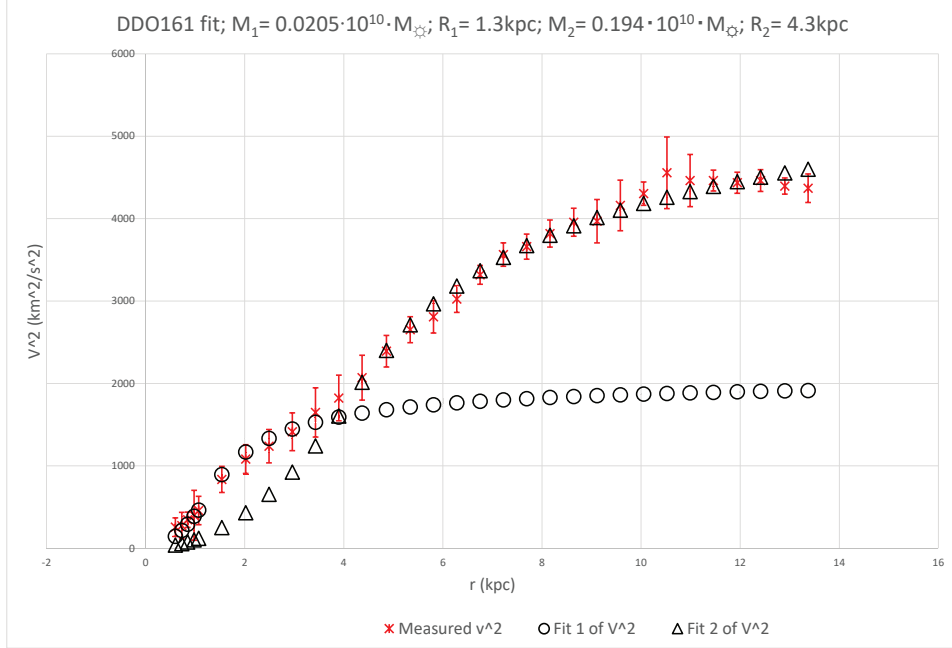


FIG. 5. DDO161, V_{orb}^2 against r .

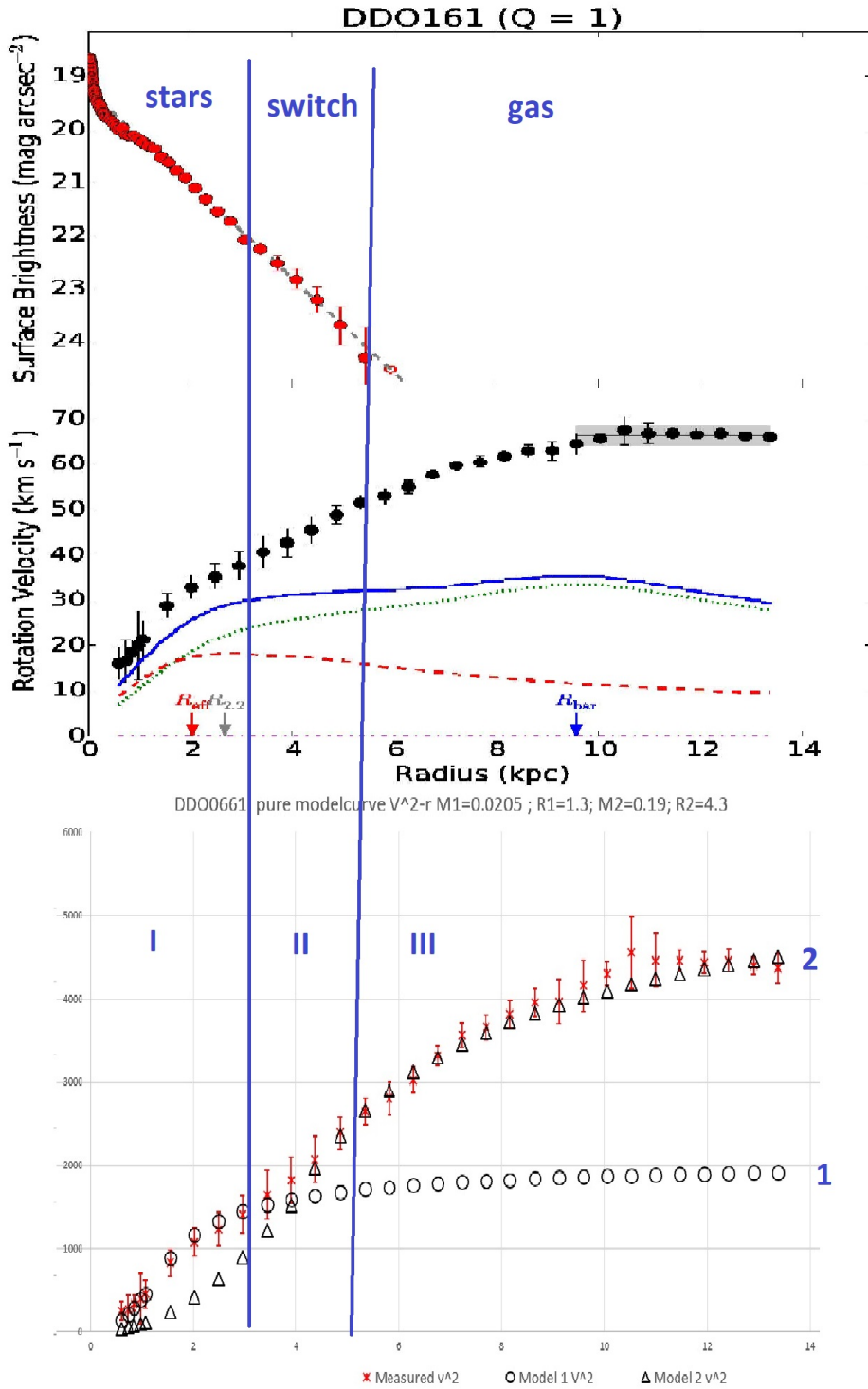


FIG. 6. DDO161, V_{orb}^2 against r , and the stars and gas mass distribution plot. The red dots are the luminous stars, the dotted line the gas contribution to the mass and the red bars line represent the stars contribution to the velocity curved, assuming the virial theorem.

IV. CONCLUSION

Twenty five percent, 43 of 175, of the rotation curves can be fit within the error margins with one model only. Most, 166 of 175, need a dual fit to remain within the error margins, with the shift from the one to the other as one goes through a distinct mass distribution shell. Some 16 of 175 galaxies are more complicated. The dual fit galaxies can be subdivided into almost single fit to almost three fit, with many clearly distinctive dual fits.

In many cases, the shift from the first model to the second correspond with the shift from star dominated to gas dominated regions as given by the SPARC database. This correspondence happens so often that it cannot be a mere coincidence.

The least daring conclusion of this paper is that huge stretches of galaxy rotation curves can be effectively plotted on constant Lagrangian curves. This needs theoretical explanation and exploration, to say the least. Especially for the more complicated galaxies, with three fits, the sections still following a constant Lagrangian curves as impressive.

The shift from one constant Lagrangian curve to the next constant Lagrangian curve is a region where the constant Lagrangian regime seems to give way to a virial regime. One gets the impression that for those galaxies, some regions appear Einsteinian and others appear Newtonian.

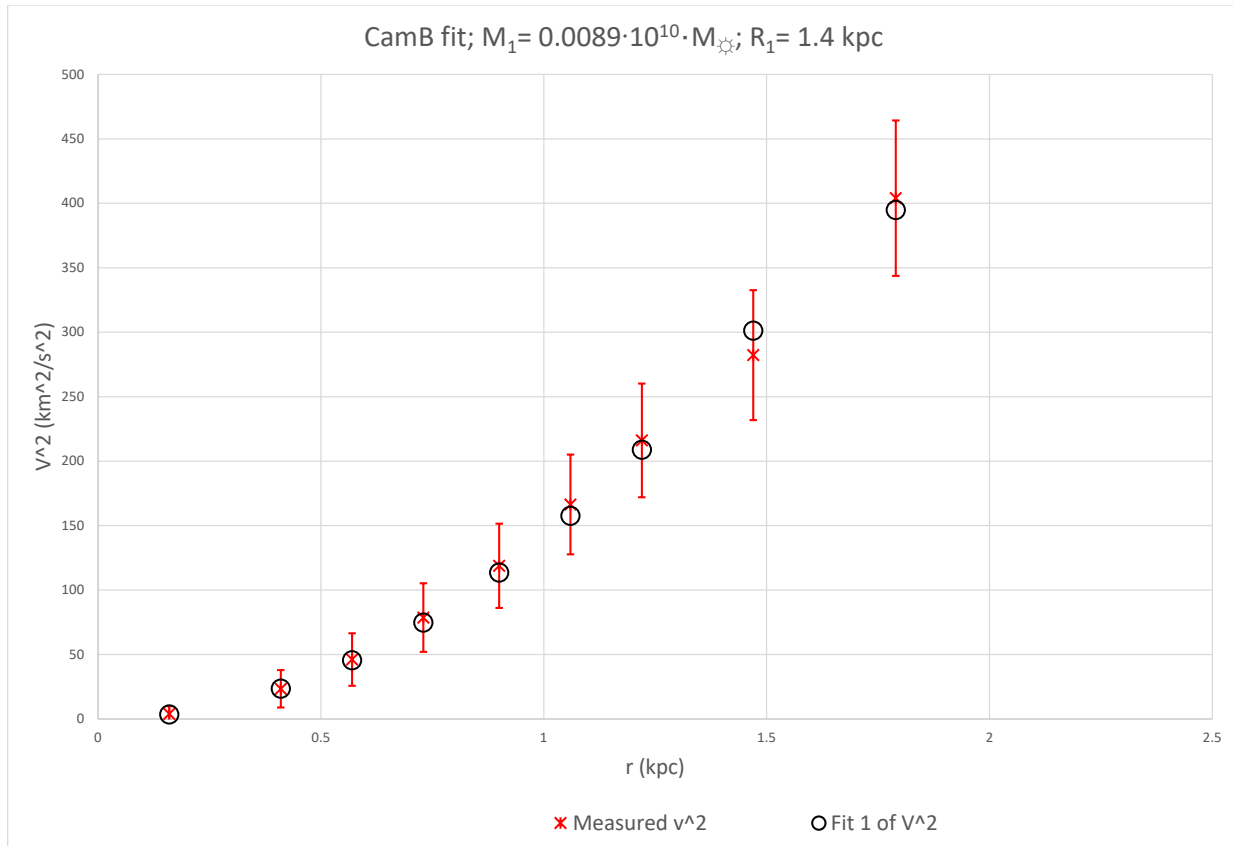
REFERENCES

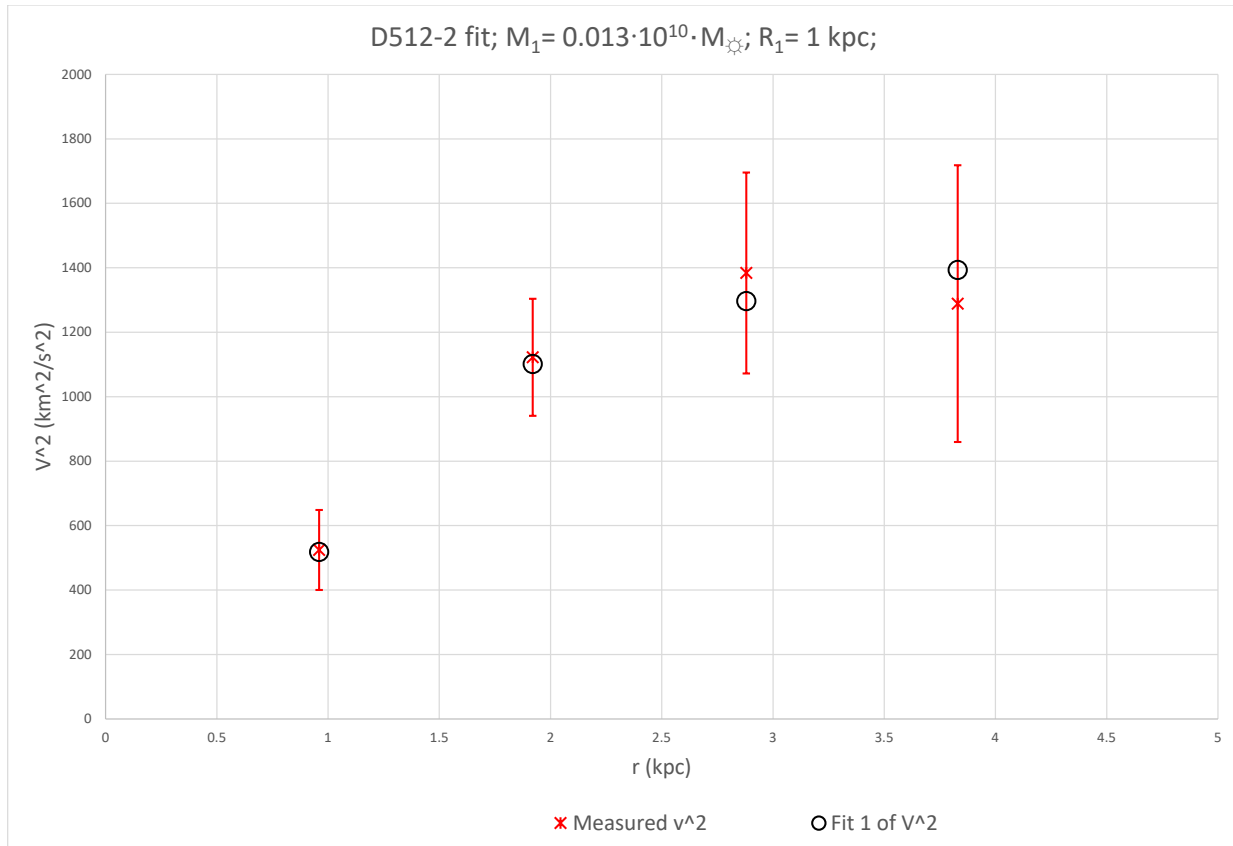
- Ashby, N. (2002, May). Relativity and the global positioning system. *Physics Today* 55(5), 41–47.
- Broeils, A. H. (1992). The mass distribution of the dwarf spiral ngc 1560. *Astronomy and Astrophysics* 256, 19–32.
- de Haas, E. P. J. (2018a). A ‘constant lagrangian’ fit of the galaxy rotation curves of the ‘f-series’ from the sparc database. *Preprint on viXra.org: Astrophysics*. [vixra:1805.0168](#).
- de Haas, E. P. J. (2018b). A ‘constant lagrangian’ model for galactic dynamics in a geodetic approach towards the galactic rotation dark matter issue. *Preprint on viXra.org: Astrophysics*. [vixra:1804.0298](#).
- de Haas, E. P. J. (2018c). Fitting some galaxy rotation curves using the ‘constant lagrangian’ model for galactic dynamics. *Preprint on viXra.org: Astrophysics*. [vixra:1804.0386](#).
- de Haas, E. P. J. (2018d). Fitting the ngc 1560 rotation curve and other galaxies in the ‘constant lagrangian’ model for galactic dynamics. *Preprint on viXra.org: Astrophysics*. [vixra:1804.0328](#).
- de Haas, E. P. J. (2018e). A stars-gas dual fit result in the ‘constant lagrangian’ model for galactic dynamics when applied to the sparc database. *Preprint on viXra.org: Astrophysics*. [vixra:1805.0047](#).
- Delva, P. and J. Lodewyck (2013). Atomic clocks: new prospects in metrology and geodesy. In *Workshop on Relativistic Positioning Systems and their Scientific Applications Brdo, Slovenia, September 19-21, 2012*. arXiv:1308.6766 [physics.atom-ph].
- Gentile, G., M. Baes, B. Famaey, and K. Van Acoleyen (2010). Mass models from high-resolution h i data of the dwarf galaxy ngc 1560. *Monthly Notices of the Royal Astronomical Society* 406(4), 2493–2503.
- Hećimović, Ž. (2013). Relativistic effects on satellite navigation. *Tehnički vjesnik* 20(1), 195–203.
- Kopeikin, S. M., I. Y. Vlasov, and W. B. Han (2017). The normal gravity field in relativistic geodesy. *ArXiv e-prints*. arXiv:1708.09456 [gr-qc].
- Lelli, F., S. S. McGaugh, and J. M. Schombert (2016, December). SPARC: Mass Models for 175 Disk Galaxies with Spitzer Photometry and Accurate Rotation Curves. *The Astronomical Journal* 152, 157.

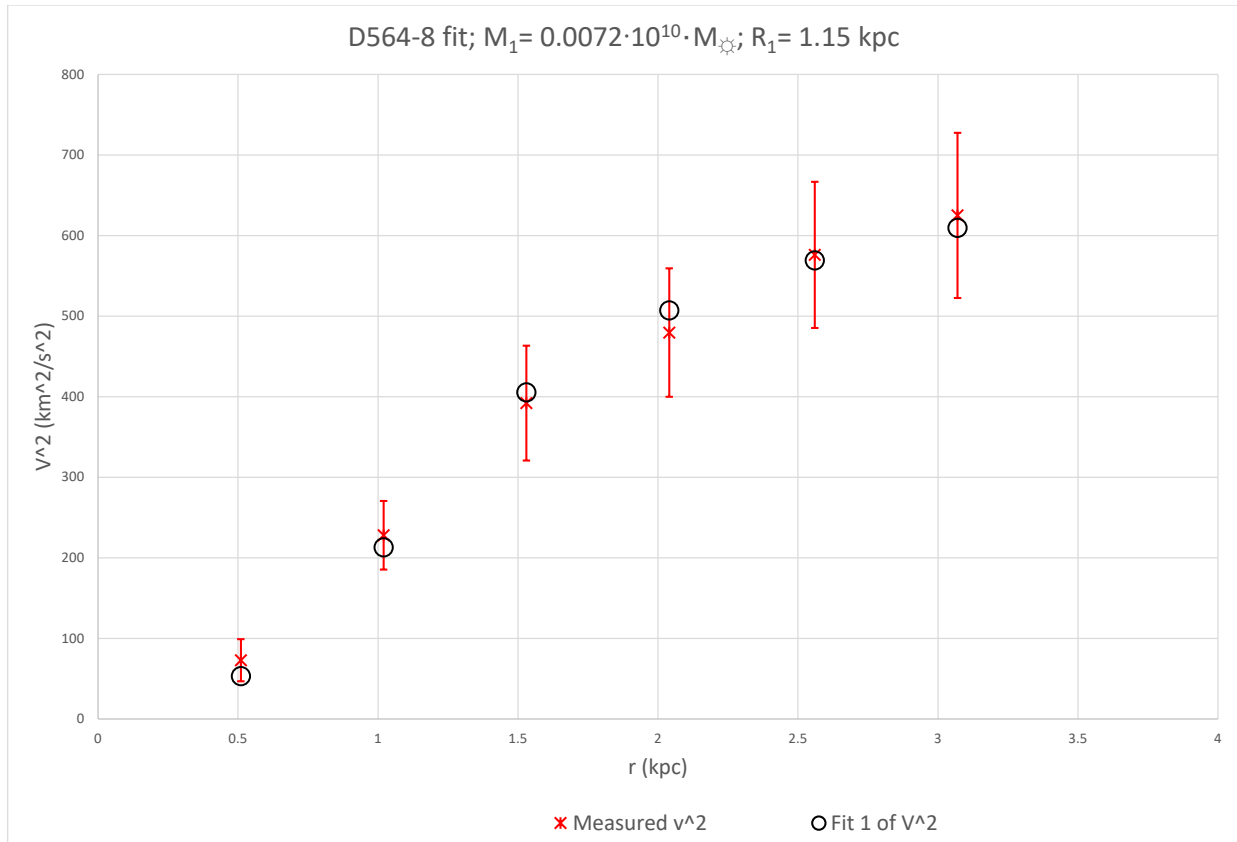
- Mayrhofer, R. and R. Pail (2012). Future satellite gravity field missions: Feasibility study of post-newtonian method. In S. Kenyon (Ed.), *Geodesy for Planet Earth*, Volume 136 of *International Association of Geodesy Symposia*, pp. 231–238. Springer International Publishing. Switzerland.
- McGaugh, S. S. (2005). The baryonic tully-fisher relation of galaxies with extended rotation curves and the stellar mass of rotating galaxies. *The Astrophysical Journal* 632, 859–871. [arXiv:astro-ph/0506750v2](https://arxiv.org/abs/astro-ph/0506750v2).
- Mercier, C. (2015). Calculation of the apparent mass of the universe. [Website access](#) (accessed on April, 14, 2018).
- Milgrom, M. (1983). A modification of the newtonian dynamics - implications for galaxies. *The Astrophysical Journal* 270, 371–387. [Astronomy Abstract Service pdf](#).
- Ruggiero, M. L., D. Bini, A. Geralico, and A. Tartaglia (2008). Emission versus fermi coordinates: applications to relativistic positioning systems. *Classical and Quantum Gravity* 25(20), 205011. arXiv:0809.0998 [gr-qc].

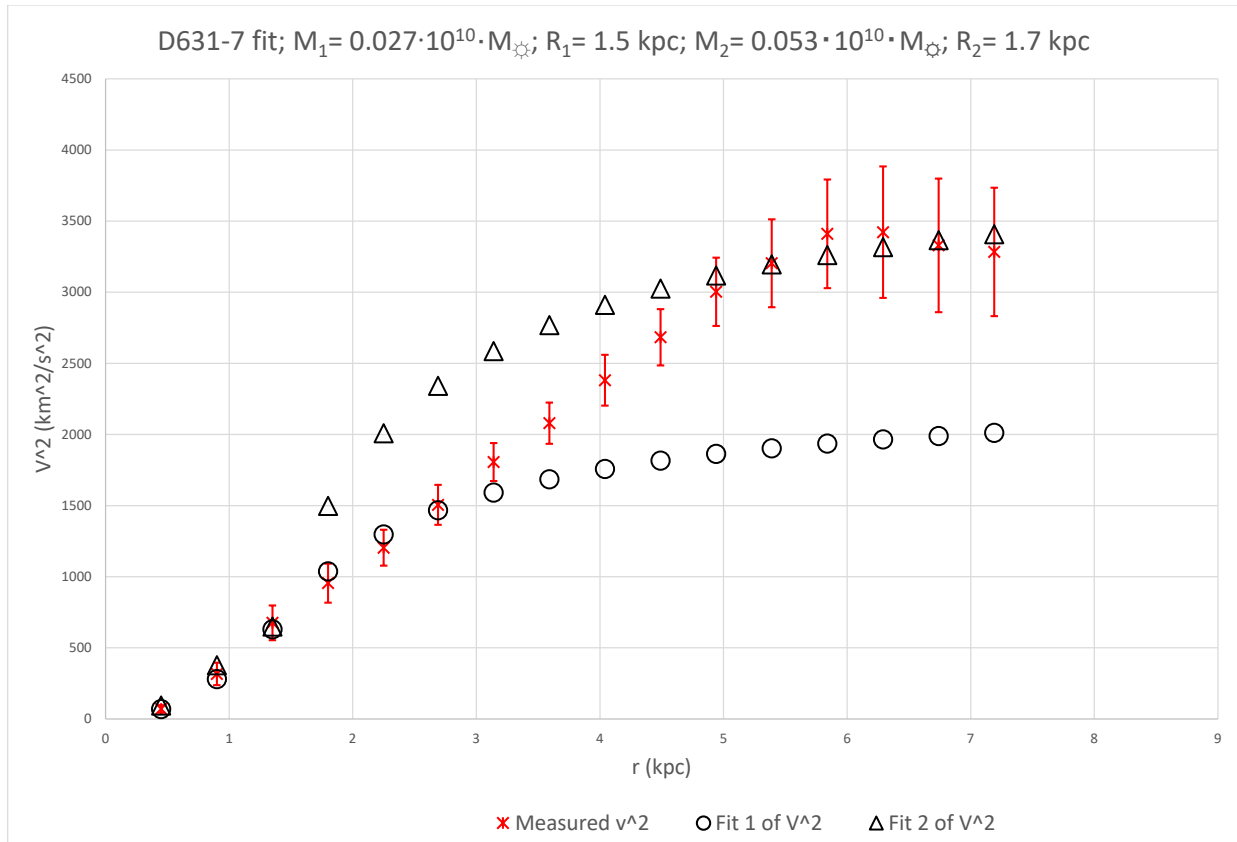
Appendix A: The fit of the 175 SPARC database galaxies.

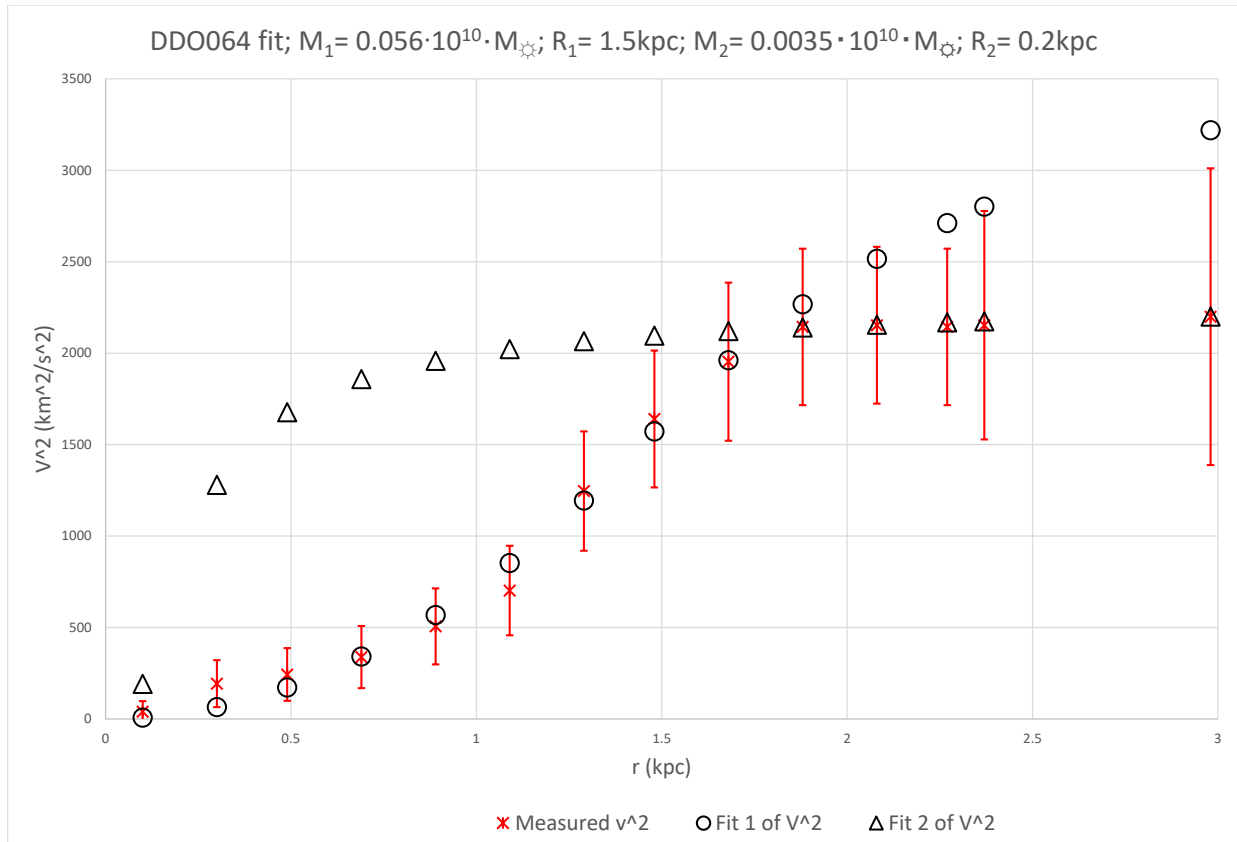
In this appendix, I present the ‘constant Lagrangian’ rotation curve fits of the sixteen galaxies whose name starts with an F in of the [SPARC database](#), including the error margins, as provided by (Lelli et al., 2016). It is to the reader to compare the results with the mass distribution graphs of SPARC (from the [MassModels-LTG.zip](#) file). As an inductive result, the fits of this database shows that, at least, huge stretches of almost all galaxy rotation curves can be plotted on a constant Lagrangian curve.

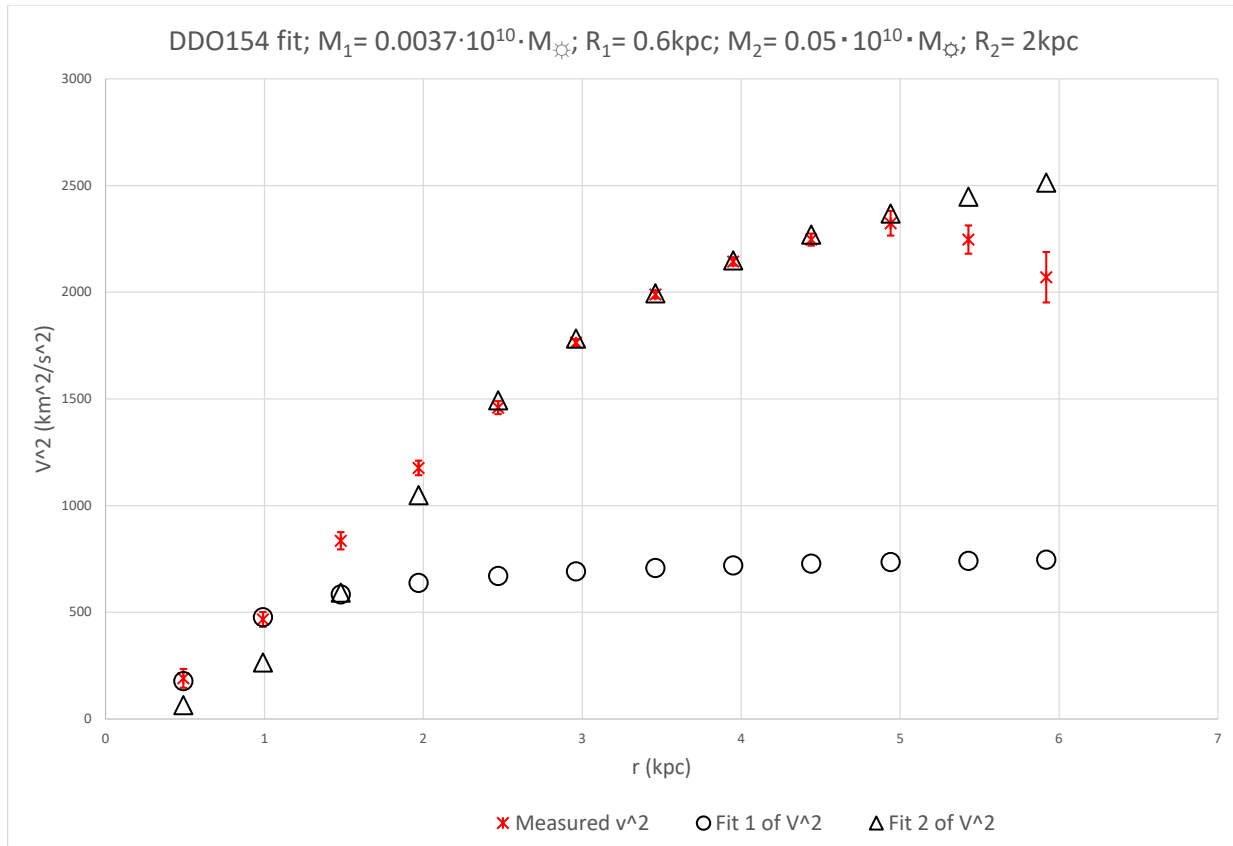


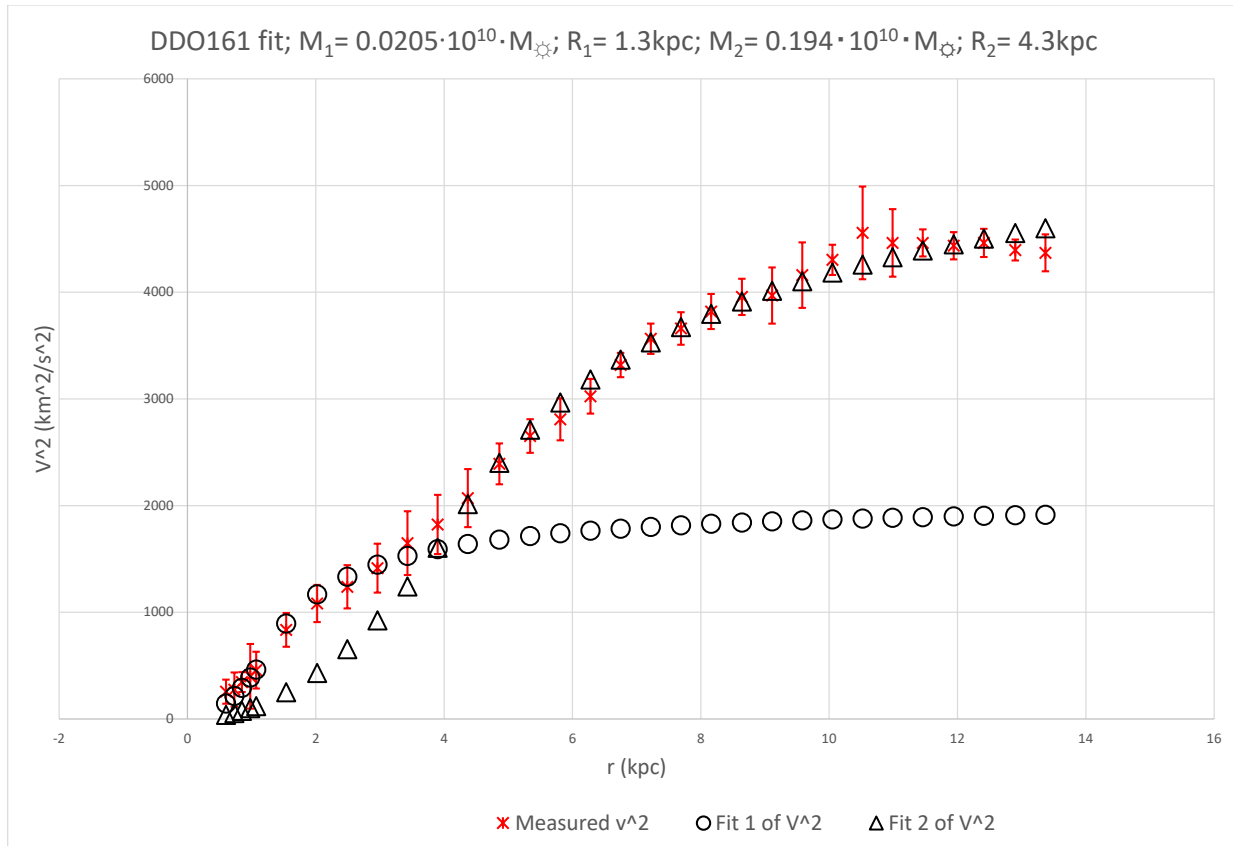


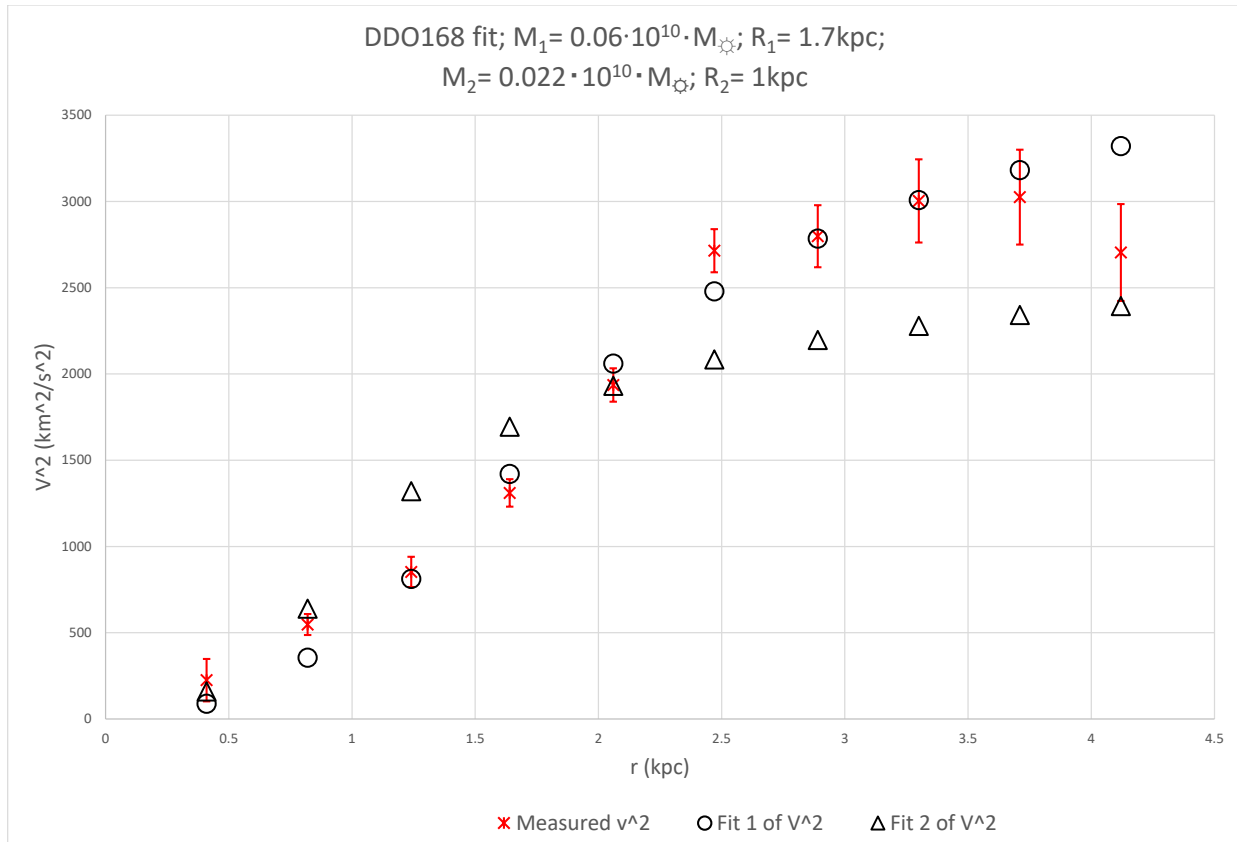


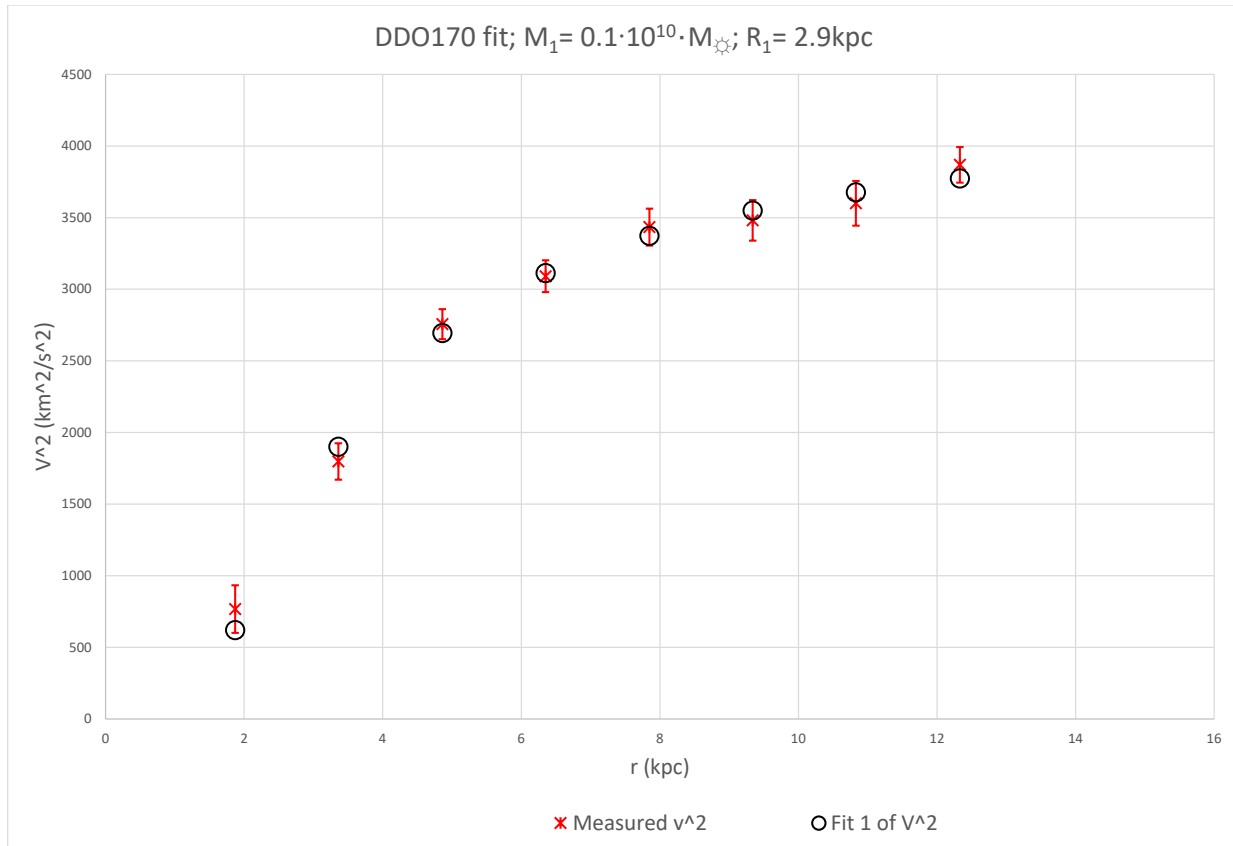




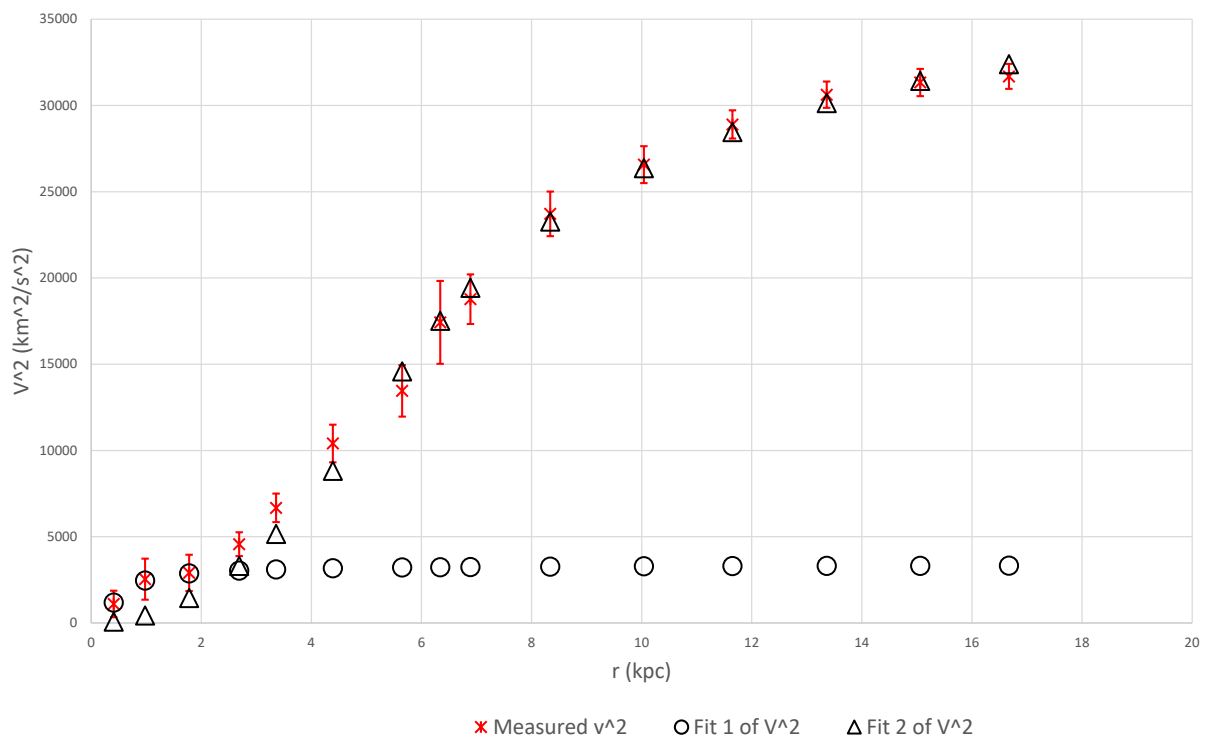


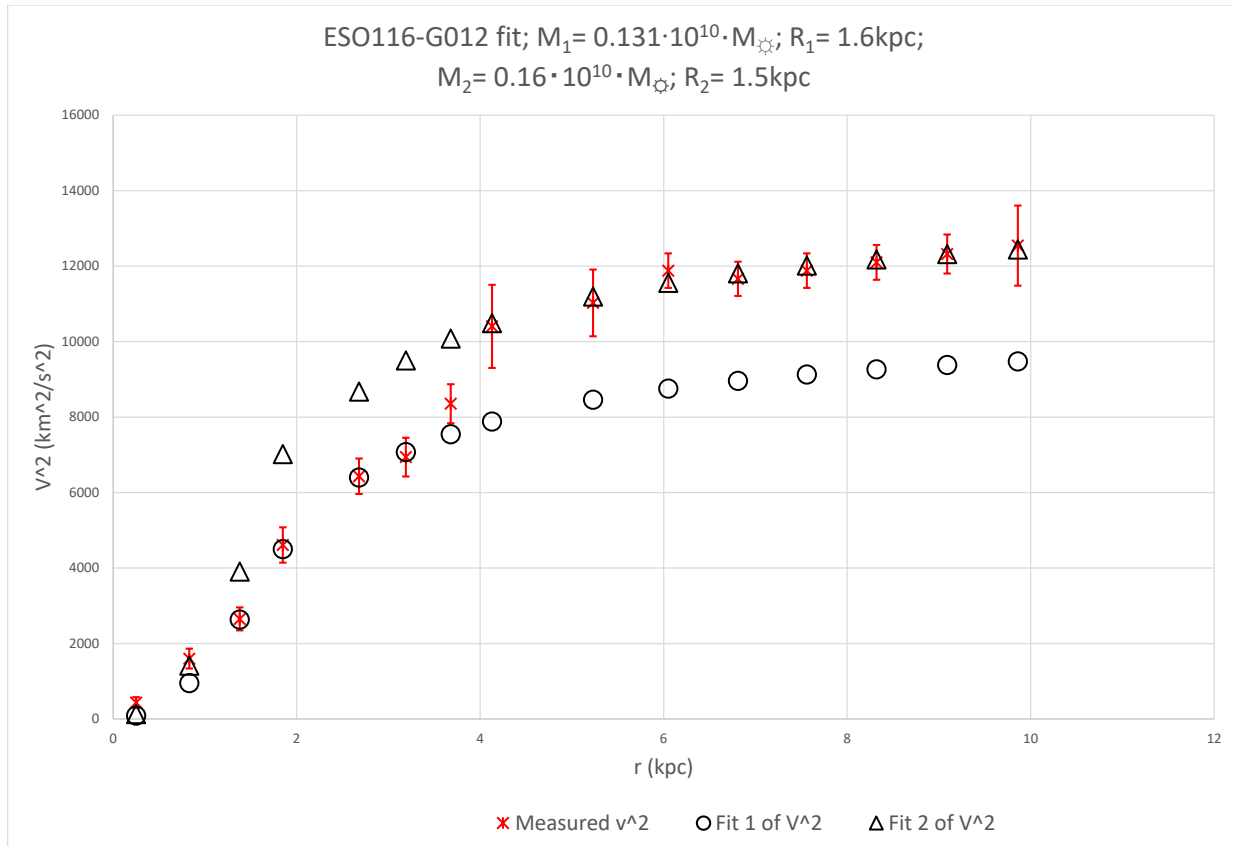




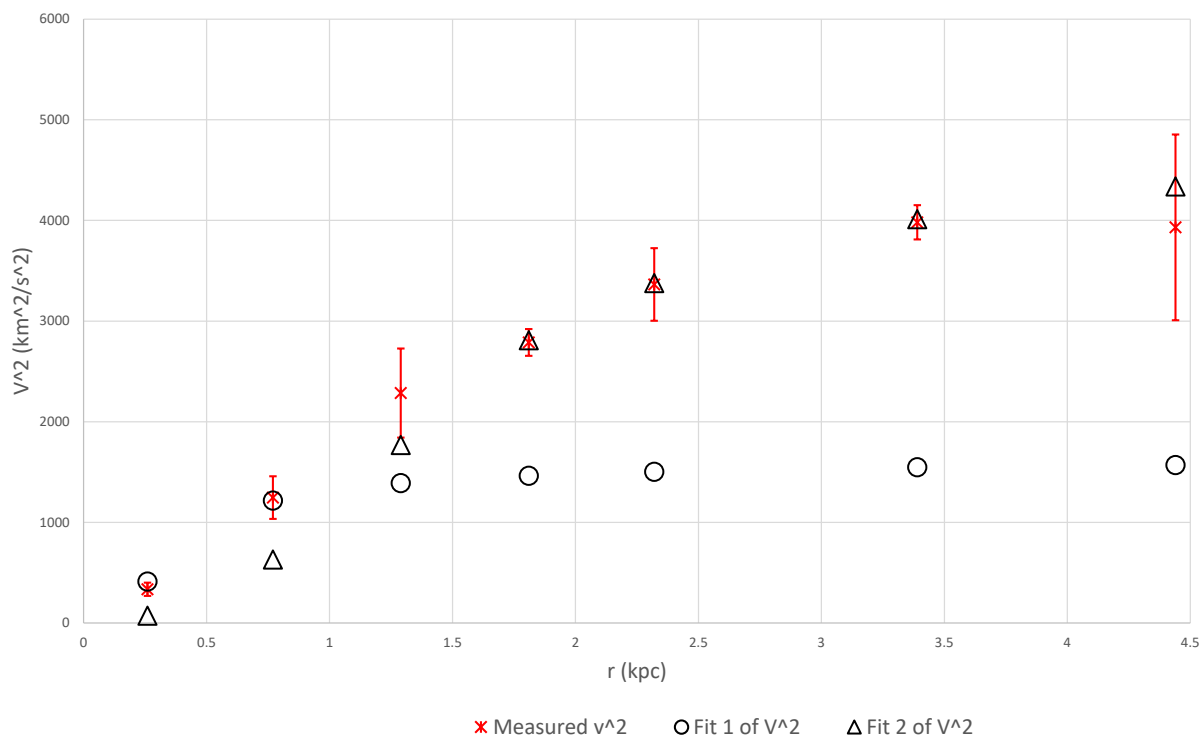


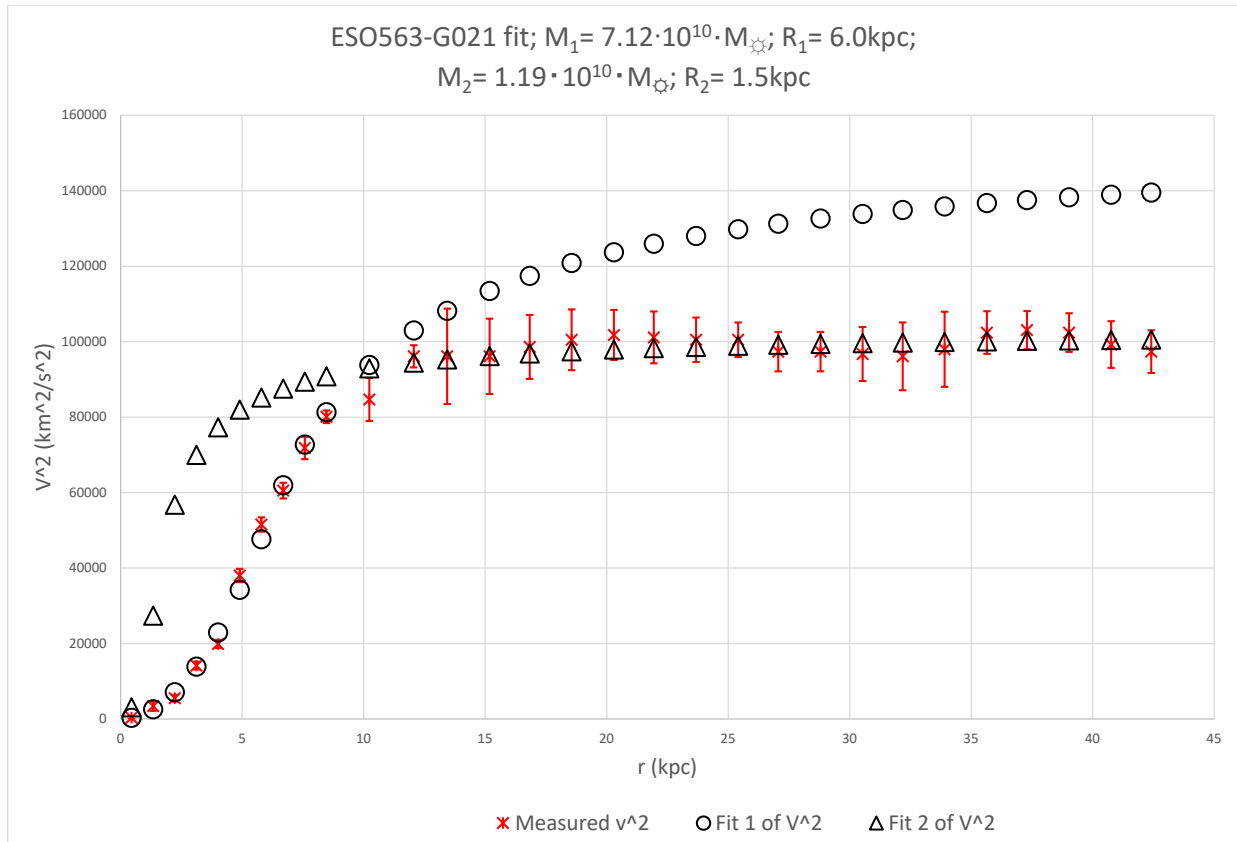
ESO079-G014 fit; $M_1 = 0.0104 \cdot 10^{10} \cdot M_{\odot}$; $R_1 = 0.4 \text{ kpc}$;
 $M_2 = 1.76 \cdot 10^{10} \cdot M_{\odot}$; $R_2 = 5.5 \text{ kpc}$

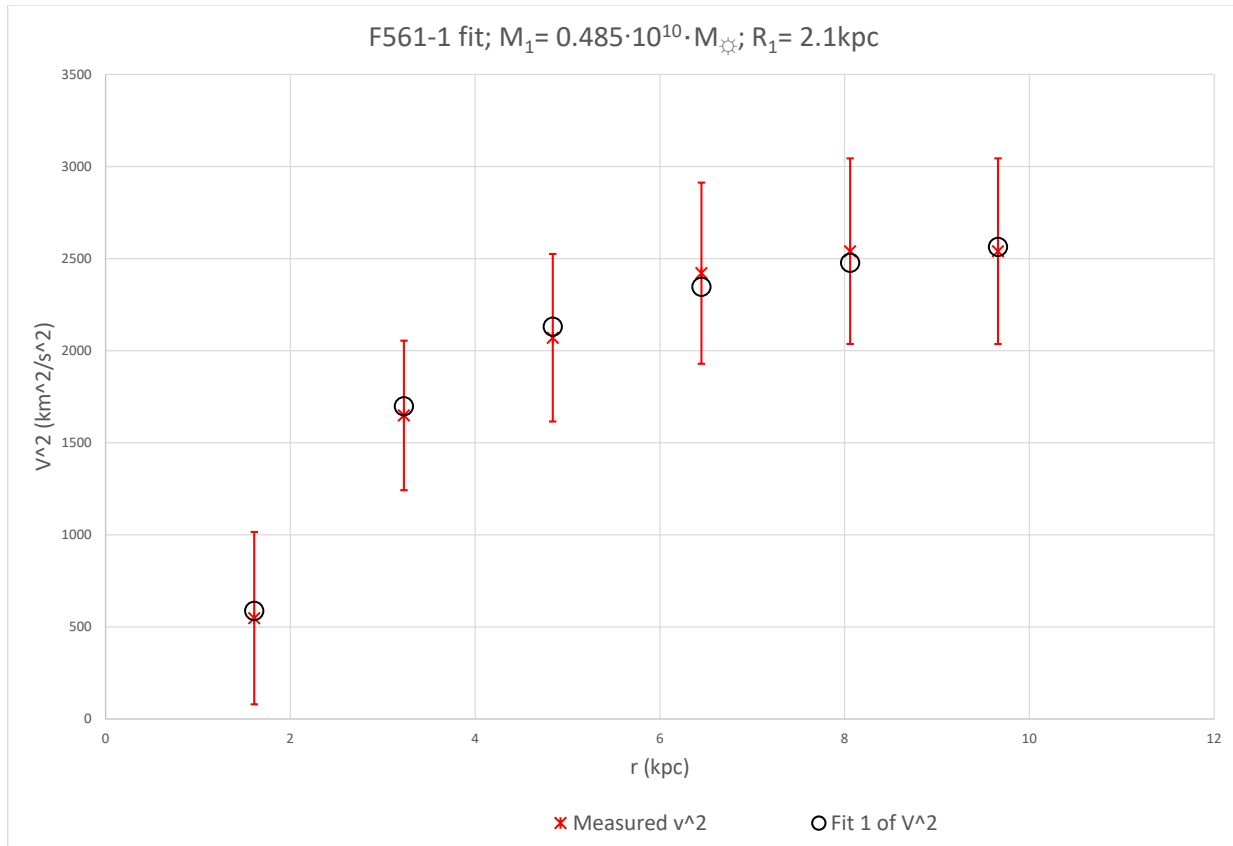


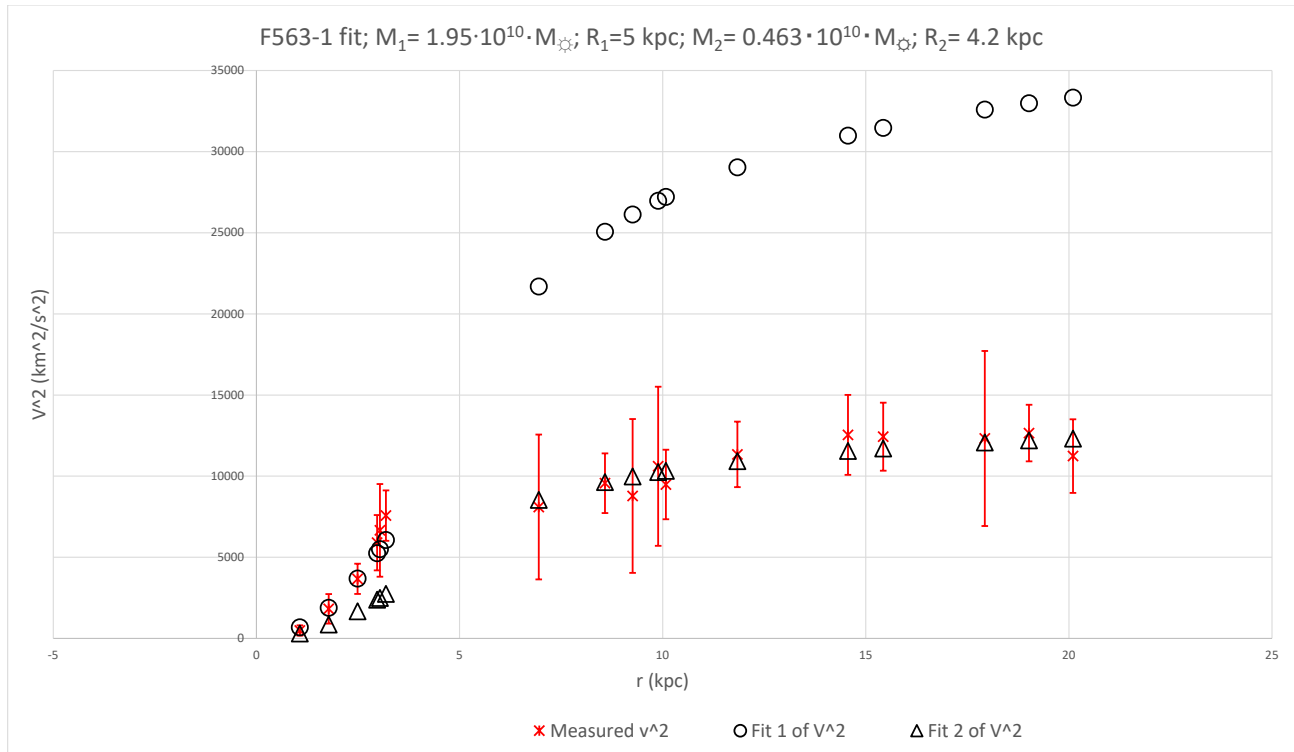


ESO444-G084 fit; $M_1 = 0.0038 \cdot 10^{10} \cdot M_{\odot}$; $R_1 = 0.3 \text{ kpc}$;
 $M_2 = 0.054 \cdot 10^{10} \cdot M_{\odot}$; $R_2 = 1.3 \text{ kpc}$

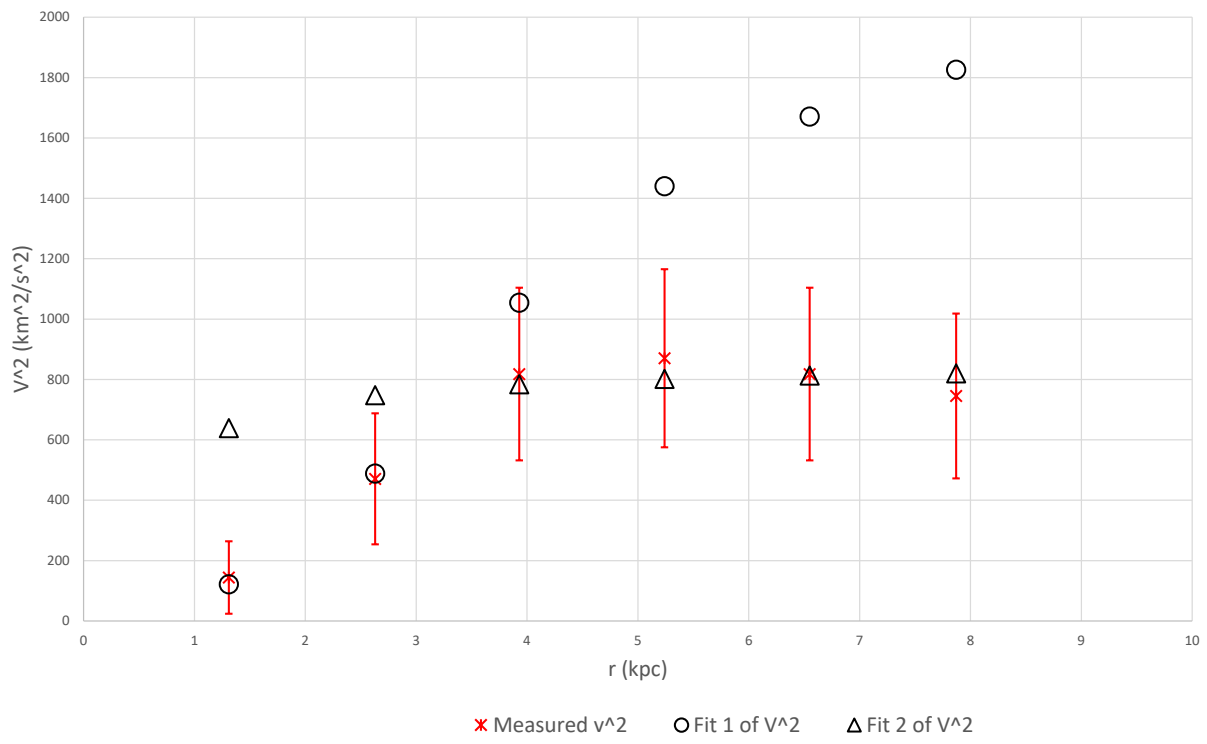




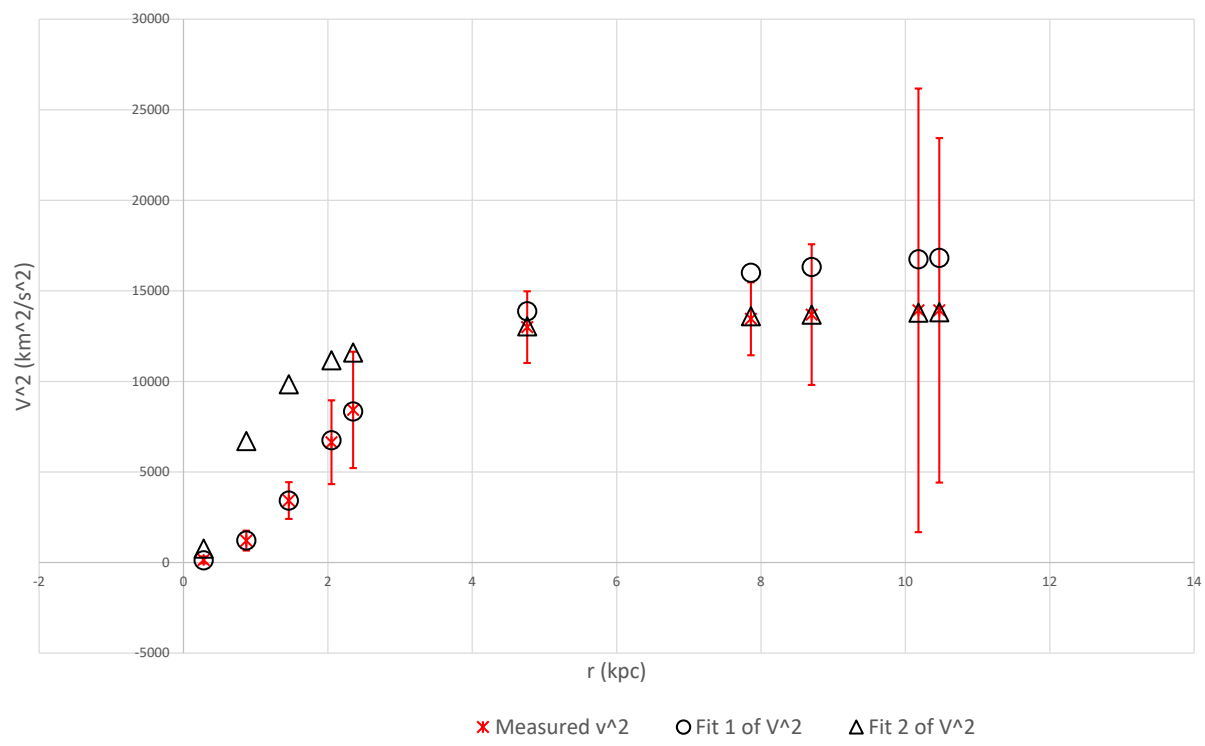


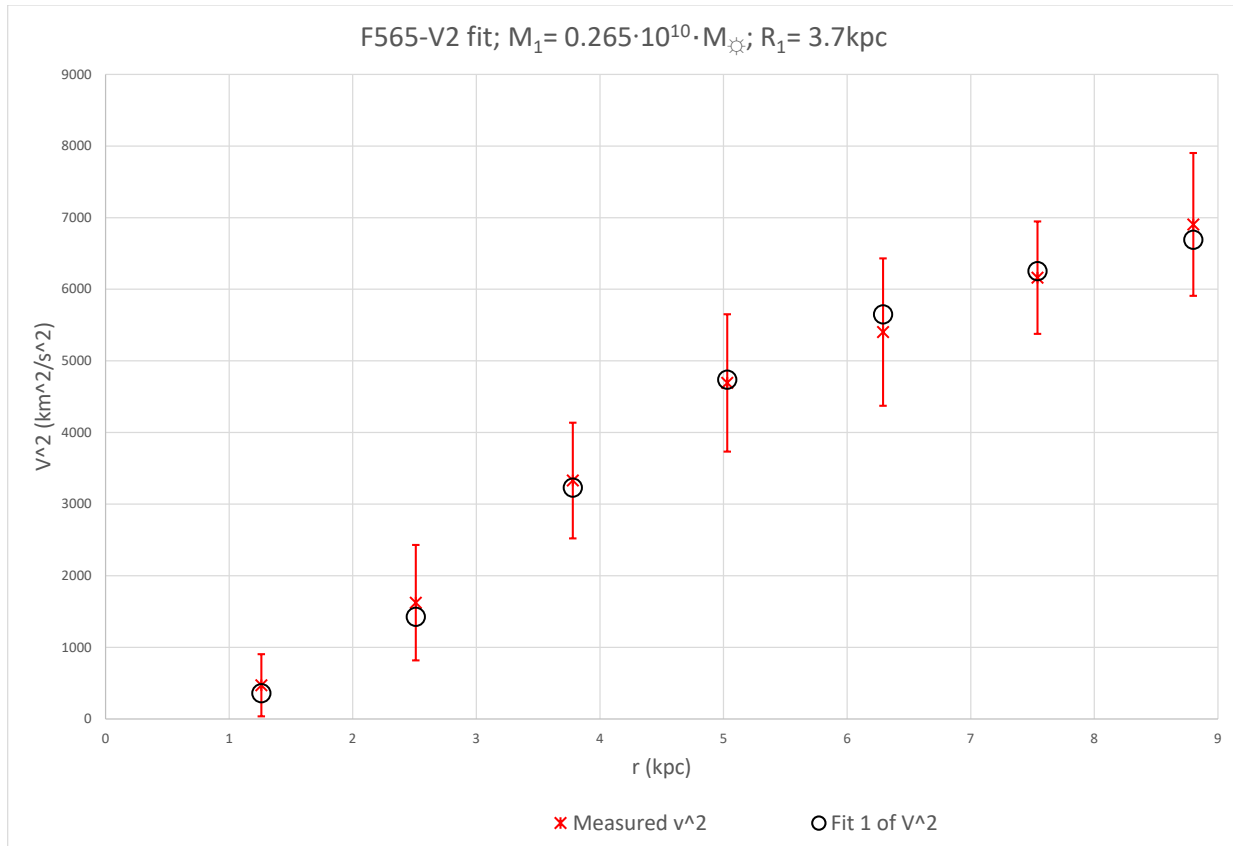


F563-V1 fit; $M_1 = 0.007 \cdot 10^{10} \cdot M_{\odot}$; $R_1 = 3.5 \text{ kpc}$;
 $M_2 = 0.0033 \cdot 10^{10} \cdot M_{\odot}$; $R_2 = 0.5 \text{ kpc}$

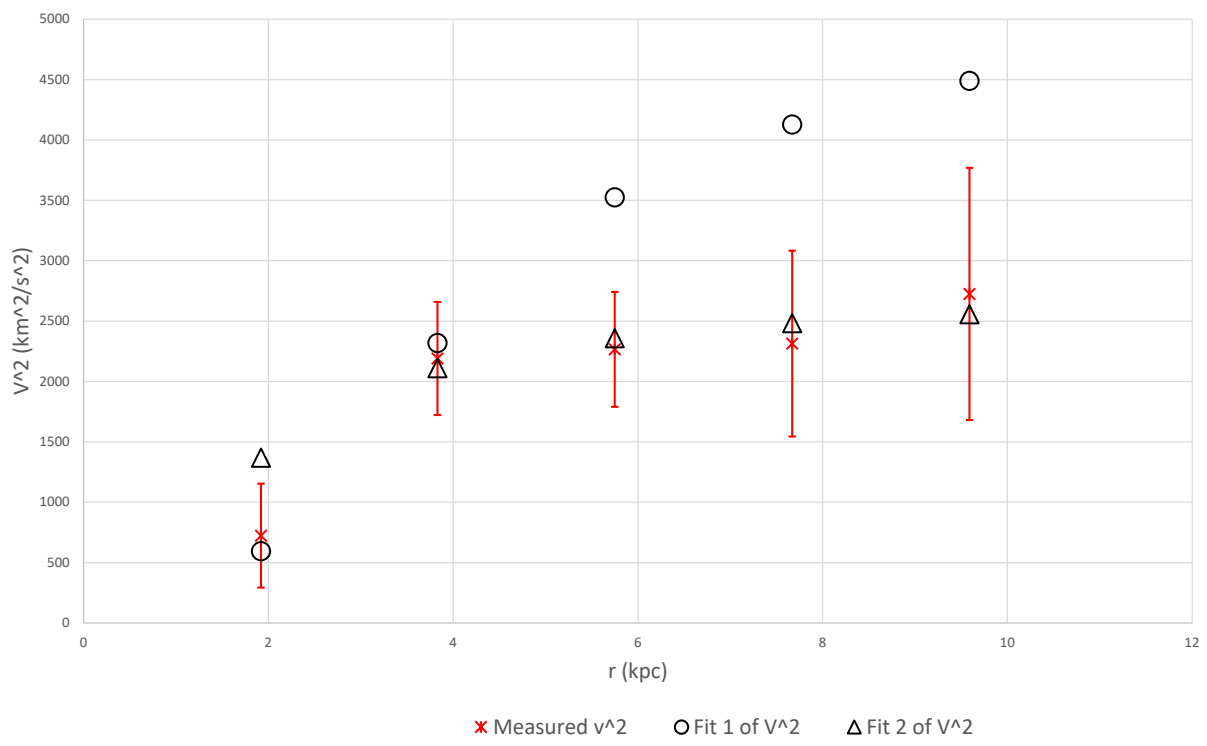


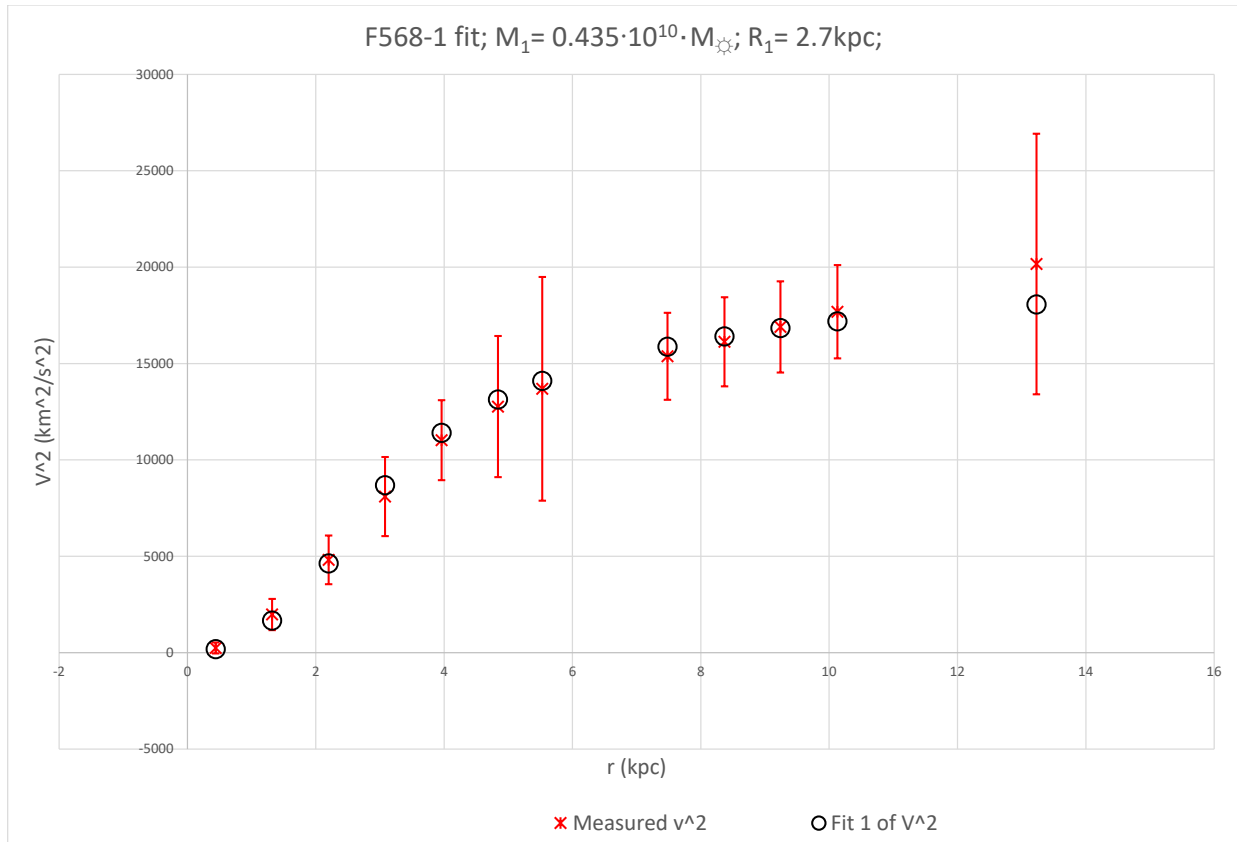
F563-V2 fit; $M_1 = 0.297 \cdot 10^{10} \cdot M_{\odot}$; $R_1 = 2 \text{ kpc}$;
 $M_2 = 0.078 \cdot 10^{10} \cdot M_{\odot}$; $R_2 = 0.7 \text{ kpc}$

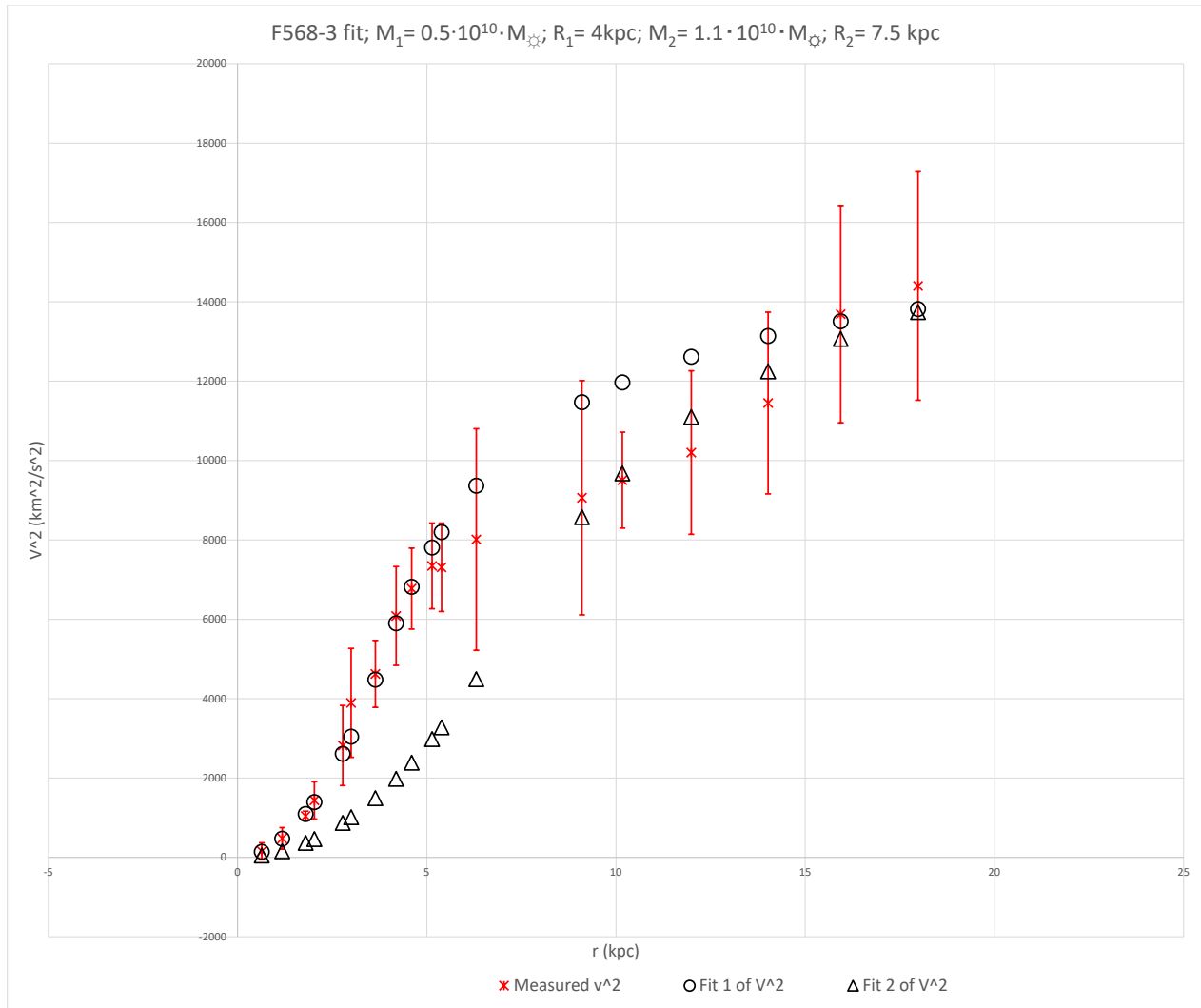




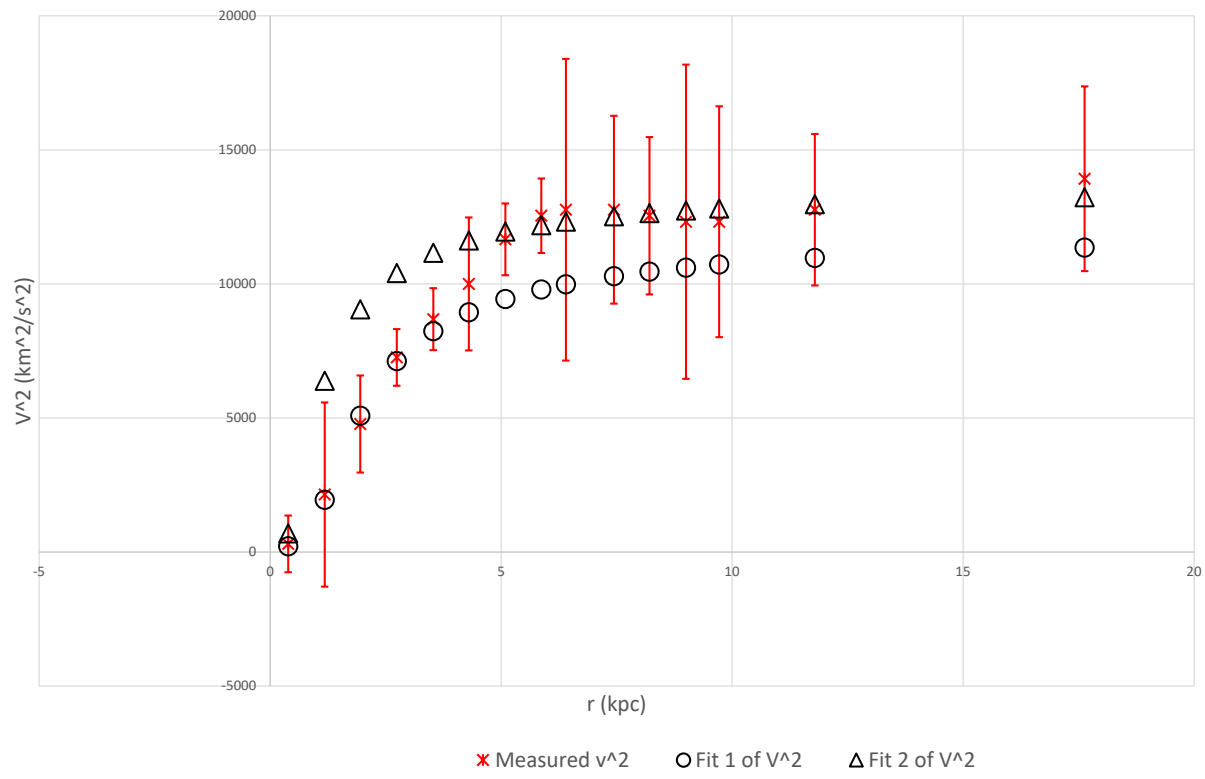
F567-2 fit; $M_1 = 1.6 \cdot 10^{10} \cdot M_{\odot}$; $R_1 = 3.5 \text{ kpc}$;
 $M_2 = 0.033 \cdot 10^{10} \cdot M_{\odot}$; $R_2 = 2.3 \text{ kpc}$



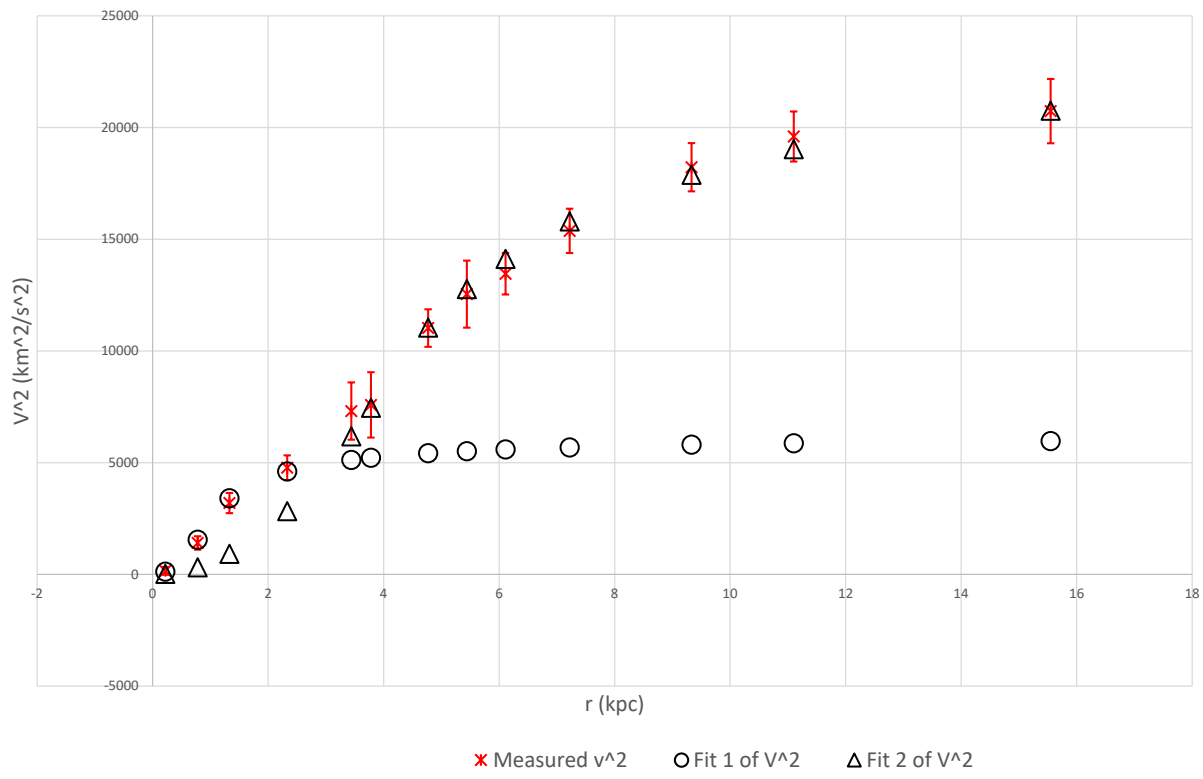


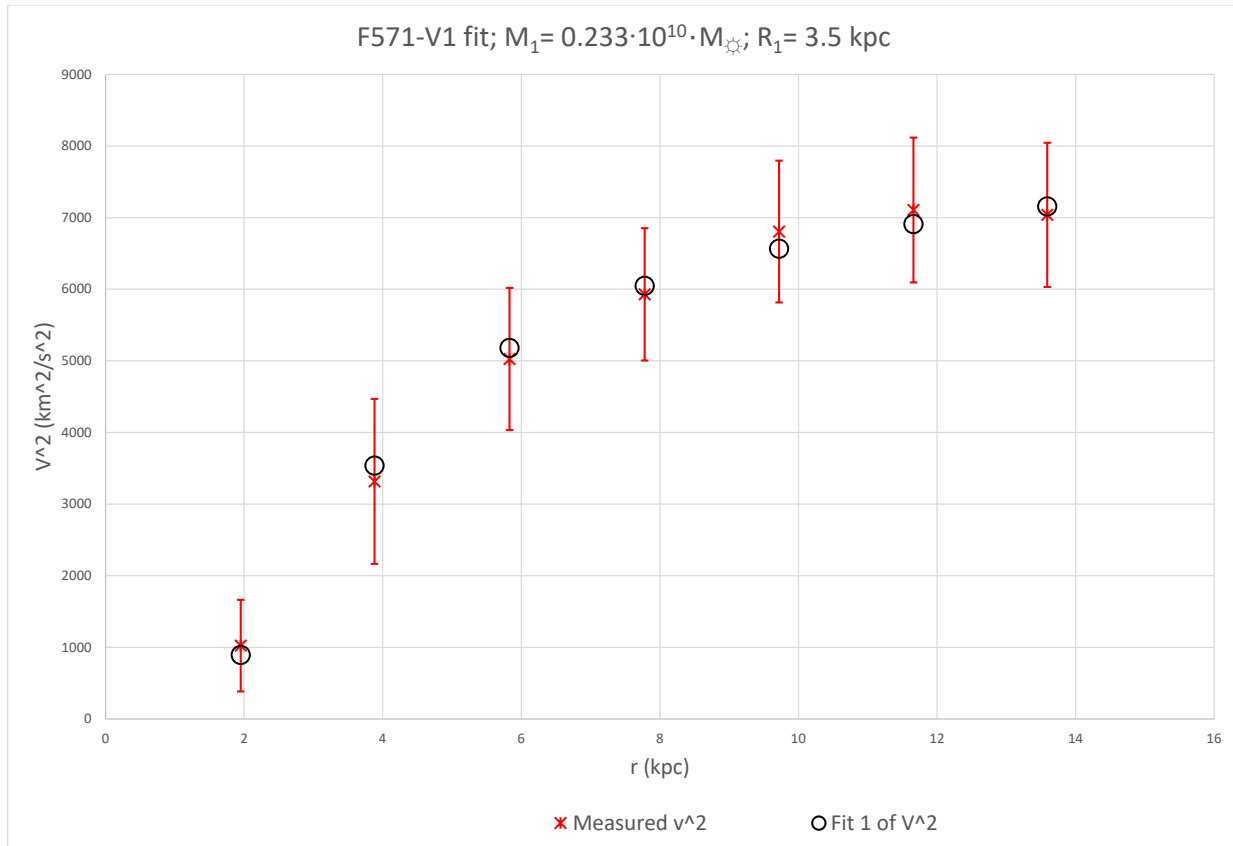


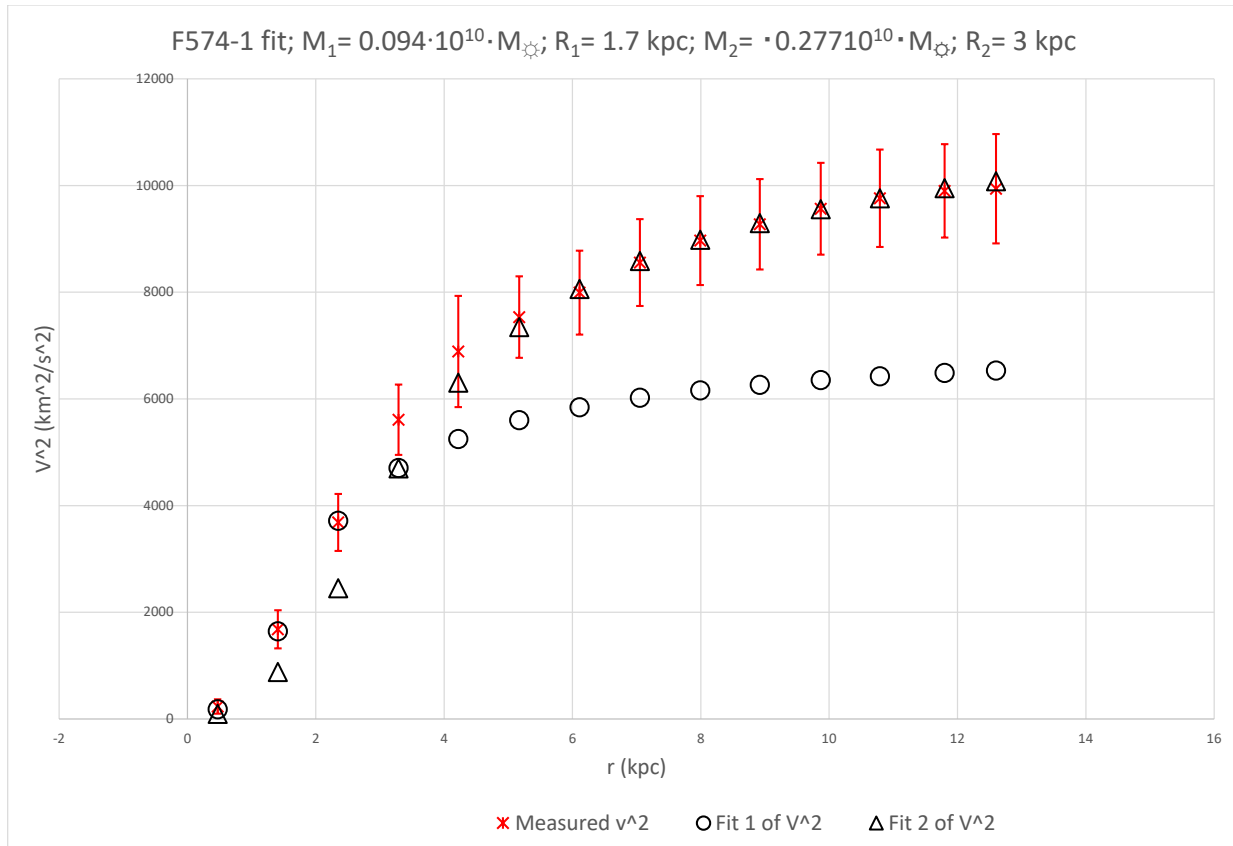
F568-V1 fit; $M_1 = 0.159 \cdot 10^{10} \cdot M_{\odot}$; $R_1 = 1.7 \text{ kpc}$; $M_2 = 0.106 \cdot 10^{10} \cdot M_{\odot}$; $R_2 = 1 \text{ kpc}$

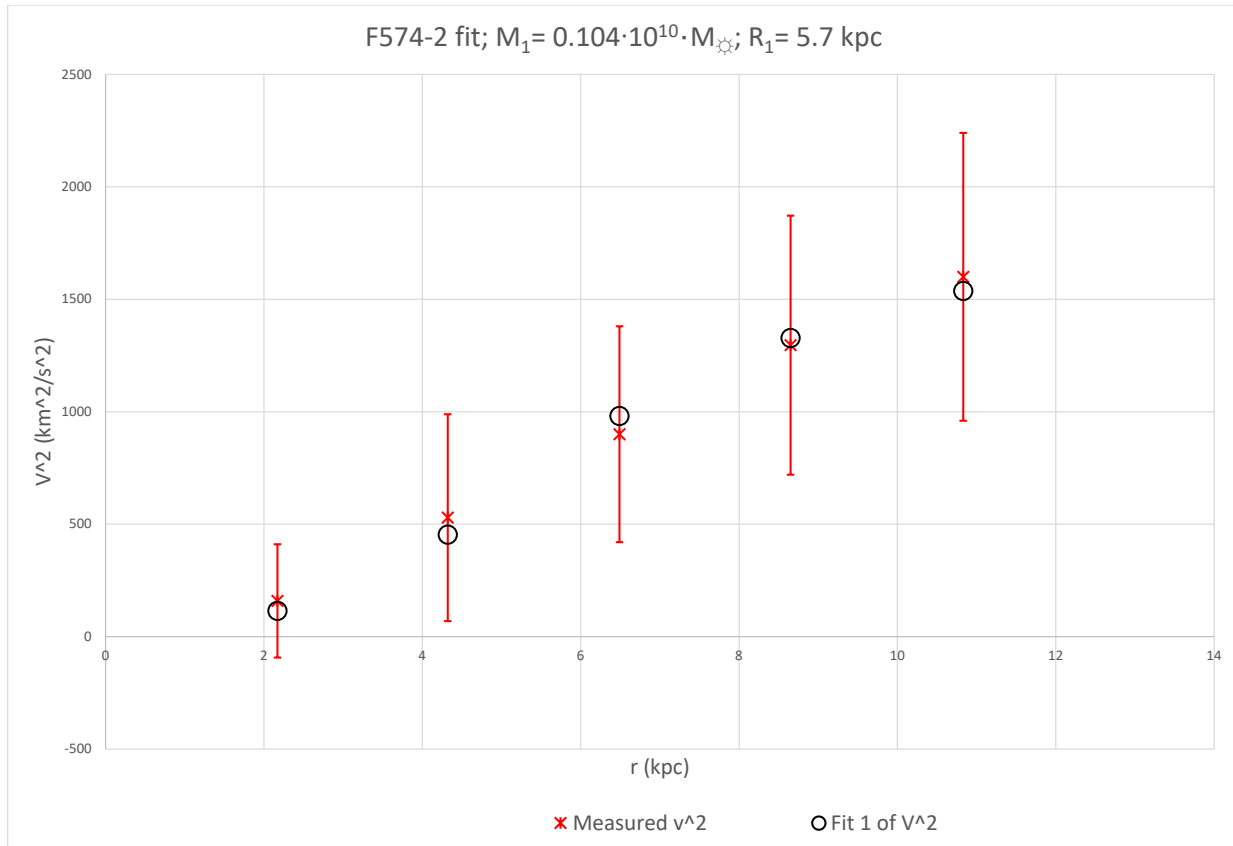


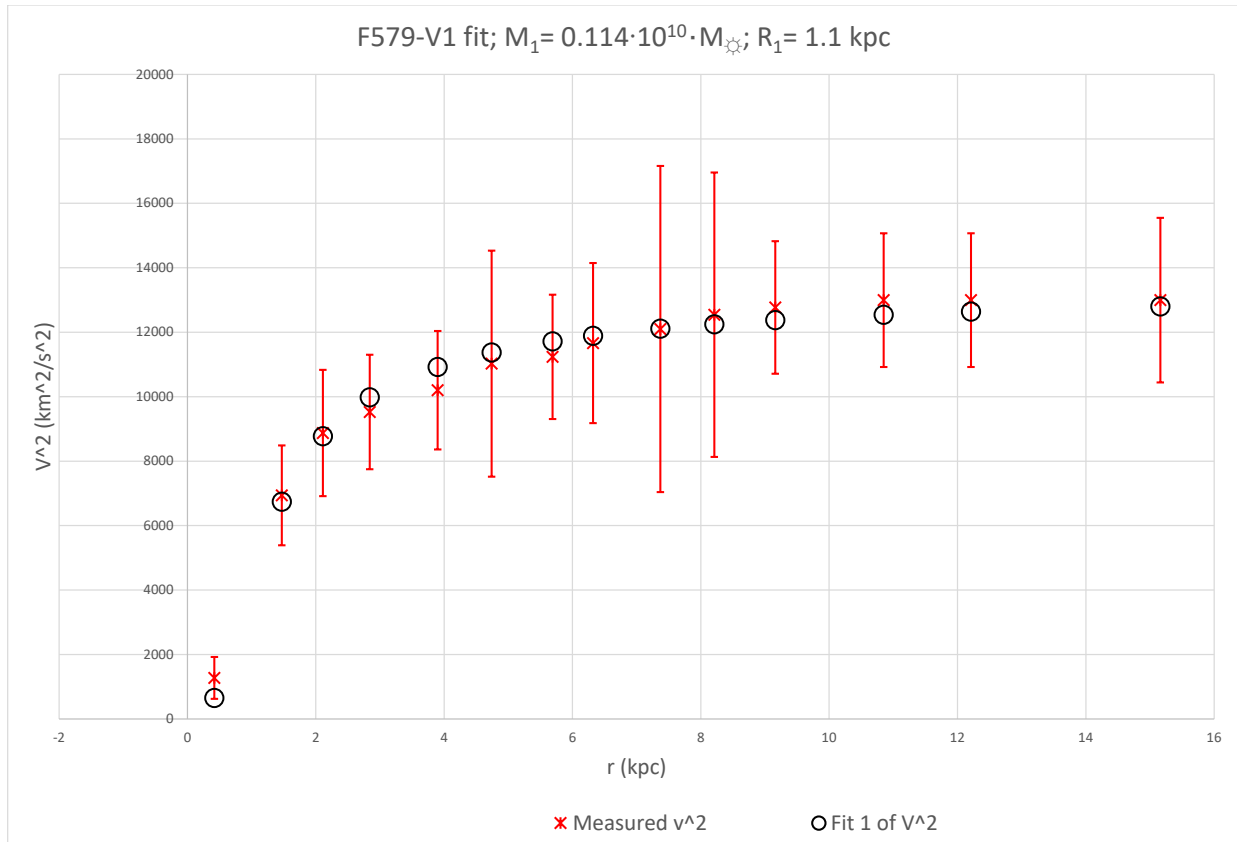
F571-8 fit; $M_1 = 0.043 \cdot 10^{10} \cdot M_{\odot}$; $R_1 = 0.9$ kpc; $M_2 = 0.772 \cdot 10^{10} \cdot M_{\odot}$; $R_2 = 4$ kpc

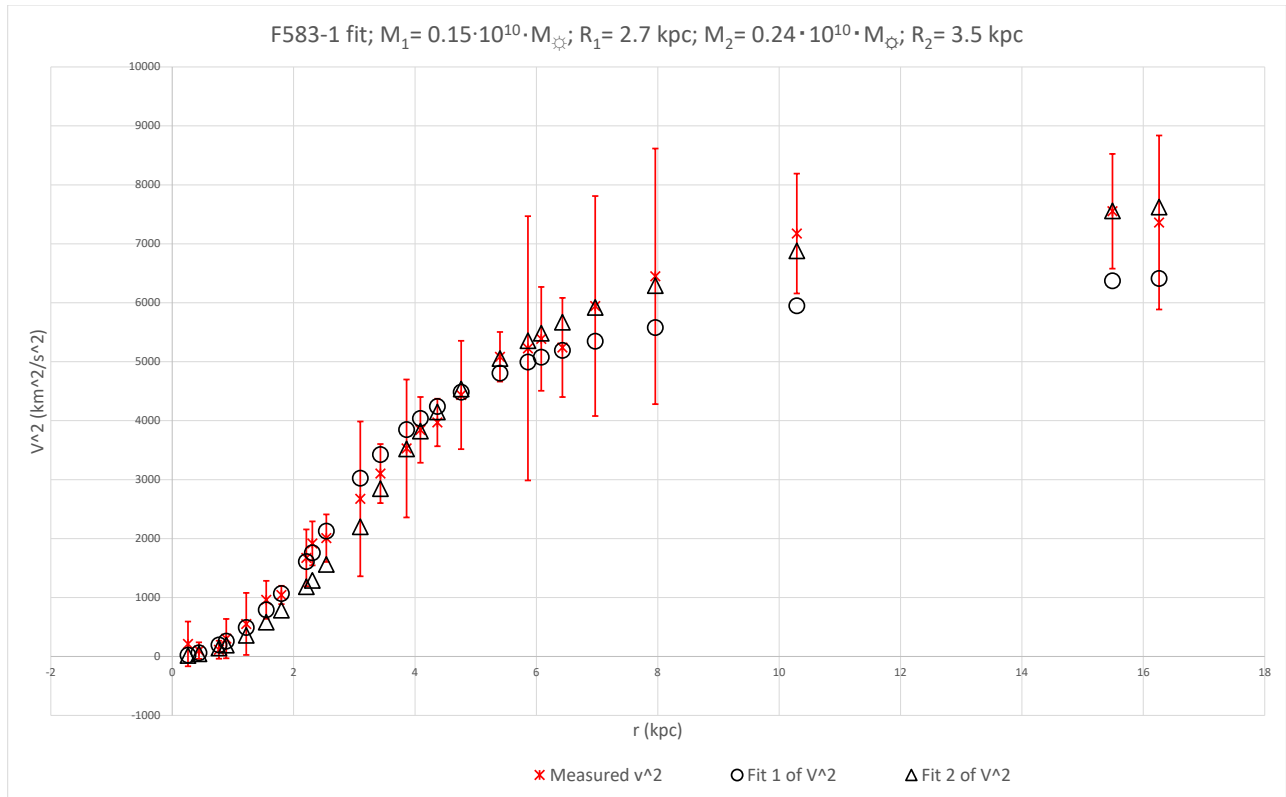




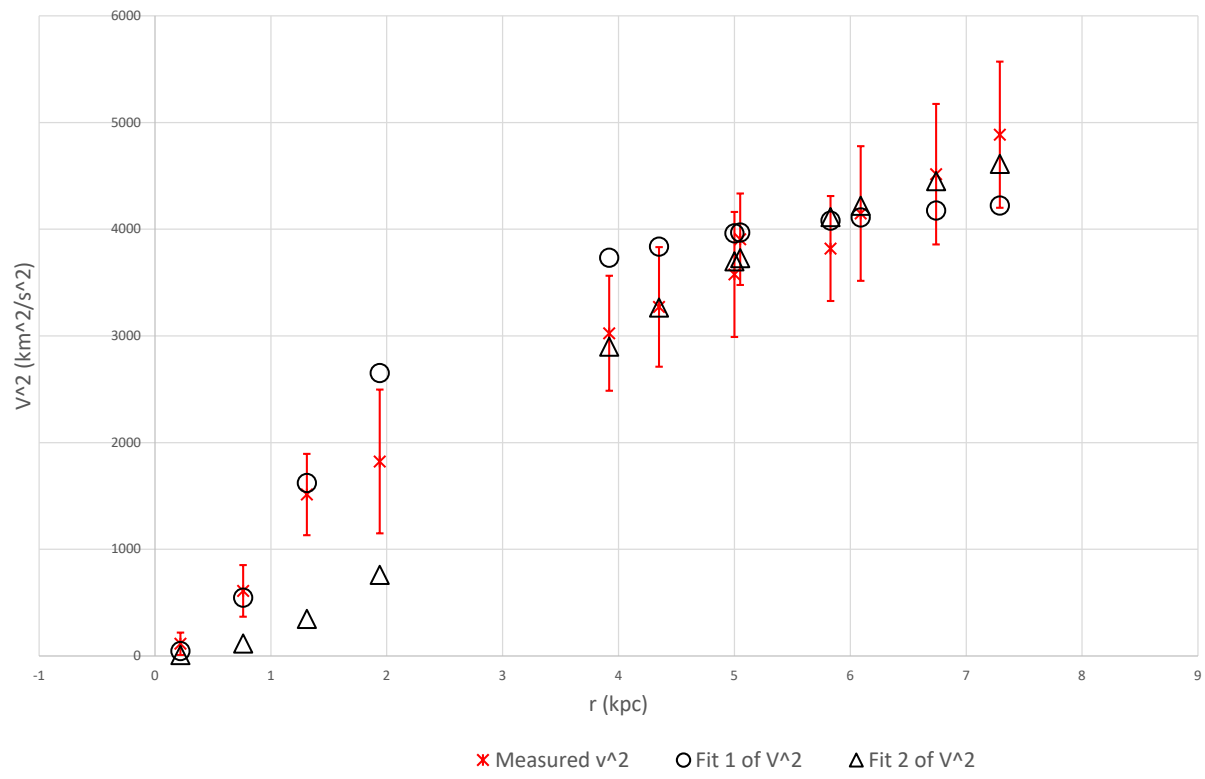




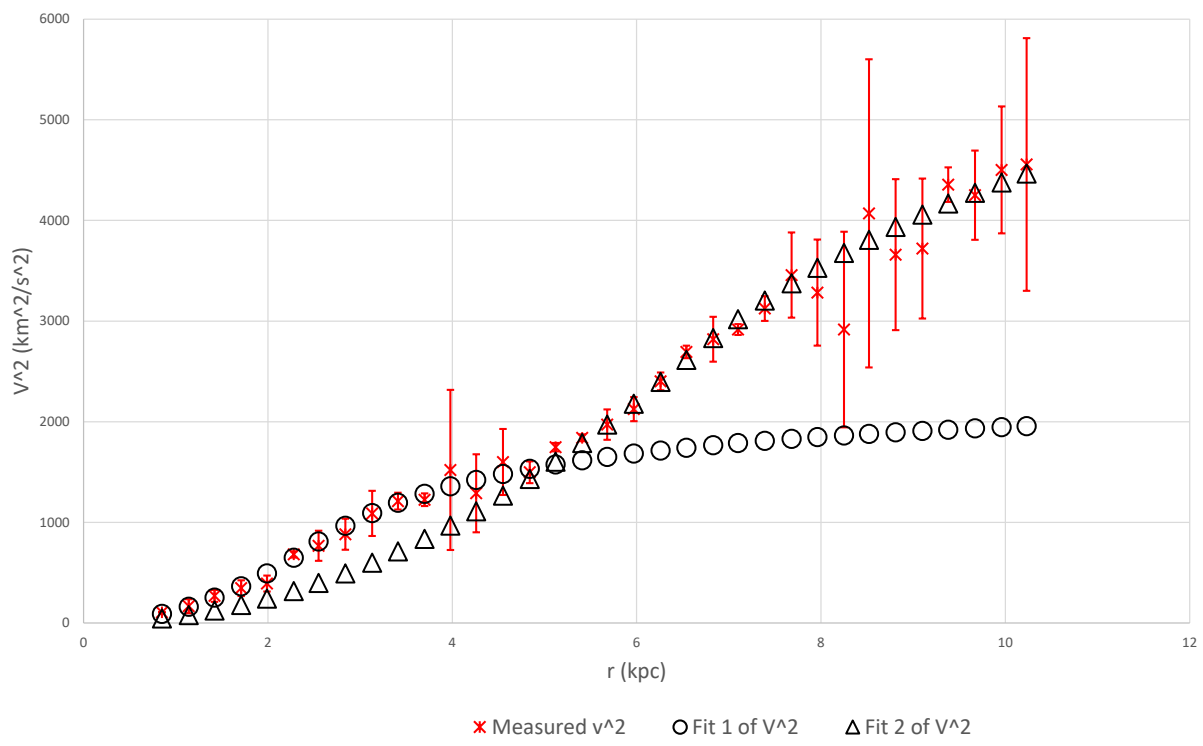


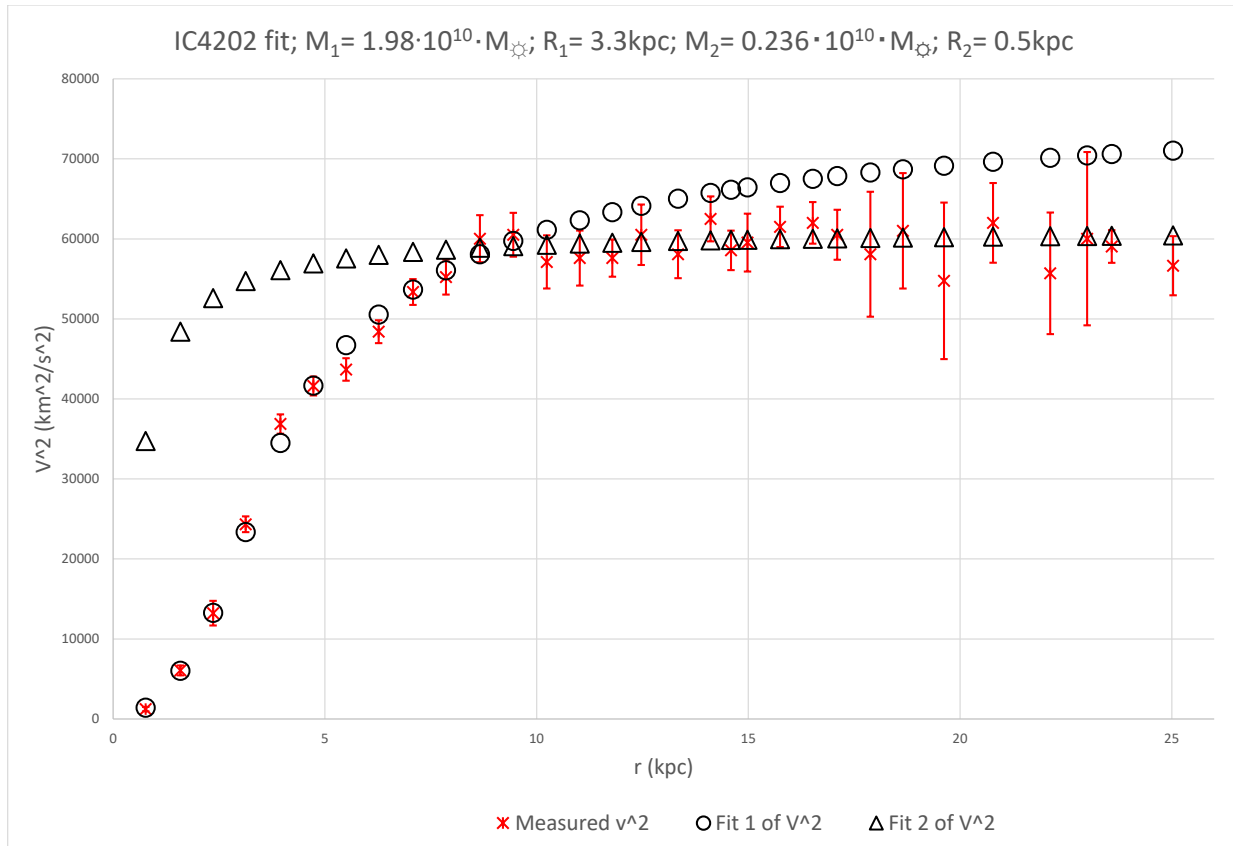


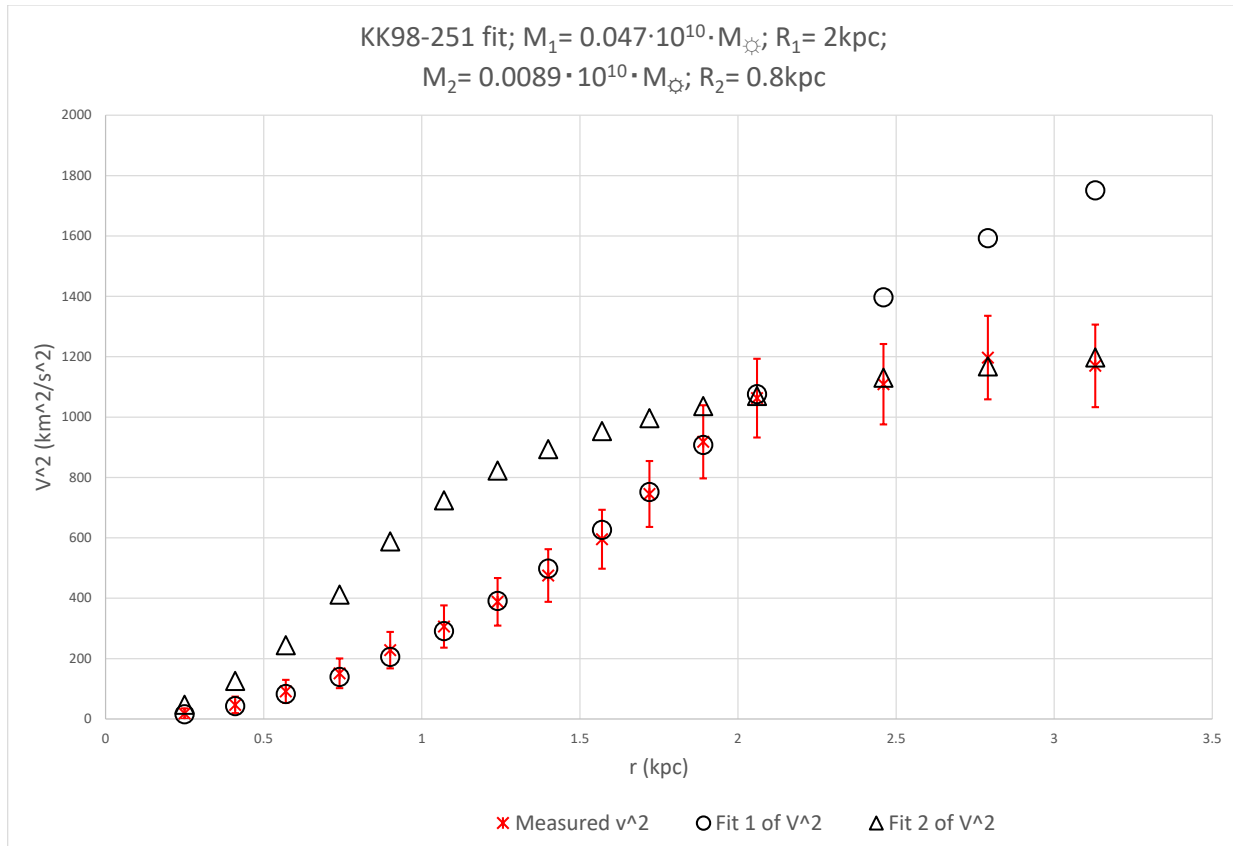
F583-4 fit; $M_1 = 0.048 \cdot 10^{10} \cdot M_{\odot}$; $R_1 = 1.3$ kpc; $M_2 = 0.168 \cdot 10^{10} \cdot M_{\odot}$; $R_2 = 3.3$ kpc

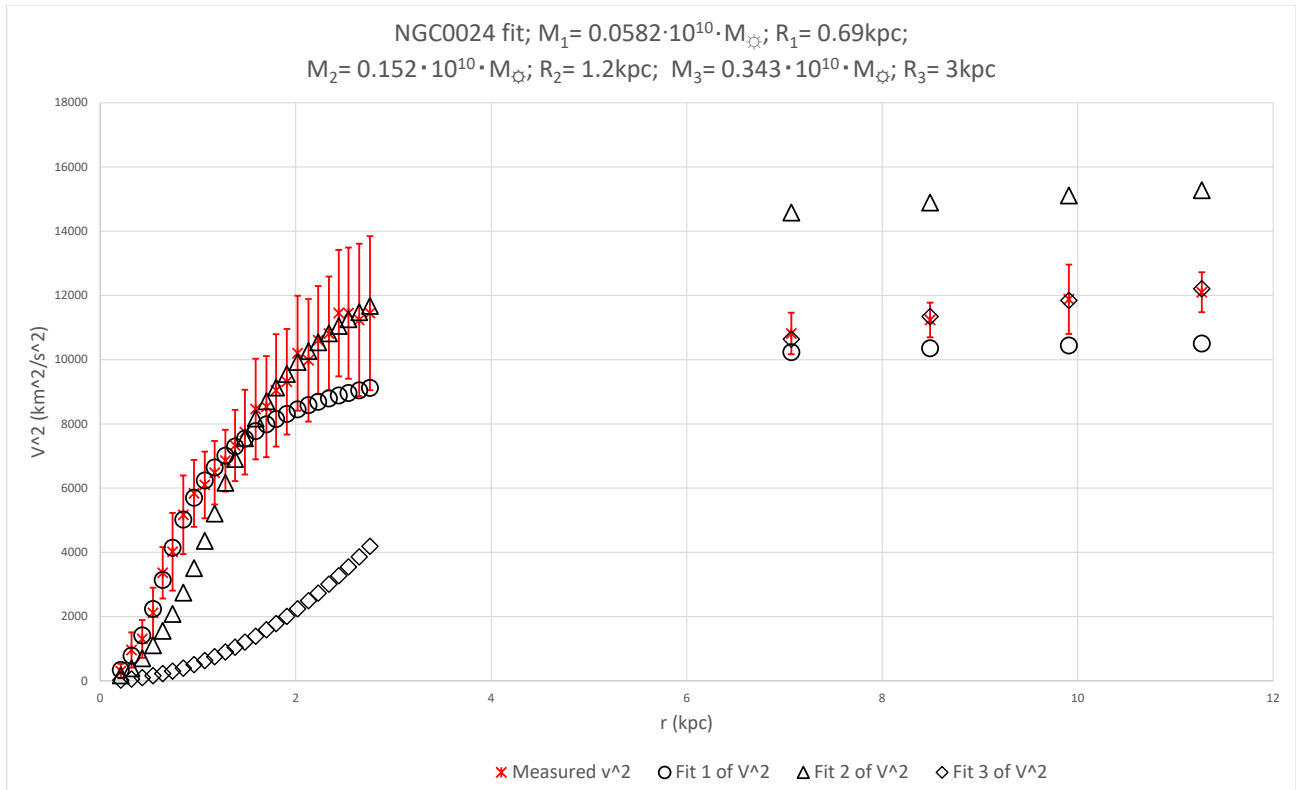


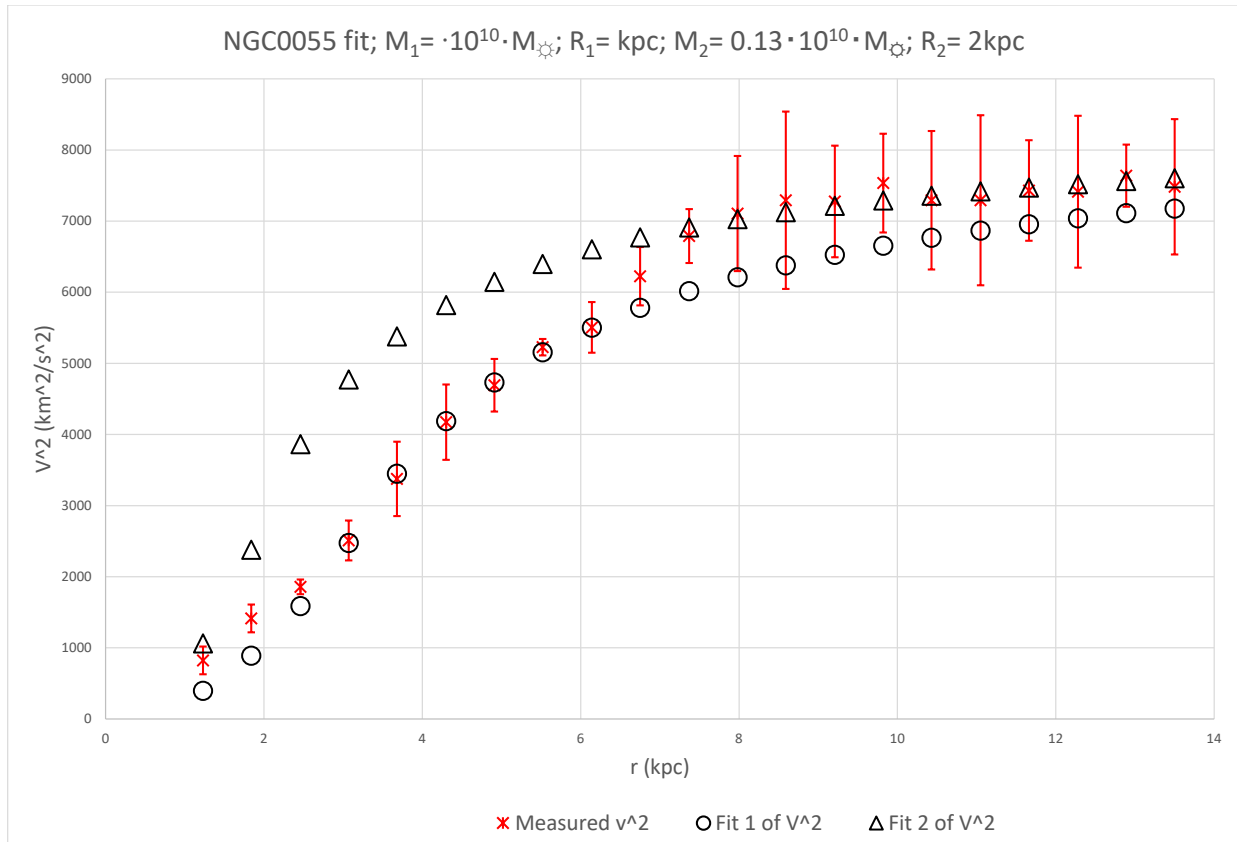
IC2574 fit; $M_1 = 0.045 \cdot 10^{10} \cdot M_{\odot}$; $R_1 = 2.5 \text{ kpc}$;
 $M_2 = 0.388 \cdot 10^{10} \cdot M_{\odot}$; $R_2 = 6.5 \text{ kpc}$

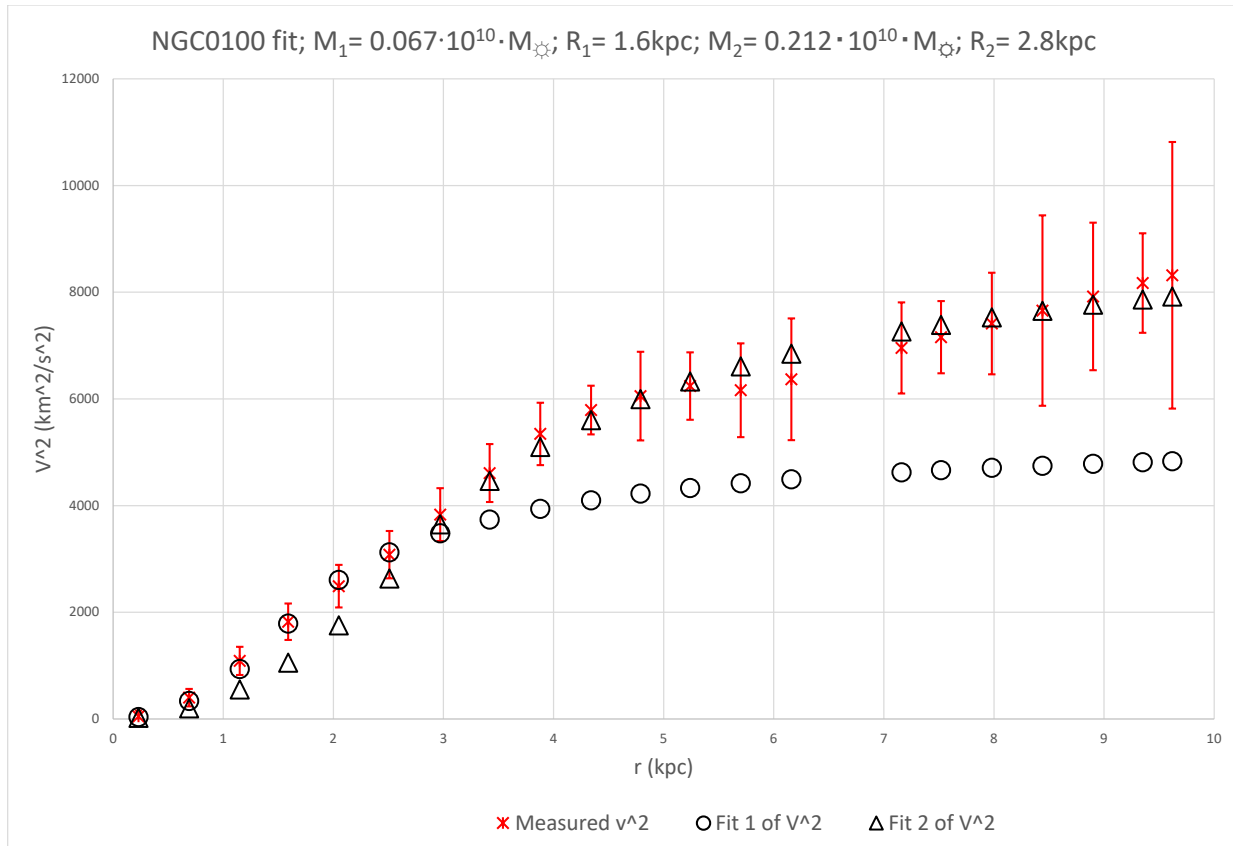


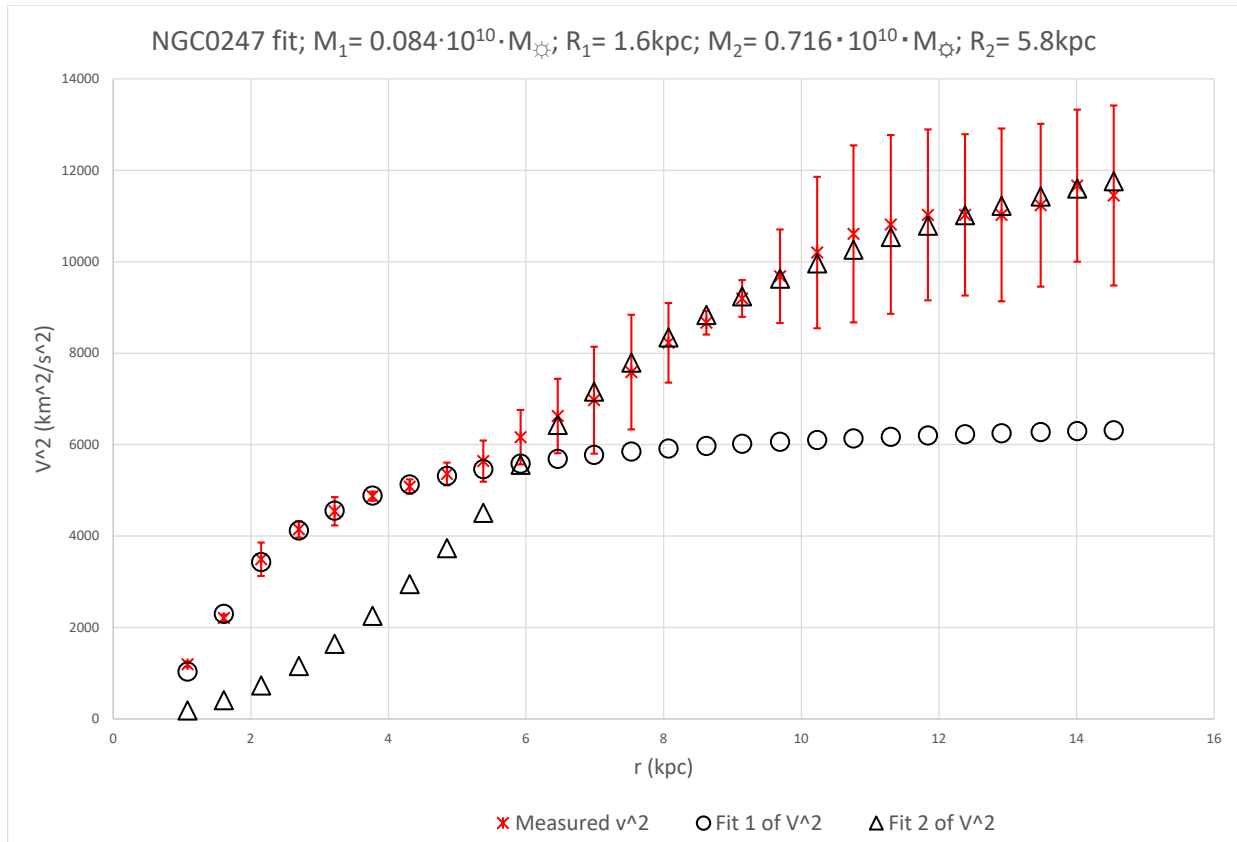




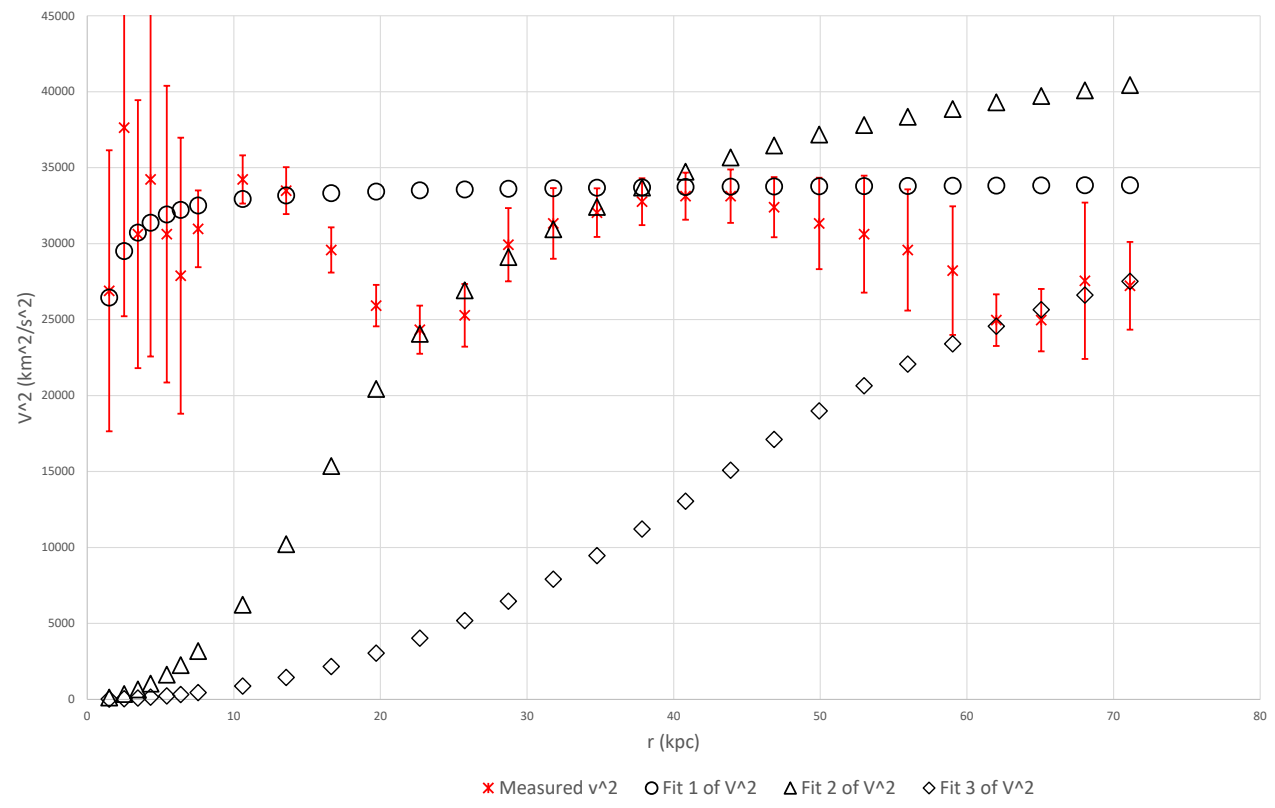


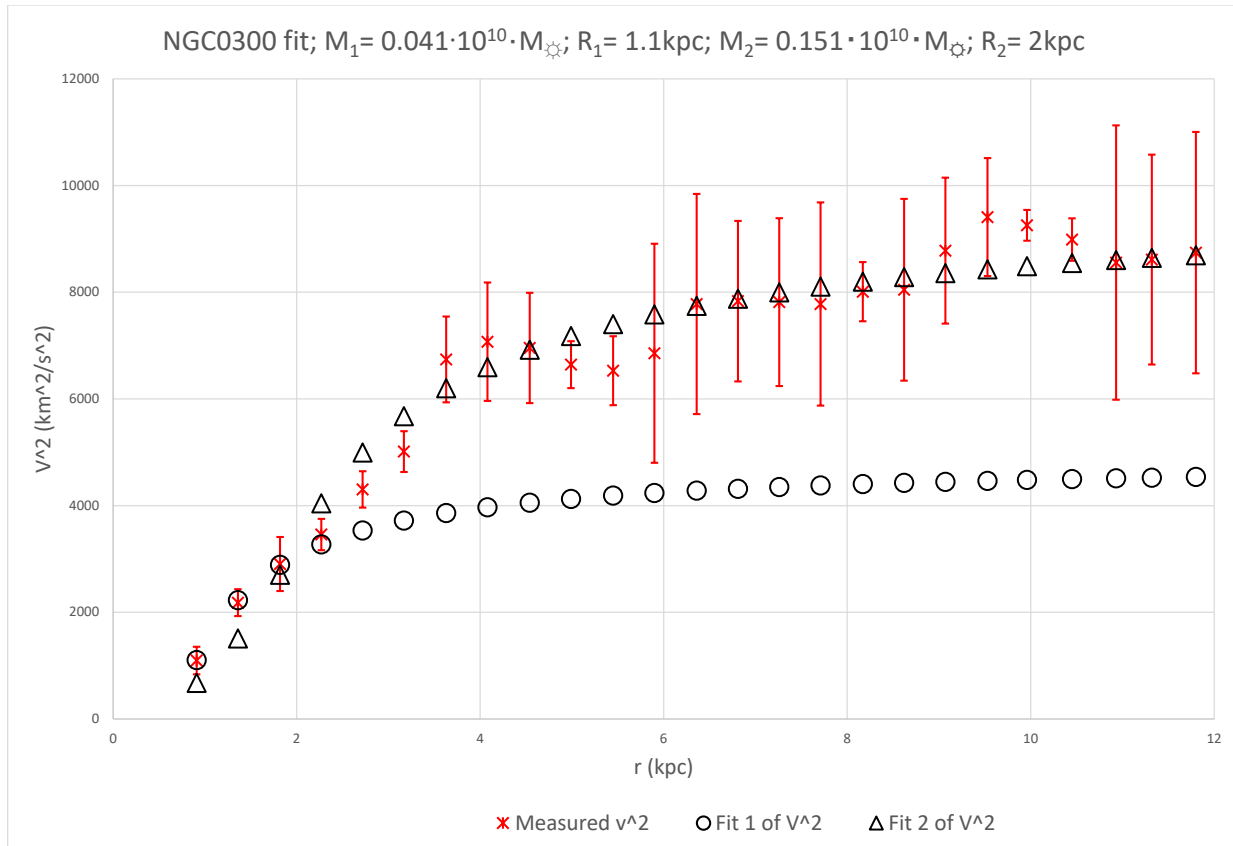


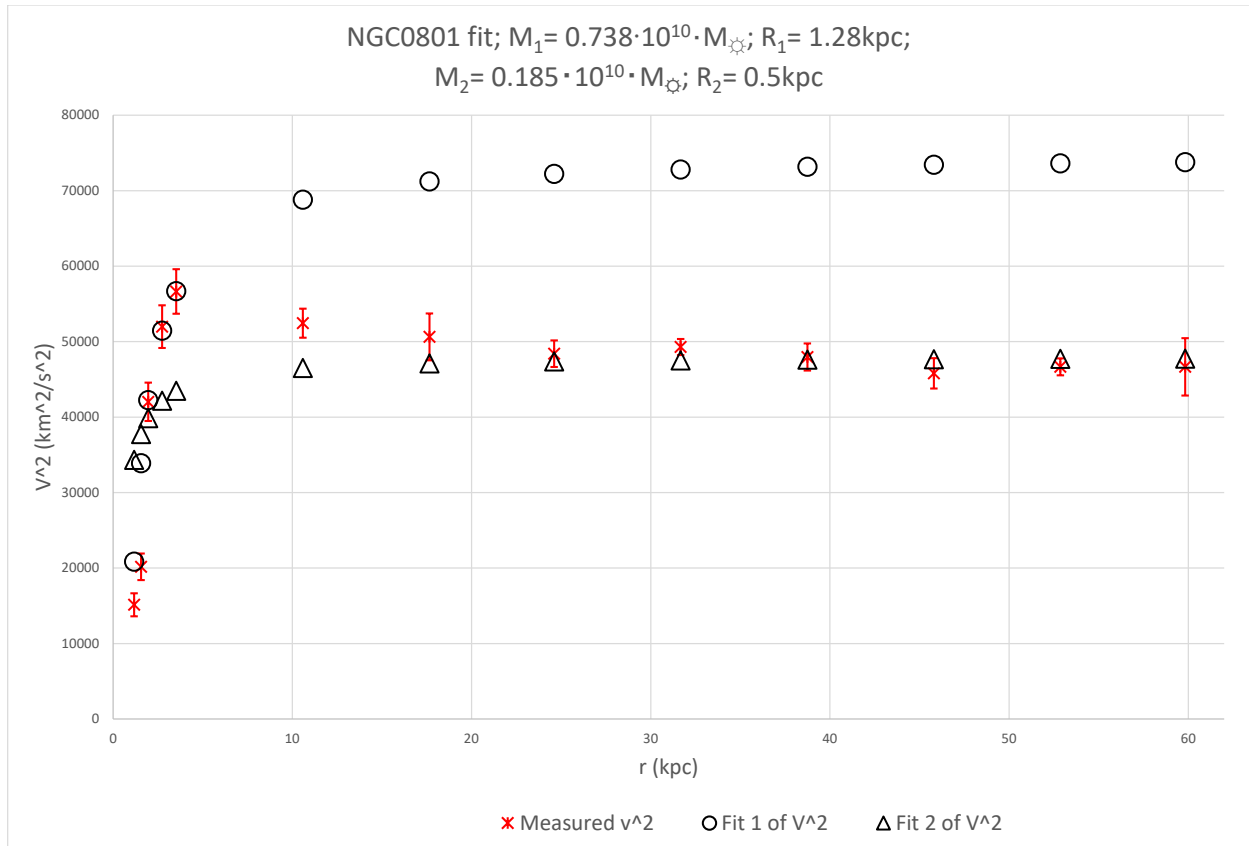


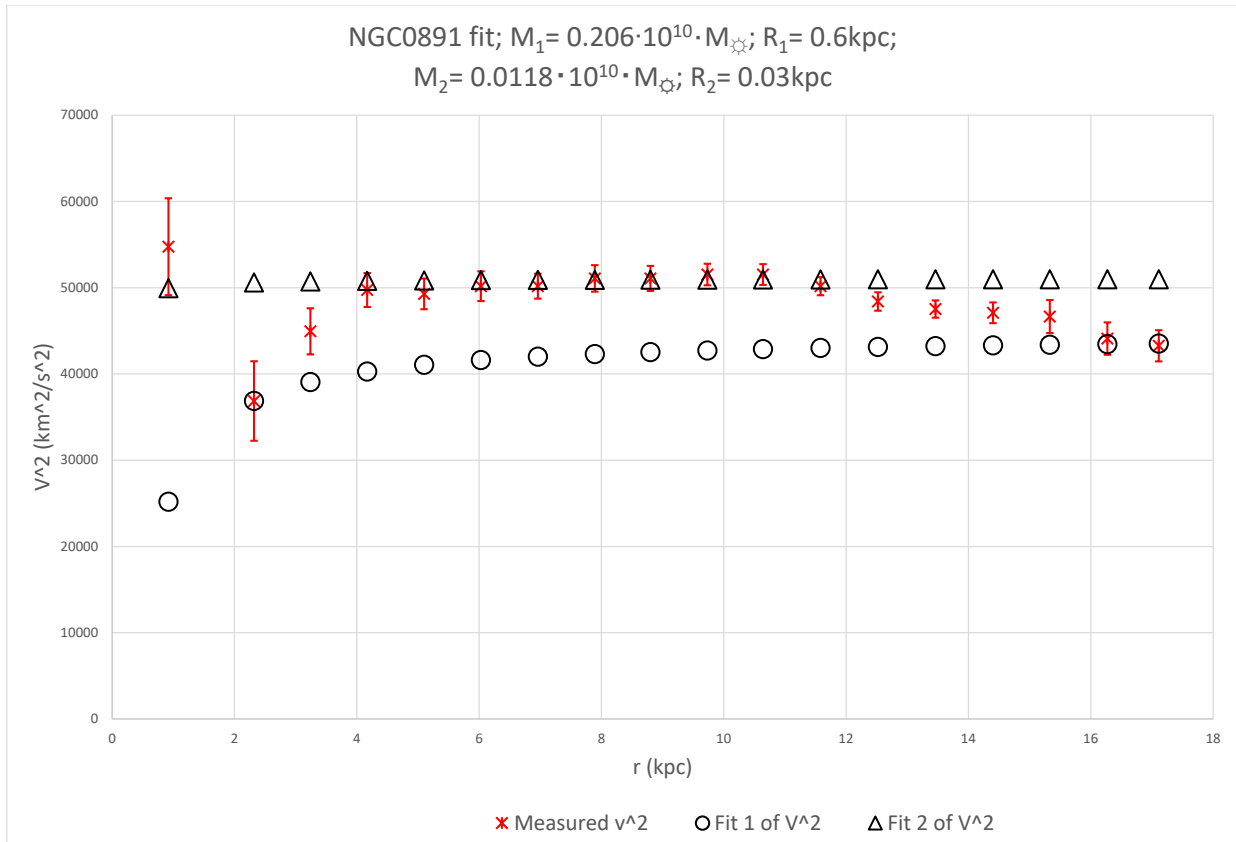


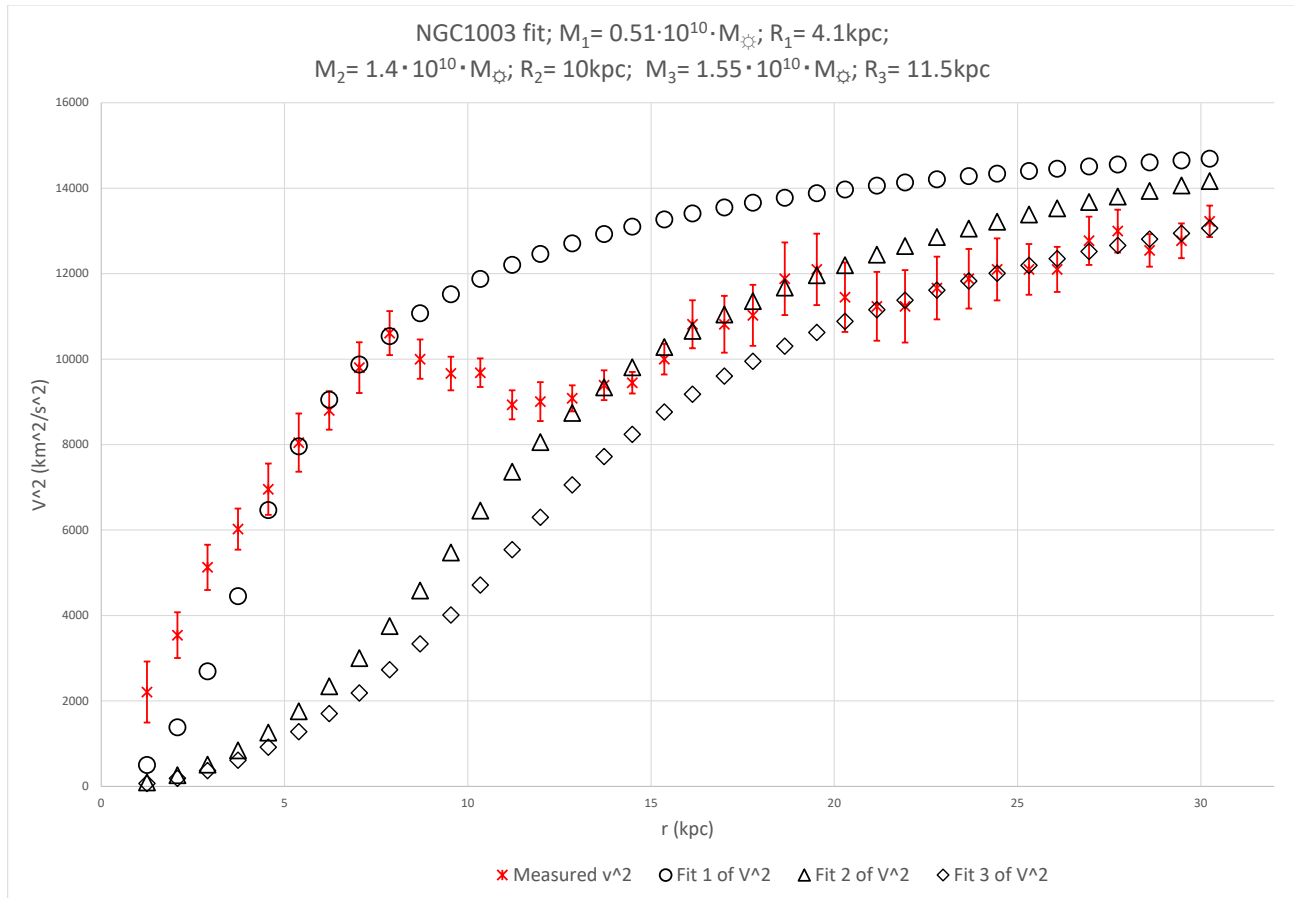
NGC0289 fit; $M_1 = 0.131 \cdot 10^{10} \cdot M_{\odot}$; $R_1 = 0.5 \text{ kpc}$;
 $M_2 = 6.3 \cdot 10^{10} \cdot M_{\odot}$; $R_2 = 17 \text{ kpc}$; $M_3 = 16.5 \cdot 10^{10} \cdot M_{\odot}$; $R_3 = 45 \text{ kpc}$



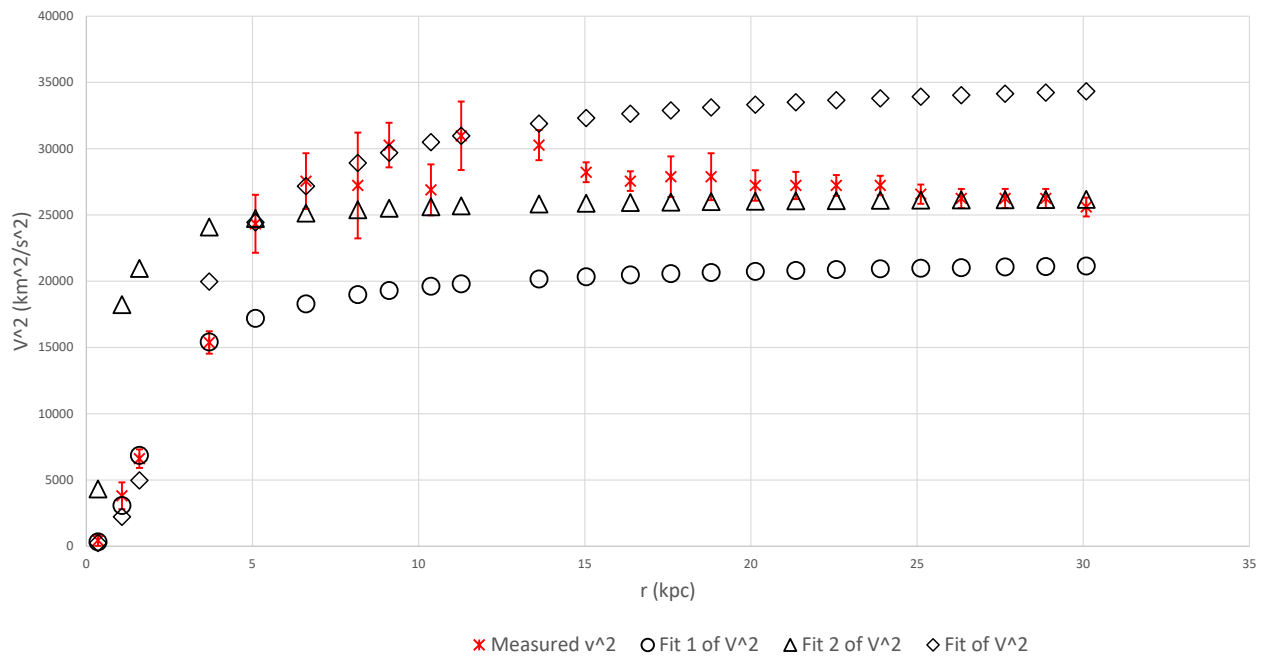




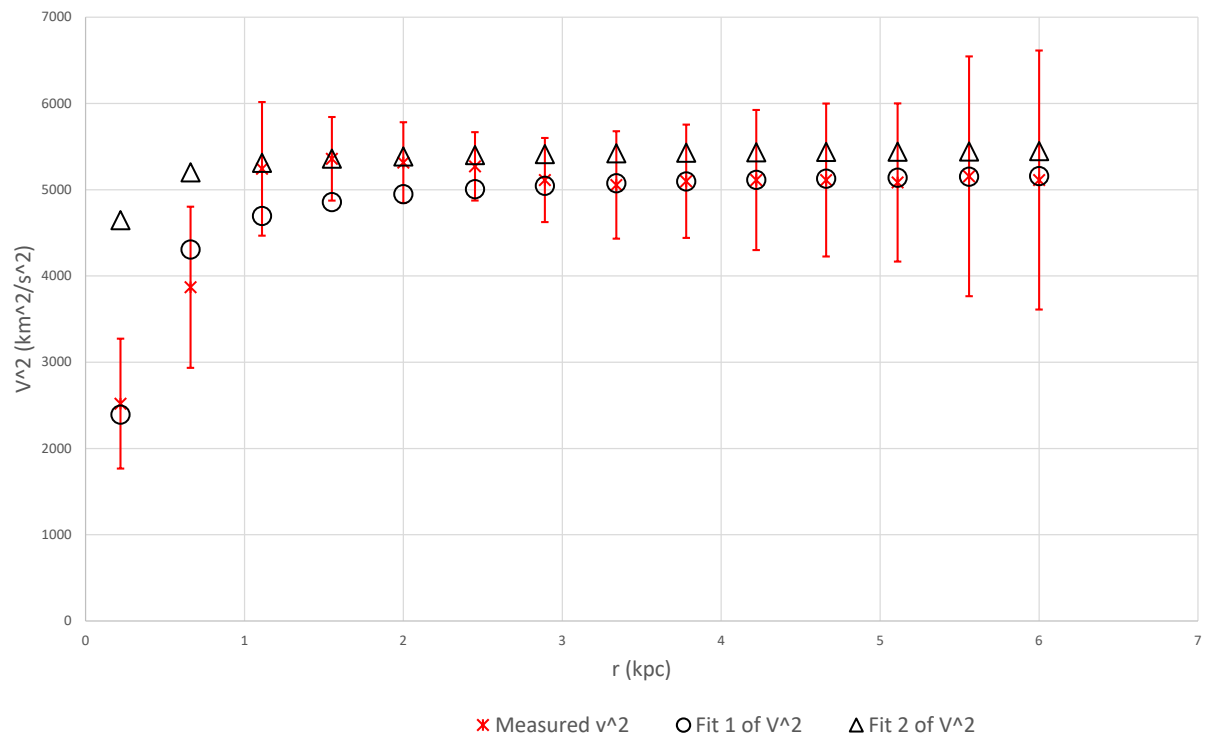




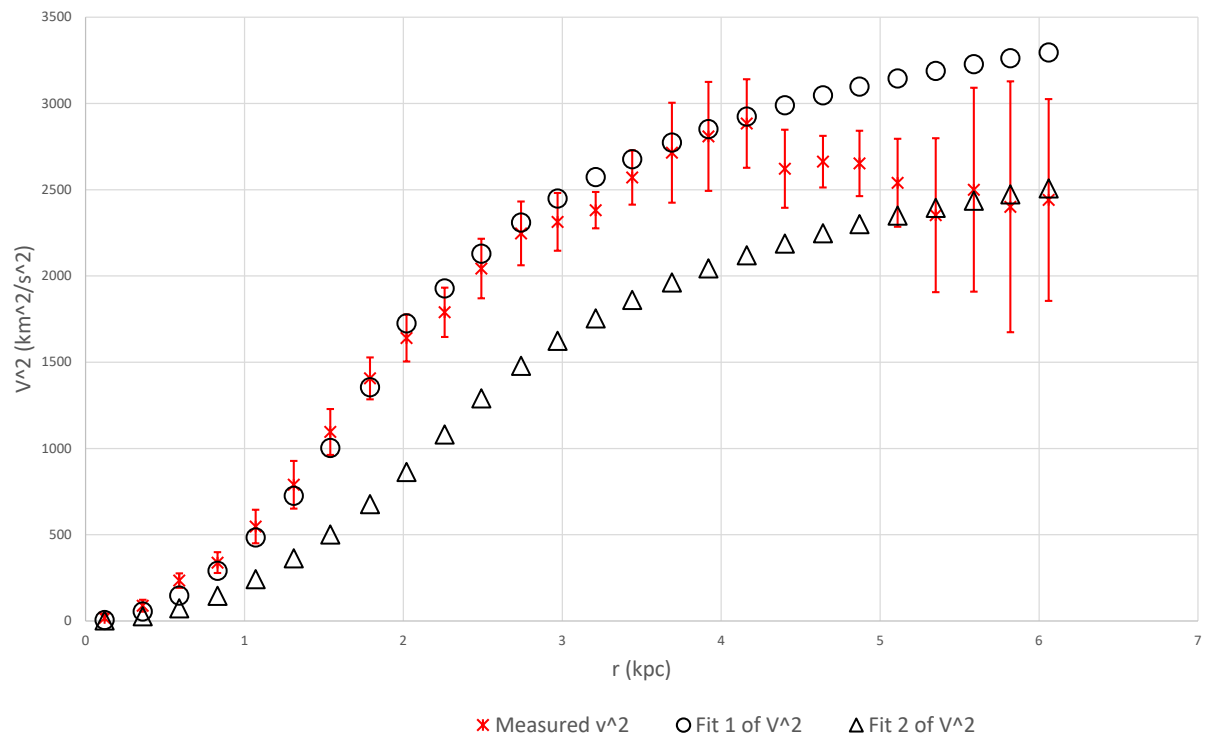
NGC1090 fit; $M_1 = \cdot 10^{10} \cdot M_{\odot}$; $R_1 = \text{kpc}$; $M_2 = 0.233 \cdot 10^{10} \cdot M_{\odot}$; $R_2 = 1.6 \text{kpc}$; $M_3 = 0.233 \cdot 10^{10} \cdot M_{\odot}$; $R_3 = 1.6 \text{kpc}$; $M_3 = 0.7 \cdot 10^{10} \cdot M_{\odot}$; $R_3 = 2.5 \text{kpc}$

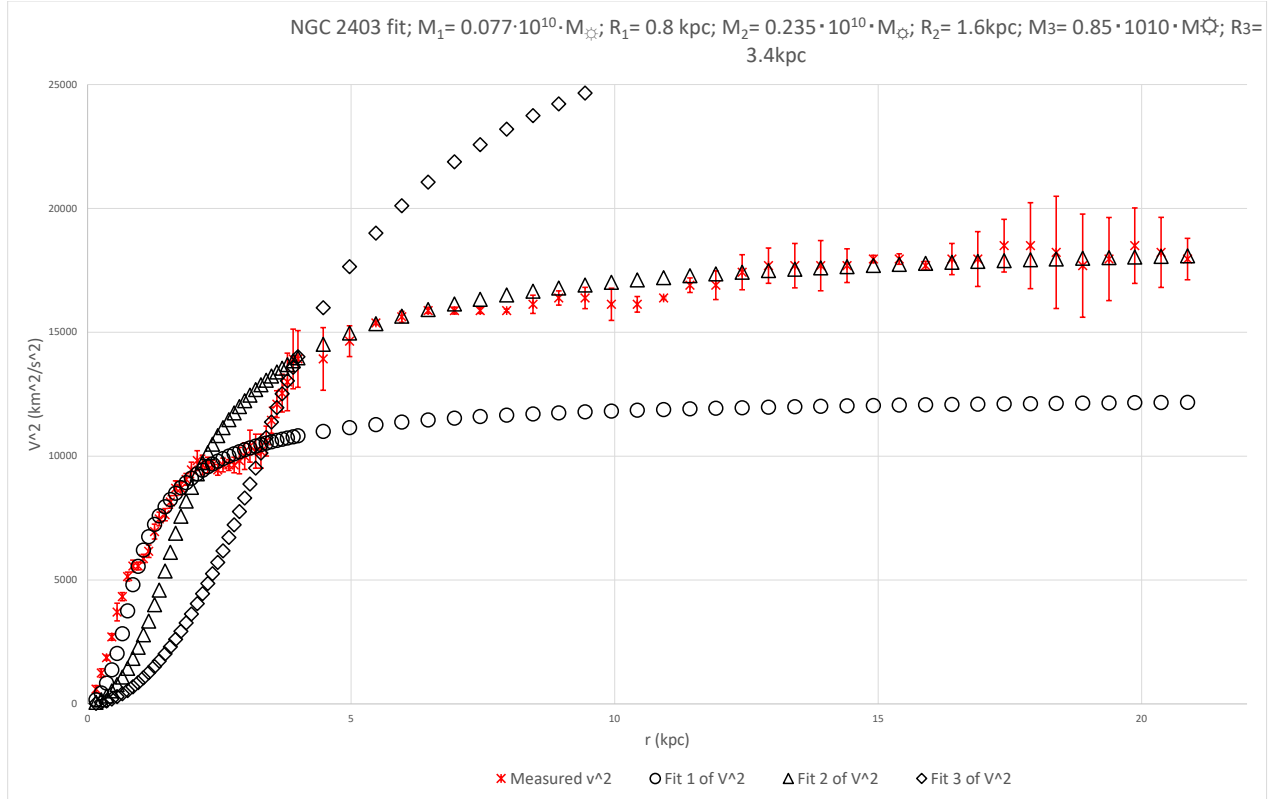


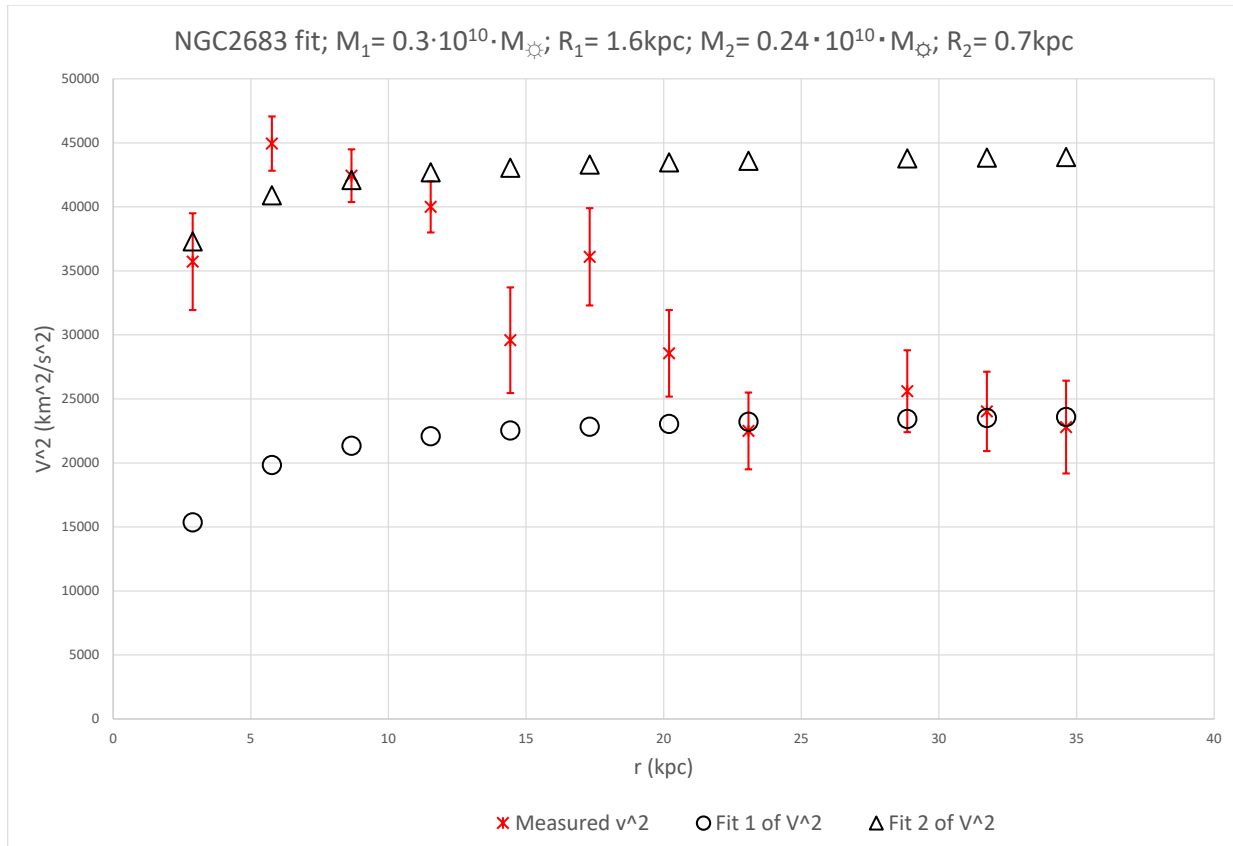
NGC1705 fit; $M_1 = 0.0073 \cdot 10^{10} \cdot M_{\odot}$; $R_1 = 0.18 \text{ kpc}$;
 $M_2 = 0.00211 \cdot 10^{10} \cdot M_{\odot}$; $R_2 = 0.05 \text{ kpc}$

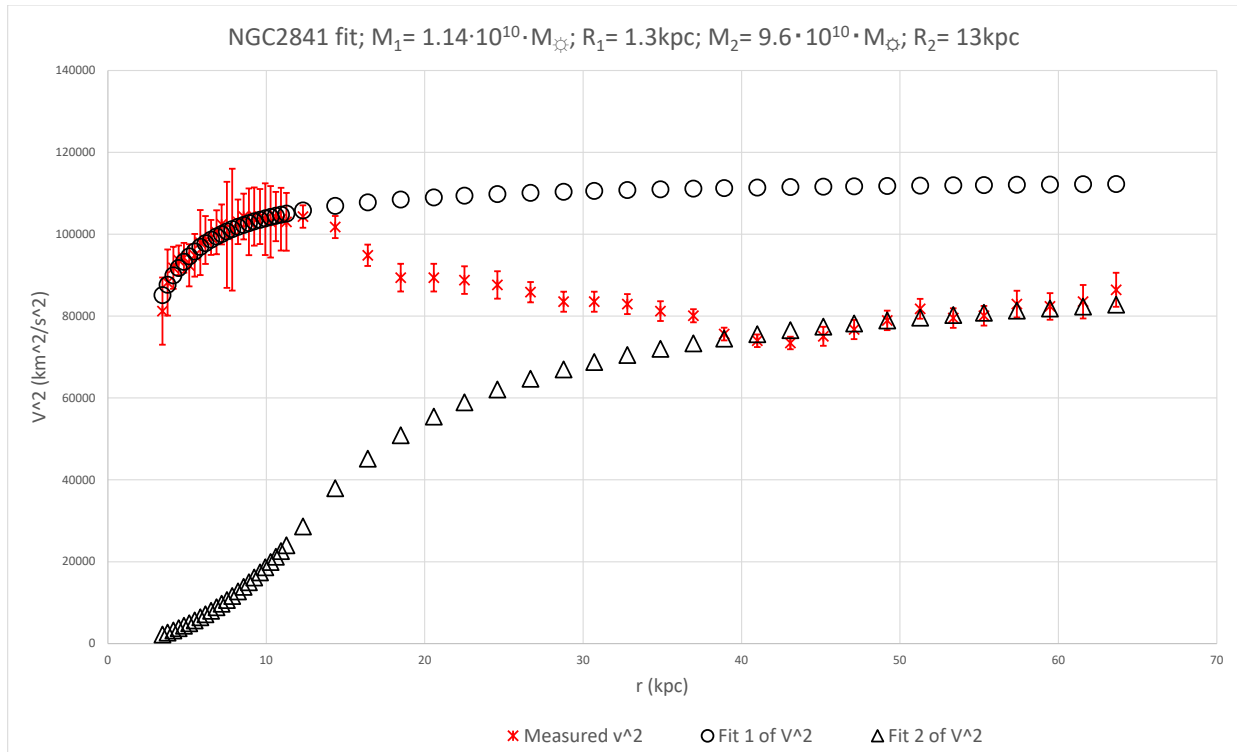


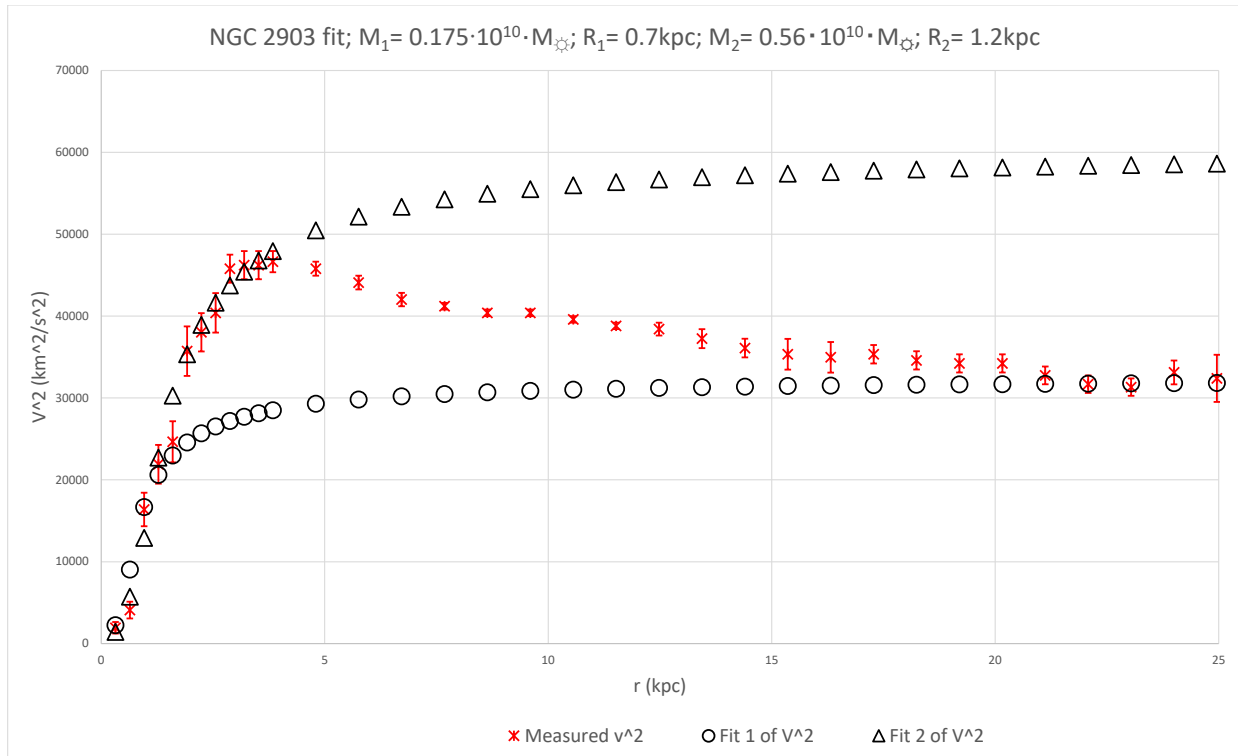
NGC 2366 fit; $M_1 = 0.057 \cdot 10^{10} \cdot M_\odot$; $R_1 = 1.8 \text{ kpc}$;
 $M_2 = 0.0595 \cdot 10^{10} \cdot M_\odot$; $R_2 = 2.3 \text{ kpc}$

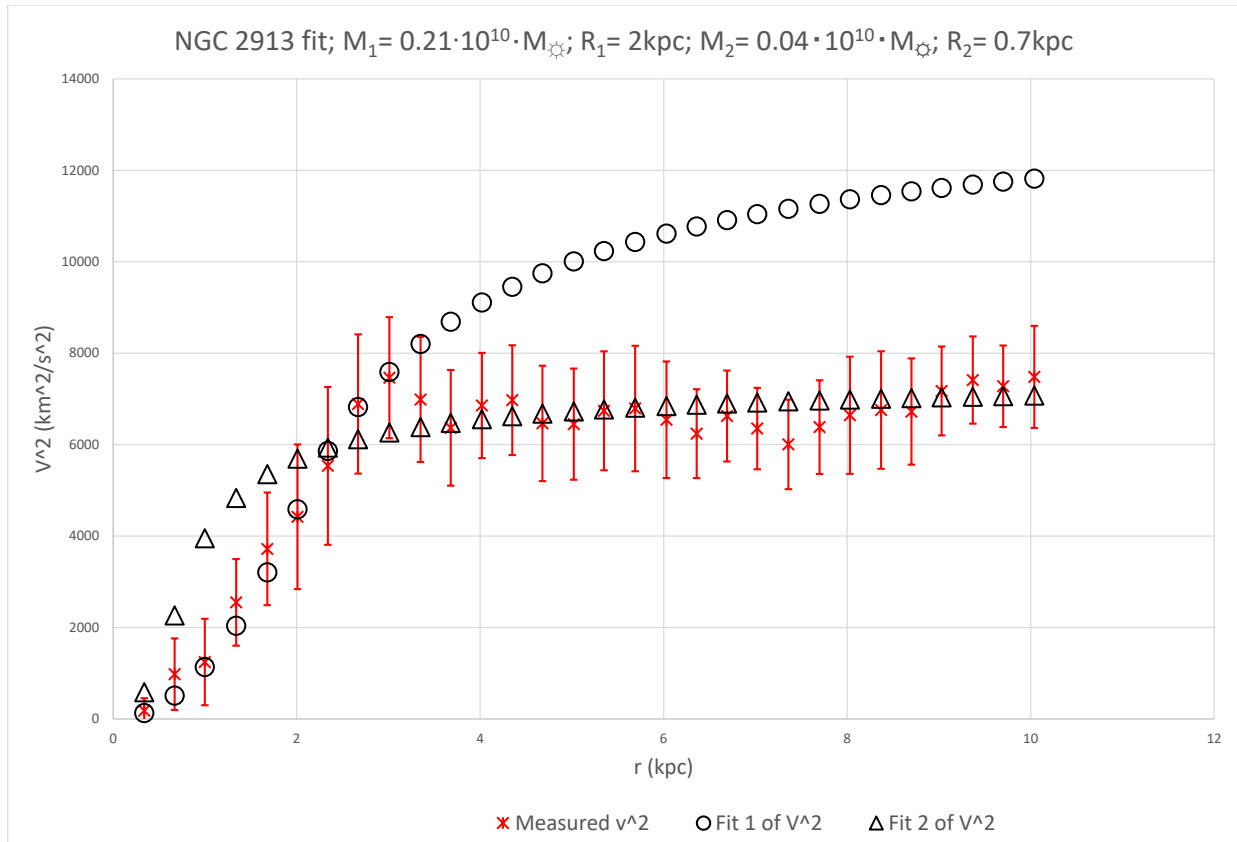


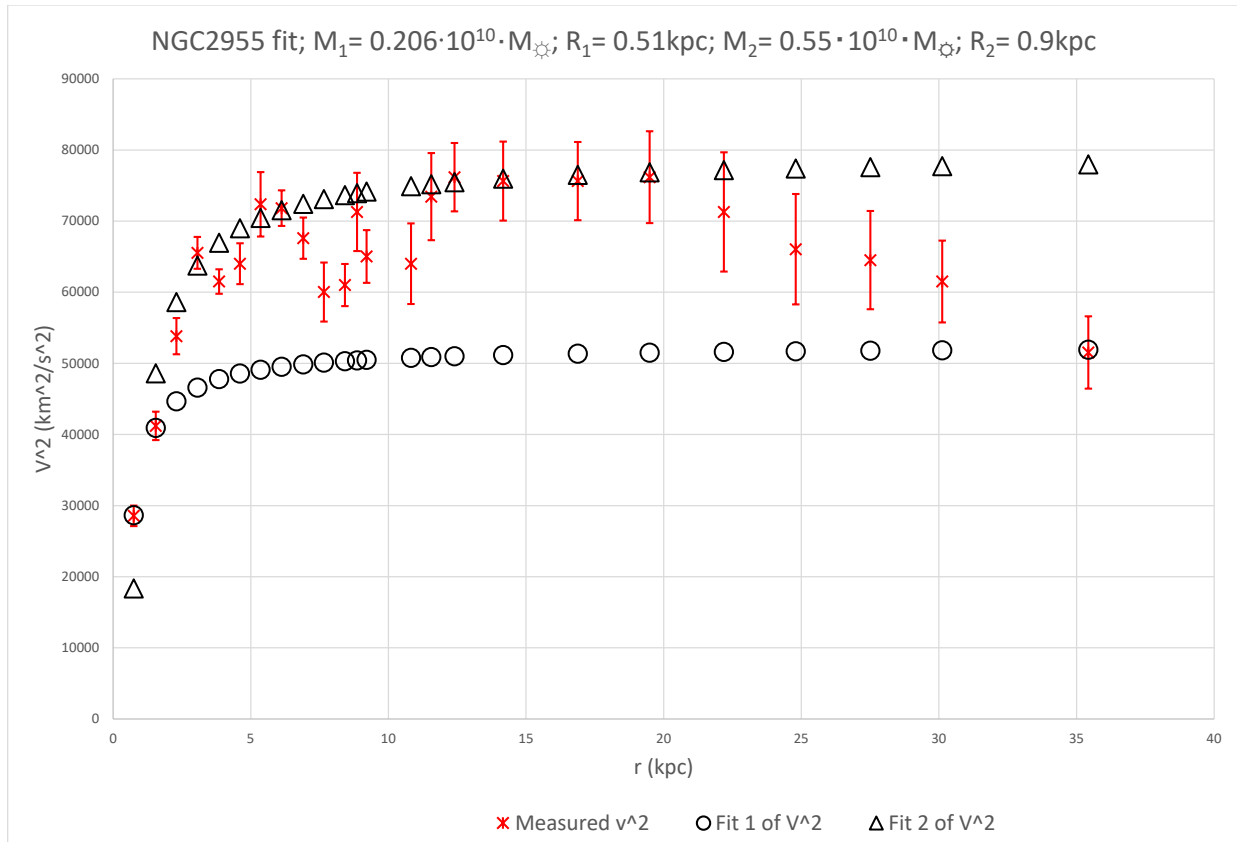


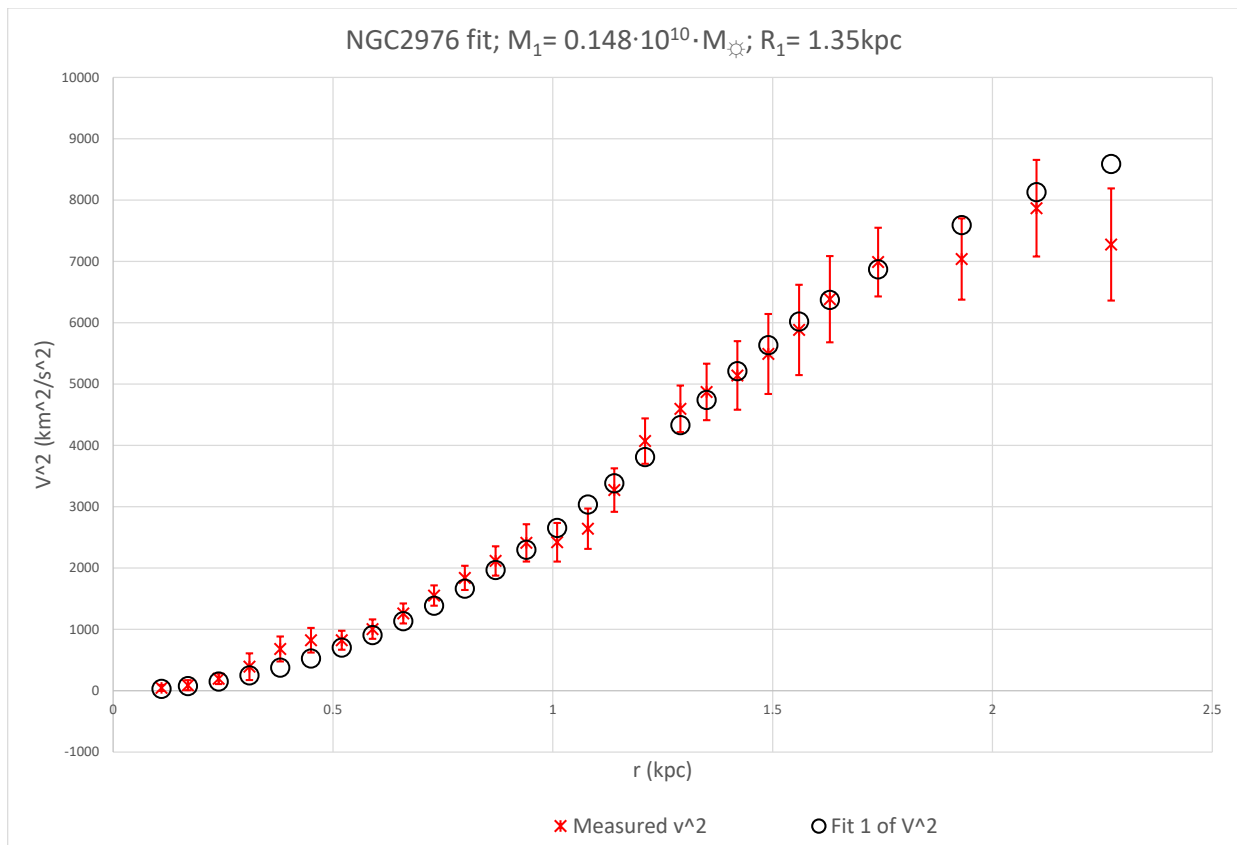




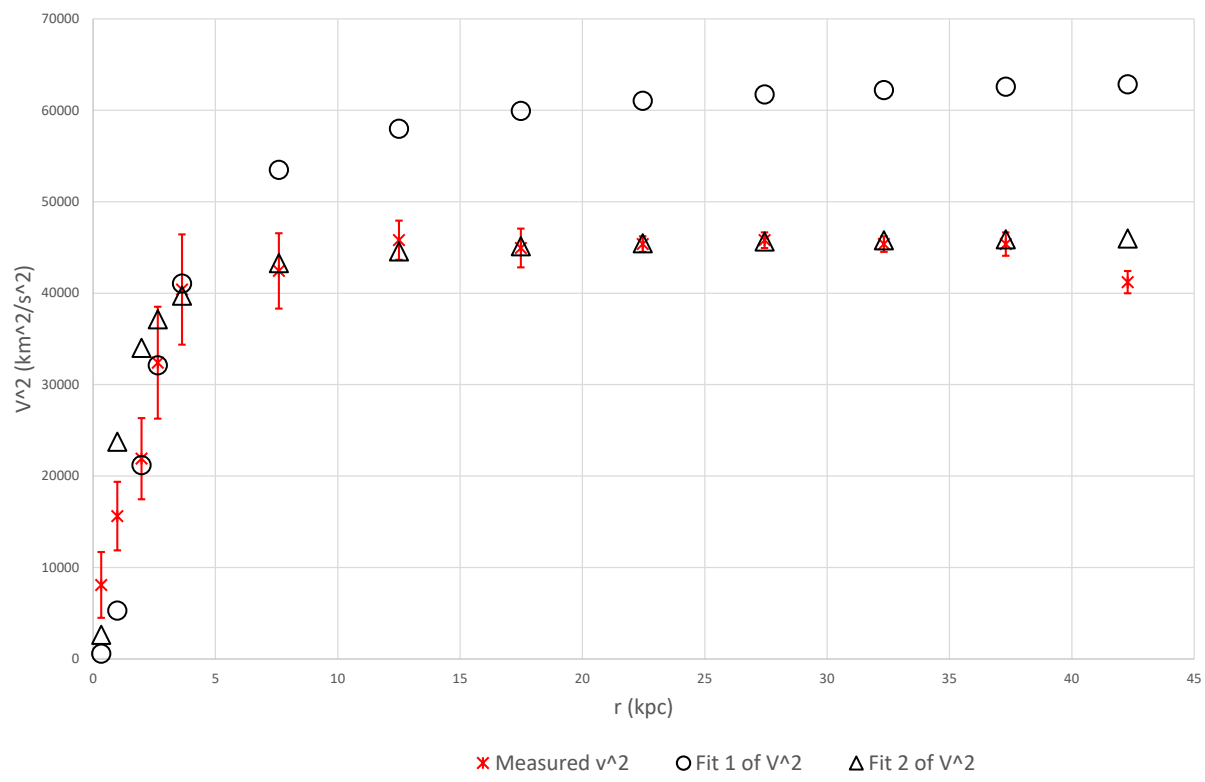


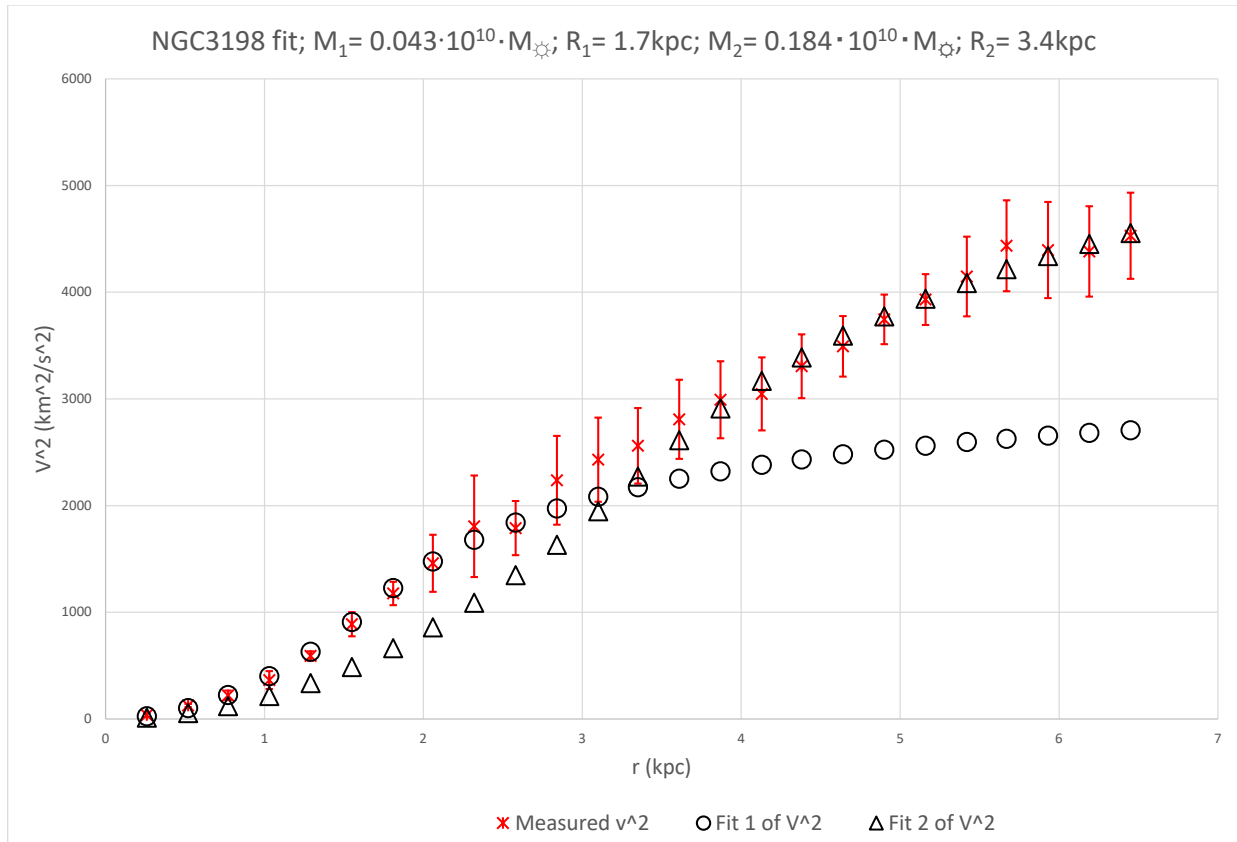


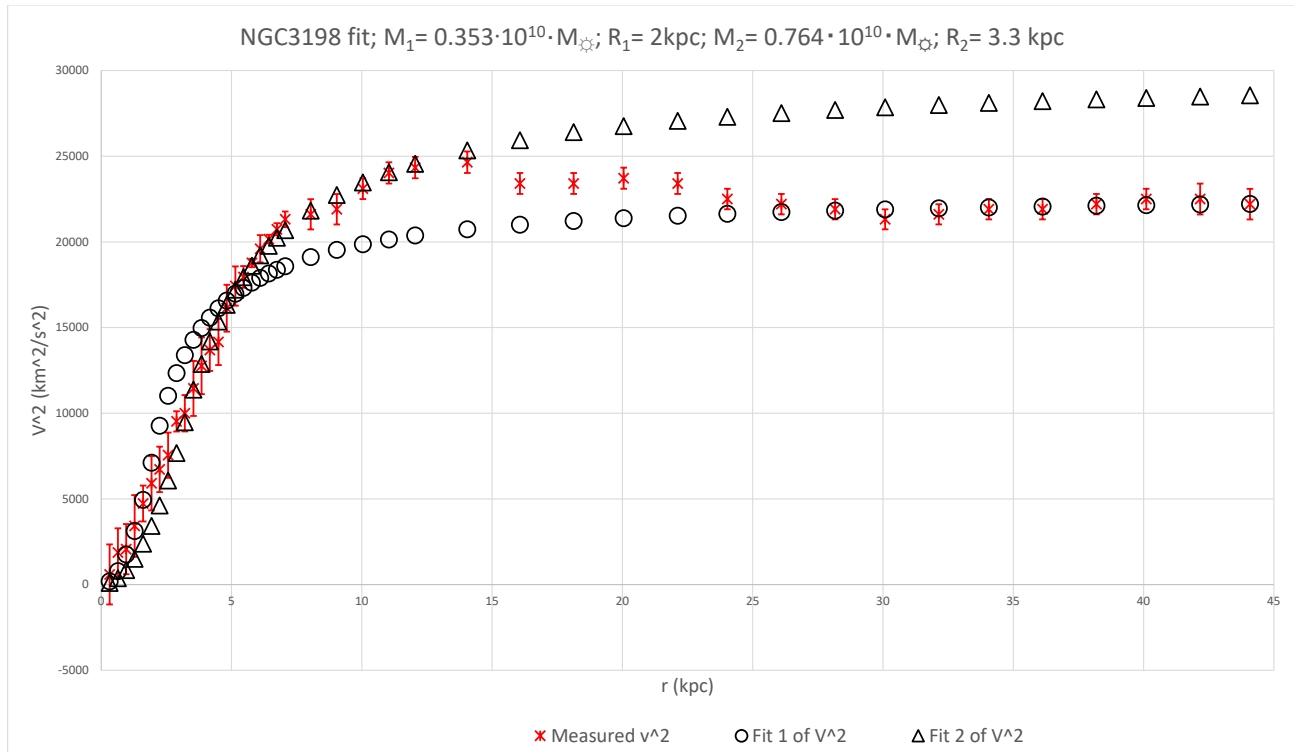


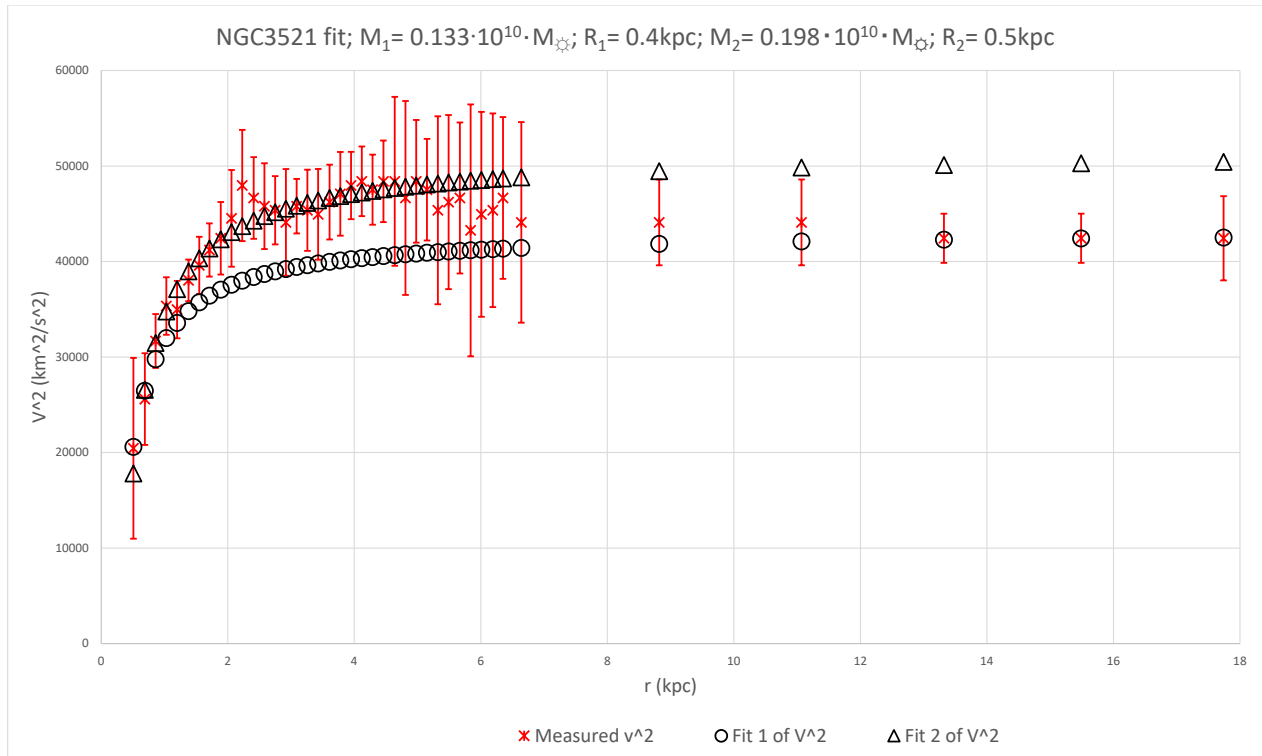


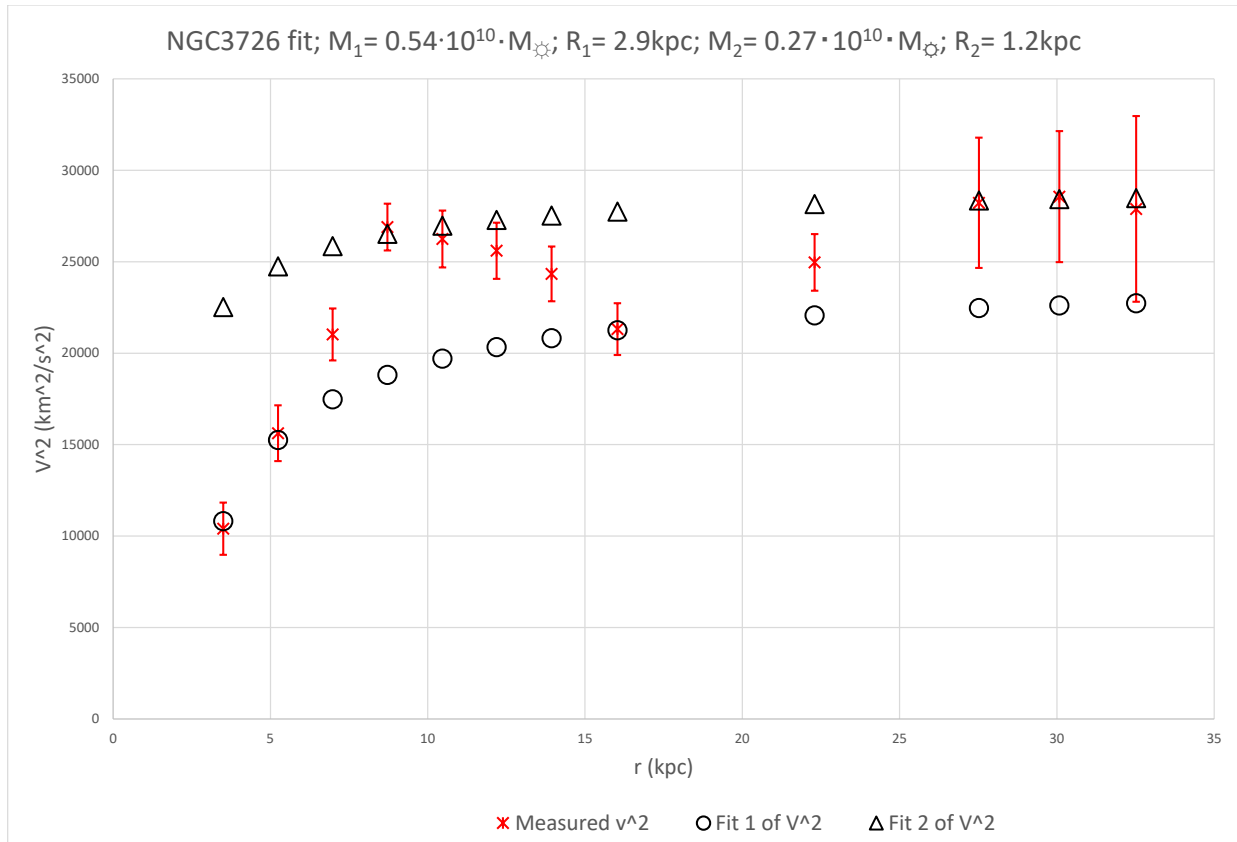
NGC2998 fit; $M_1 = 1 \cdot 10^{10} \cdot M_{\odot}$; $R_1 = 2 \text{ kpc}$; $M_2 = 0.287 \cdot 10^{10} \cdot M_{\odot}$; $R_2 = 0.8 \text{ kpc}$



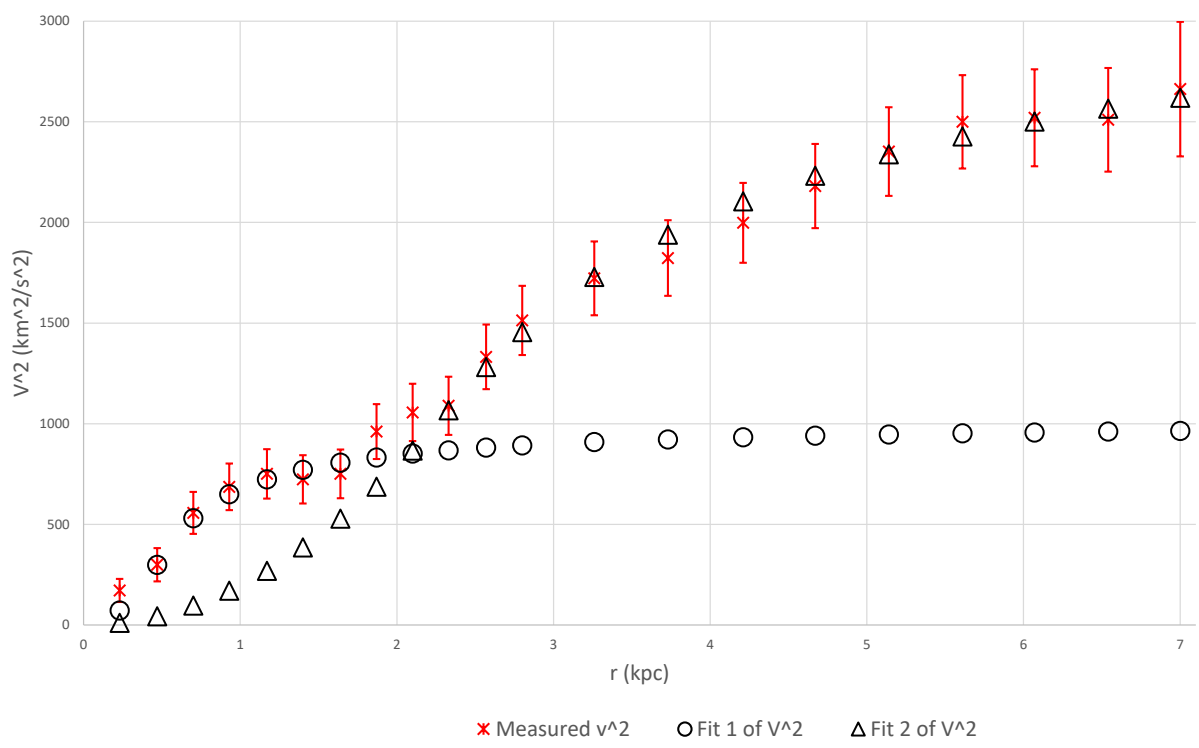


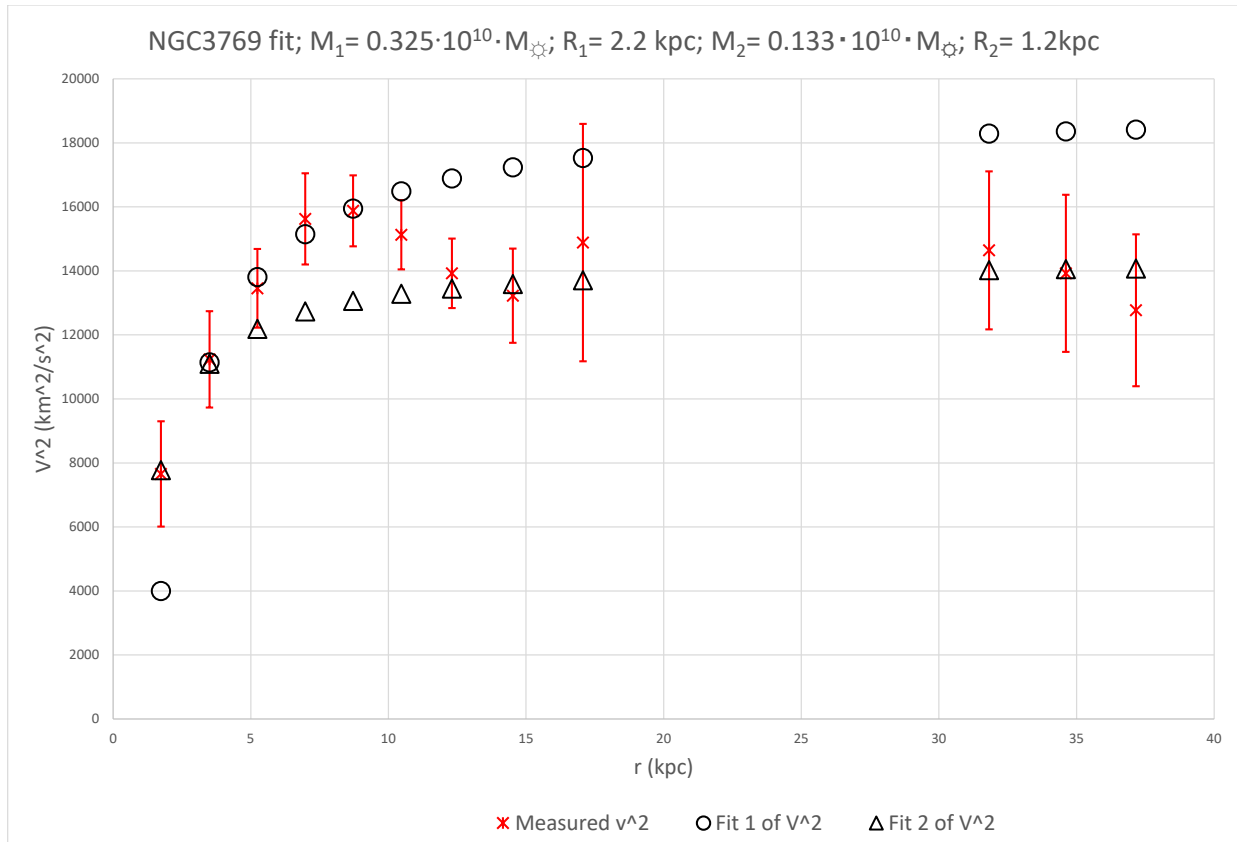


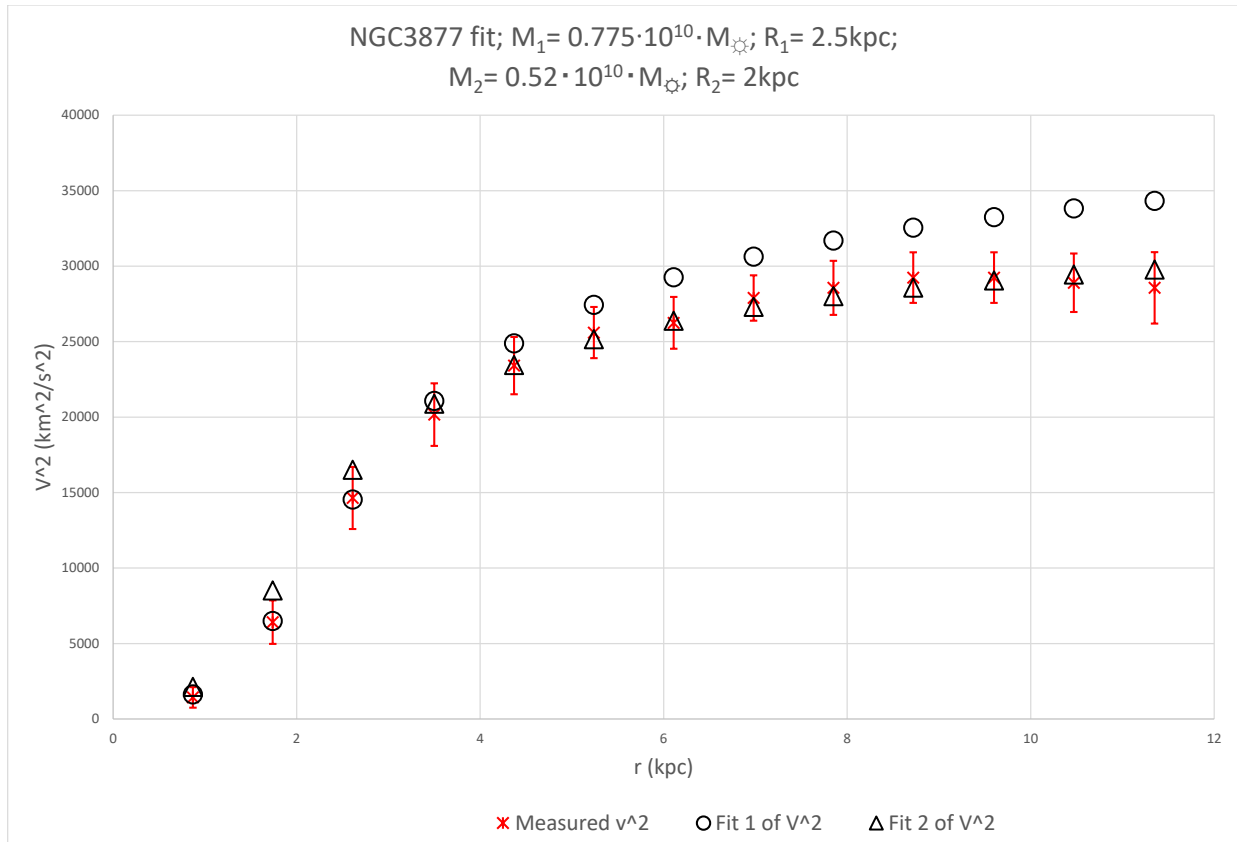


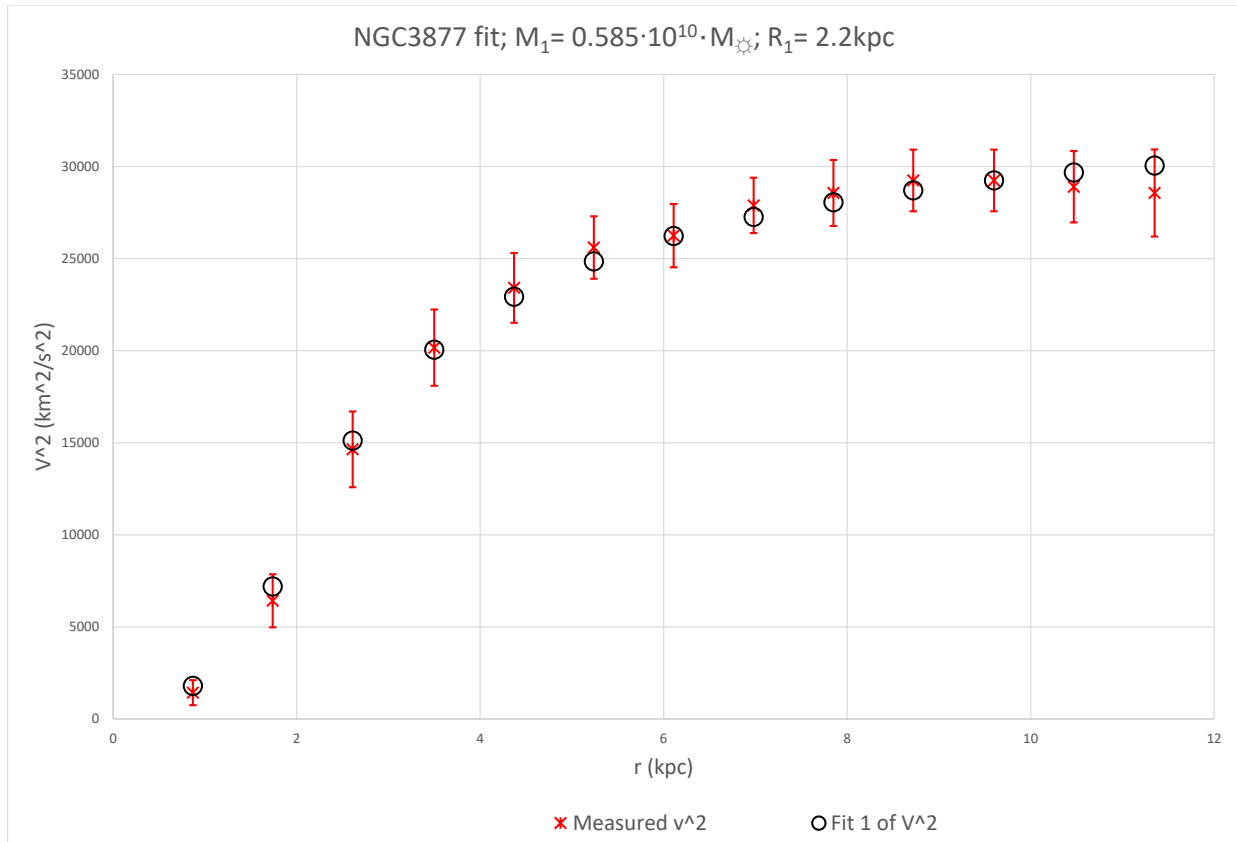


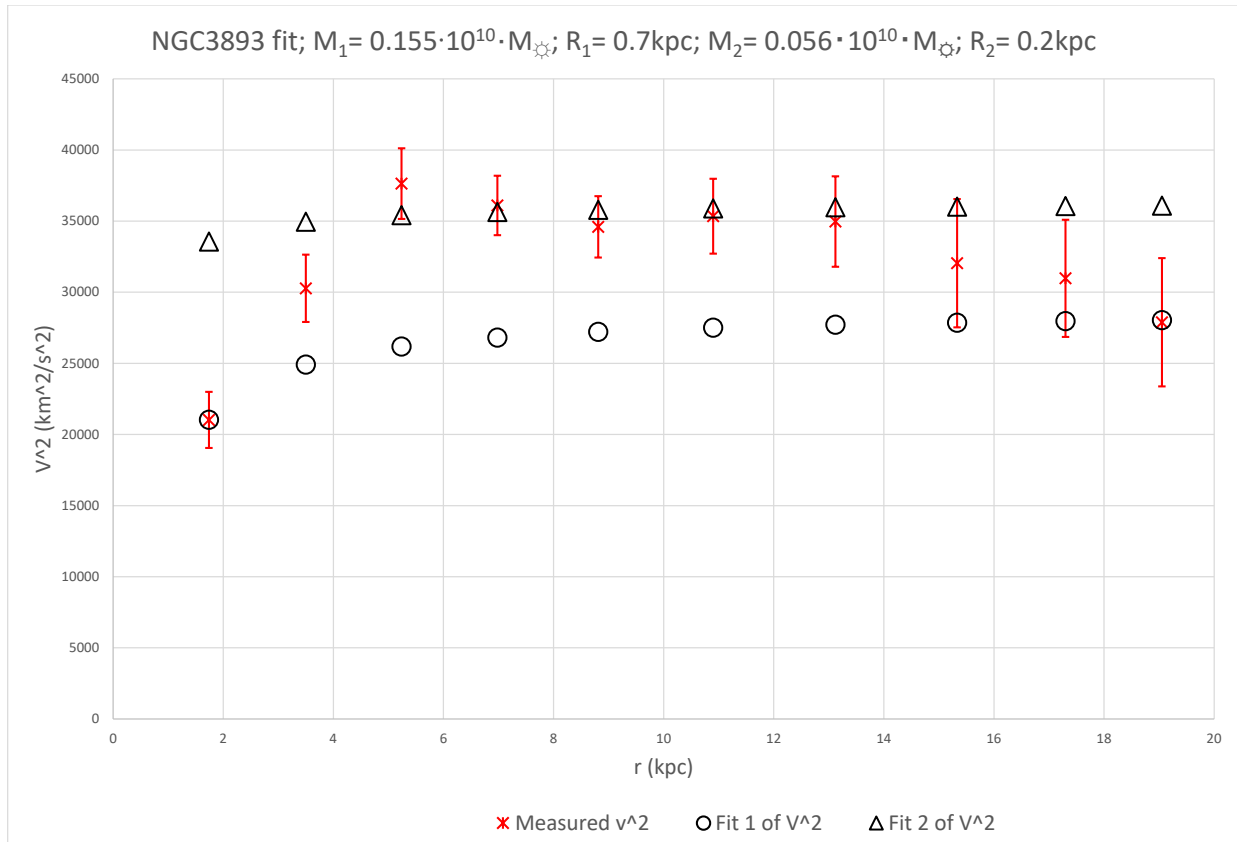
NGC3741 fit; $M_1 = 0.0039 \cdot 10^{10} \cdot M_{\odot}$; $R_1 = 0.5 \text{ kpc}$;
 $M_2 = 0.0628 \cdot 10^{10} \cdot M_{\odot}$; $R_2 = 2.4 \text{ kpc}$

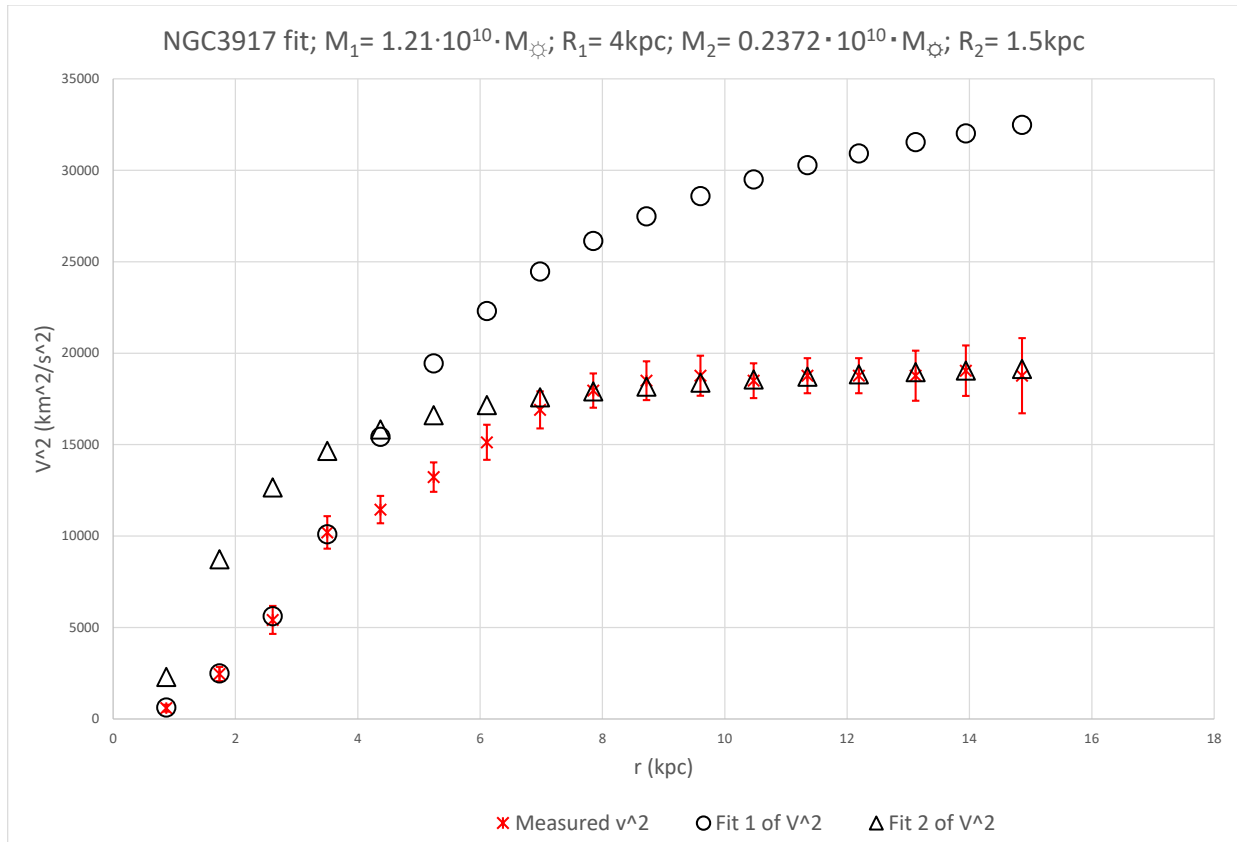


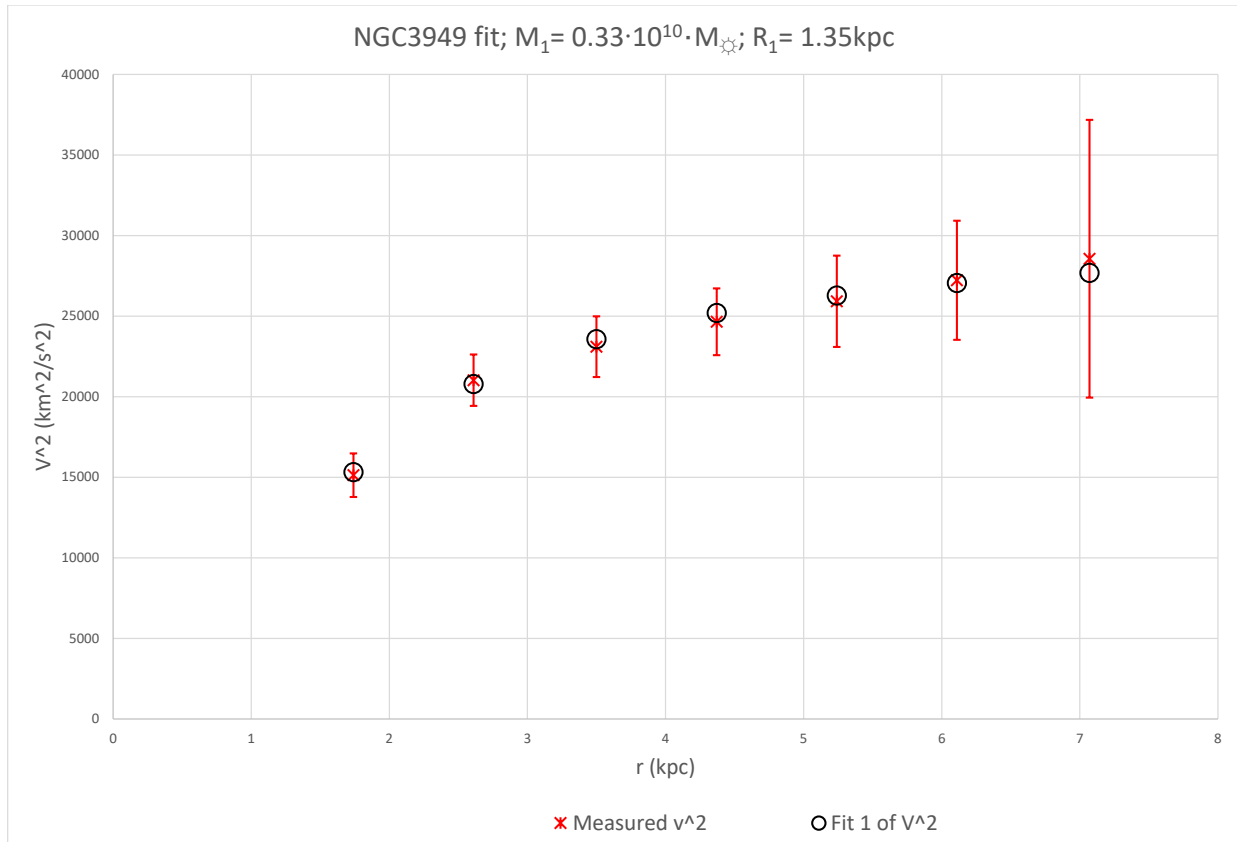




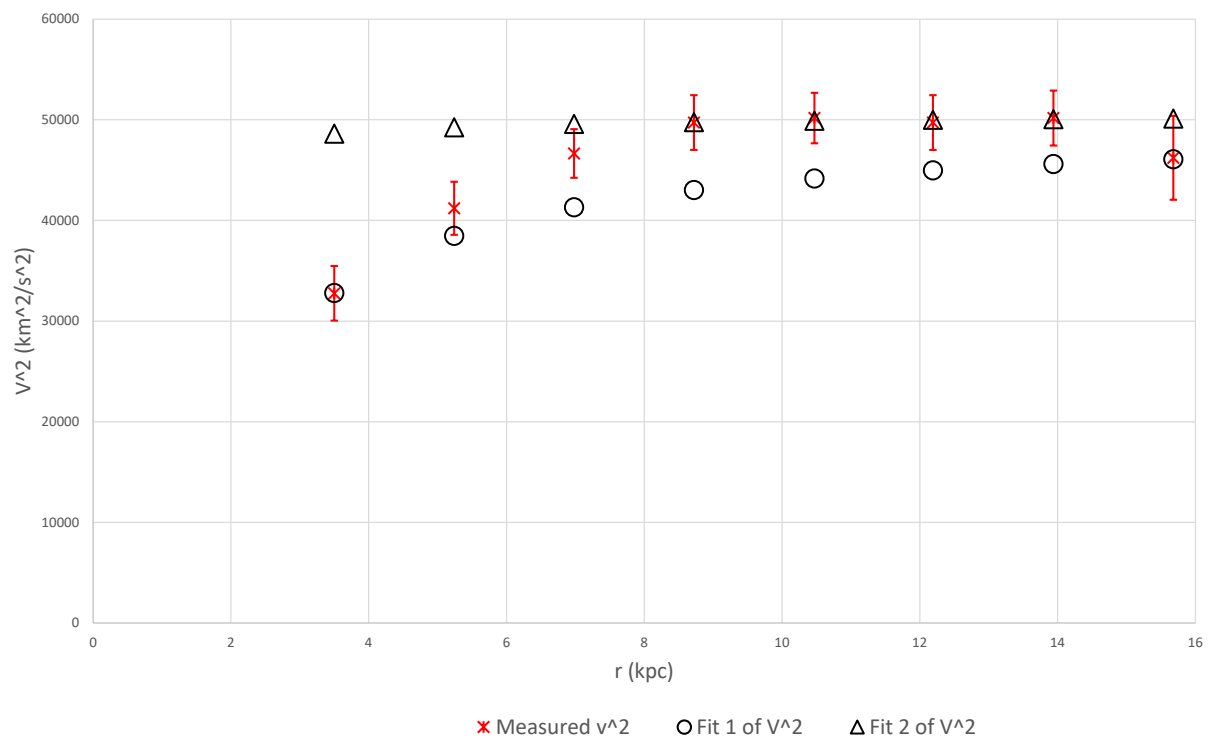


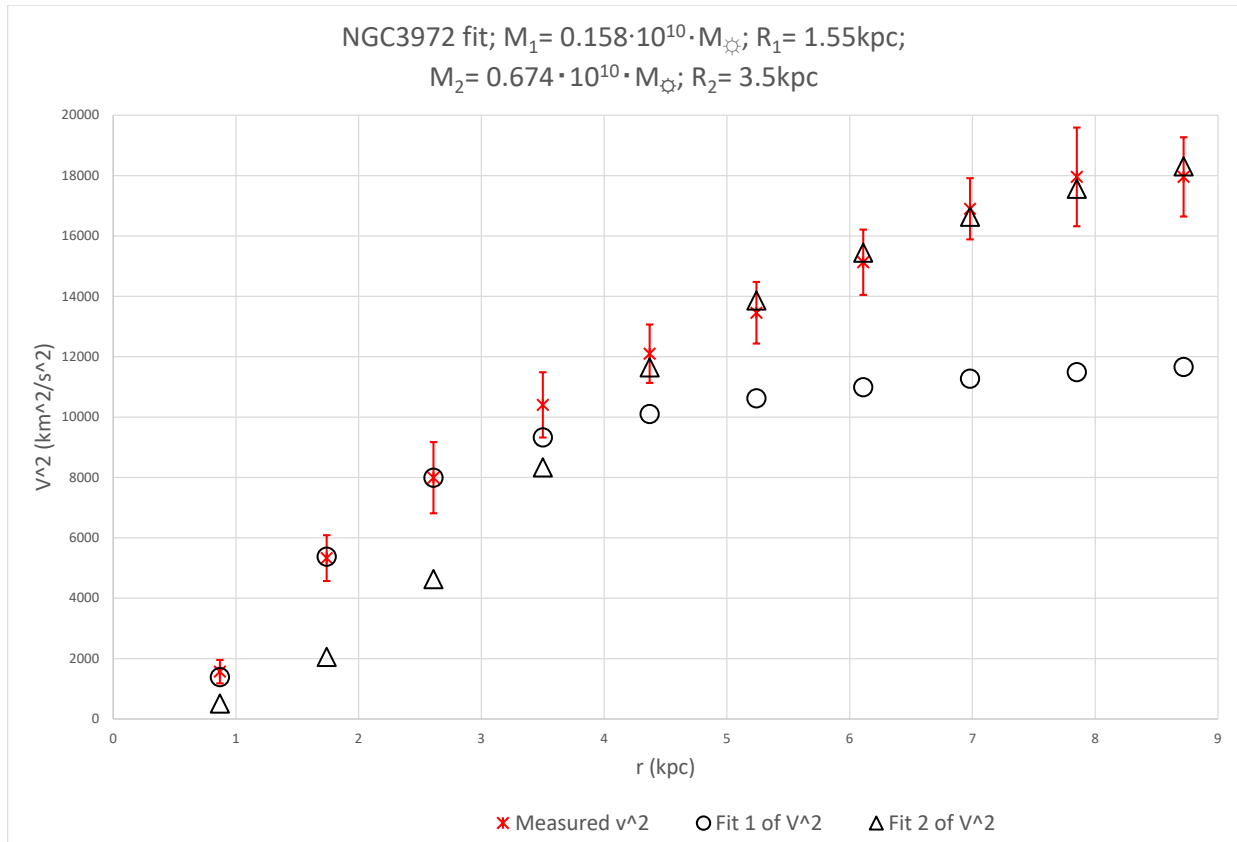


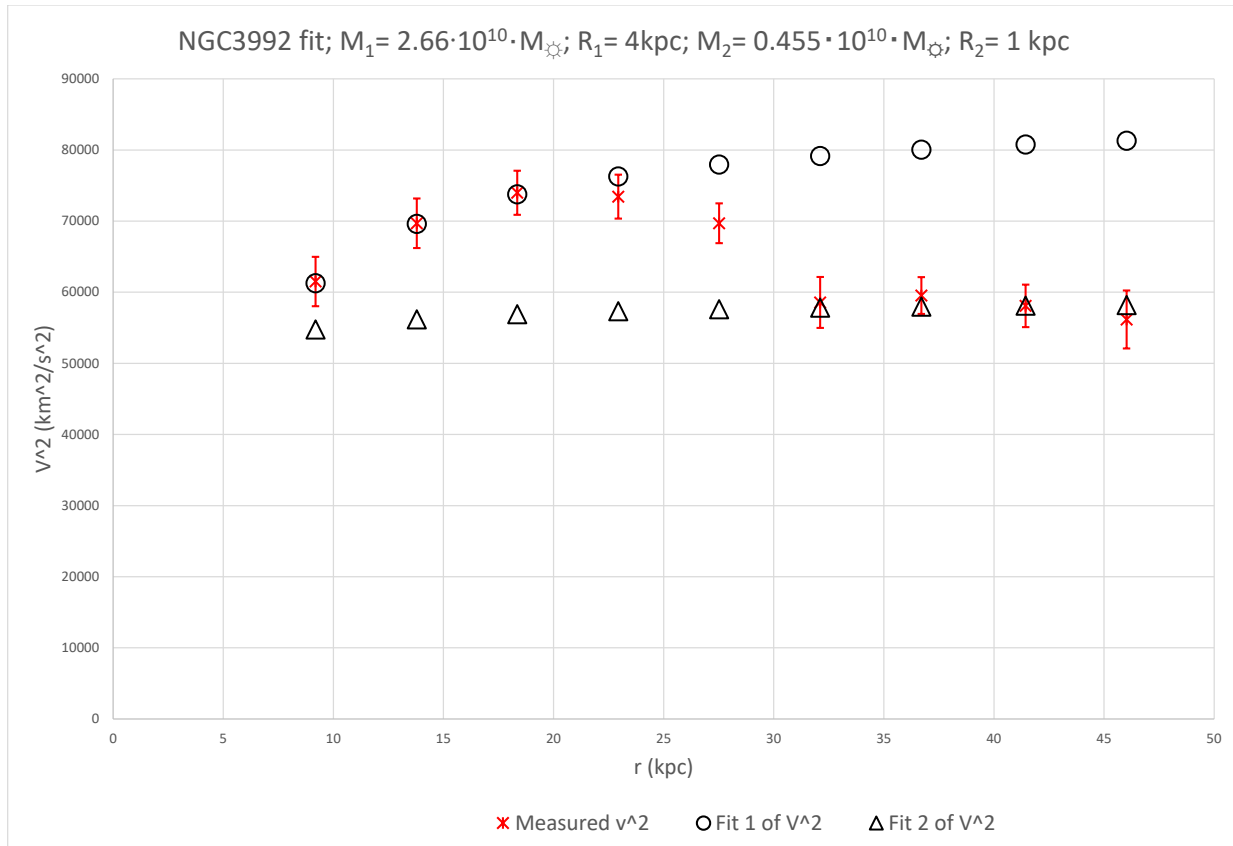


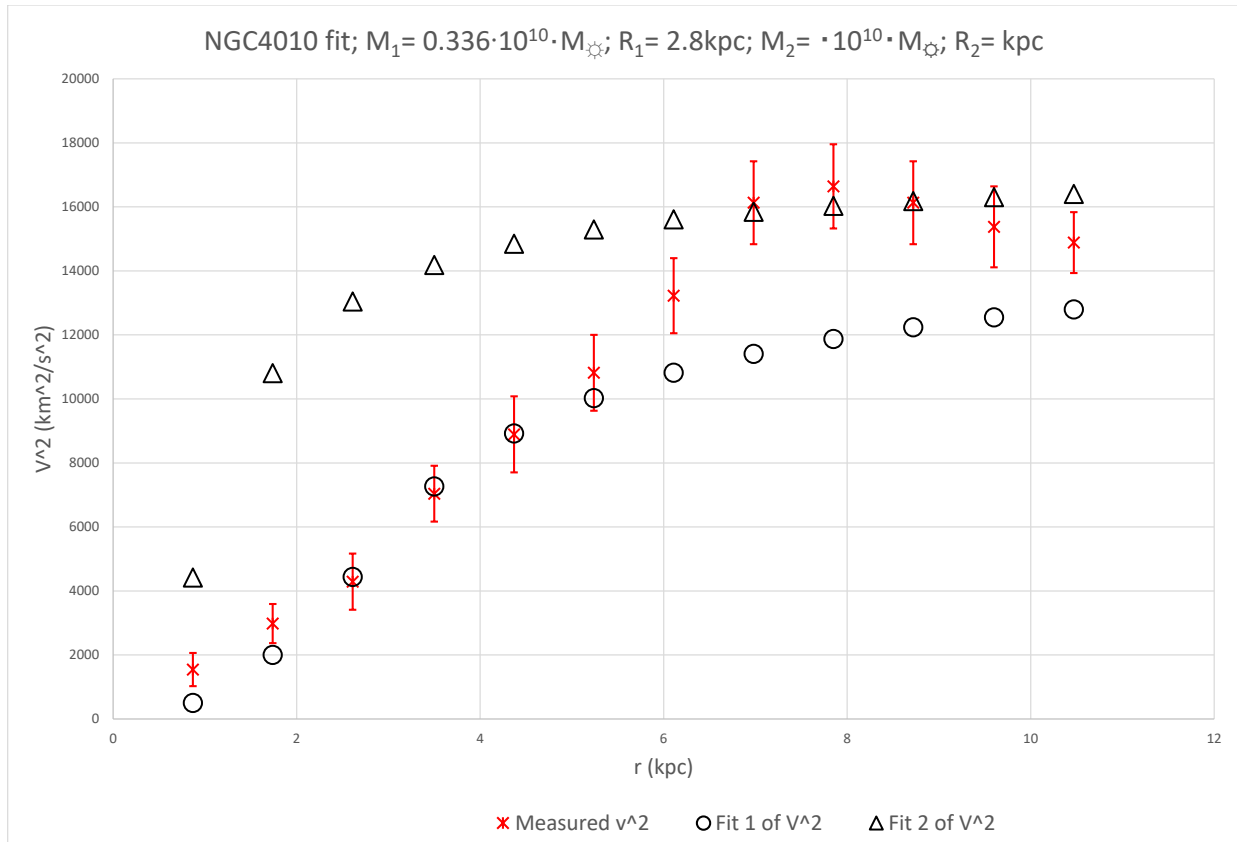


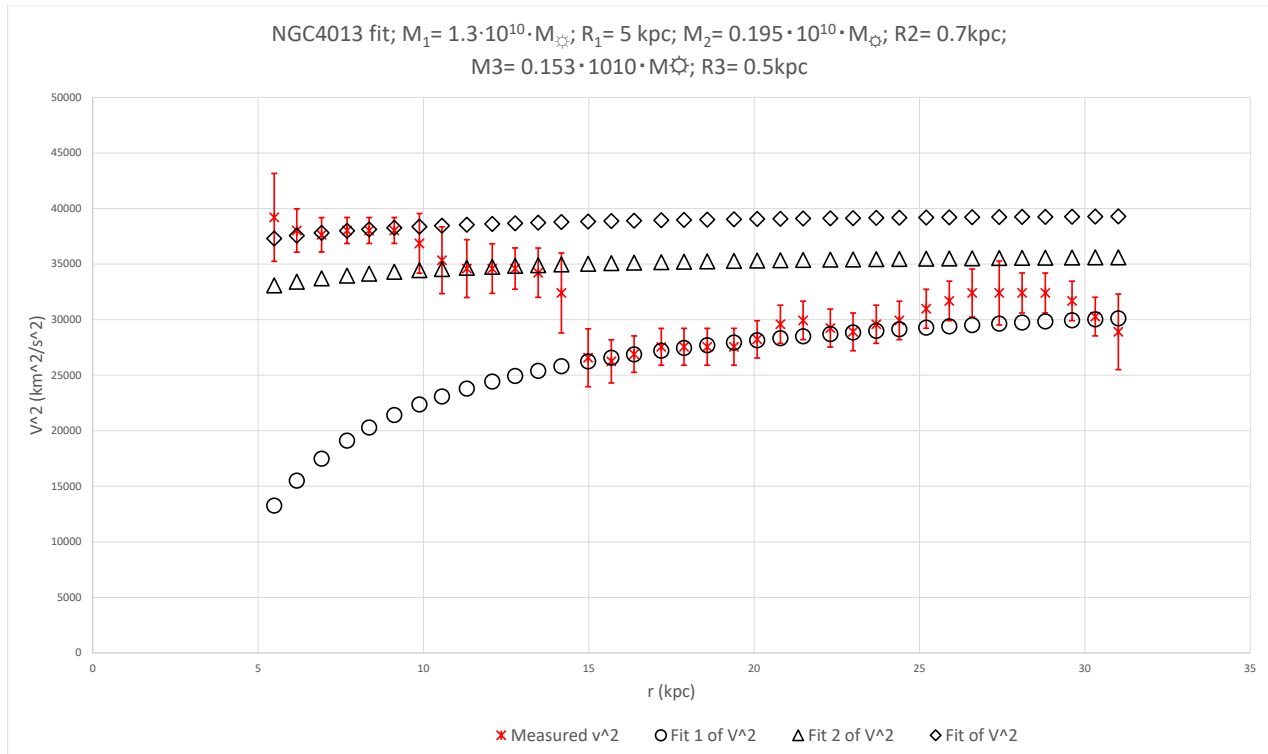
NGC3953 fit; $M_1 = 0.692 \cdot 10^{10} \cdot M_{\odot}$; $R_1 = 1.8 \text{ kpc}$;
 $M_2 = 0.0779 \cdot 10^{10} \cdot M_{\odot}$; $R_2 = 0.2 \text{ kpc}$

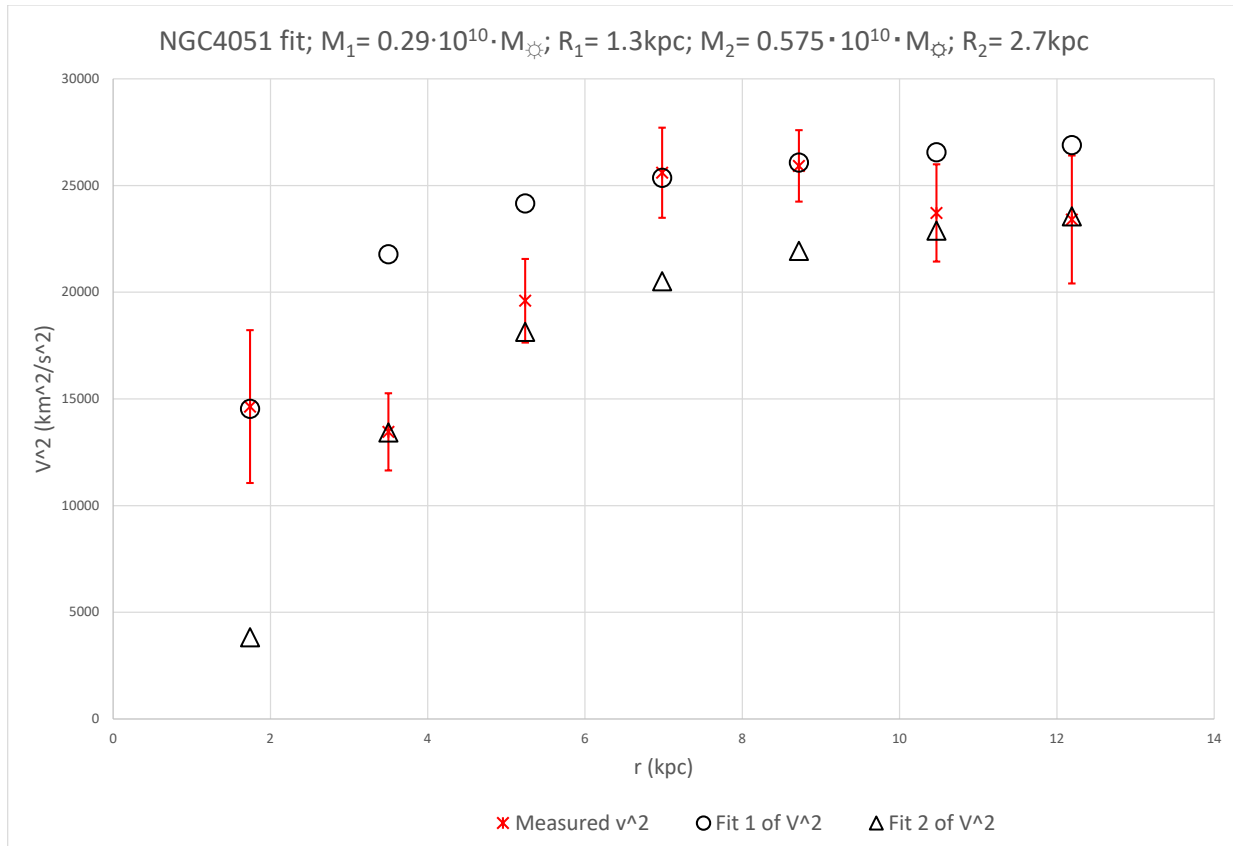


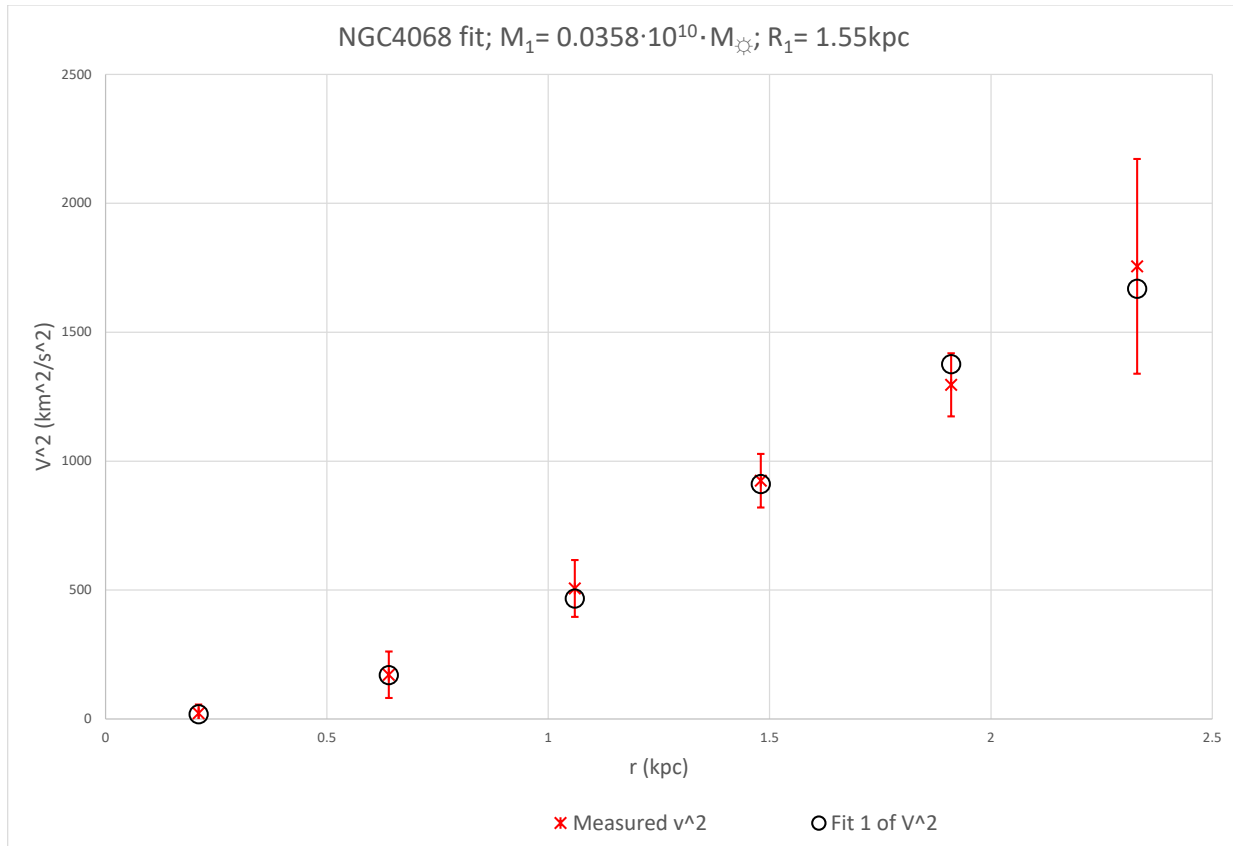


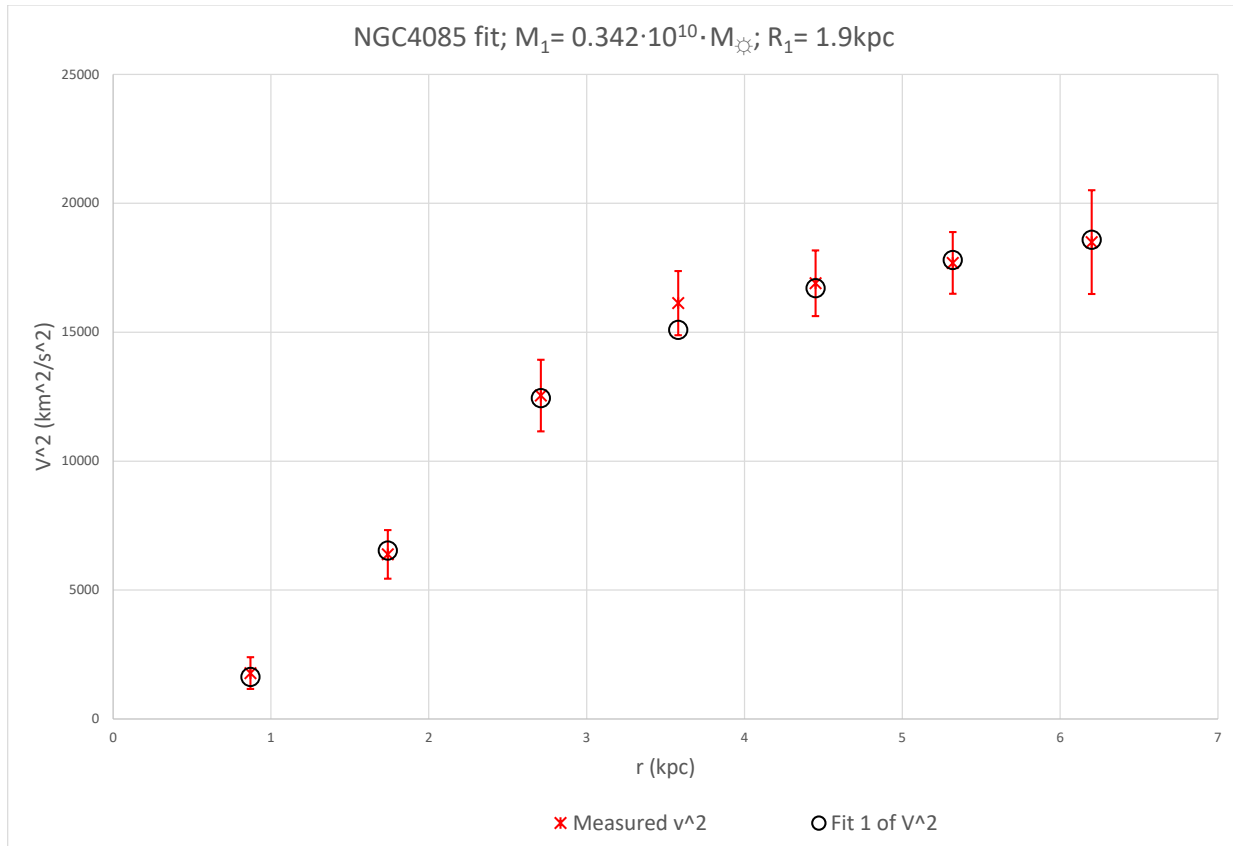




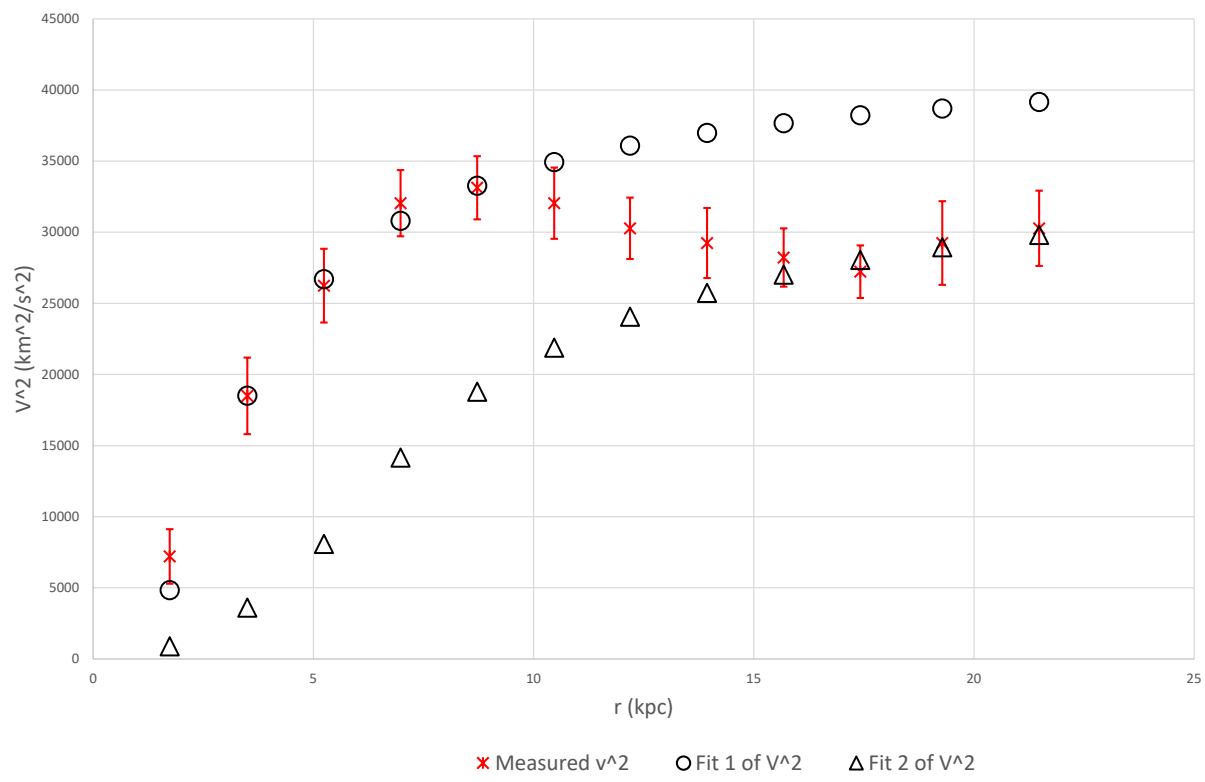


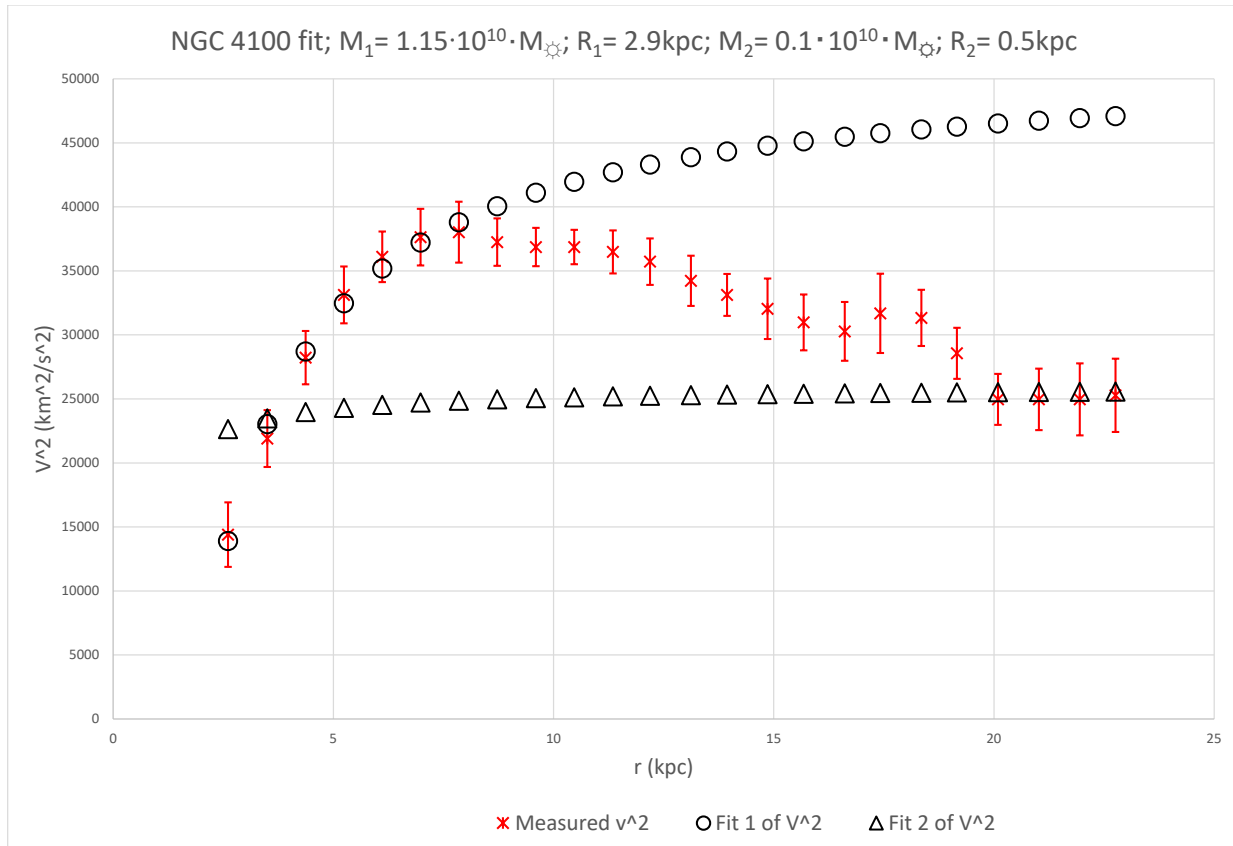




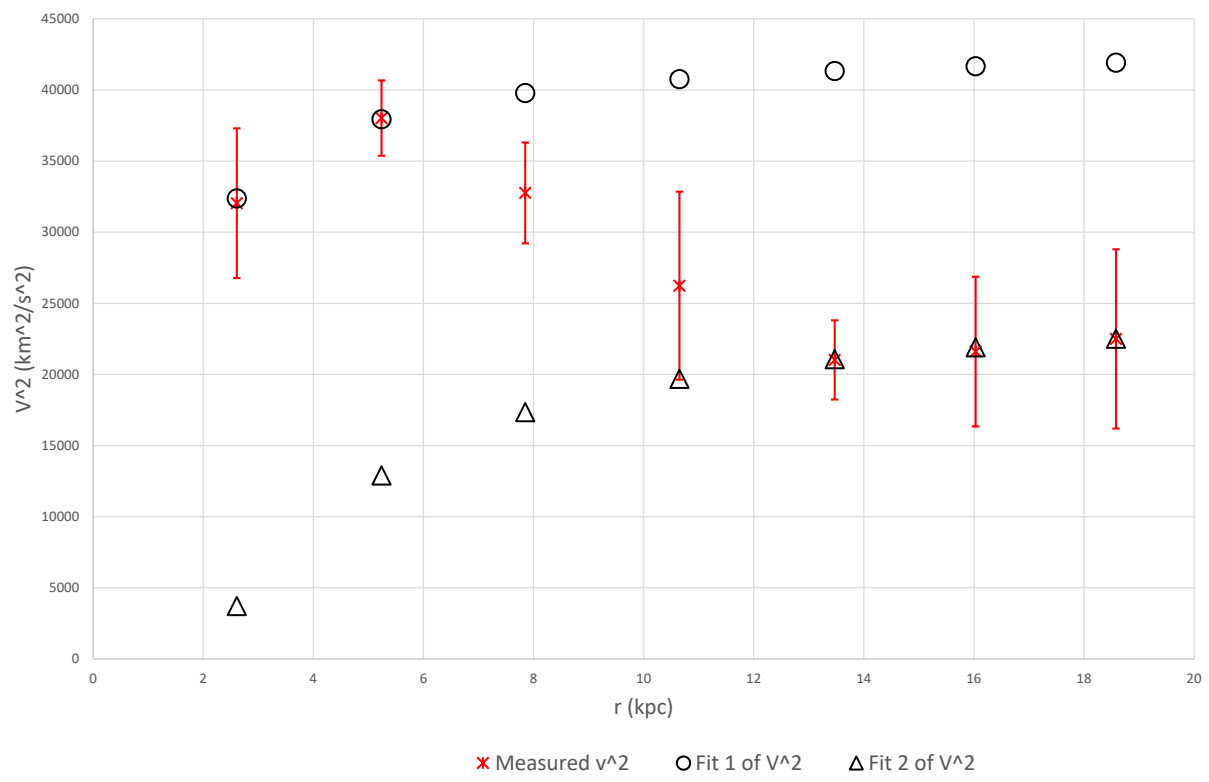


NGC4088 fit; $M_1 = 0.998 \cdot 10^{10} \cdot M_{\odot}$; $R_1 = 3 \text{ kpc}$; $M_2 = 1.87 \cdot 10^{10} \cdot M_{\odot}$; $R_2 = 6.5 \text{ kpc}$

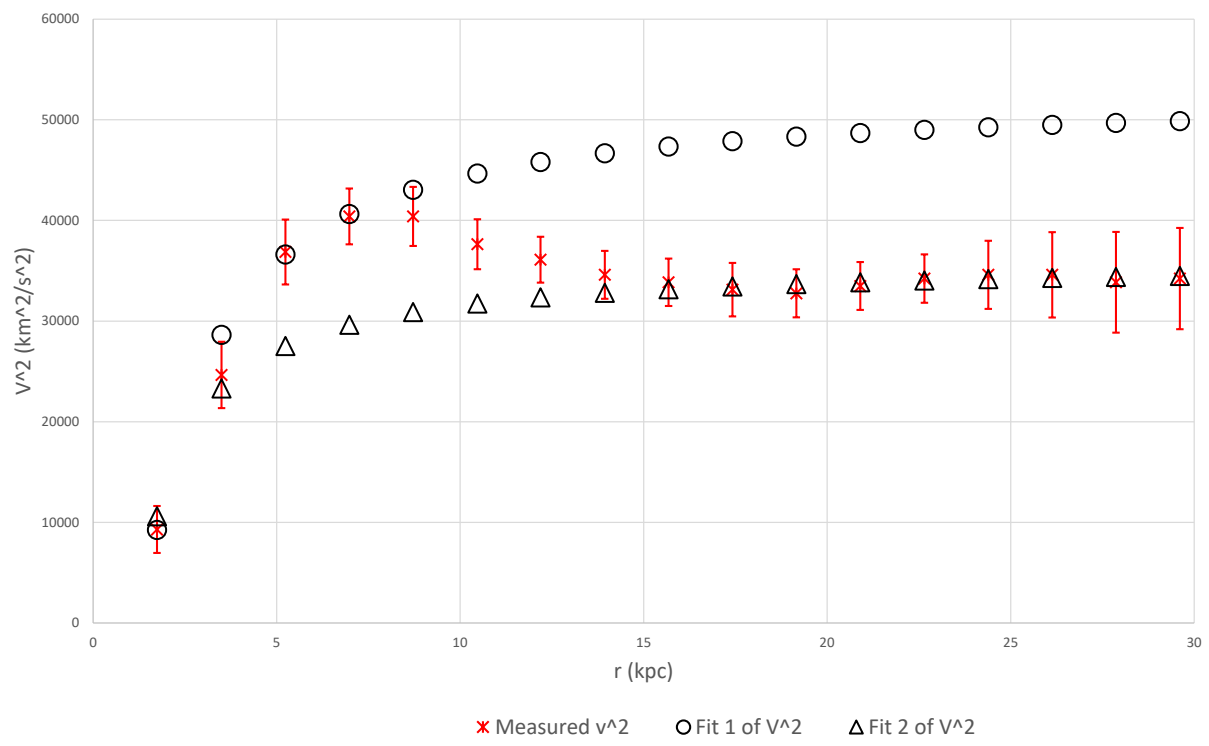


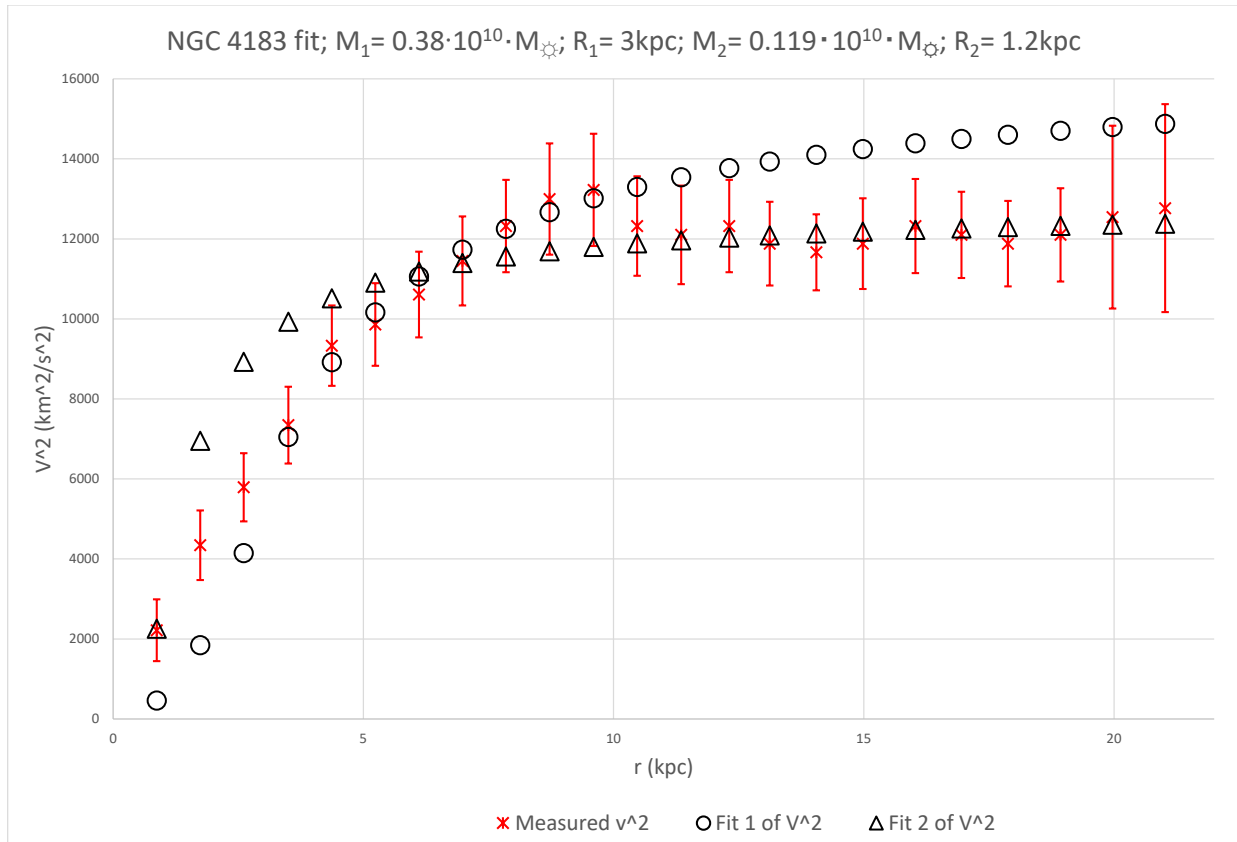


NGC4138 fit; $M_1 = 0.335 \cdot 10^{10} \cdot M_{\odot}$; $R_1 = 1 \text{ kpc}$; $M_2 = 0.81 \cdot 10^{10} \cdot M_{\odot}$; $R_2 = 4 \text{ kpc}$

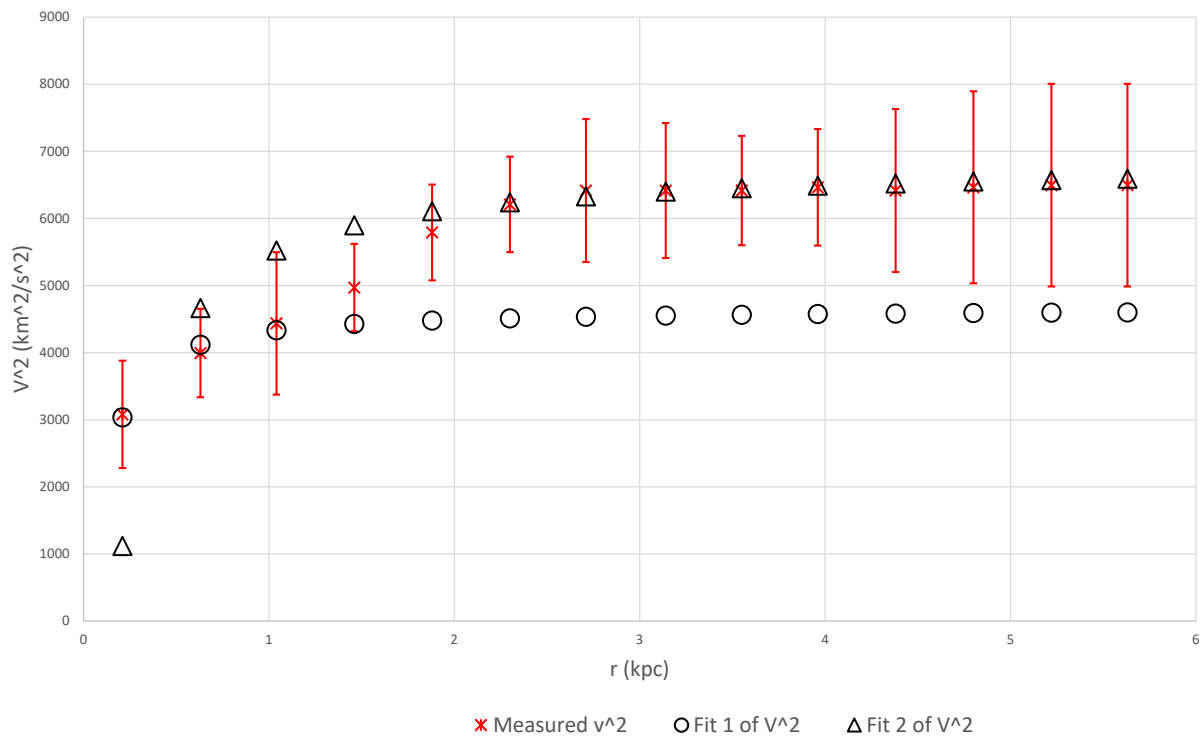


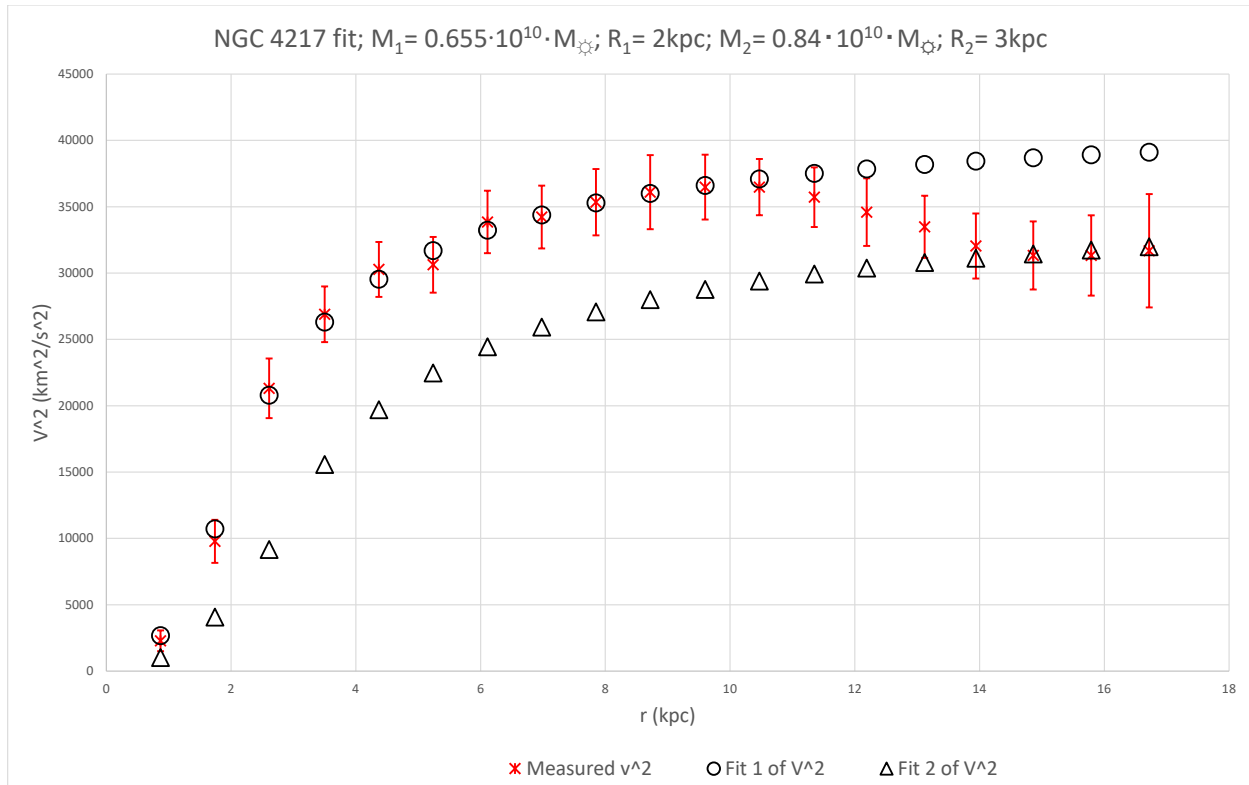
NGC4157 fit; $M_1 = 0.975 \cdot 10^{10} \cdot M_{\odot}$; $R_1 = 2.4 \text{kpc}$;
 $M_2 = 0.513 \cdot 10^{10} \cdot M_{\odot}$; $R_2 = 1.85 \text{kpc}$



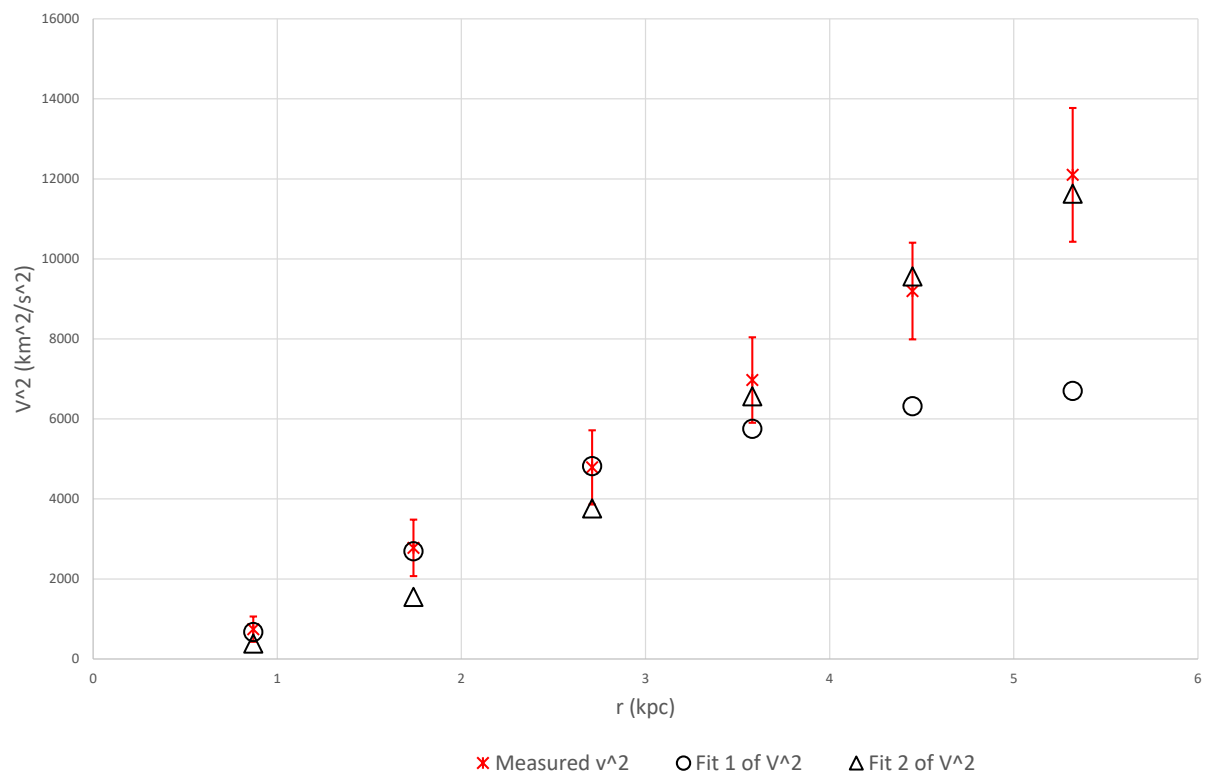


NGC4214 fit; $M_1 = 0.00395 \cdot 10^{10} \cdot M_{\odot}$; $R_1 = 0.11 \text{kpc}$;
 $M_2 = 0.0158 \cdot 10^{10} \cdot M_{\odot}$; $R_2 = 0.3 \text{kpc}$

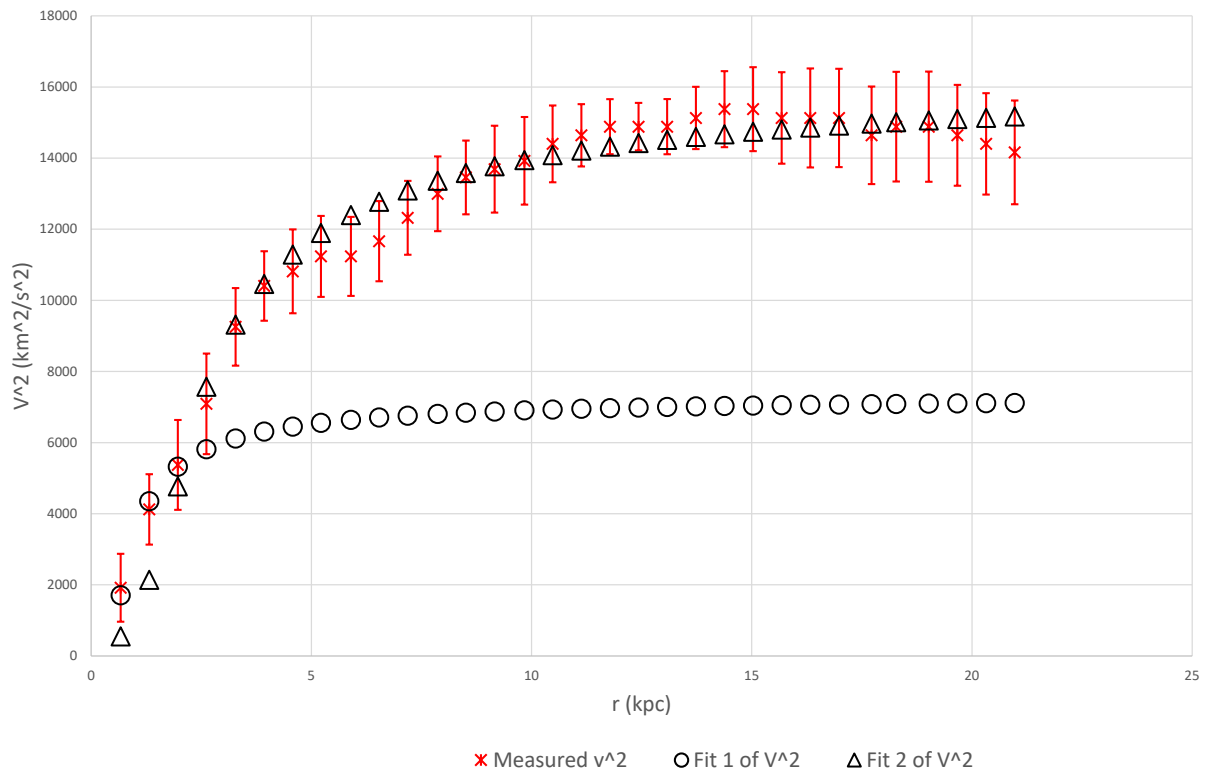


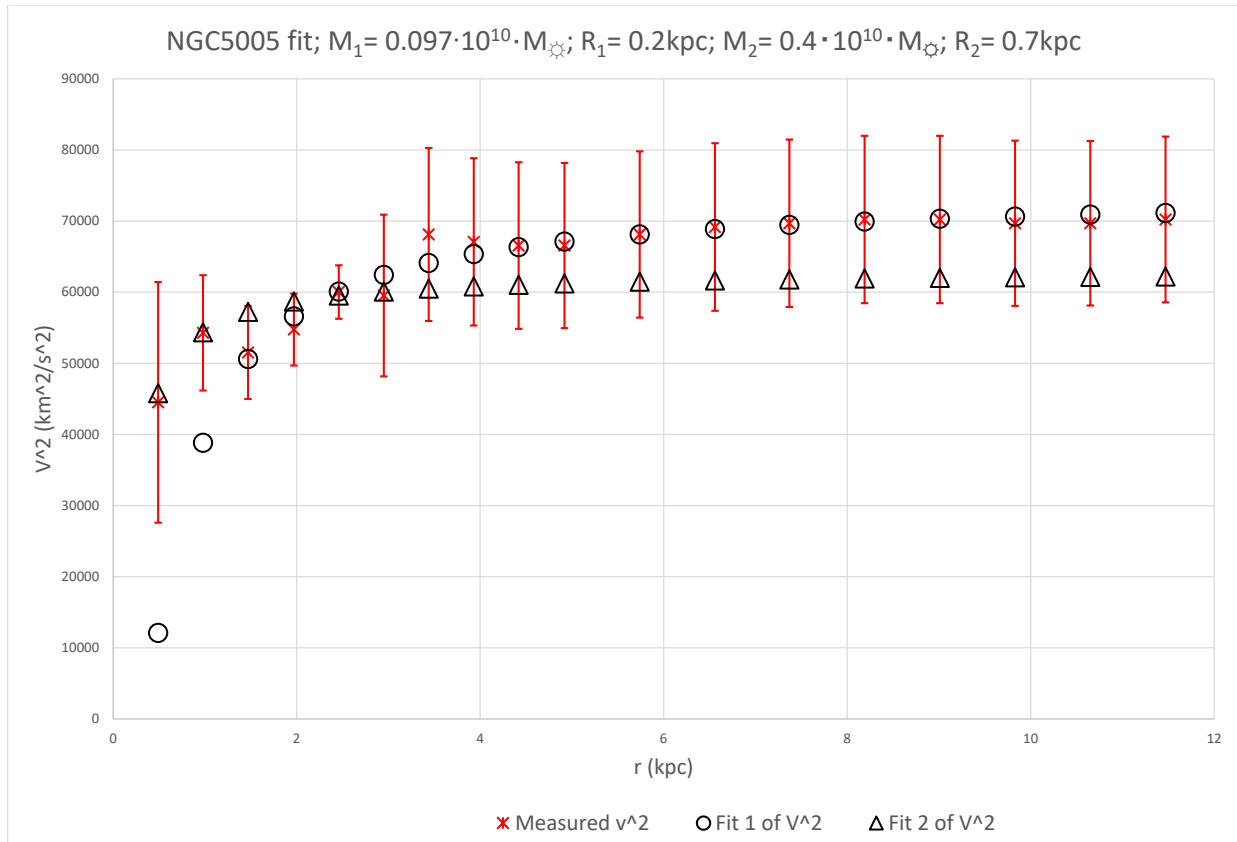


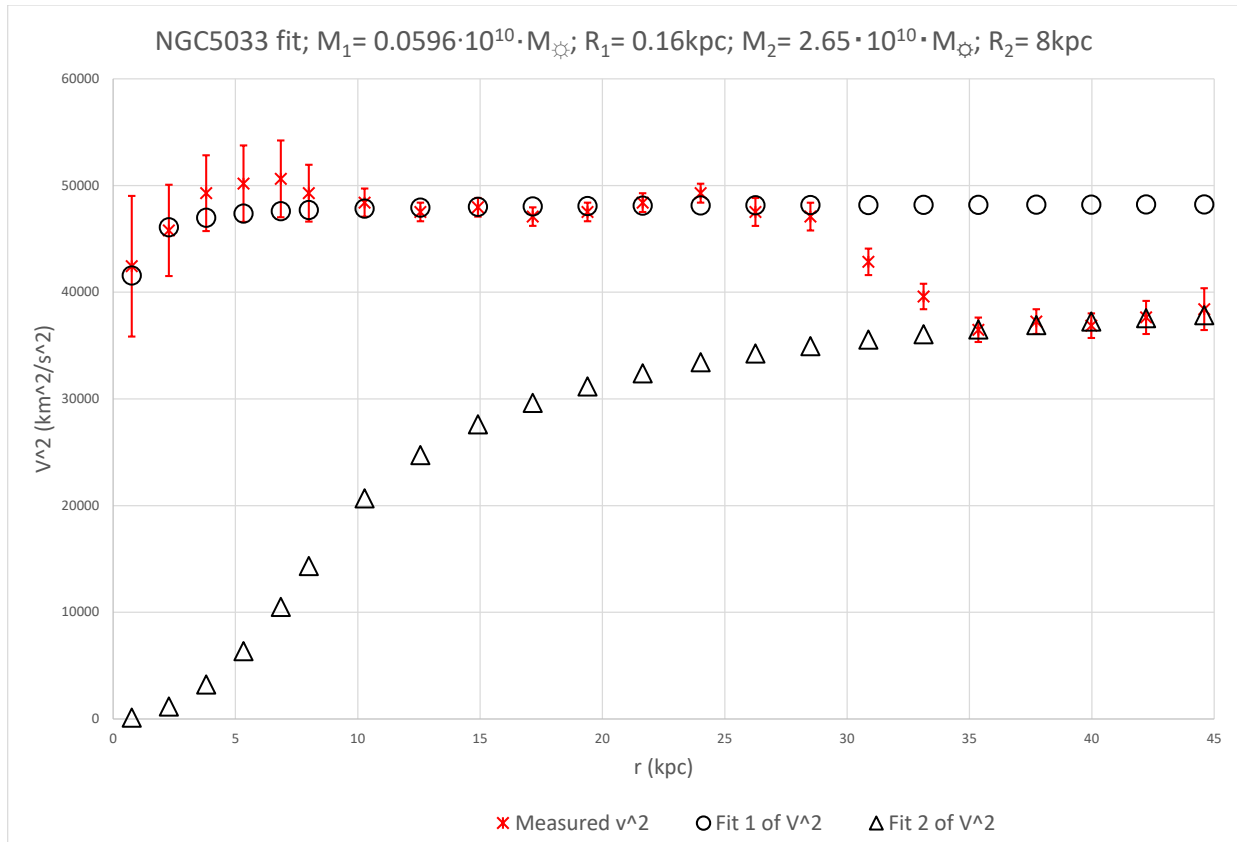
NGC4389 fit; $M_1 = 0.12 \cdot 10^{10} \cdot M_{\odot}$; $R_1 = 1.8 \text{ kpc}$; $M_2 = 0.65 \cdot 10^{10} \cdot M_{\odot}$; $R_2 = 3.8 \text{ kpc}$

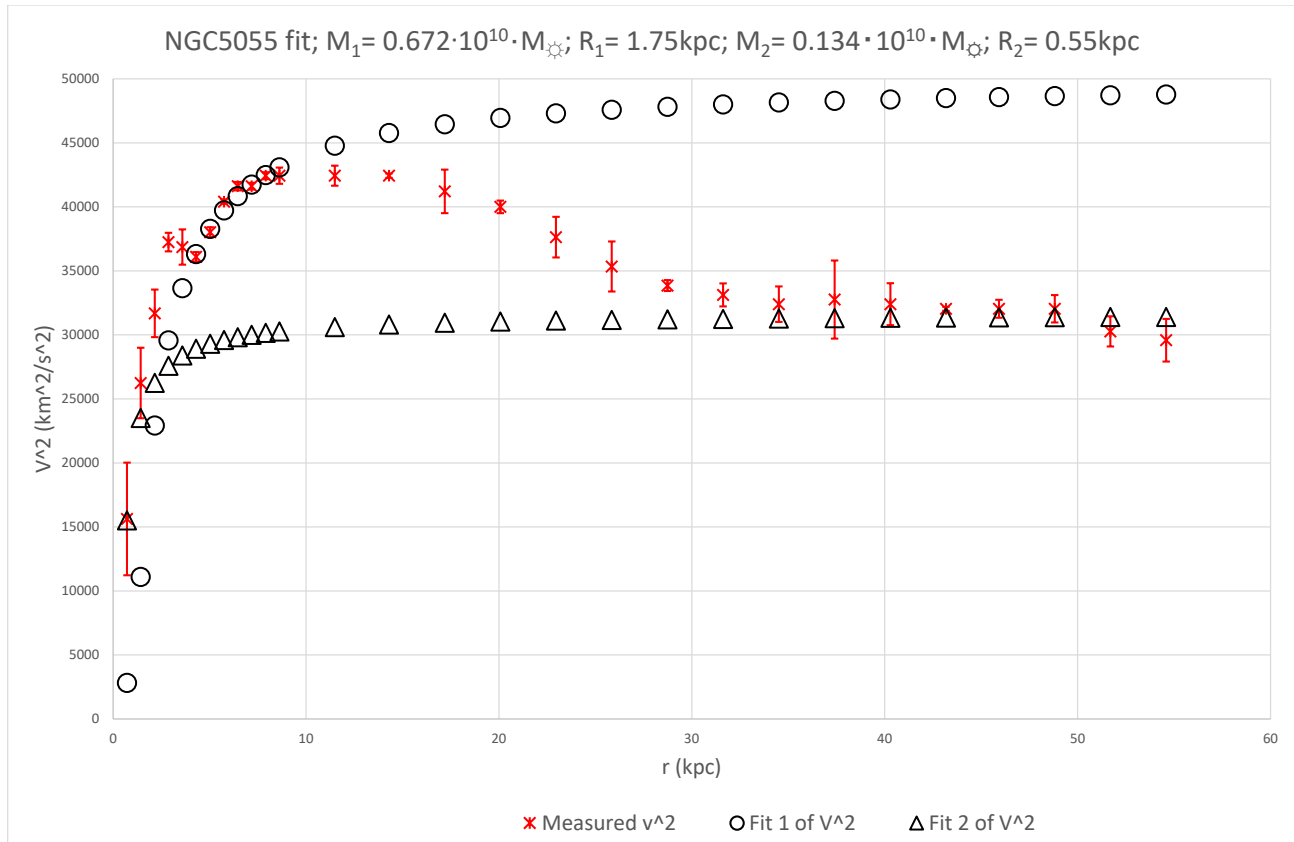


NGC4559 fit; $M_1 = 0.045 \cdot 10^{10} \cdot M_{\odot}$; $R_1 = 0.8 \text{ kpc}$; $M_2 = 0.263 \cdot 10^{10} \cdot M_{\odot}$; $R_2 = 2.1 \text{ kpc}$

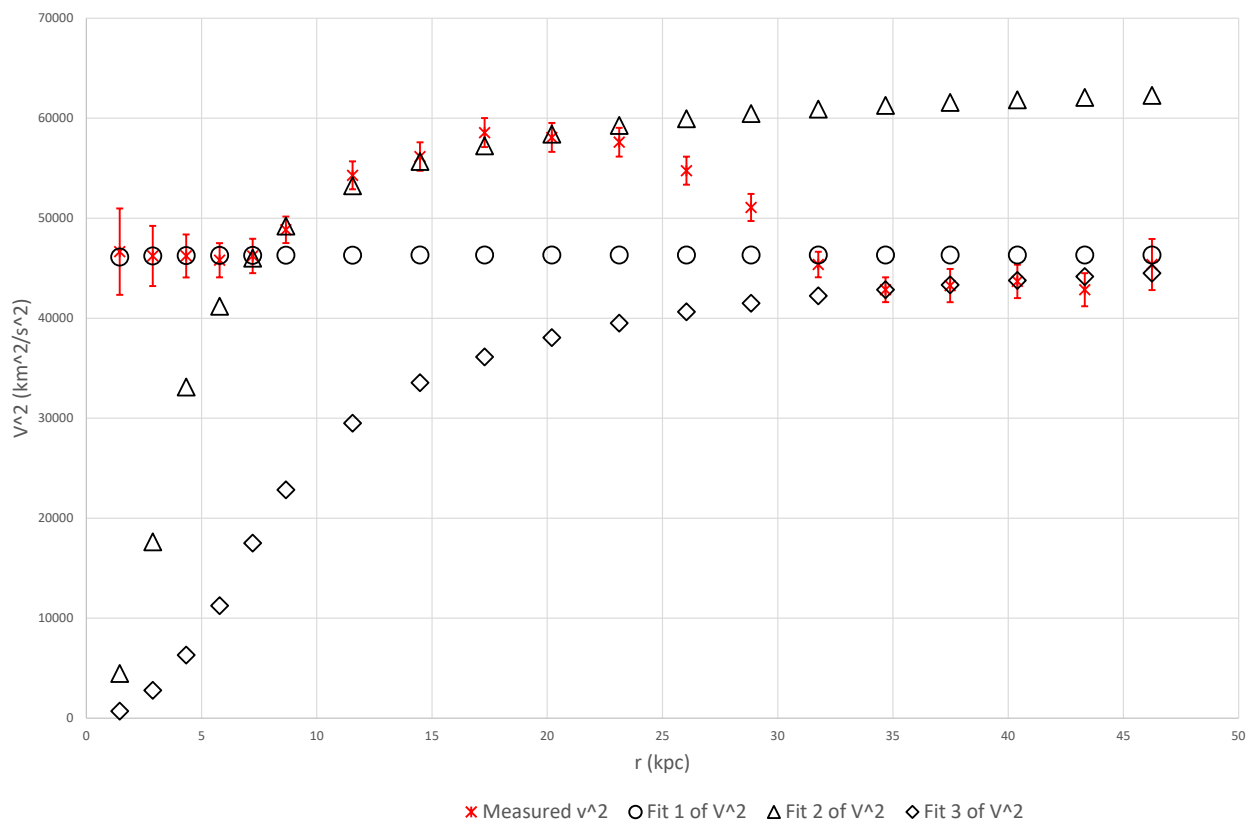




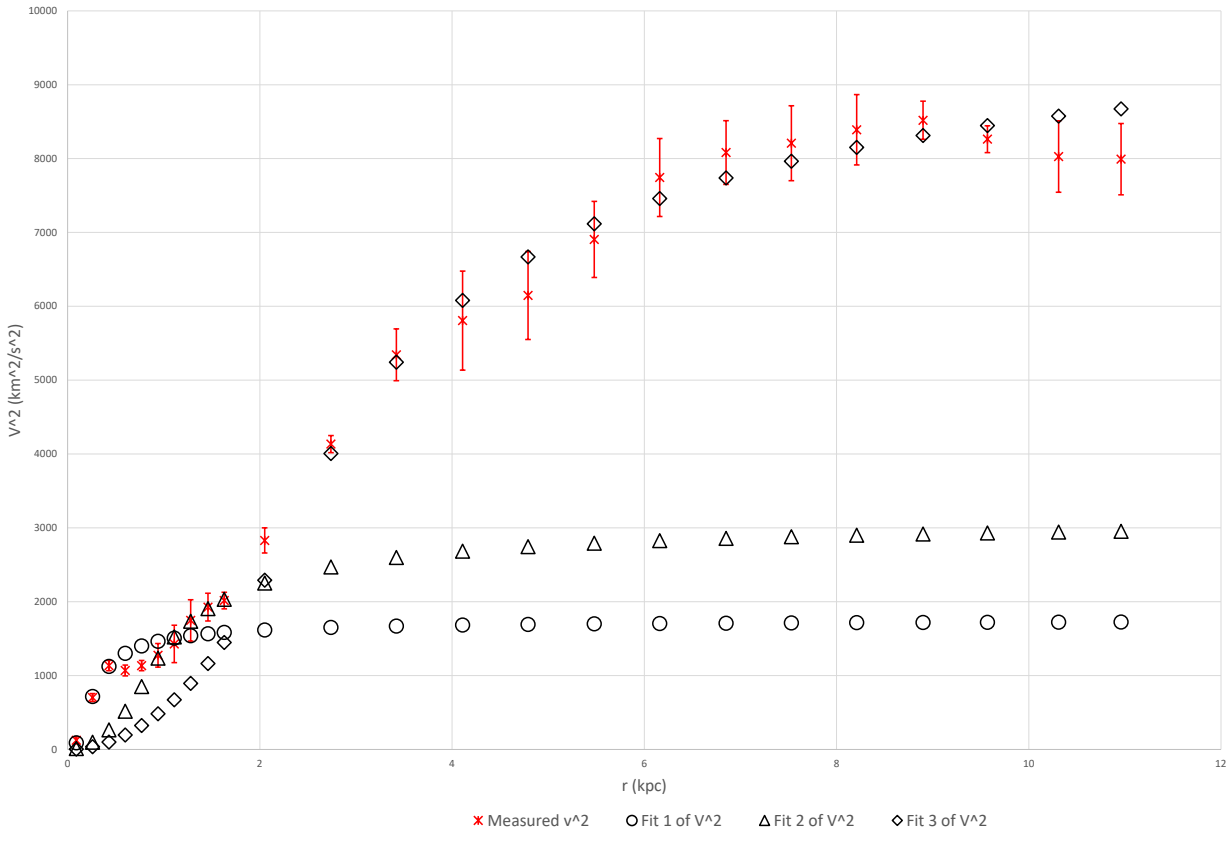


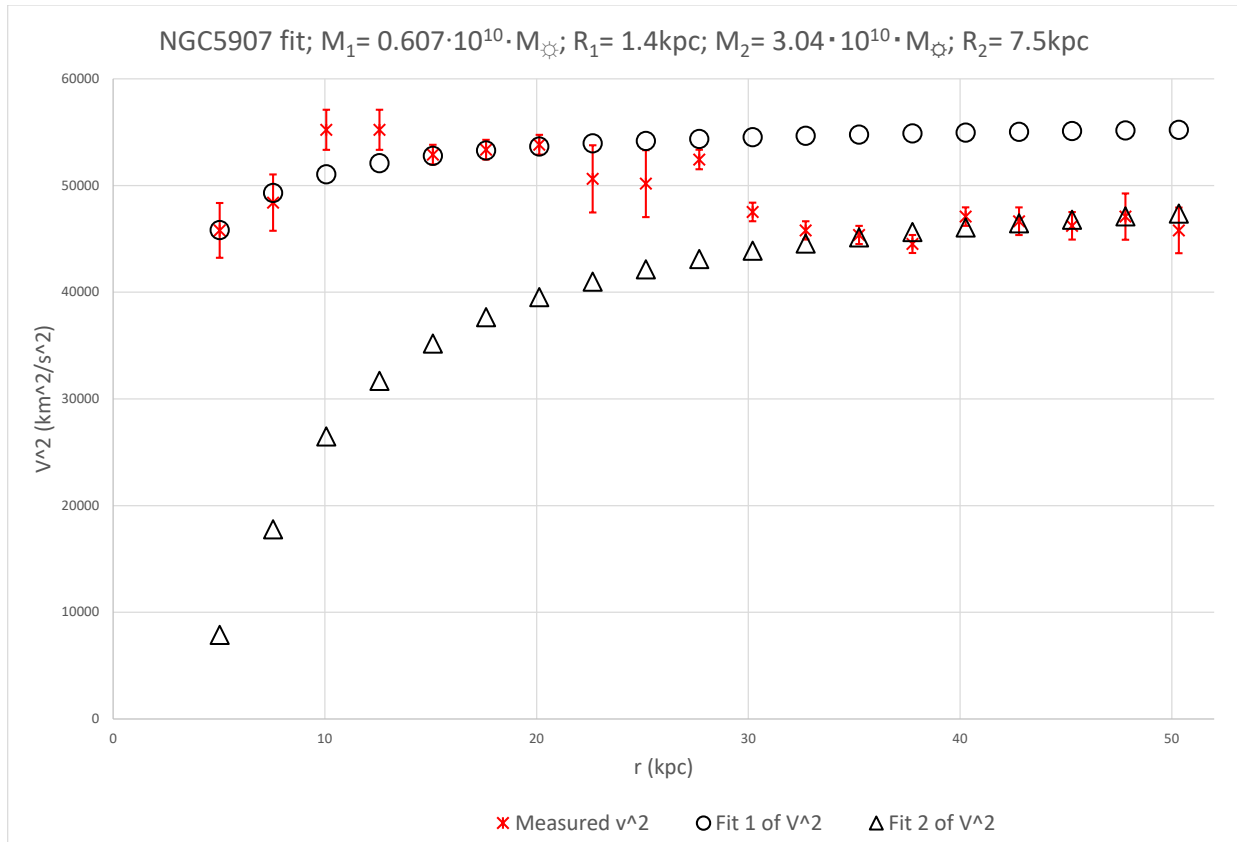


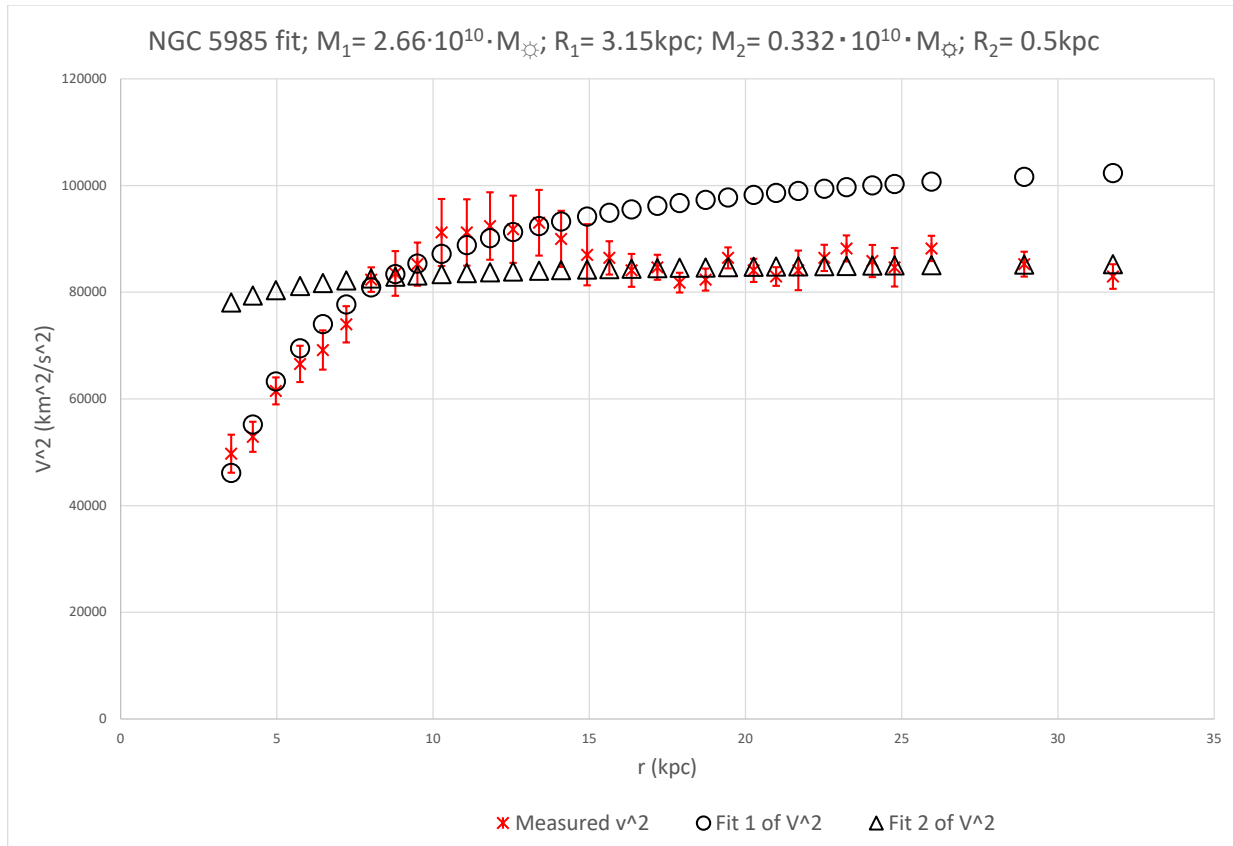
NGC5371 fit; $M_1 = 0.00357 \cdot 10^{10} \cdot M_{\odot}$; $R_1 = 0.01 \text{ kpc}$; $M_2 = 1.61 \cdot 10^{10} \cdot M_{\odot}$; $R_2 = 3.2 \text{ kpc}$;
 $M_3 = 2.67 \cdot 10^{10} \cdot M_{\odot}$; $R_3 = 7 \text{ kpc}$

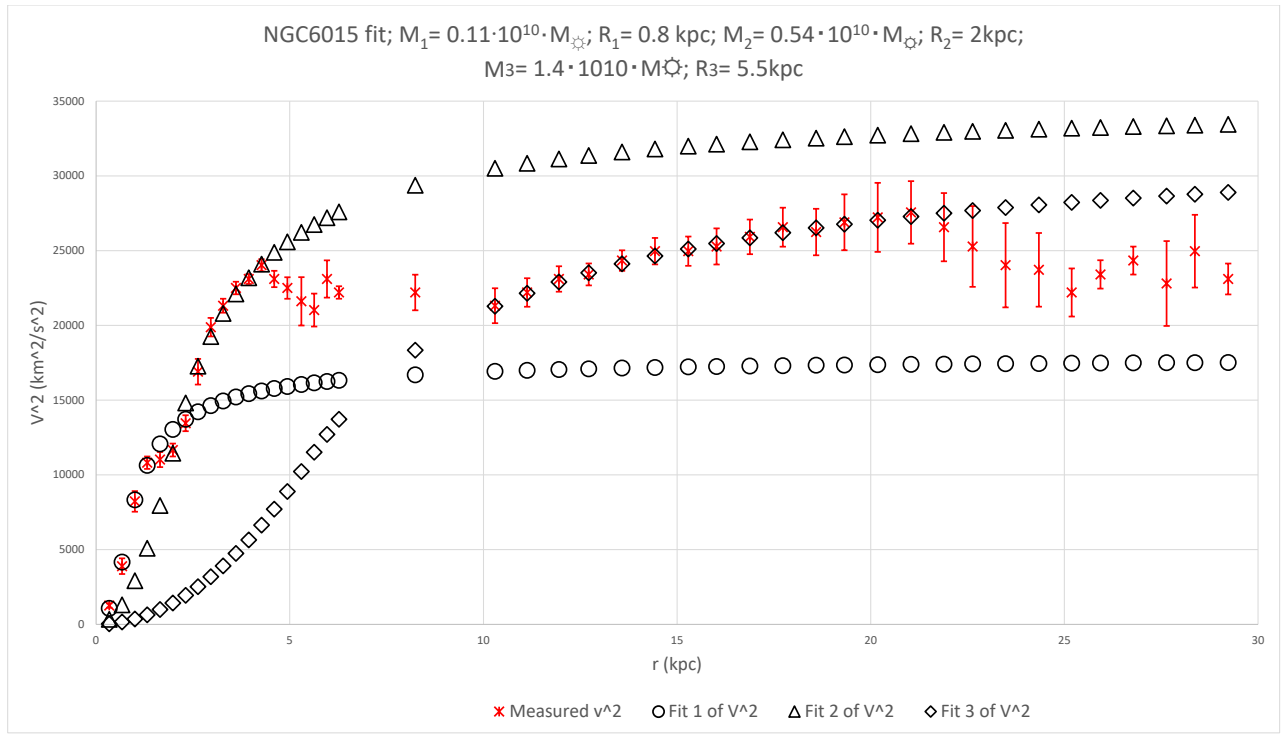


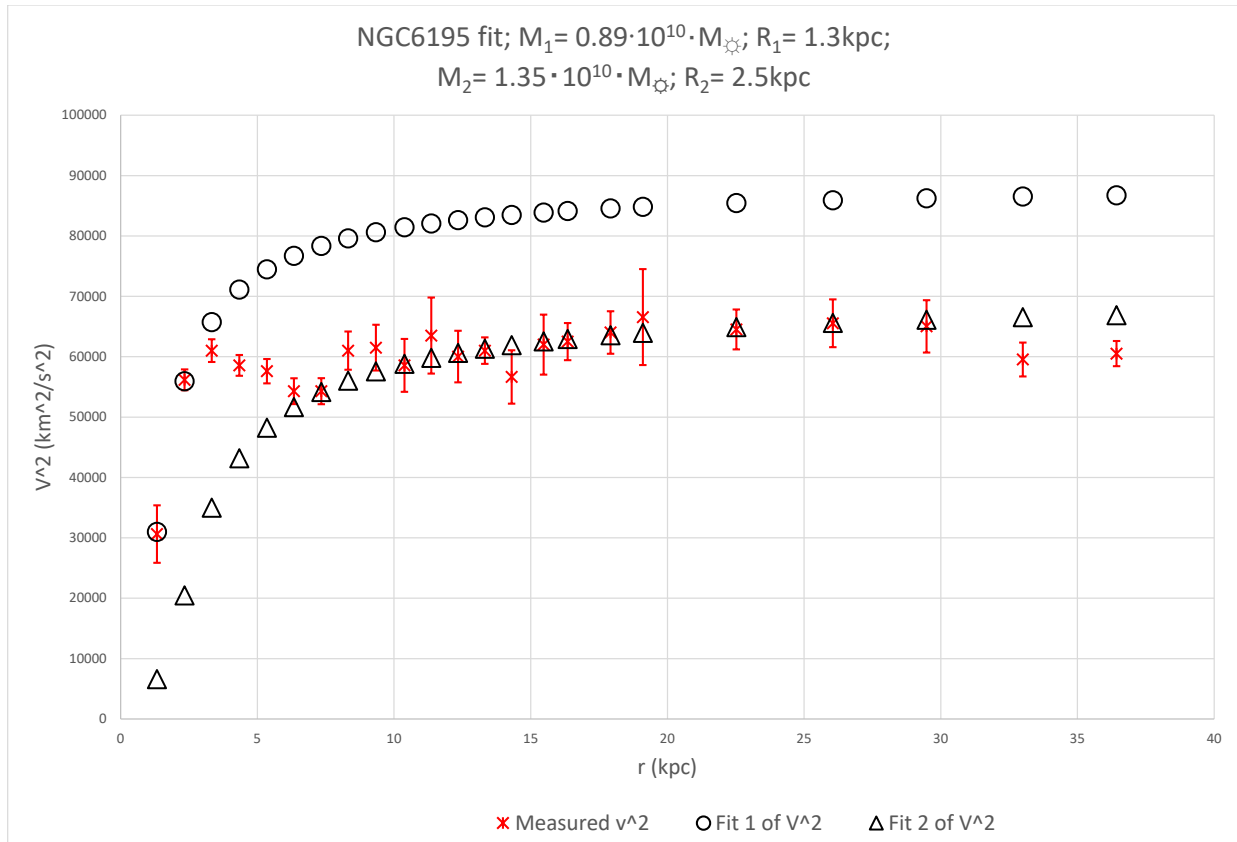
NGC5585 fit; $M_1 = 0.0031 \cdot 10^{10} \cdot M_{\odot}$; $R_1 = 0.23$ kpc; $M_2 = 0.0204 \cdot 10^{10} \cdot M_{\odot}$; $R_2 = 0.85$ kpc;
 $M_3 = 0.197 \cdot 10^{10} \cdot M_{\odot}$; $R_3 = 2.5$ kpc



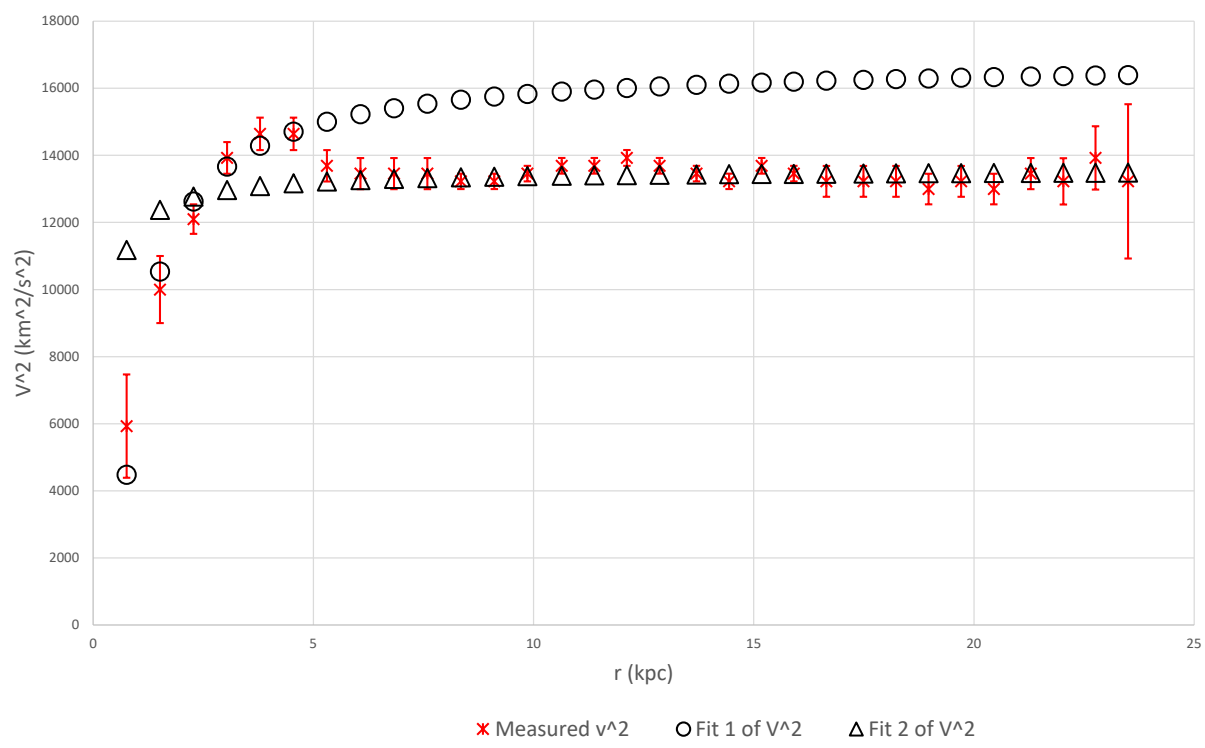


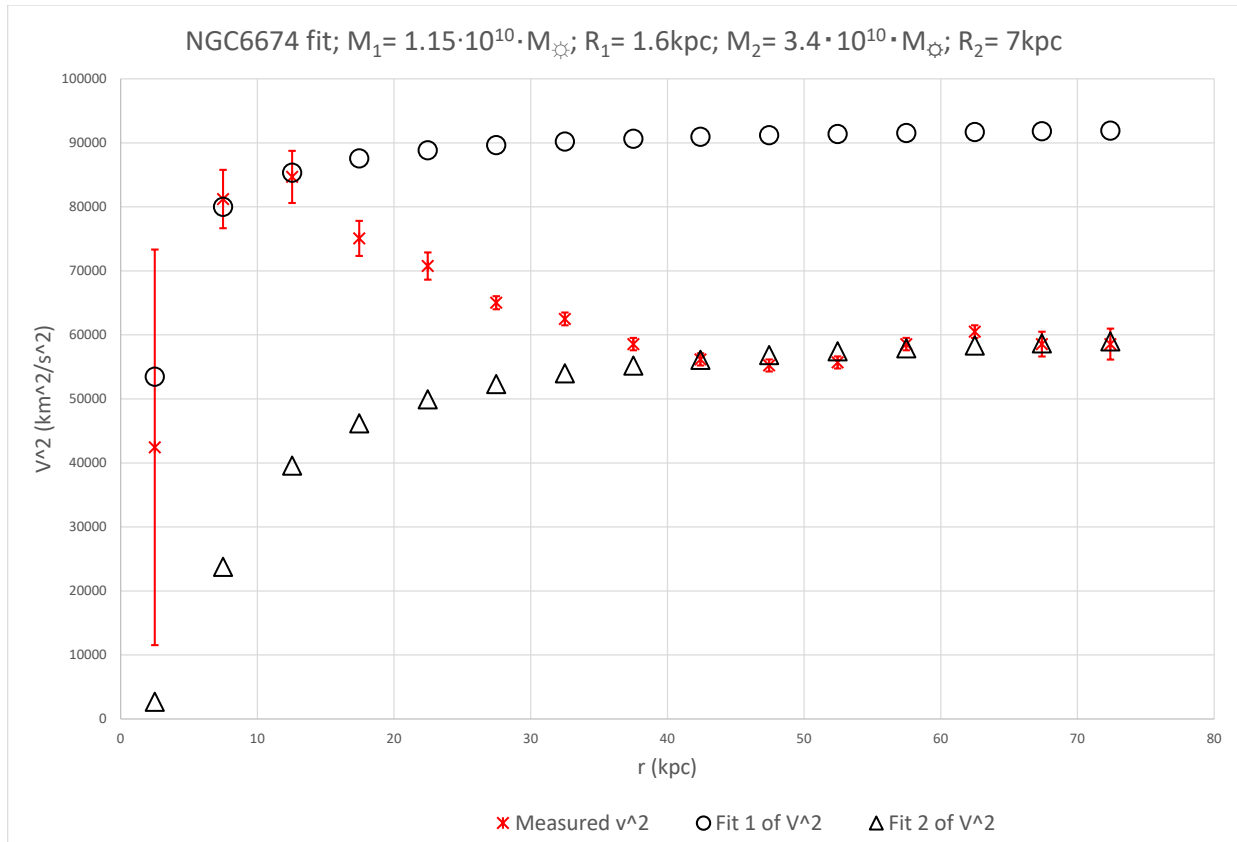


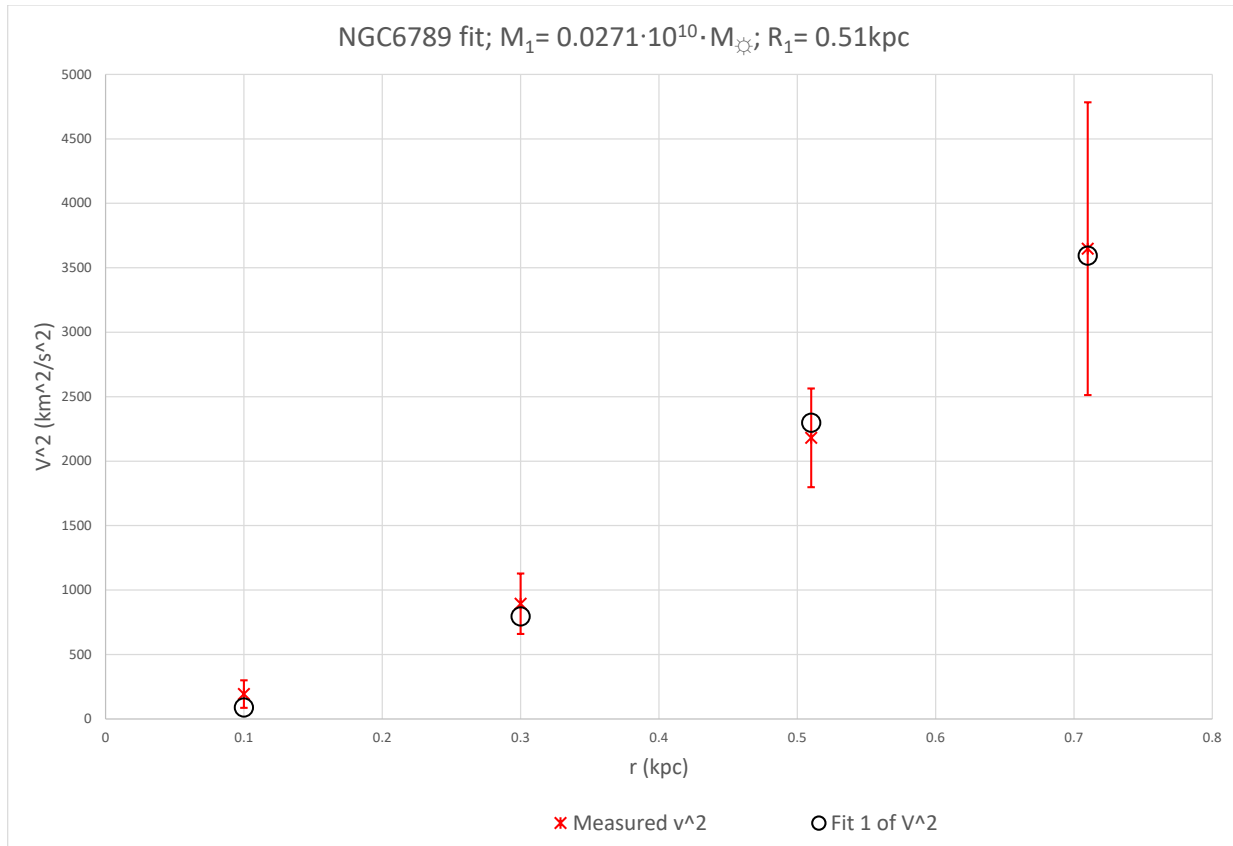




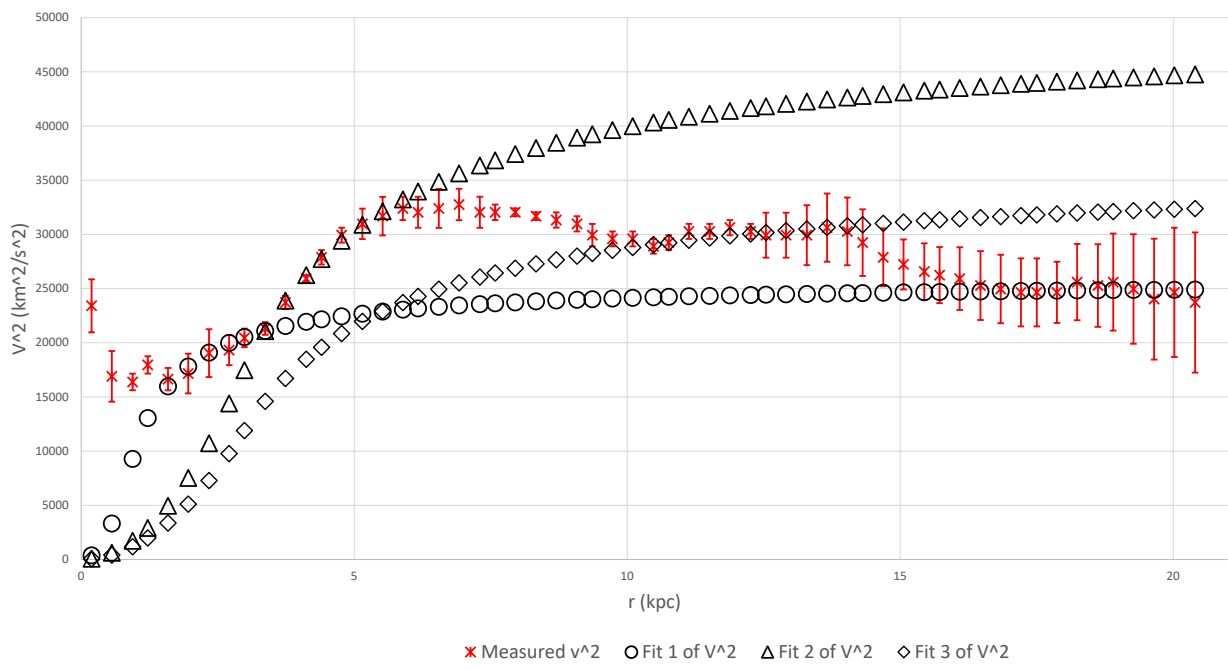
NGC6503 fit; $M_1 = 0.11 \cdot 10^{10} \cdot M_{\odot}$; $R_1 = 0.85 \text{ kpc}$;
 $M_2 = 0.0209 \cdot 10^{10} \cdot M_{\odot}$; $R_2 = 0.2 \text{ kpc}$

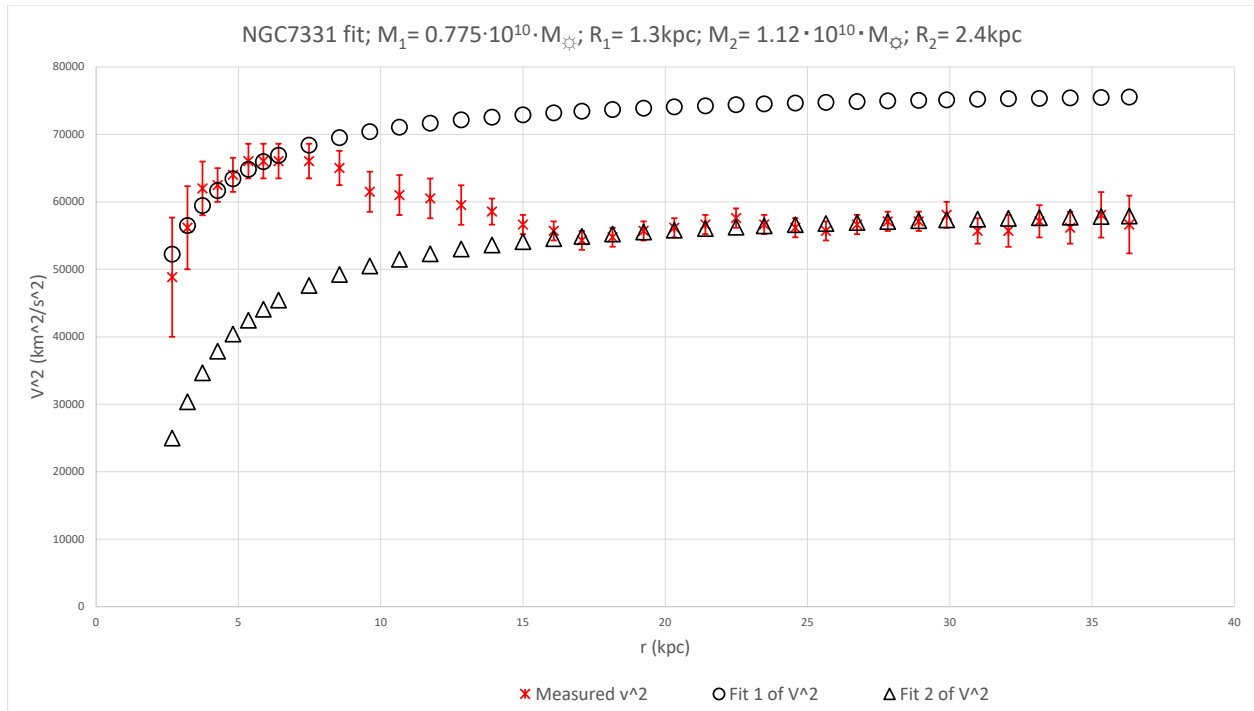


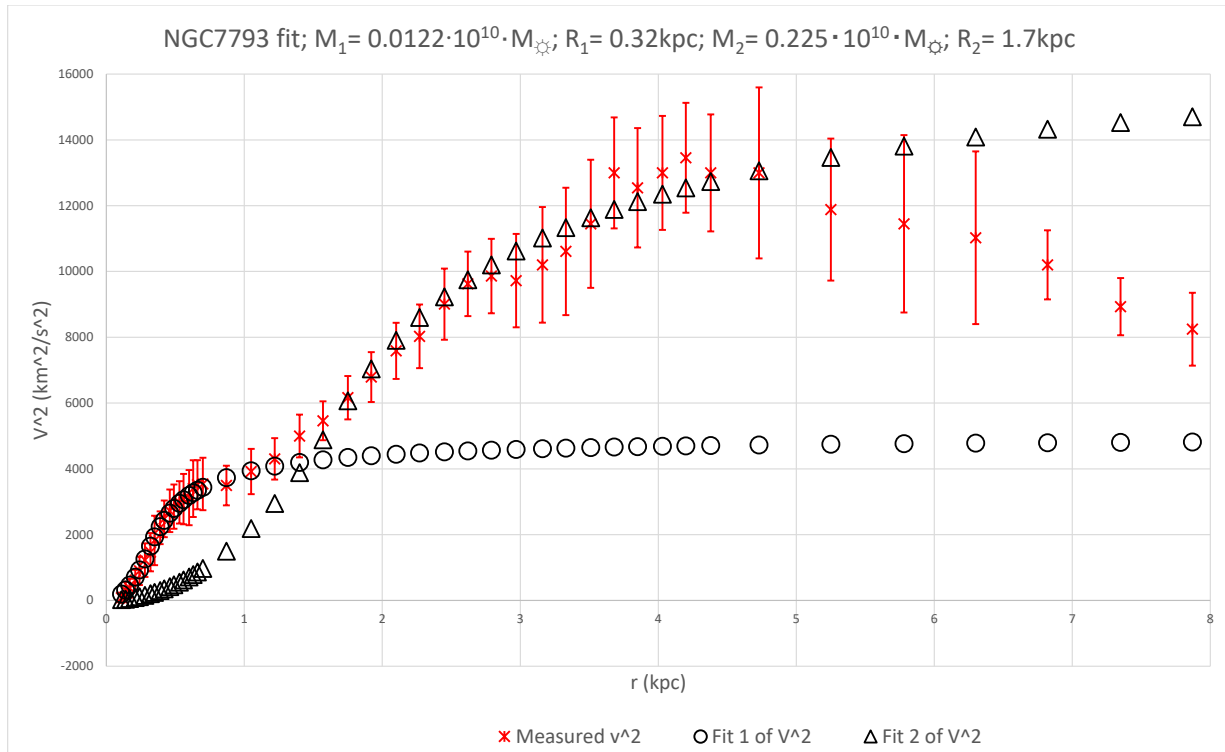


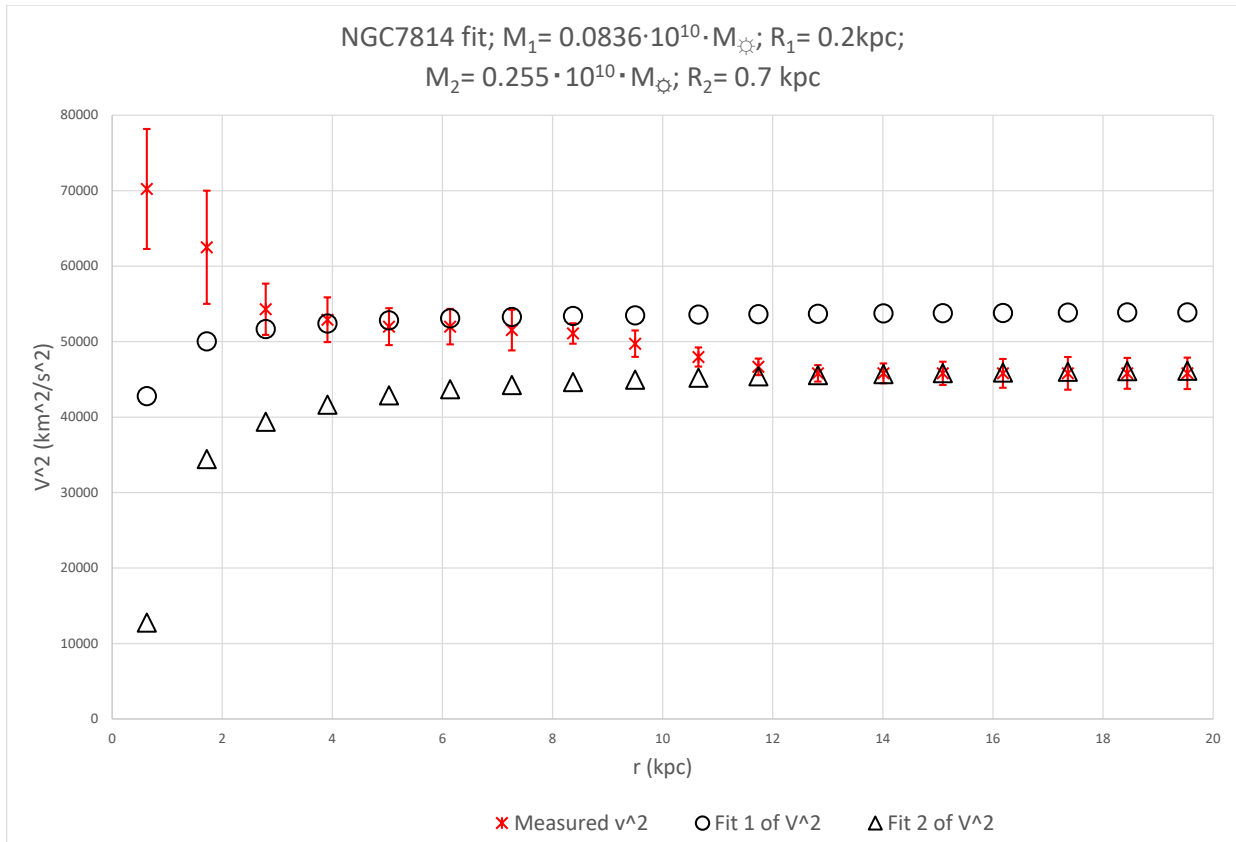


NGC6946 fit; $M_1 = 0.178 \cdot 10^{10} \cdot M_{\odot}$; $R_1 = 0.9 \text{ kpc}$; $M_2 = 1.105 \cdot 10^{10} \cdot M_{\odot}$; $R_2 = 2.9 \text{ kpc}$;
 $M_3 = 0.83 \cdot 10^{10} \cdot M_{\odot}$; $R_3 = 3 \text{ kpc}$

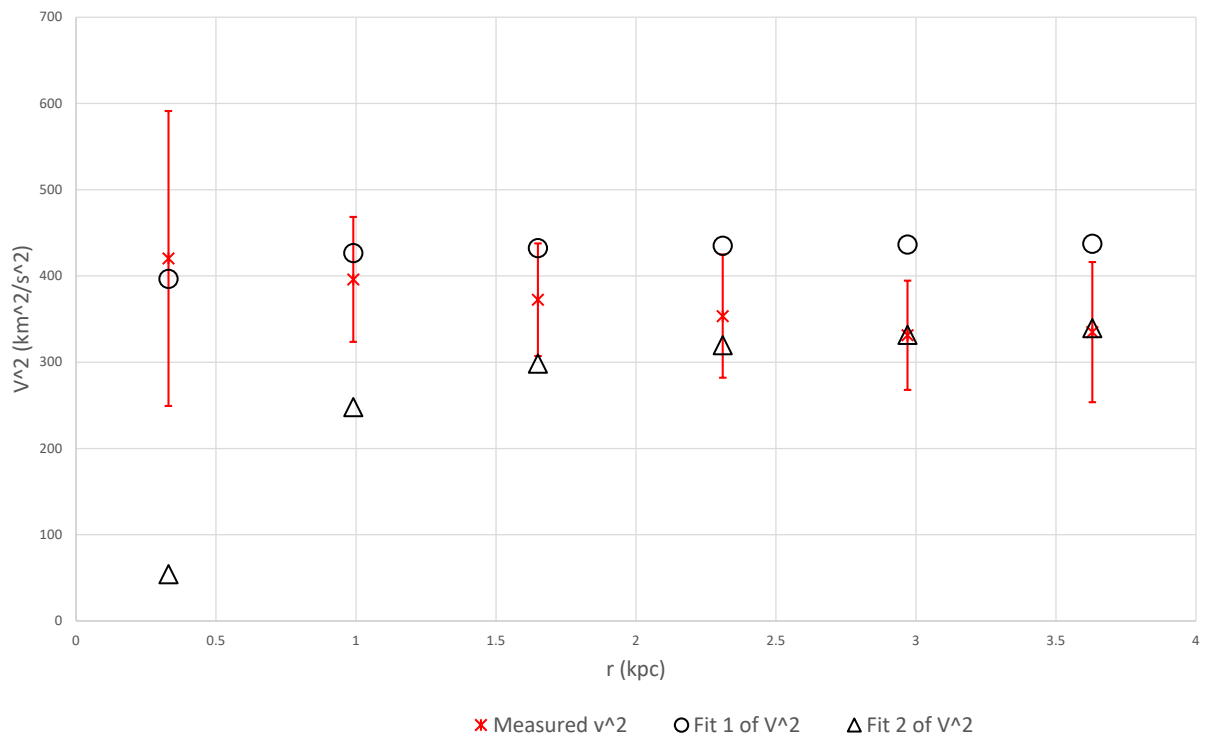


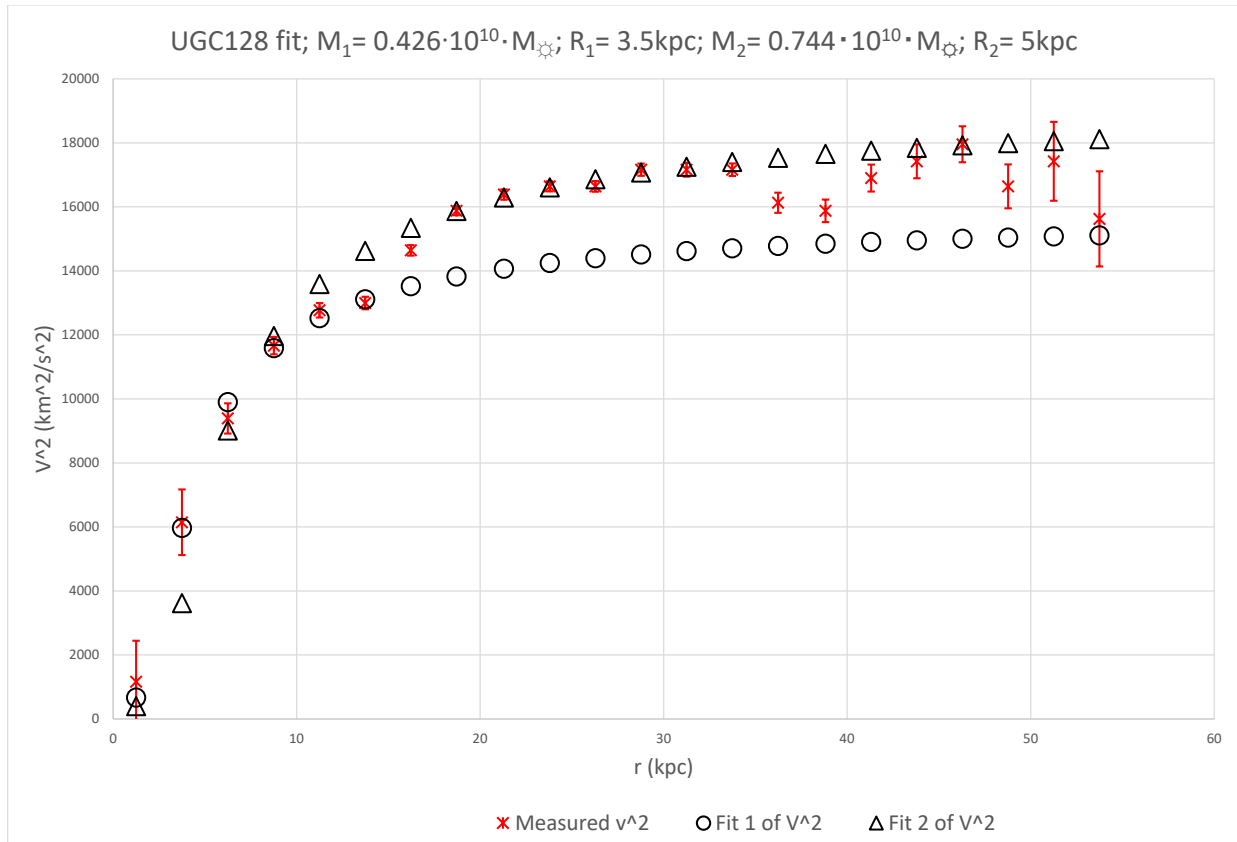


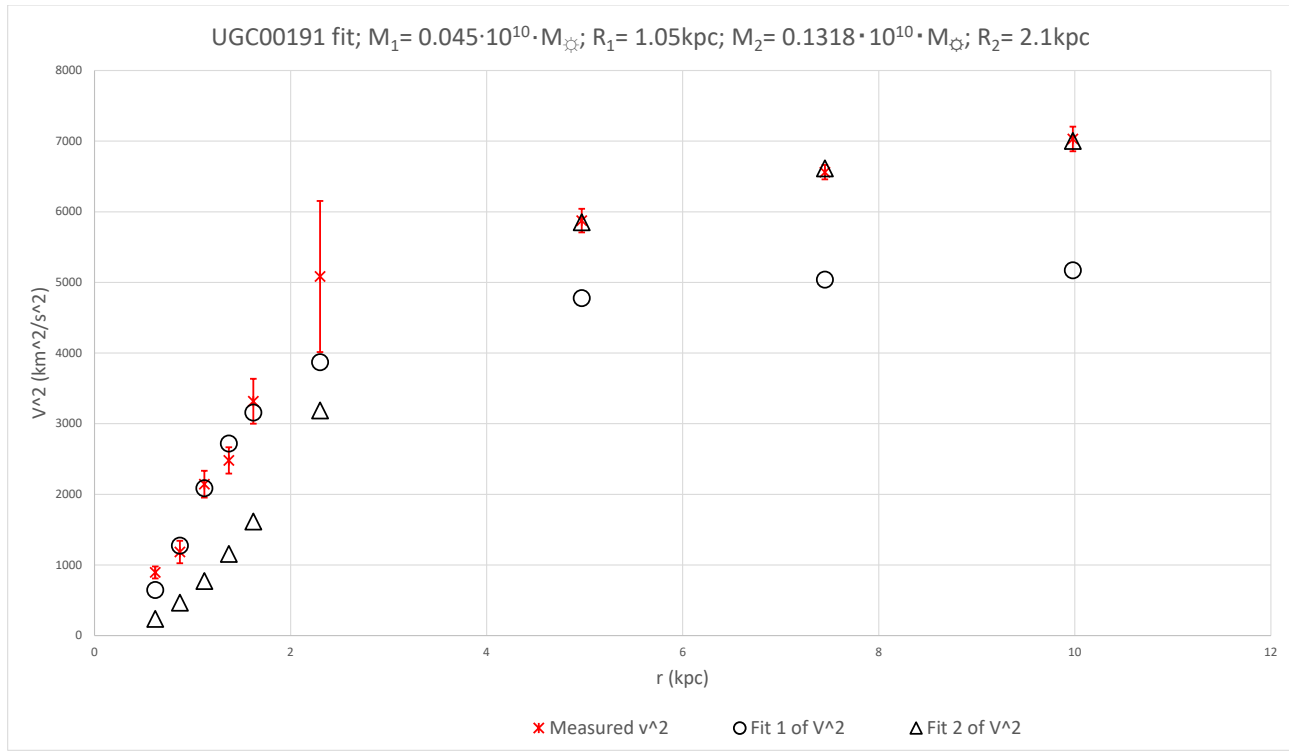


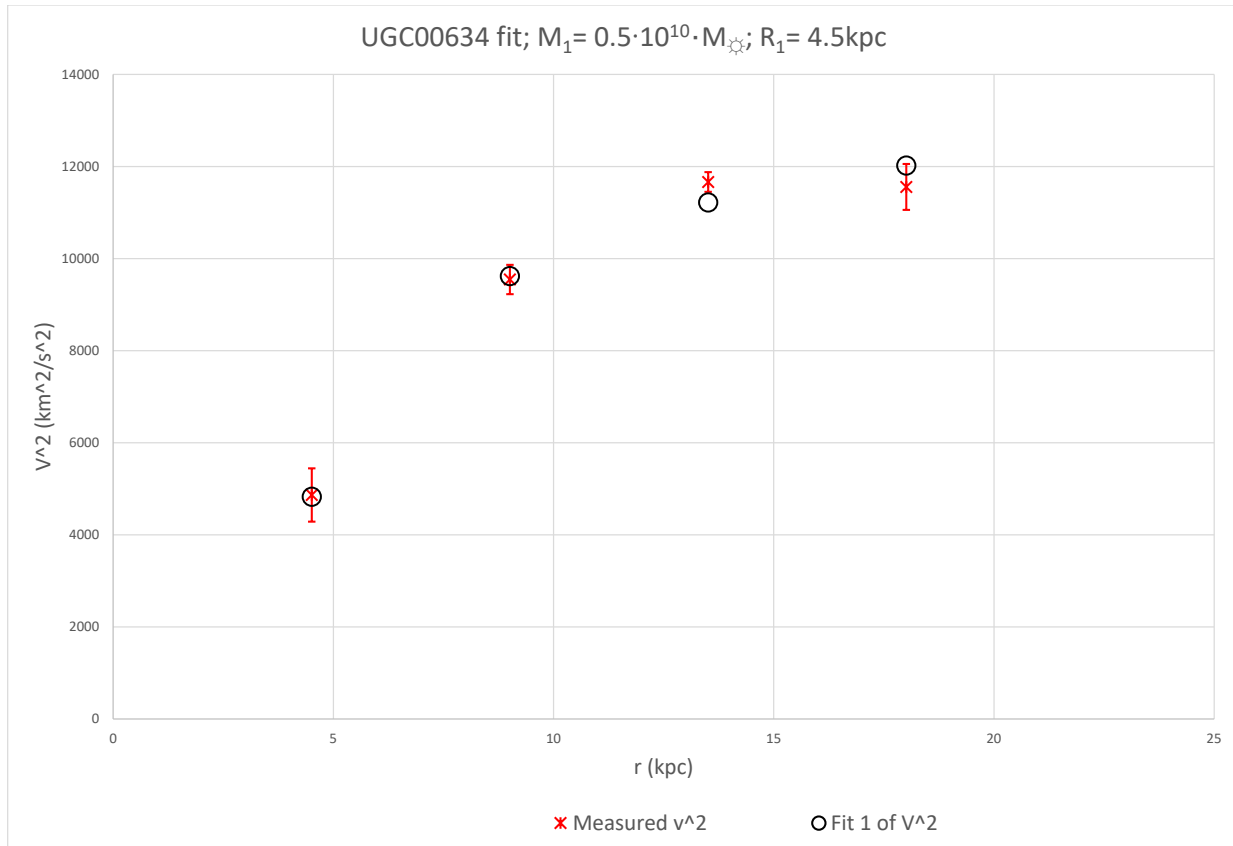


PGC51017 fit; $M_1 = 0.00017 \cdot 10^{10} \cdot M_{\odot}$; $R_1 = 0.05 \text{ kpc}$;
 $M_2 = 0.00144 \cdot 10^{10} \cdot M_{\odot}$; $R_2 = 0.5 \text{ kpc}$

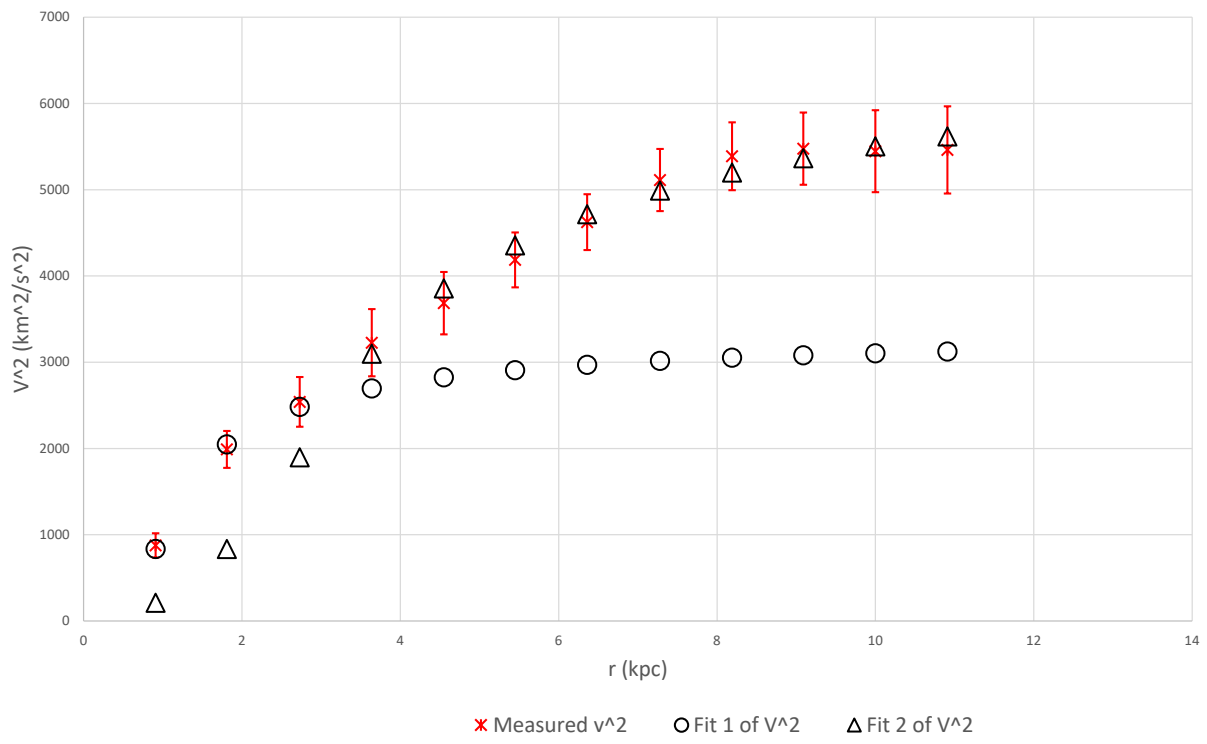




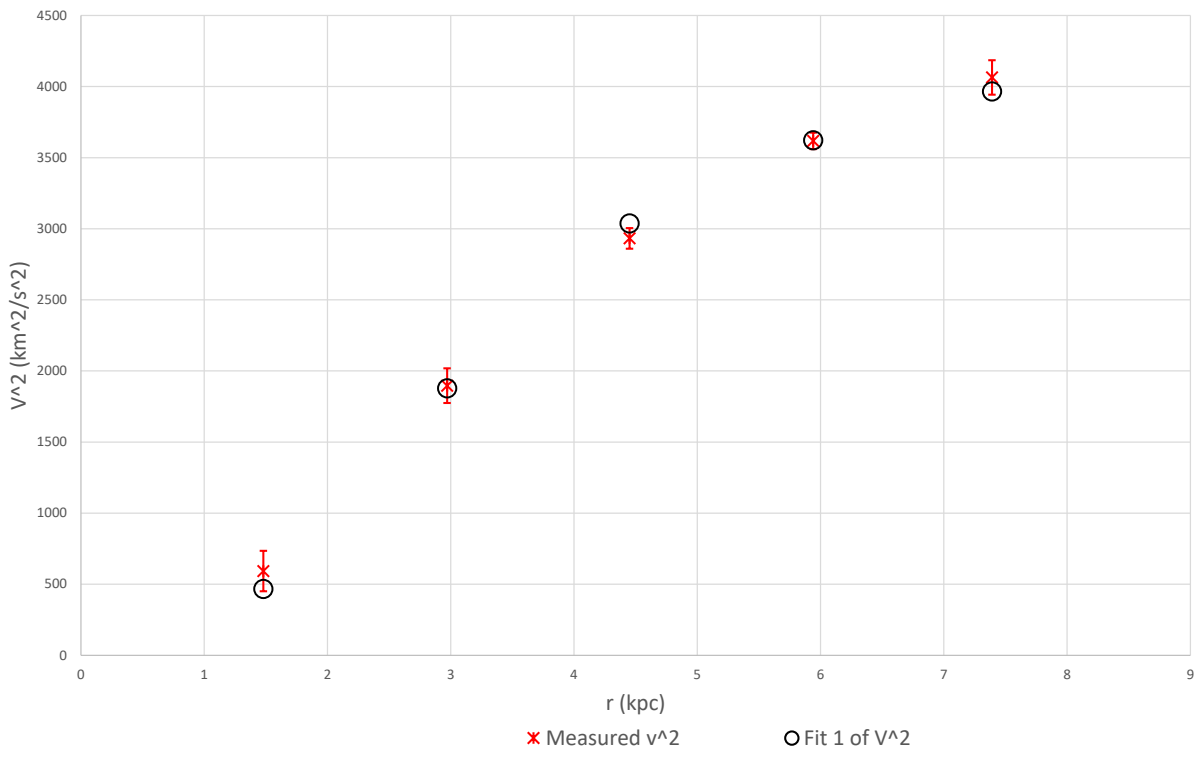




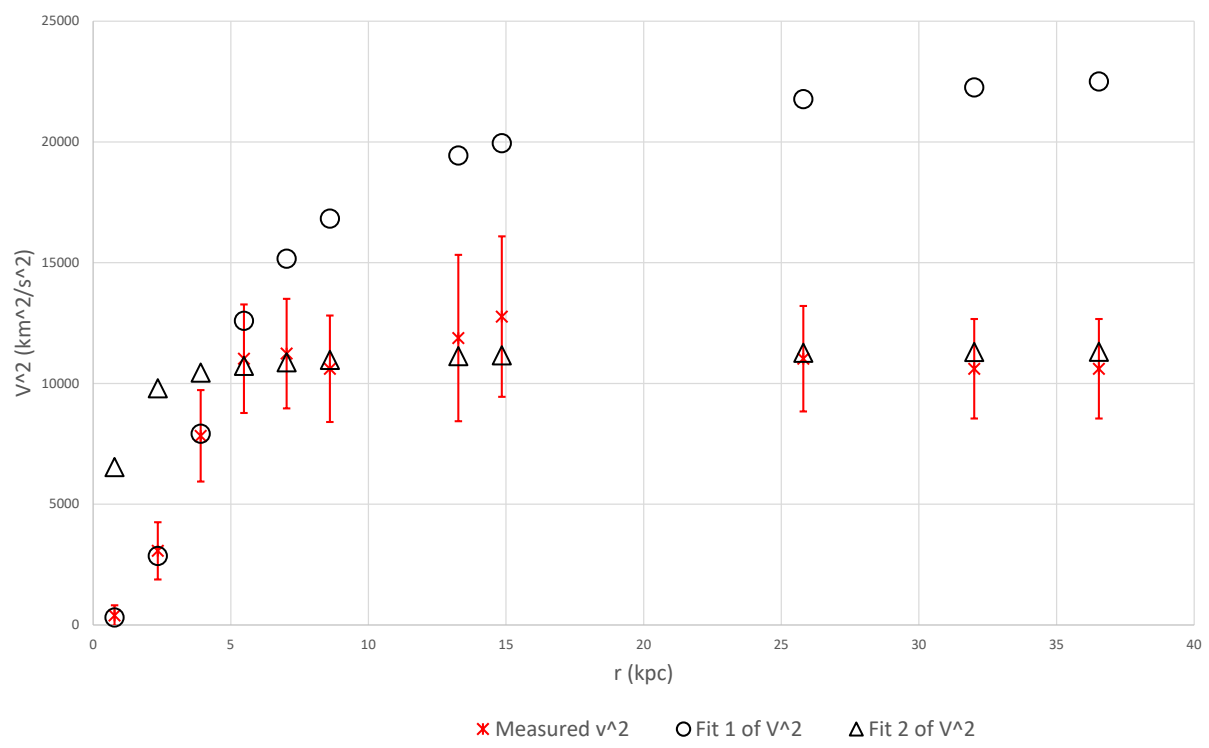
UGC00731 fit; $M_1 = 0.027 \cdot 10^{10} \cdot M_{\odot}$; $R_1 = 1.05 \text{ kpc}$;
 $M_2 = 0.159 \cdot 10^{10} \cdot M_{\odot}$; $R_2 = 3 \text{ kpc}$

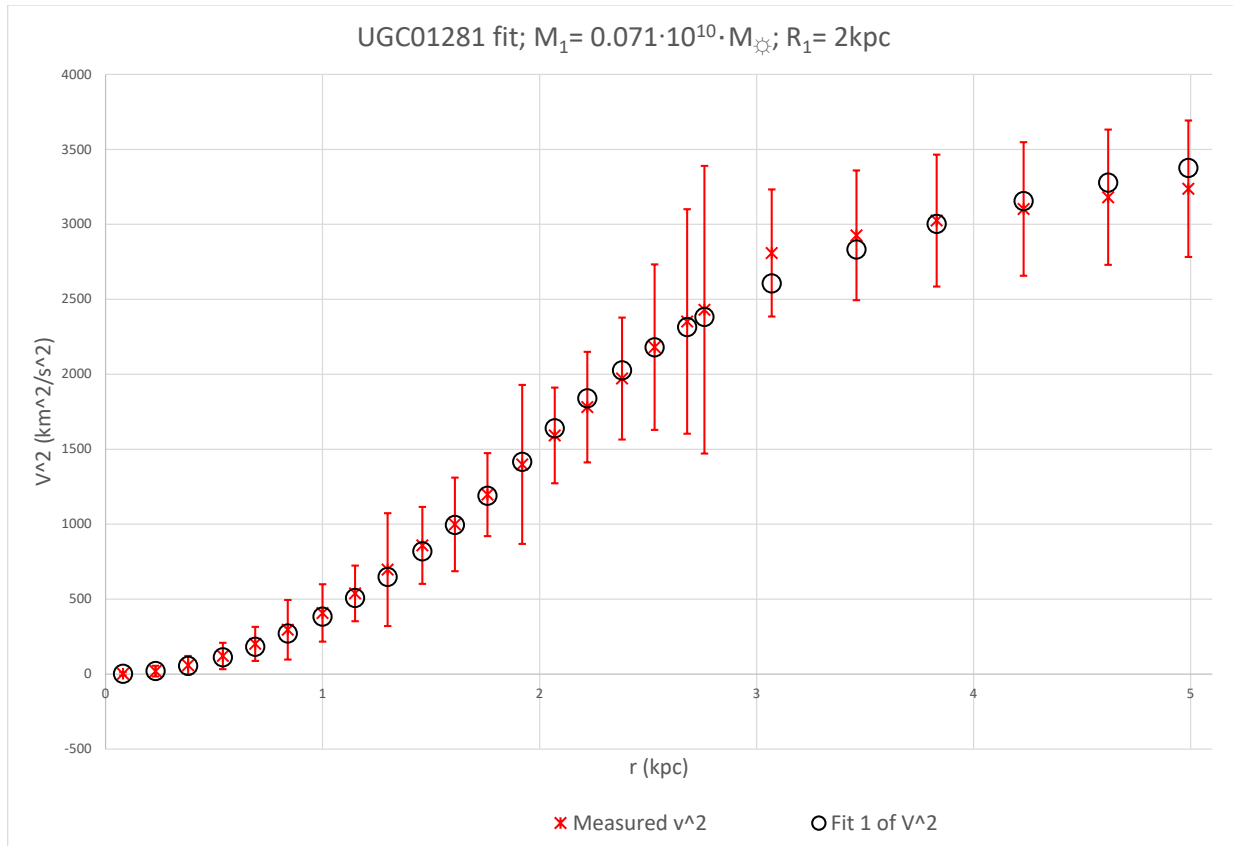


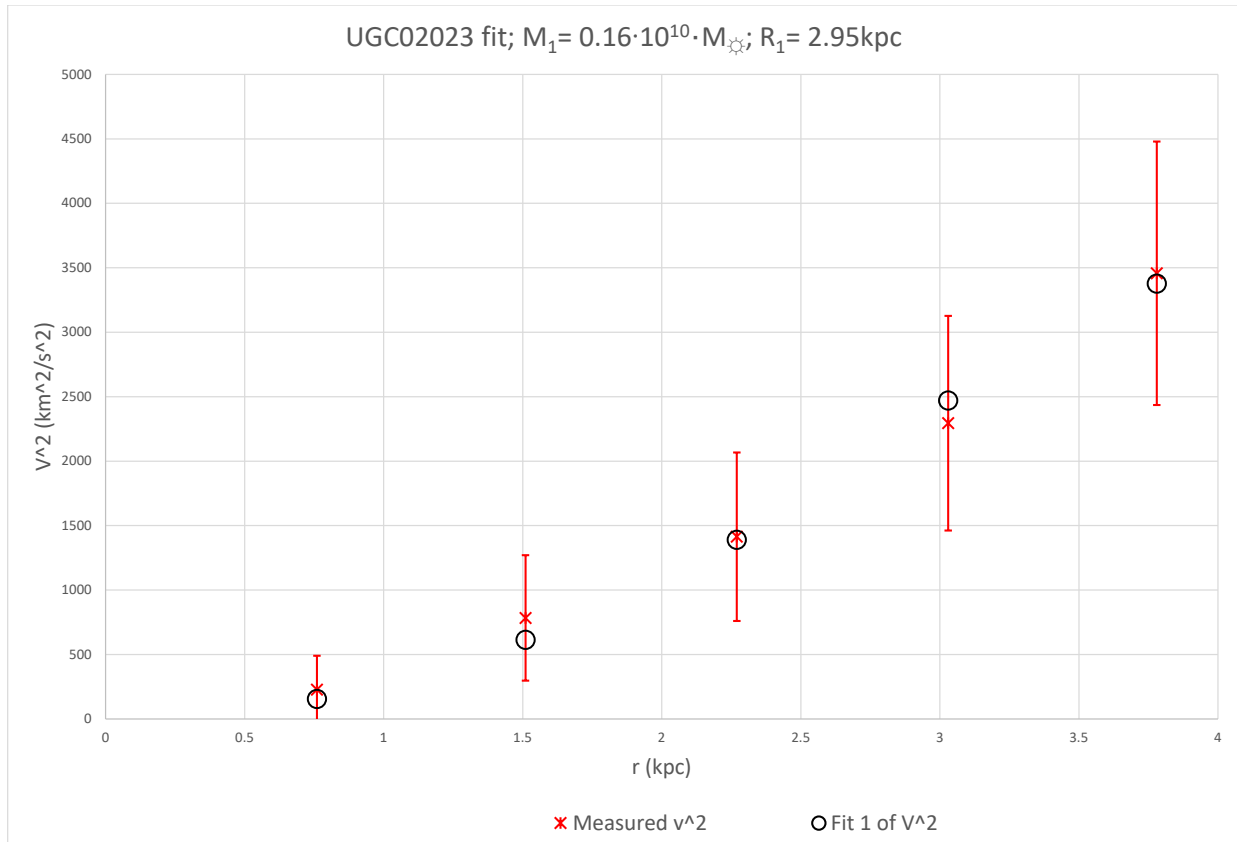
UGC00891 fit; $M_1 = 0.12 \cdot 10^{10} \cdot M_{\odot}$; $R_1 = 2.9 \text{ kpc}$



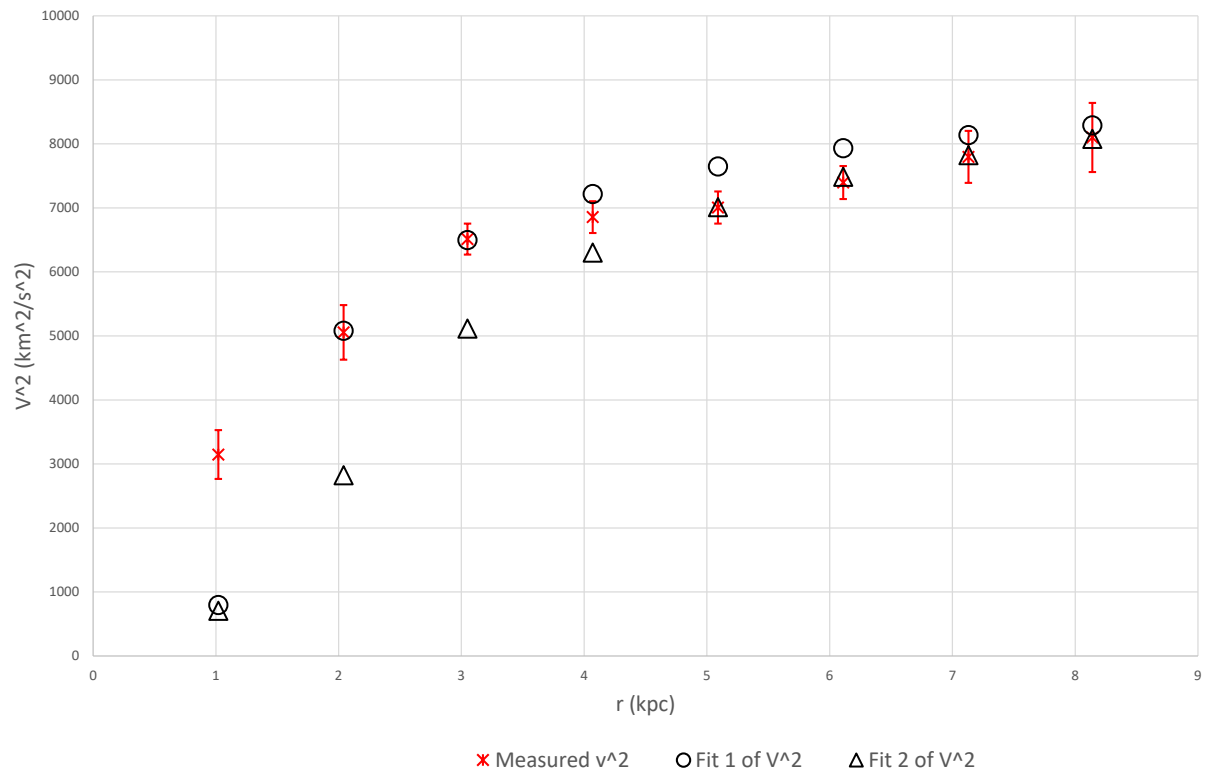
UGC01230 fit; $M_1 = 0.738 \cdot 10^{10} \cdot M_{\odot}$; $R_1 = 3.95 \text{ kpc}$;
 $M_2 = 0.044 \cdot 10^{10} \cdot M_{\odot}$; $R_2 = 0.5 \text{ kpc}$



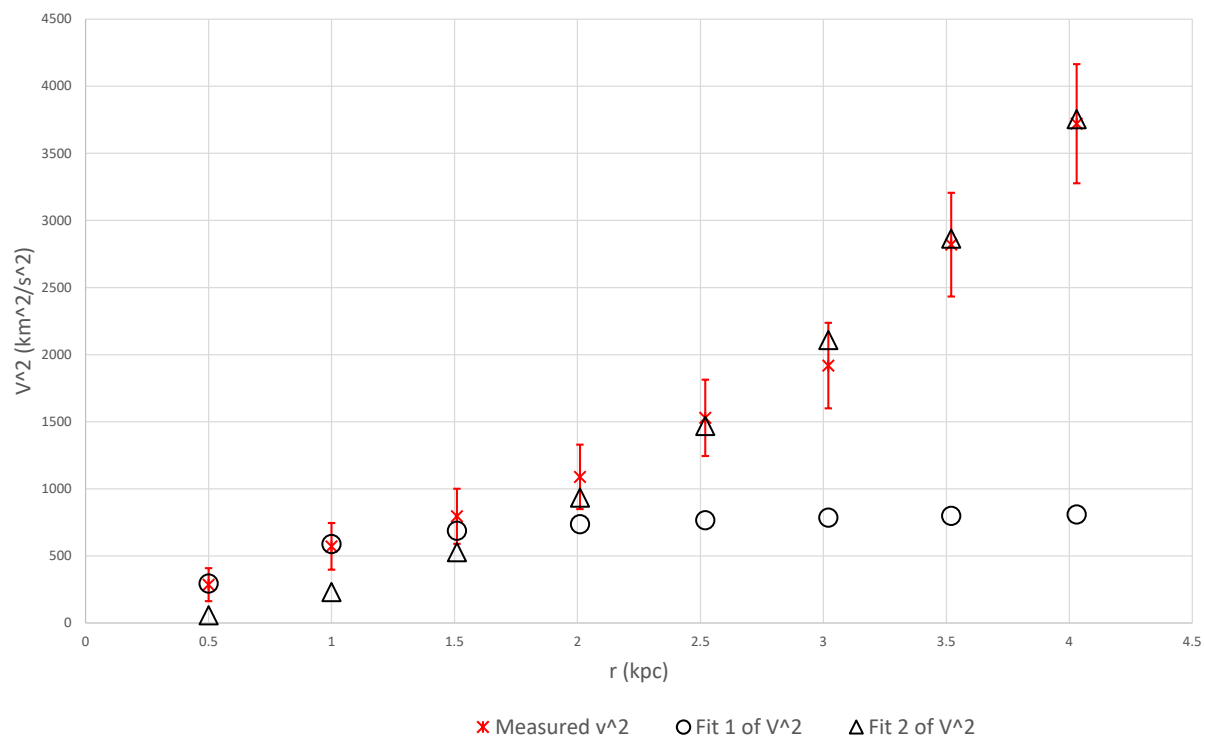


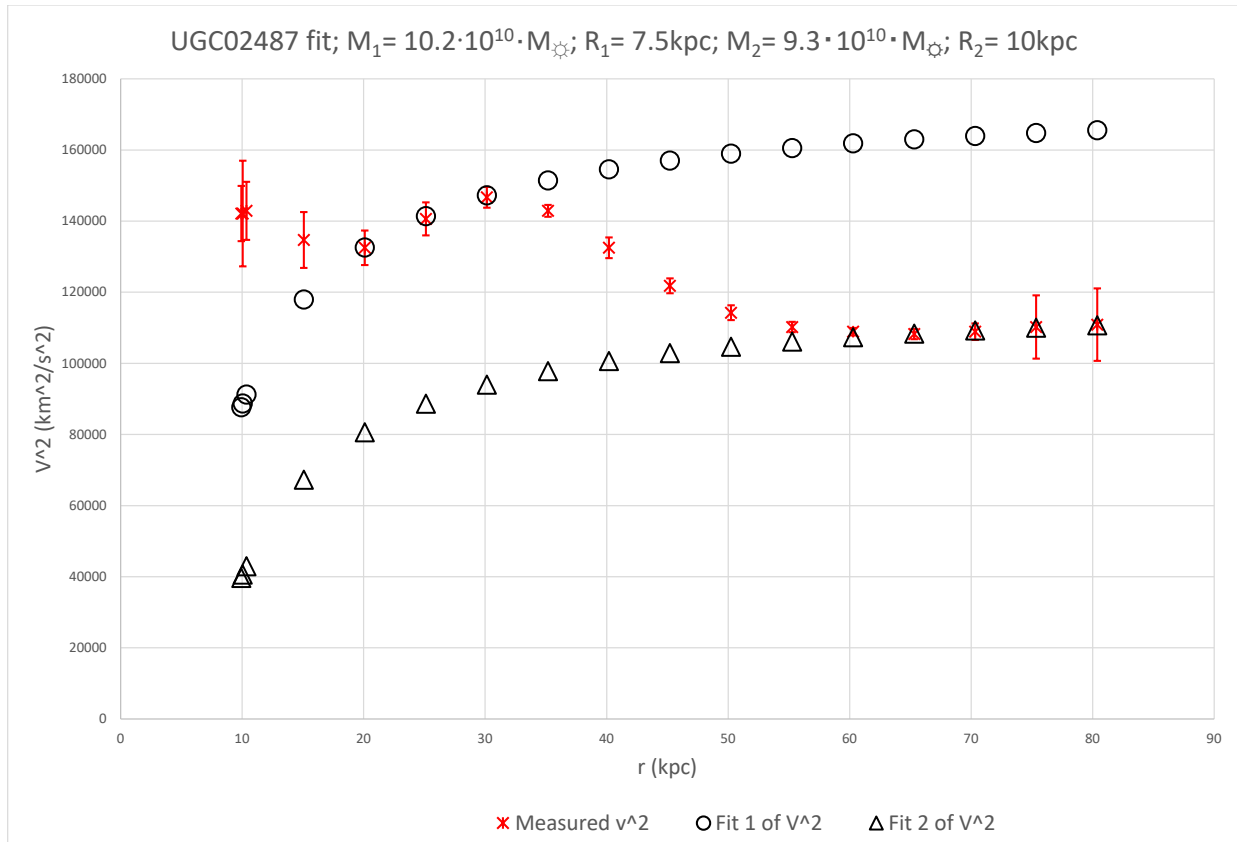


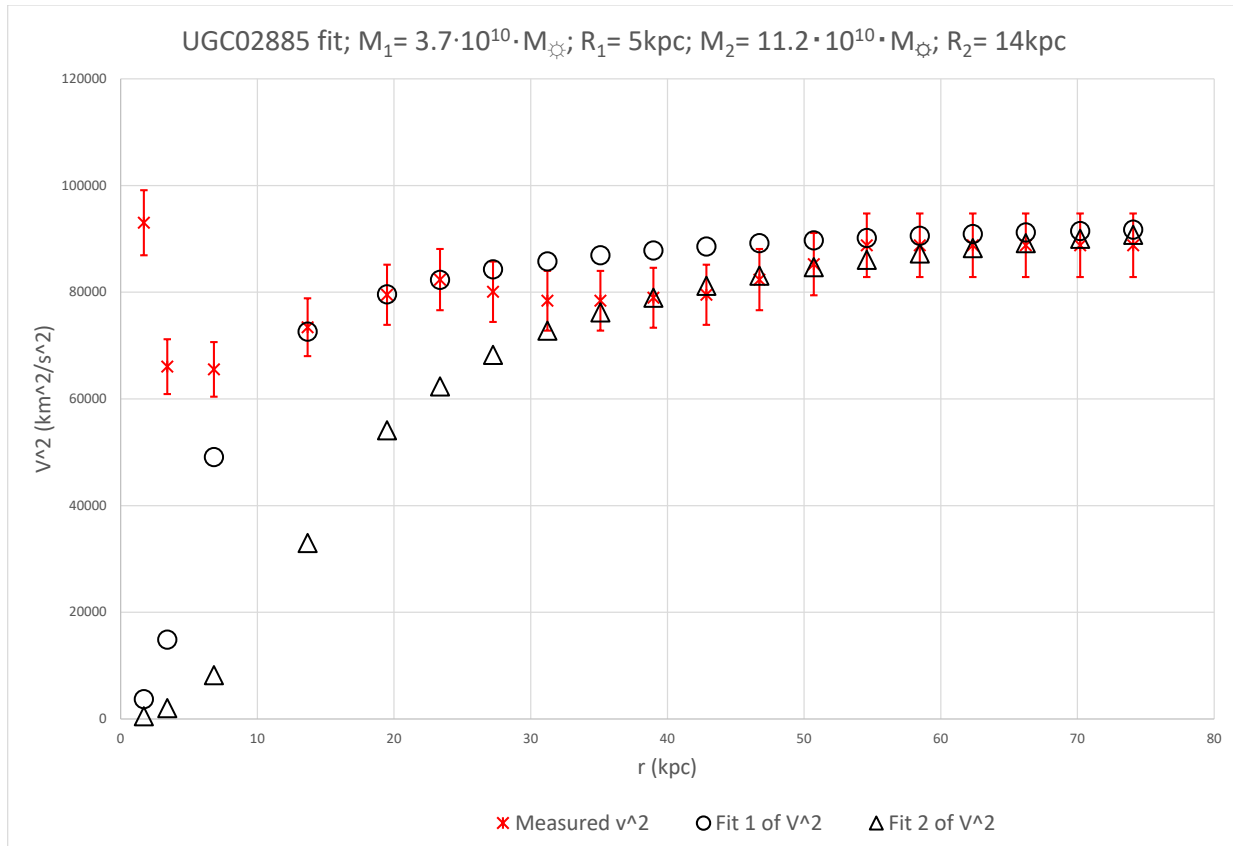
UGC02259 fit; $M_1 = 0.101 \cdot 10^{10} \cdot M_{\odot}$; $R_1 = 1.4 \text{ kpc}$; $M_2 = 0.167 \cdot 10^{10} \cdot M_{\odot}$; $R_2 = 2.2 \text{ kpc}$

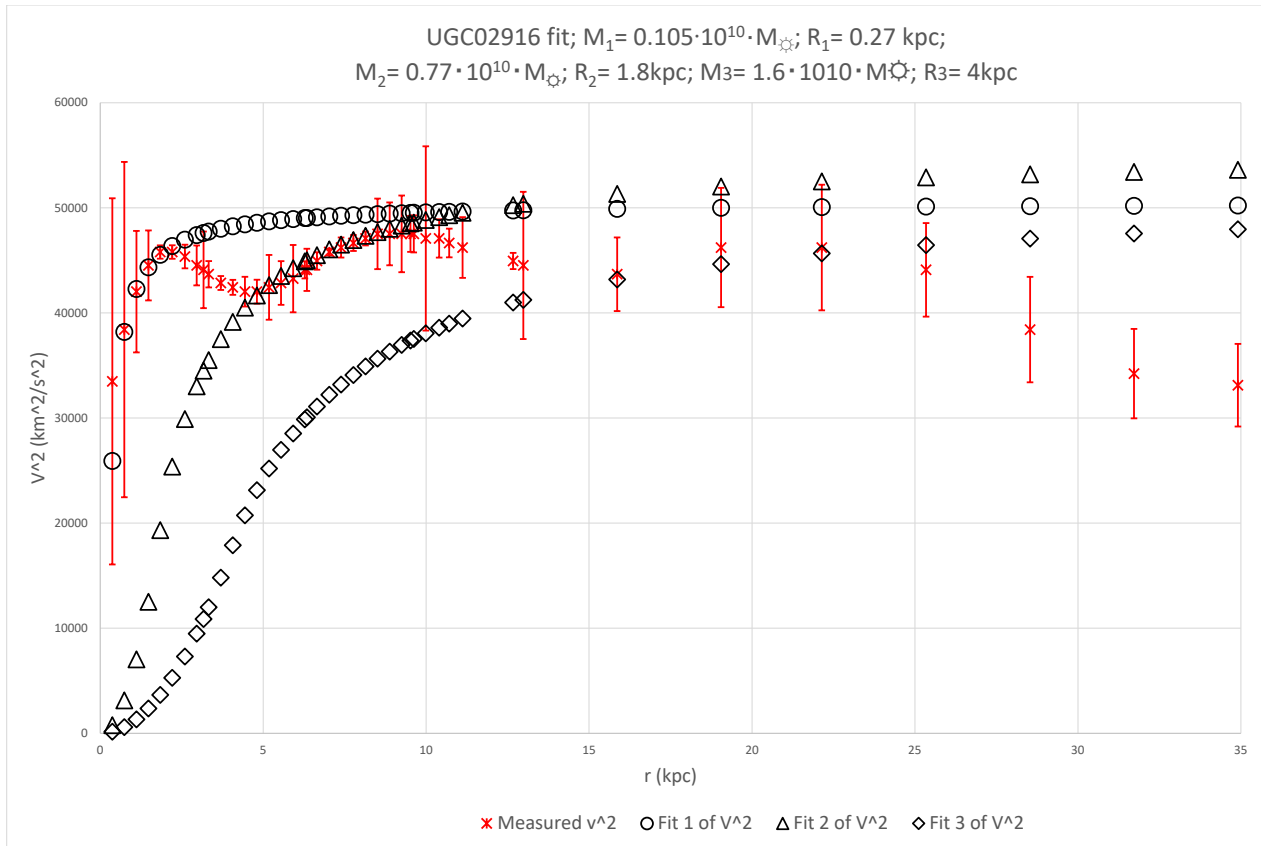


UGC02455 fit; $M_1 = 0.0034 \cdot 10^{10} \cdot M_{\odot}$; $R_1 = 0.5 \text{ kpc}$;
 $M_2 = 0.342 \cdot 10^{10} \cdot M_{\odot}$; $R_2 = 4 \text{ kpc}$

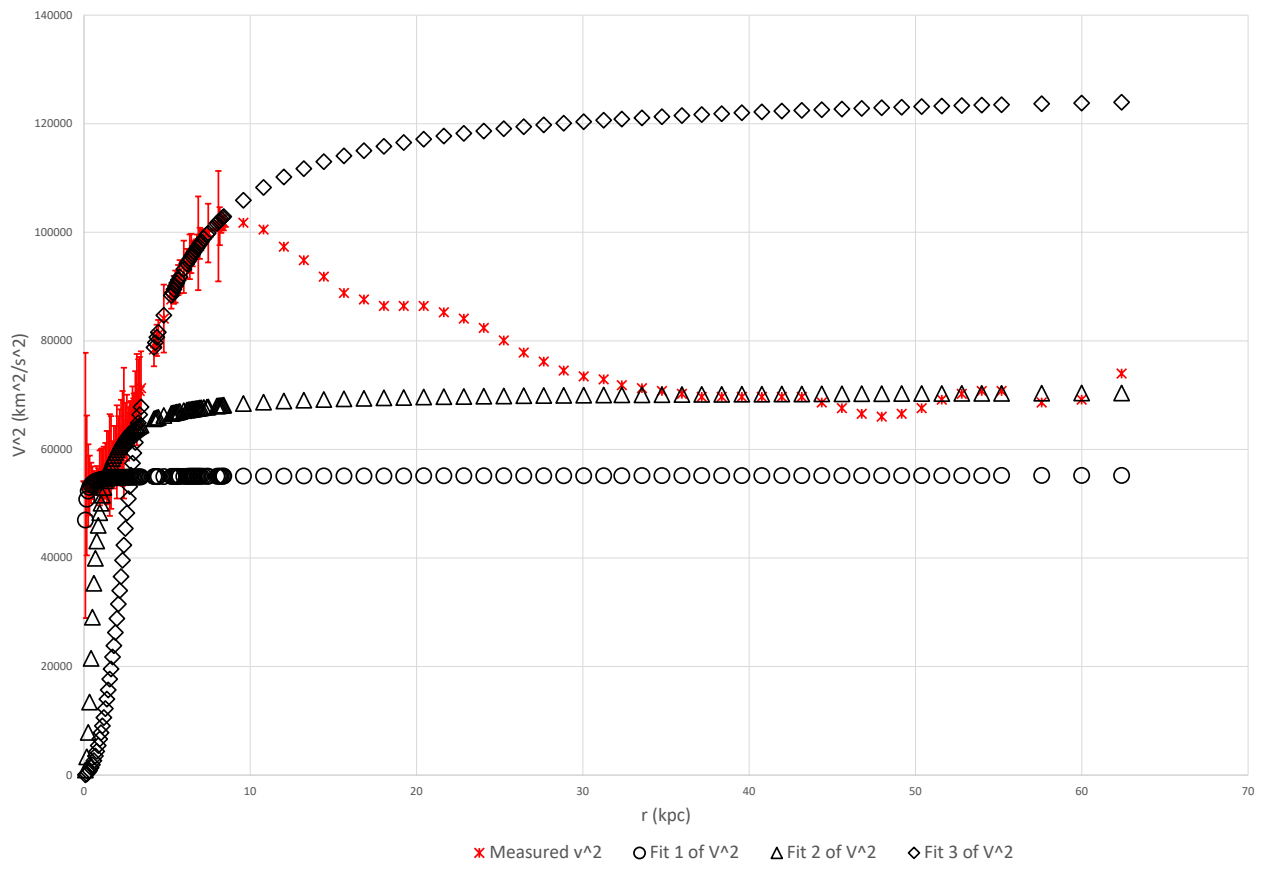


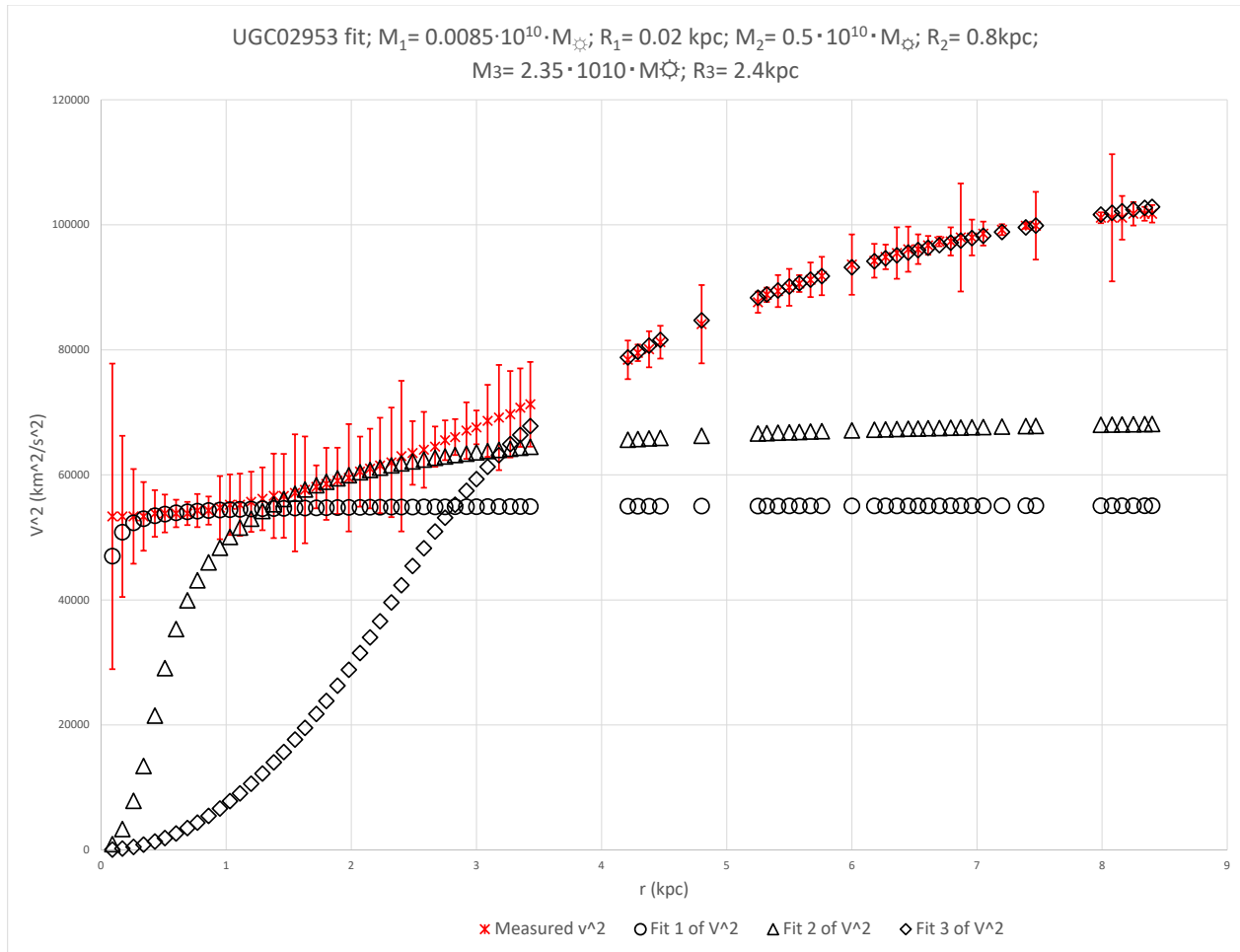


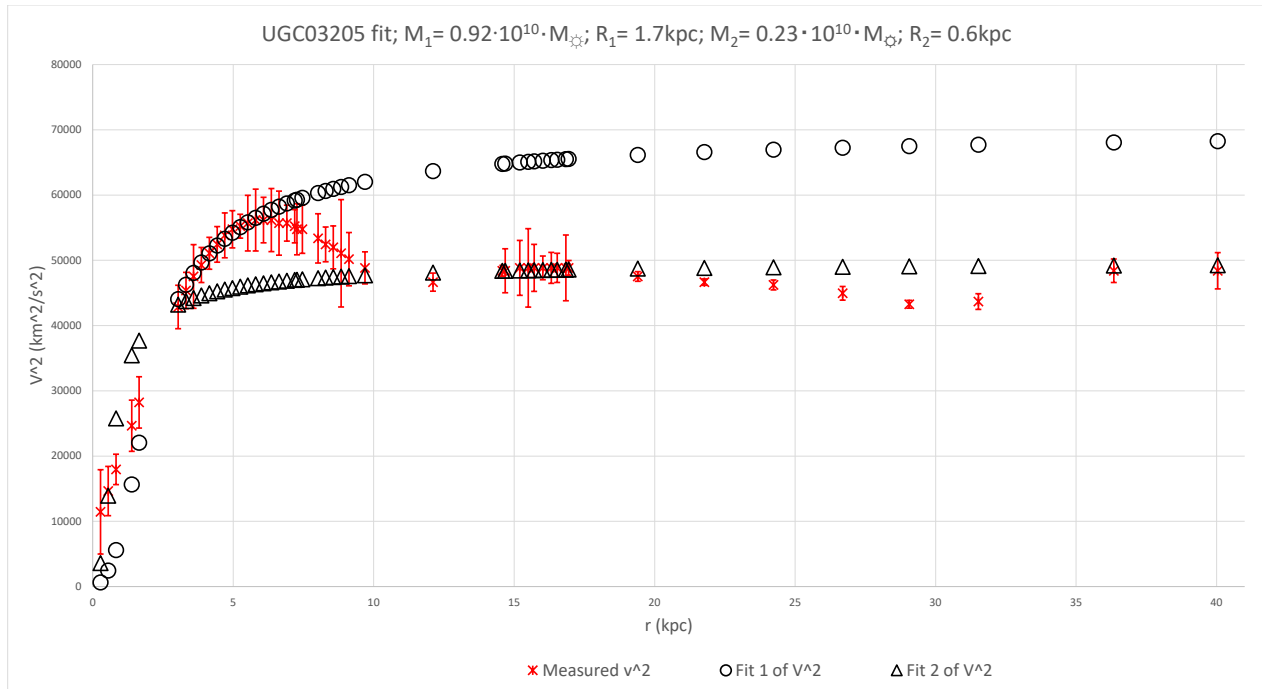


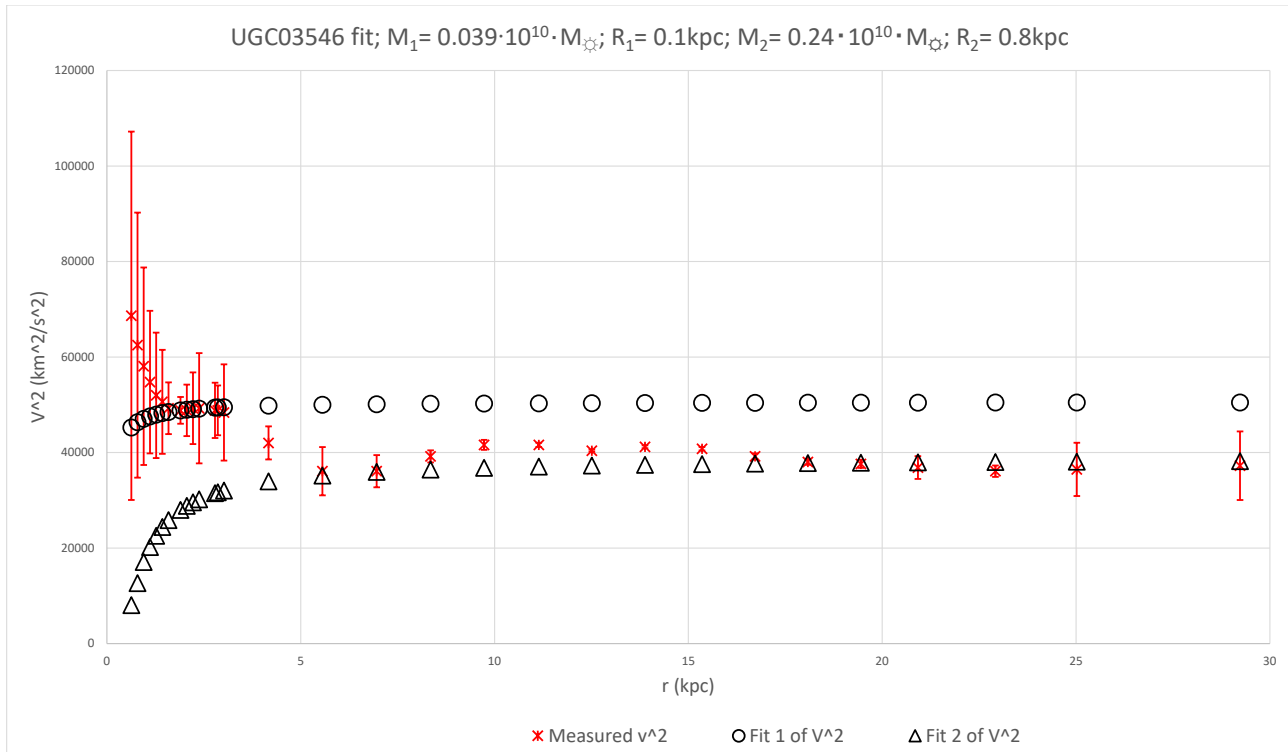


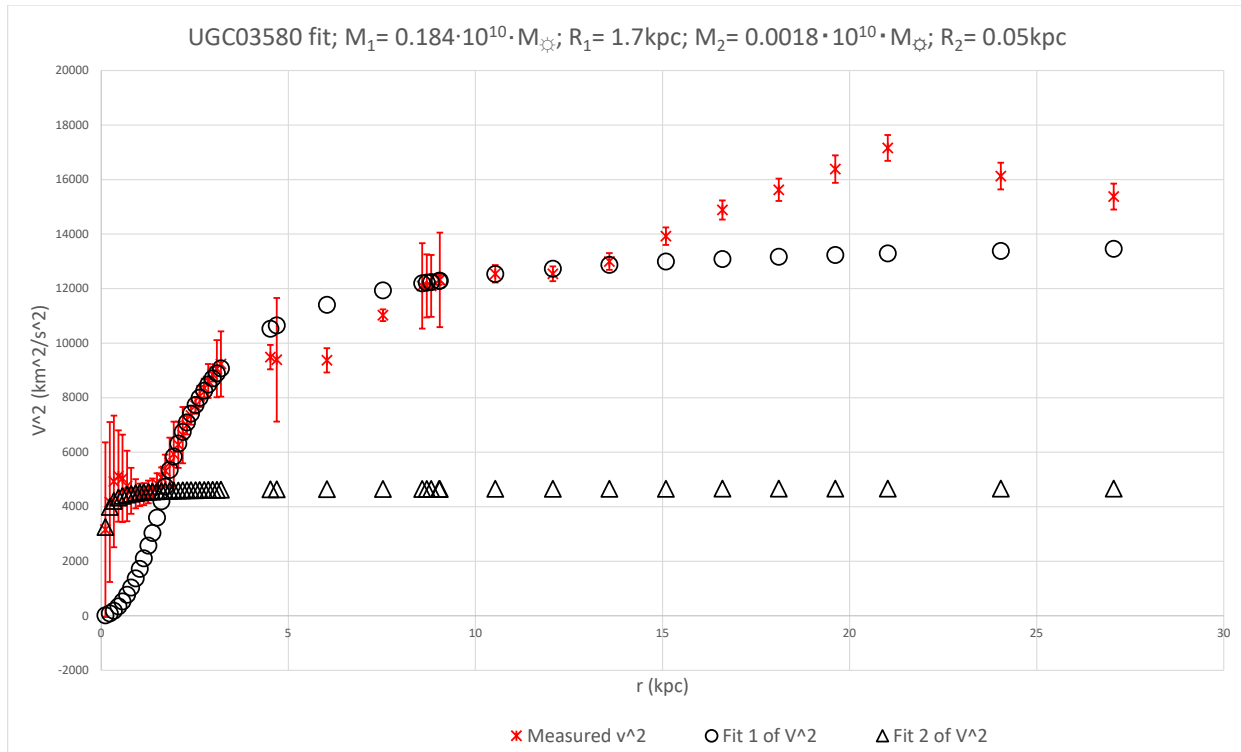
UGC02953 fit; $M_1 = 0.0085 \cdot 10^{10} \cdot M_{\odot}$; $R_1 = 0.02 \text{ kpc}$; $M_2 = 0.245 \cdot 10^{10} \cdot M_{\odot}$; $R_2 = 0.45 \text{ kpc}$;
 $M_3 = 2.35 \cdot 10^{10} \cdot M_{\odot}$; $R_3 = 2.4 \text{ kpc}$



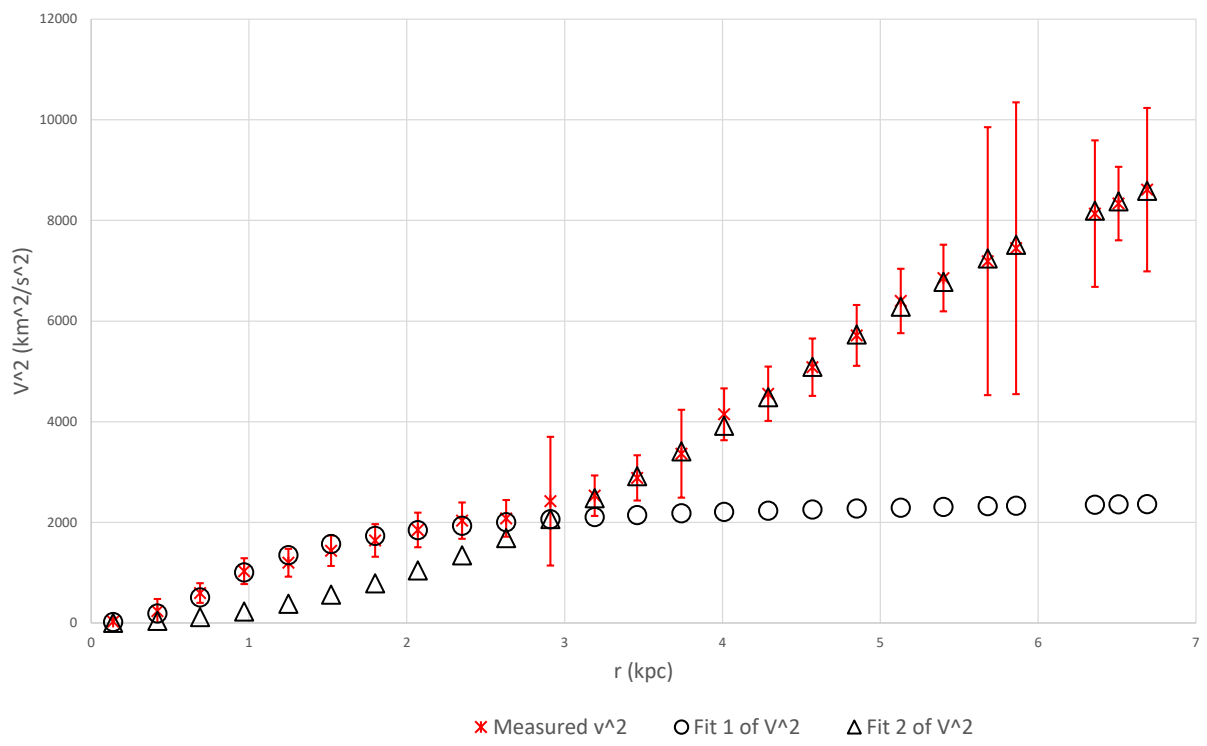




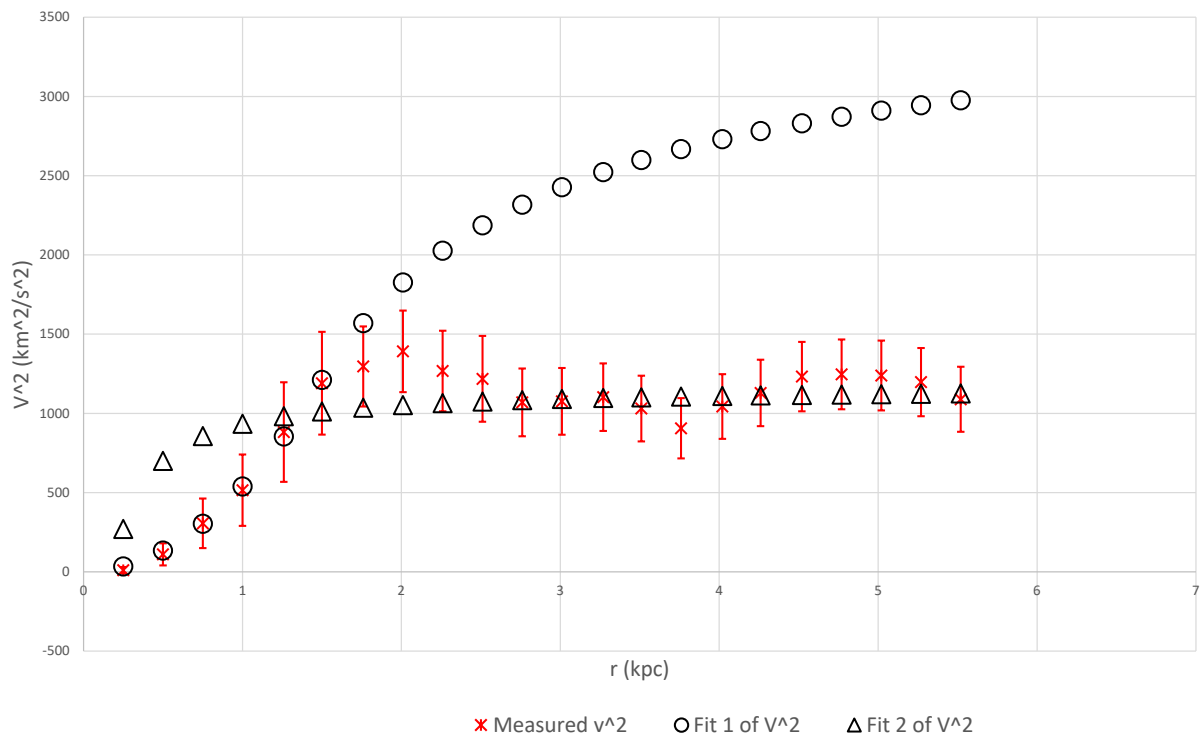


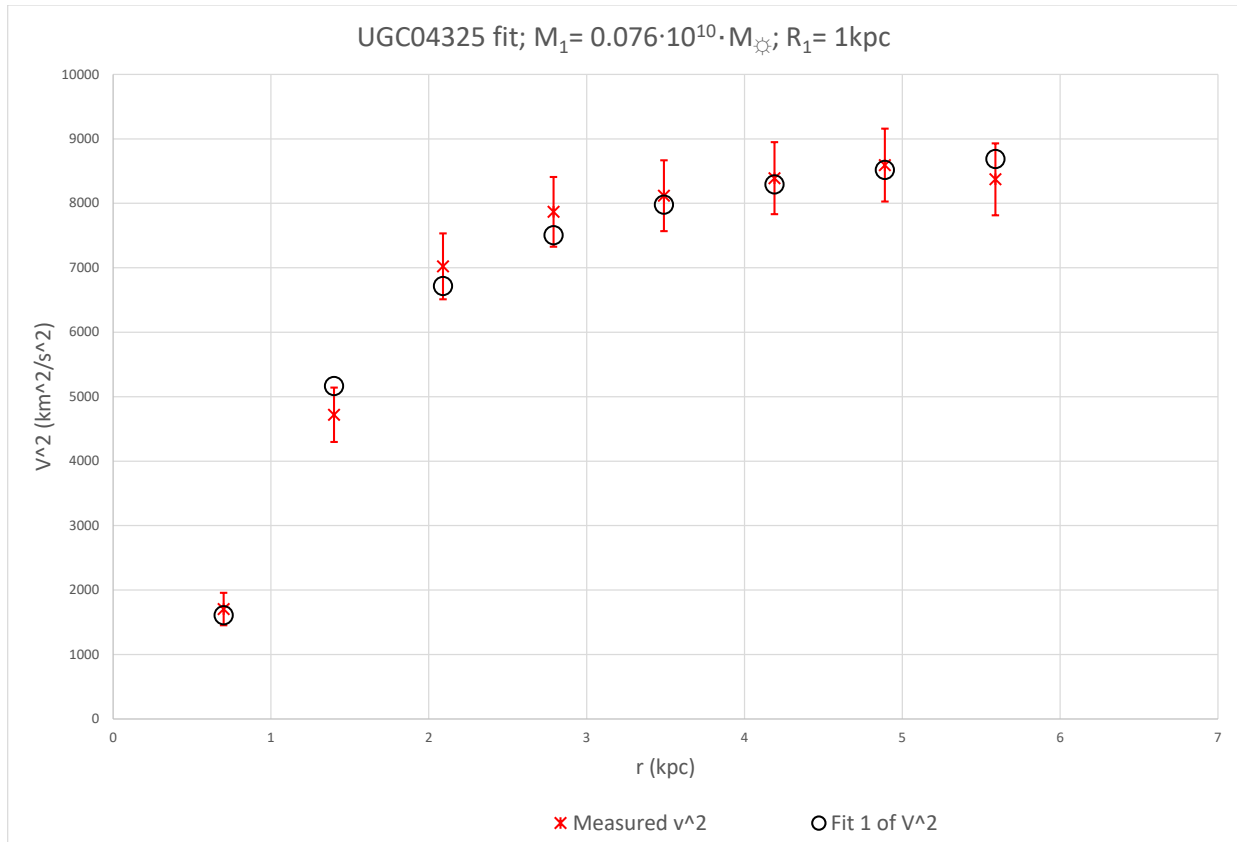


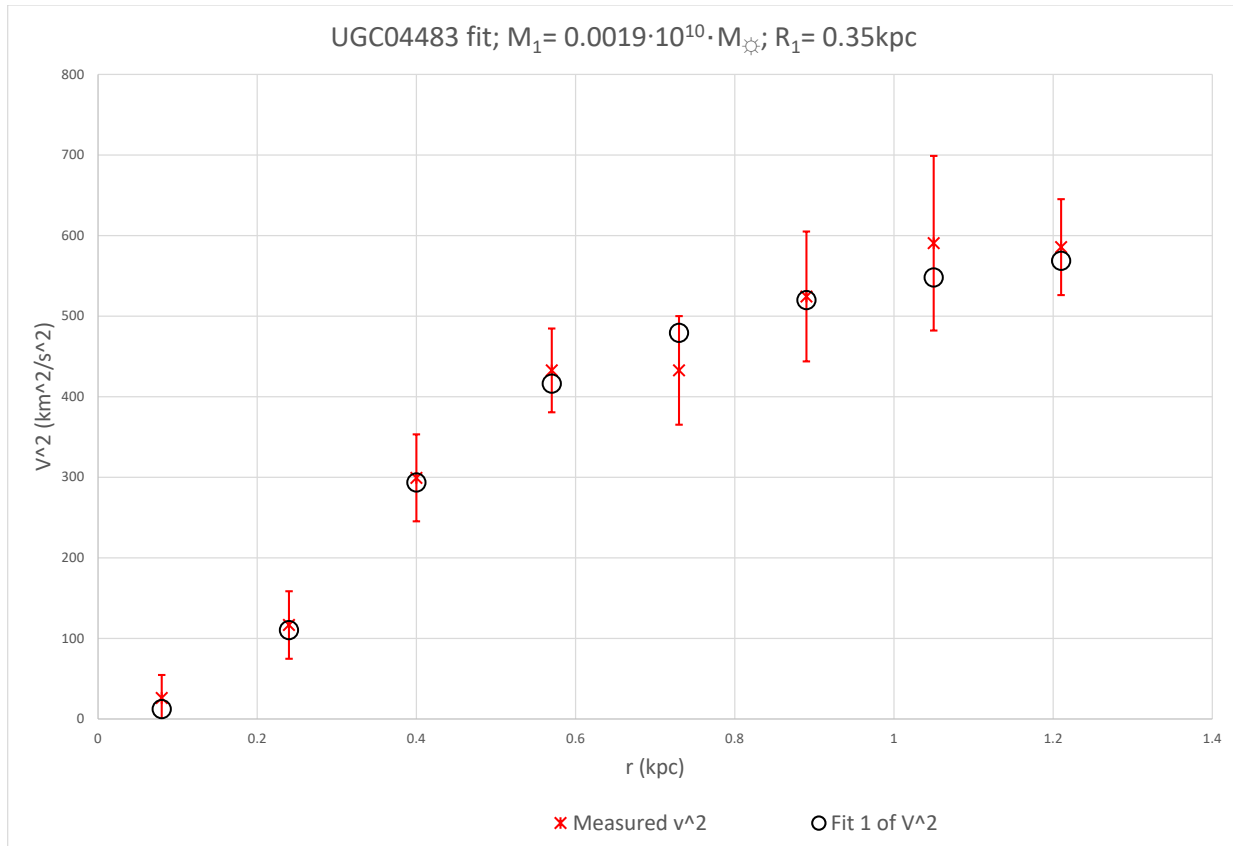
UGC04278 fit; $M_1 = 0.018 \cdot 10^{10} \cdot M_{\odot}$; $R_1 = 0.9 \text{ kpc}$;
 $M_2 = 0.585 \cdot 10^{10} \cdot M_{\odot}$; $R_2 = 4.7 \text{ kpc}$

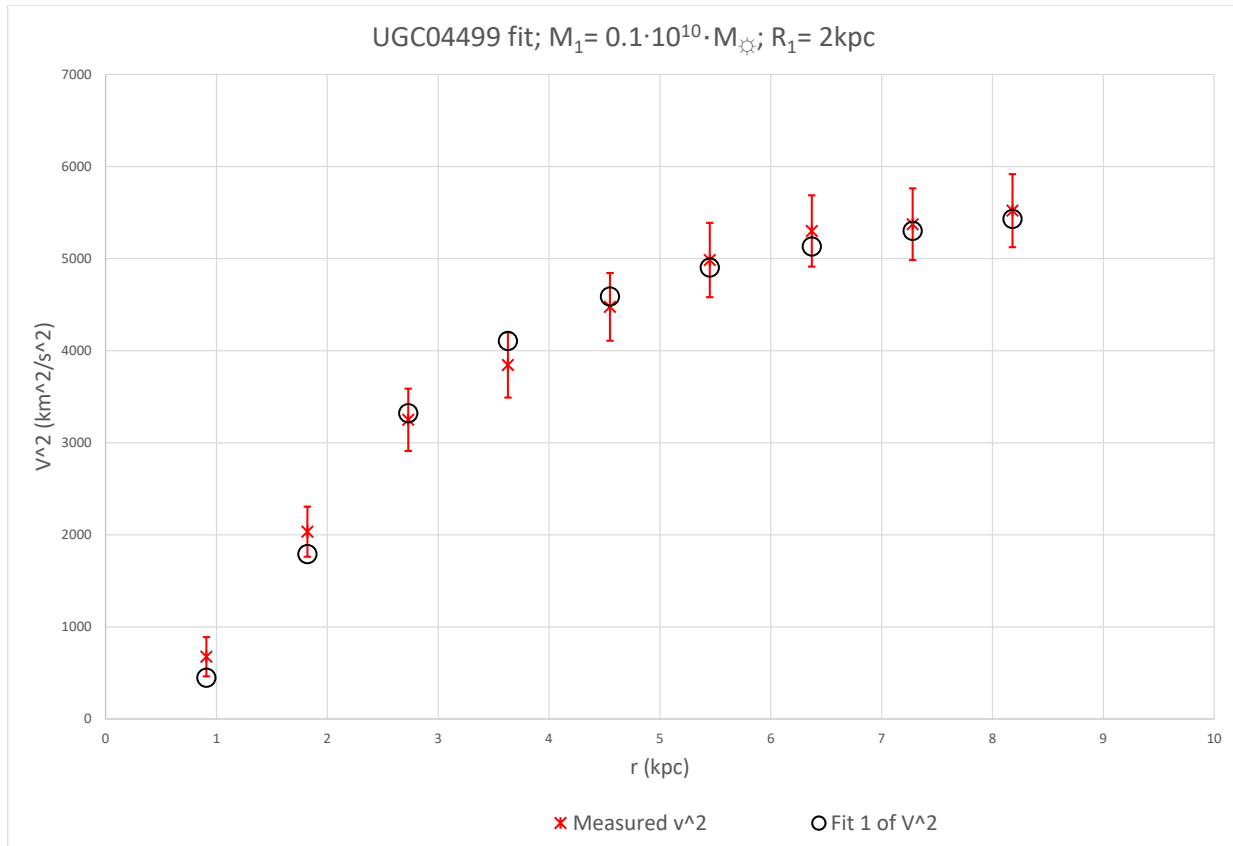


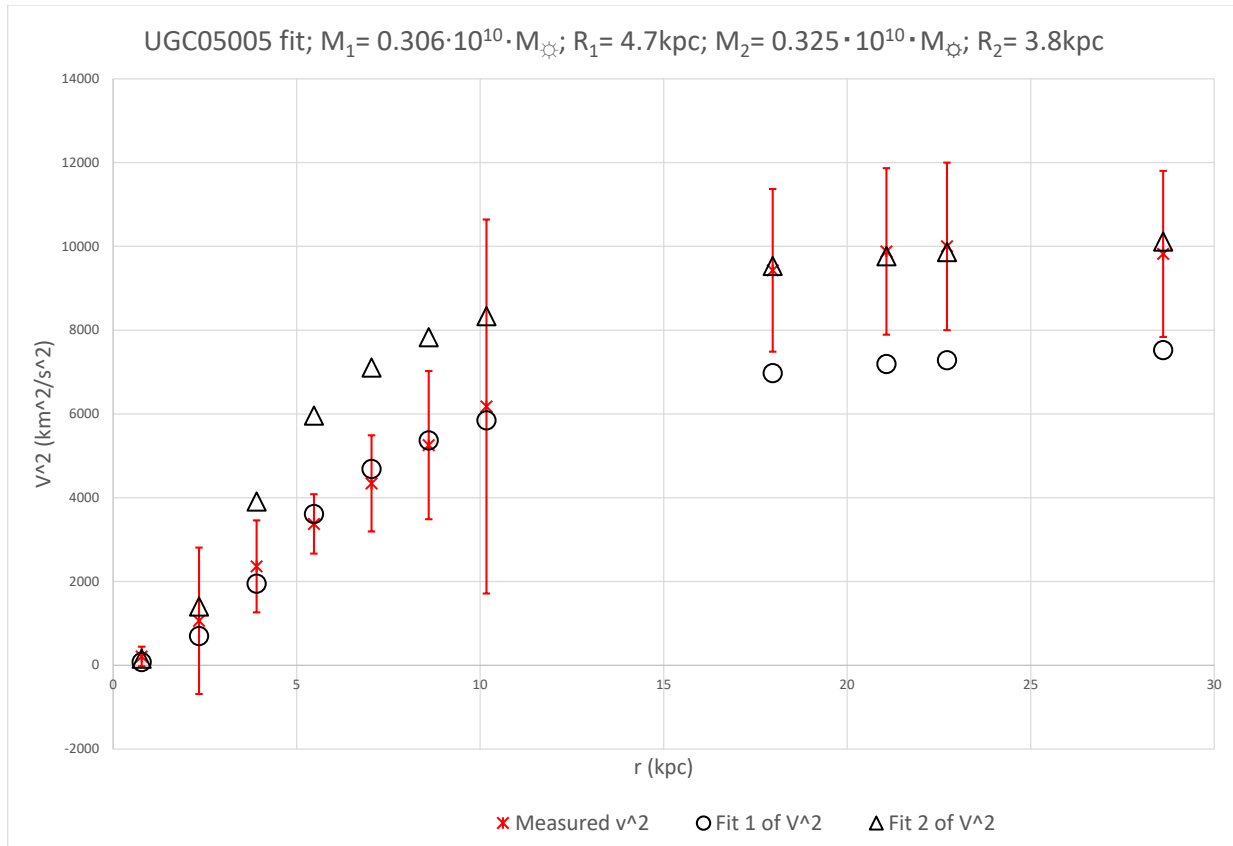
UGC04305 fit; $M_1 = 0.042 \cdot 10^{10} \cdot M_{\odot}$; $R_1 = 1.5 \text{ kpc}$;
 $M_2 = 0.0027 \cdot 10^{10} \cdot M_{\odot}$; $R_2 = 0.3 \text{ kpc}$

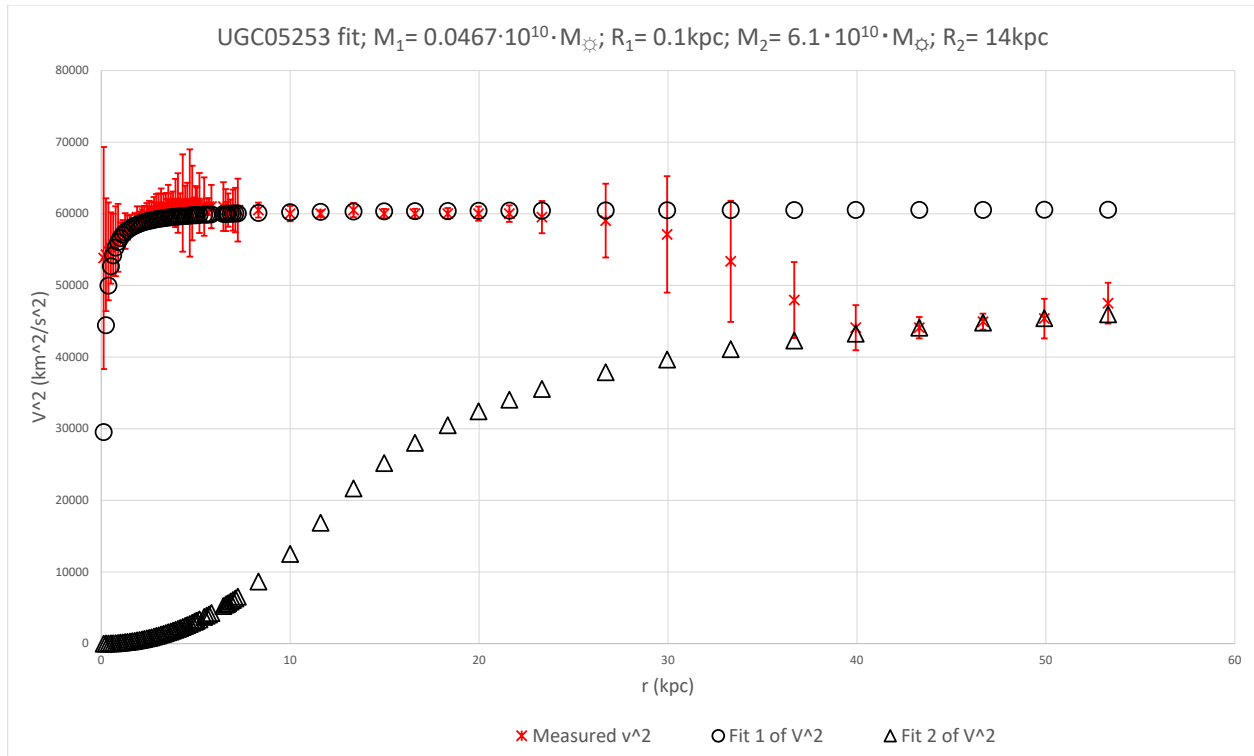


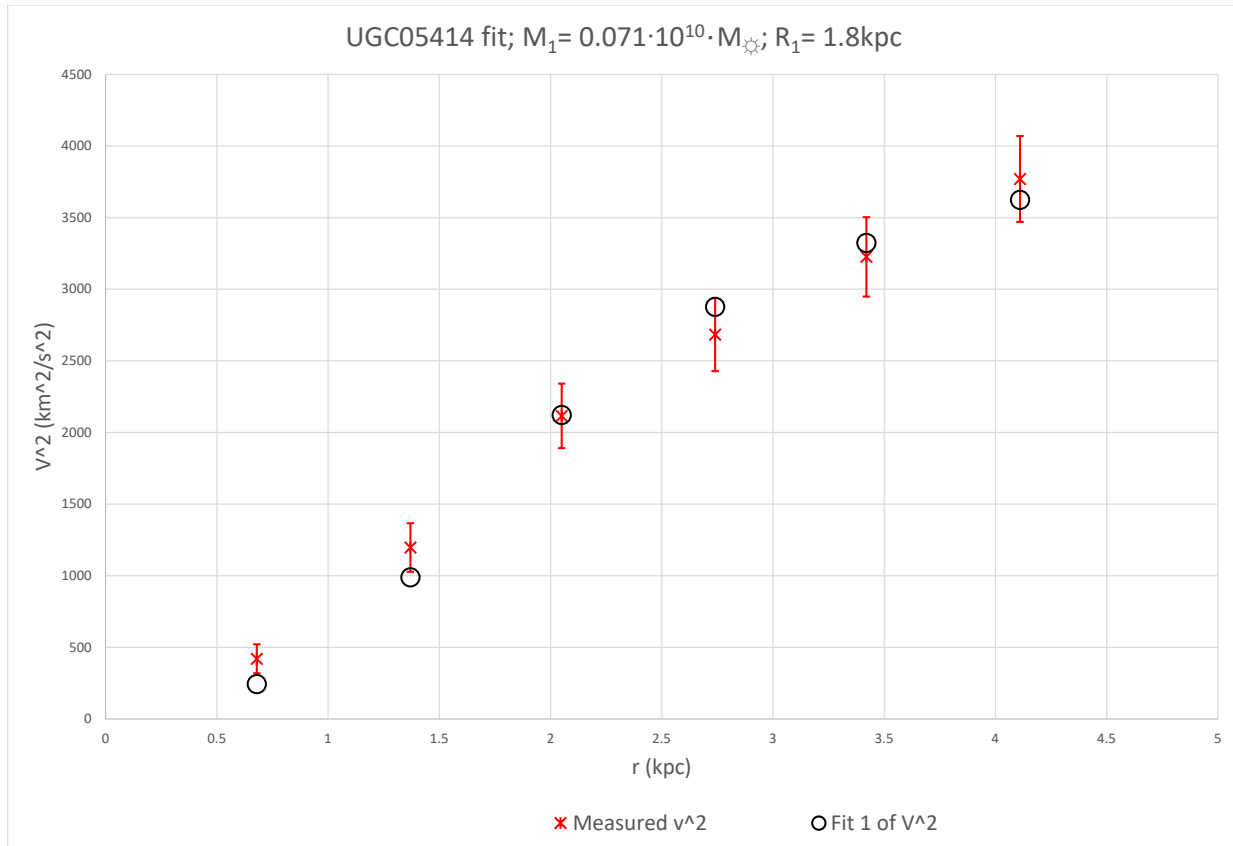


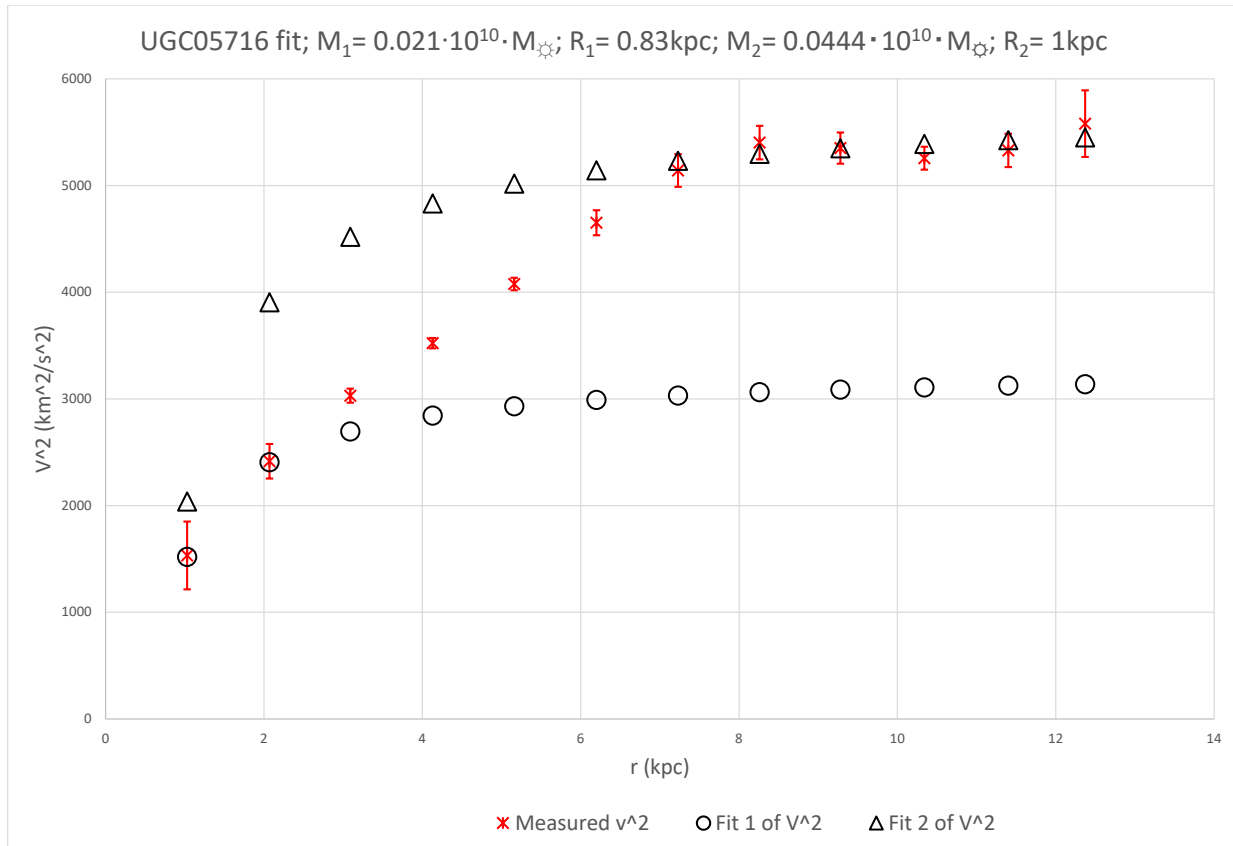




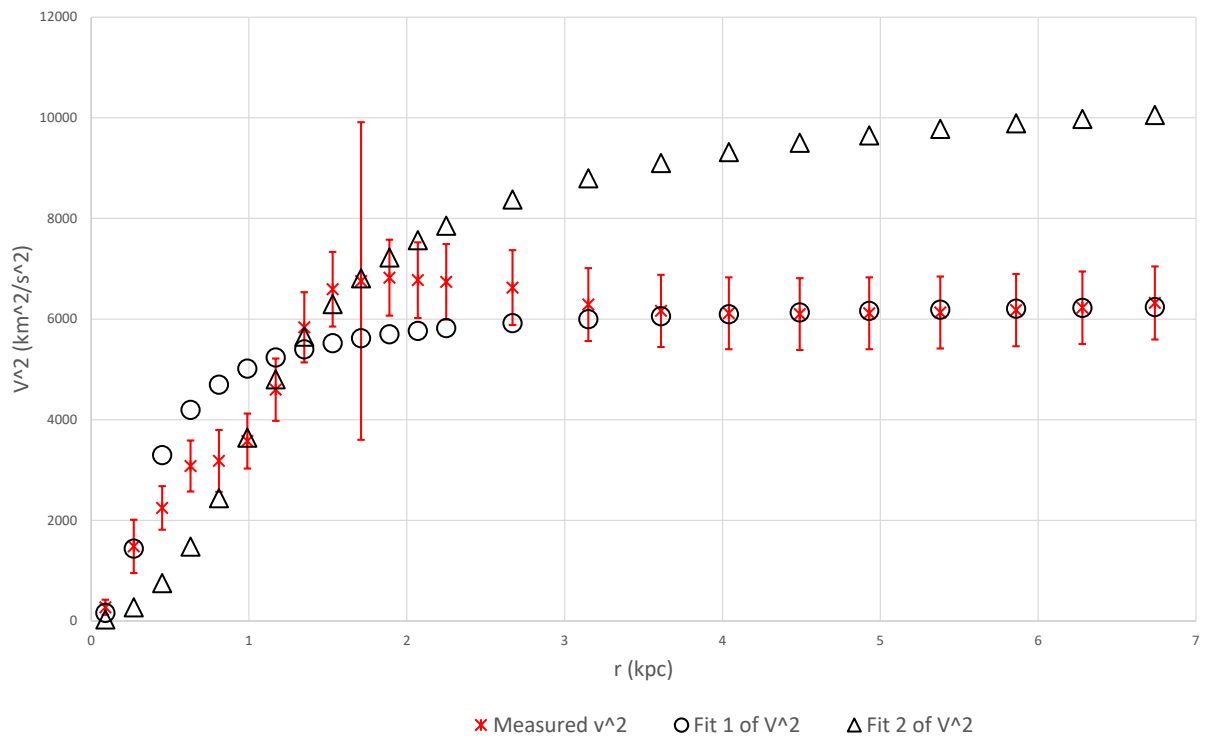


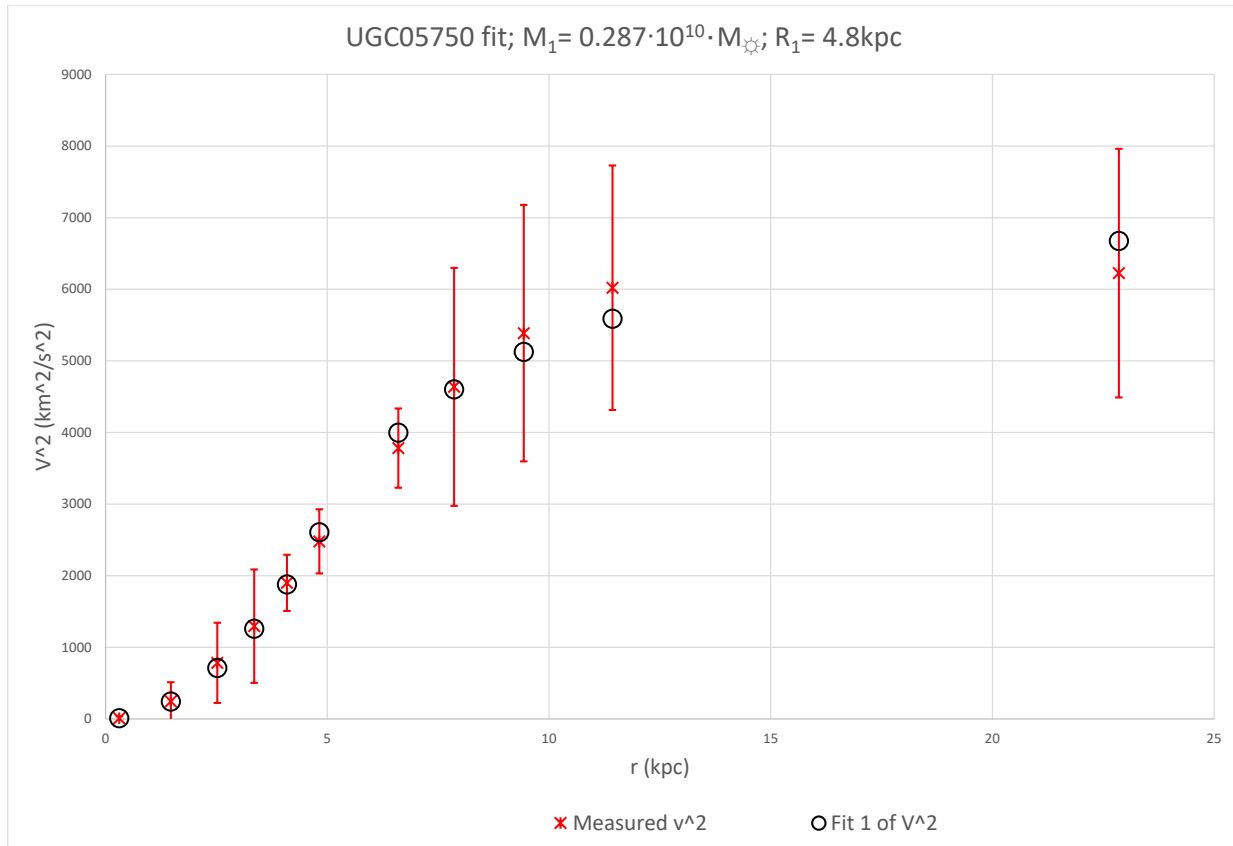




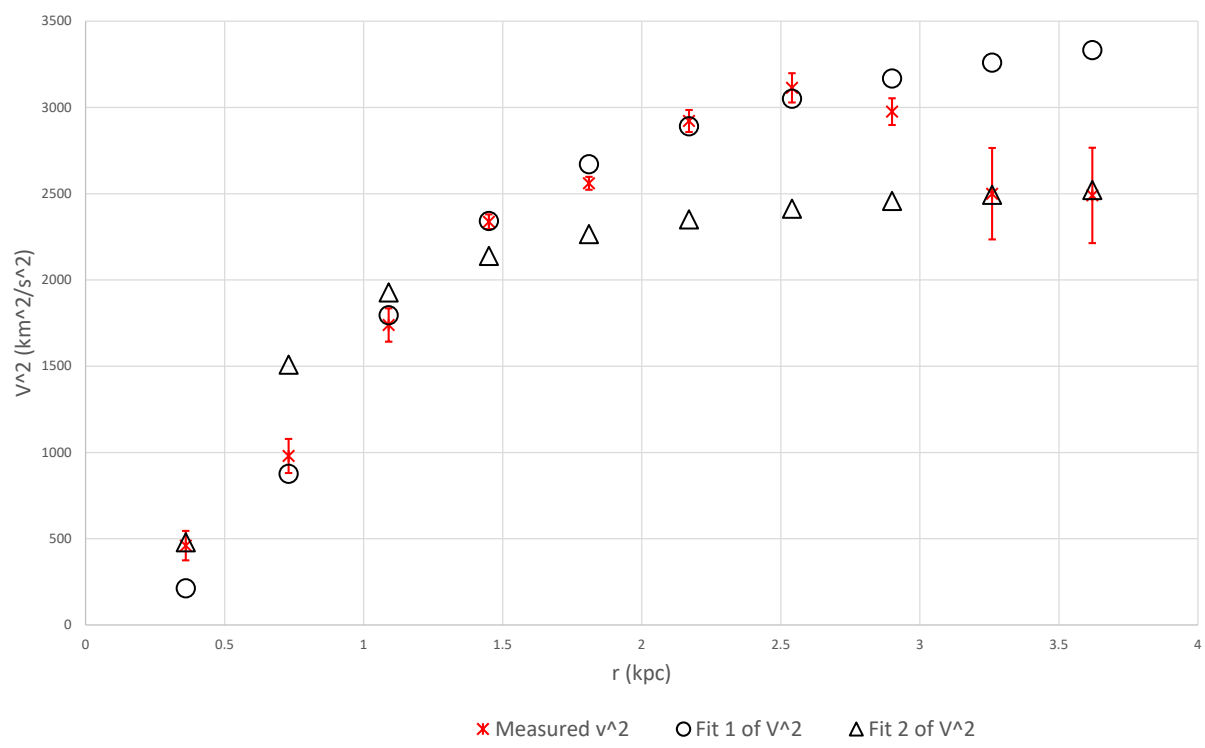


UGC05721 fit; $M_1 = 0.0164 \cdot 10^{10} \cdot M_{\odot}$; $R_1 = 0.33 \text{ kpc}$;
 $M_2 = 0.086 \cdot 10^{10} \cdot M_{\odot}$; $R_2 = 1 \text{ kpc}$

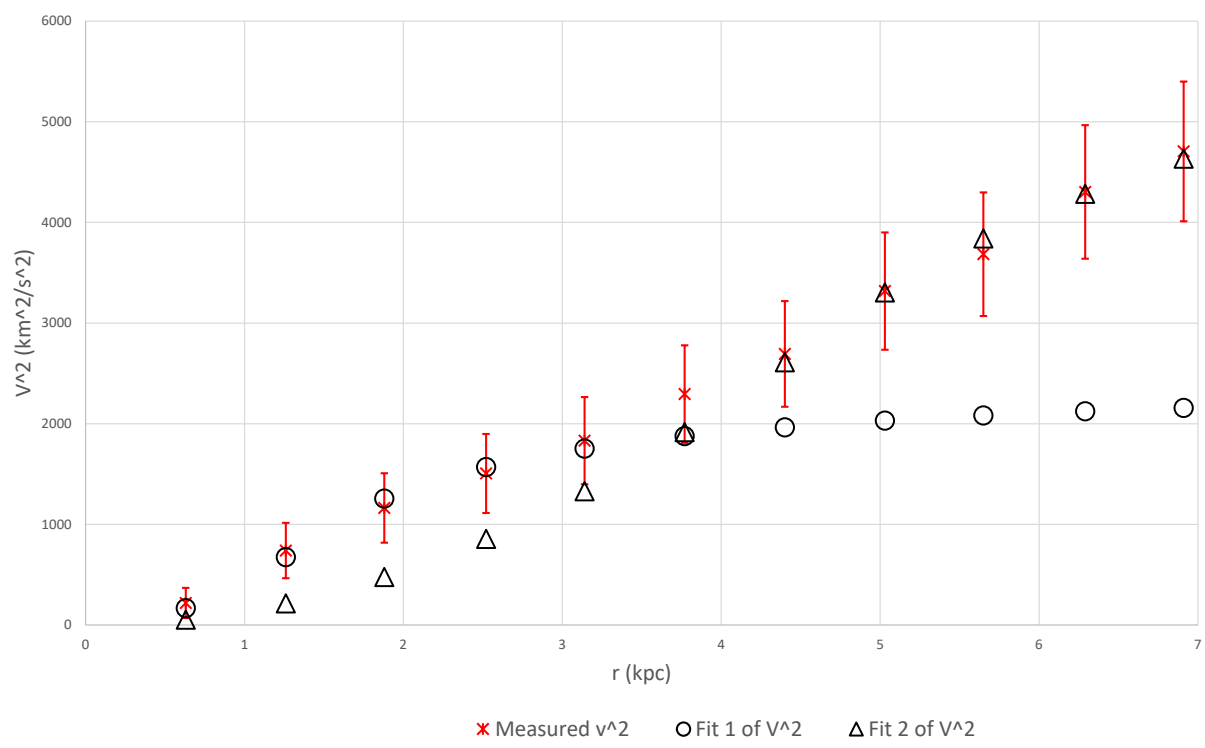




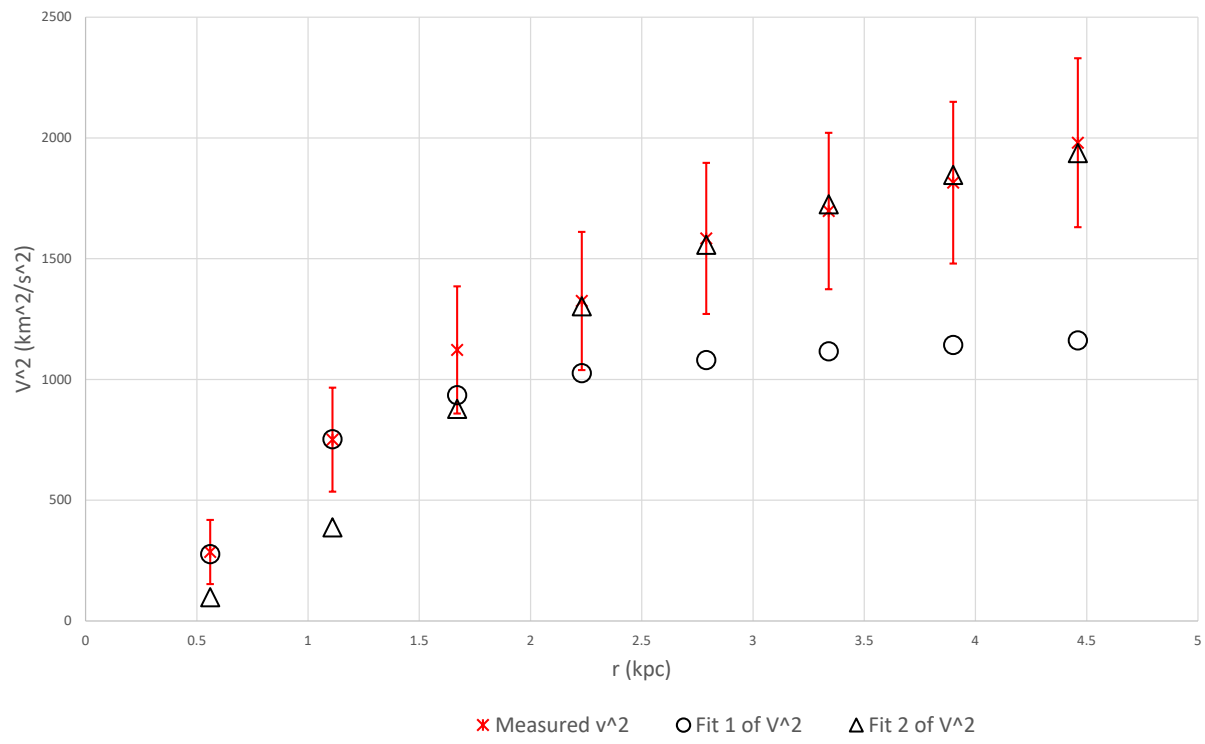
UGC05764 fit; $M_1 = 0.0277 \cdot 10^{10} \cdot M_{\odot}$; $R_1 = 0.9 \text{ kpc}$;
 $M_2 = 0.0107 \cdot 10^{10} \cdot M_{\odot}$; $R_2 = 0.5 \text{ kpc}$



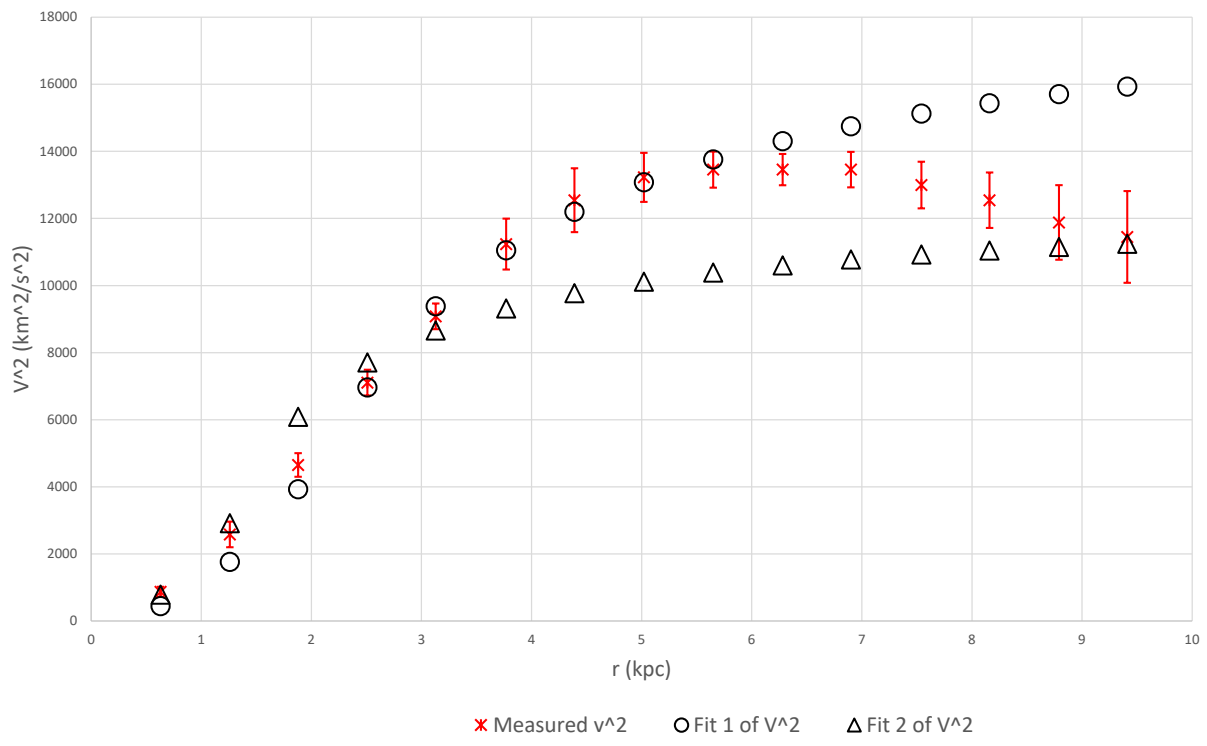
UGC05829 fit; $M_1 = 0.0269 \cdot 10^{10} \cdot M_{\odot}$; $R_1 = 1.4 \text{ kpc}$;
 $M_2 = 0.284 \cdot 10^{10} \cdot M_{\odot}$; $R_2 = 4.5 \text{ kpc}$

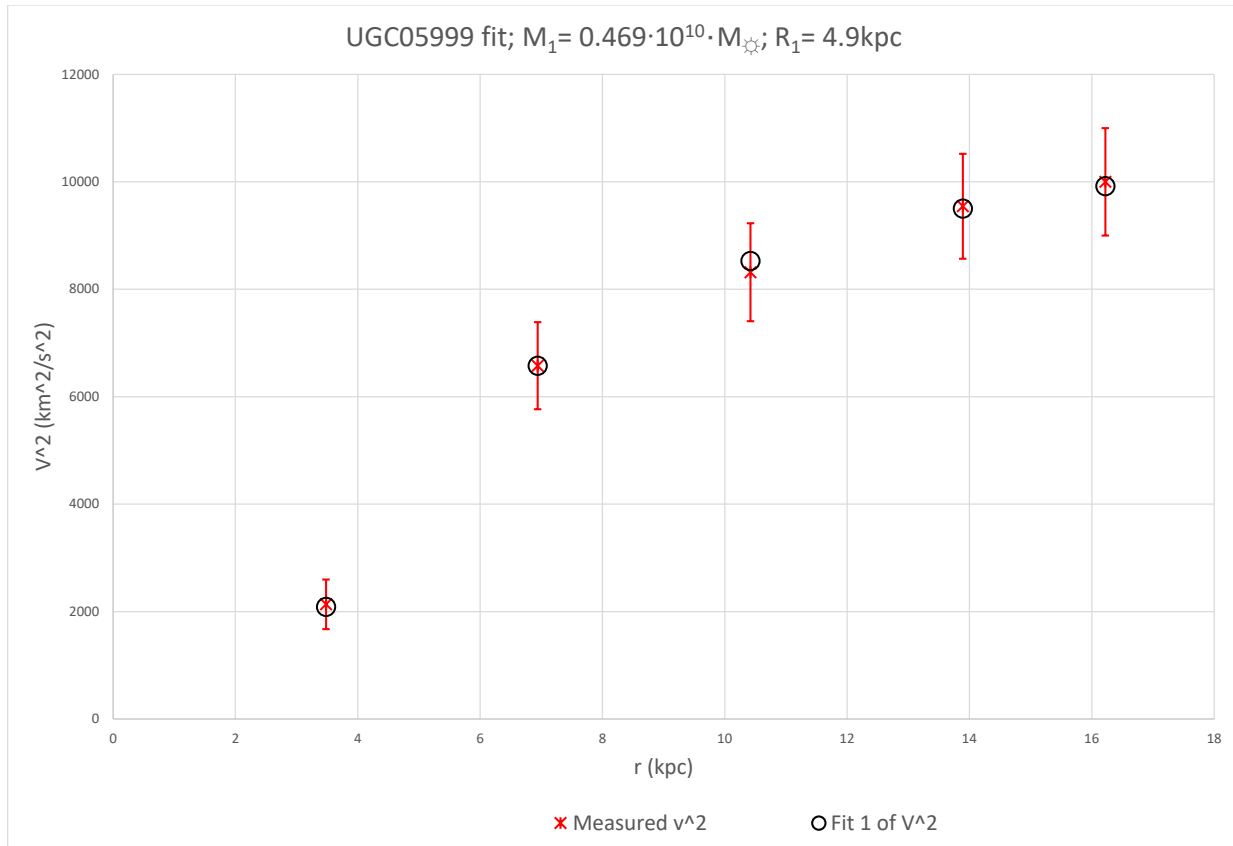


UGC05918 fit; $M_1 = 0.007 \cdot 10^{10} \cdot M_{\odot}$; $R_1 = 0.7 \text{ kpc}$;
 $M_2 = 0.037 \cdot 10^{10} \cdot M_{\odot}$; $R_2 = 1.65 \text{ kpc}$

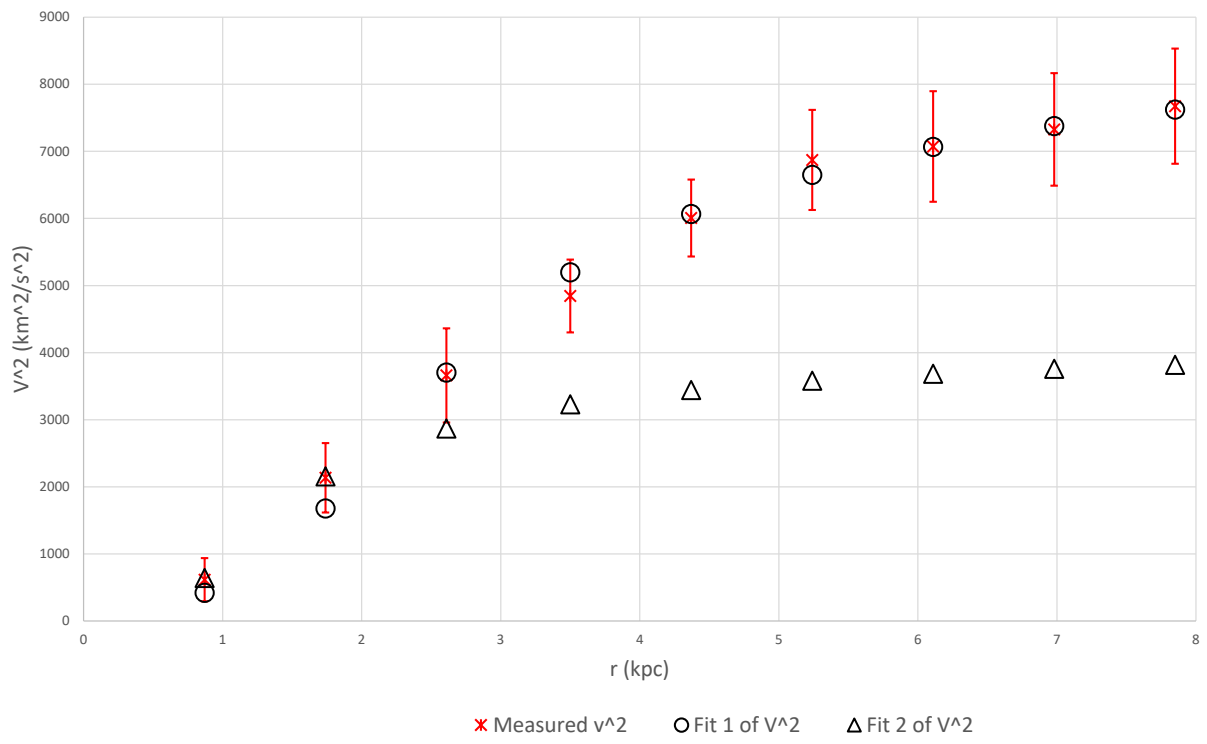


UGC05986 fit; $M_1 = 0.355 \cdot 10^{10} \cdot M_{\odot}$; $R_1 = 2.4 \text{ kpc}$;
 $M_2 = 0.14 \cdot 10^{10} \cdot M_{\odot}$; $R_2 = 1.45 \text{ kpc}$

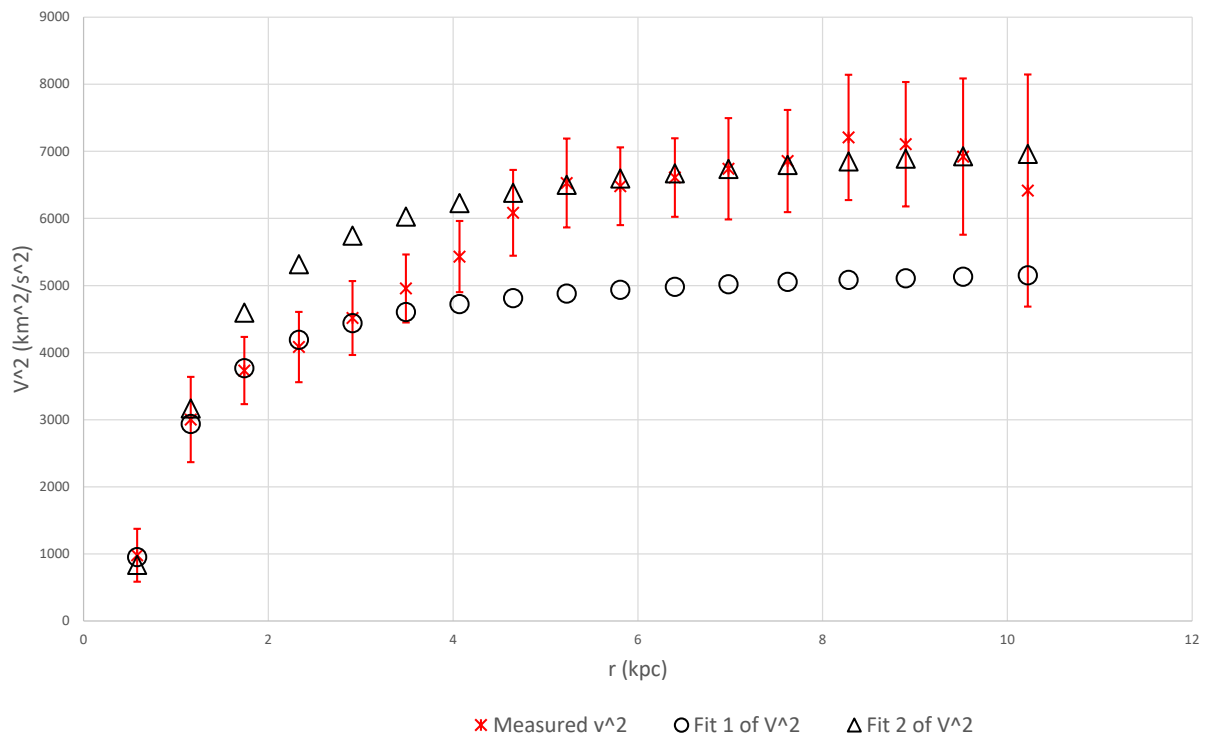


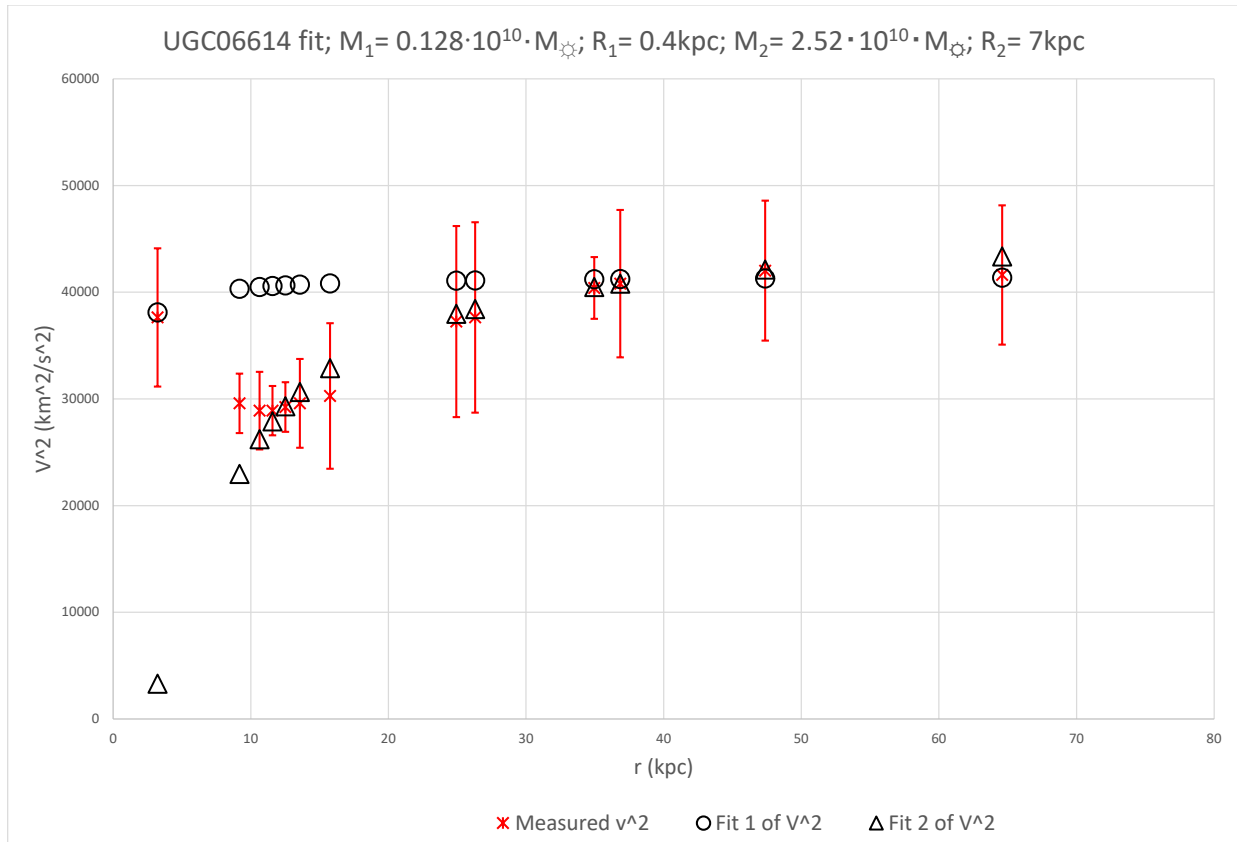


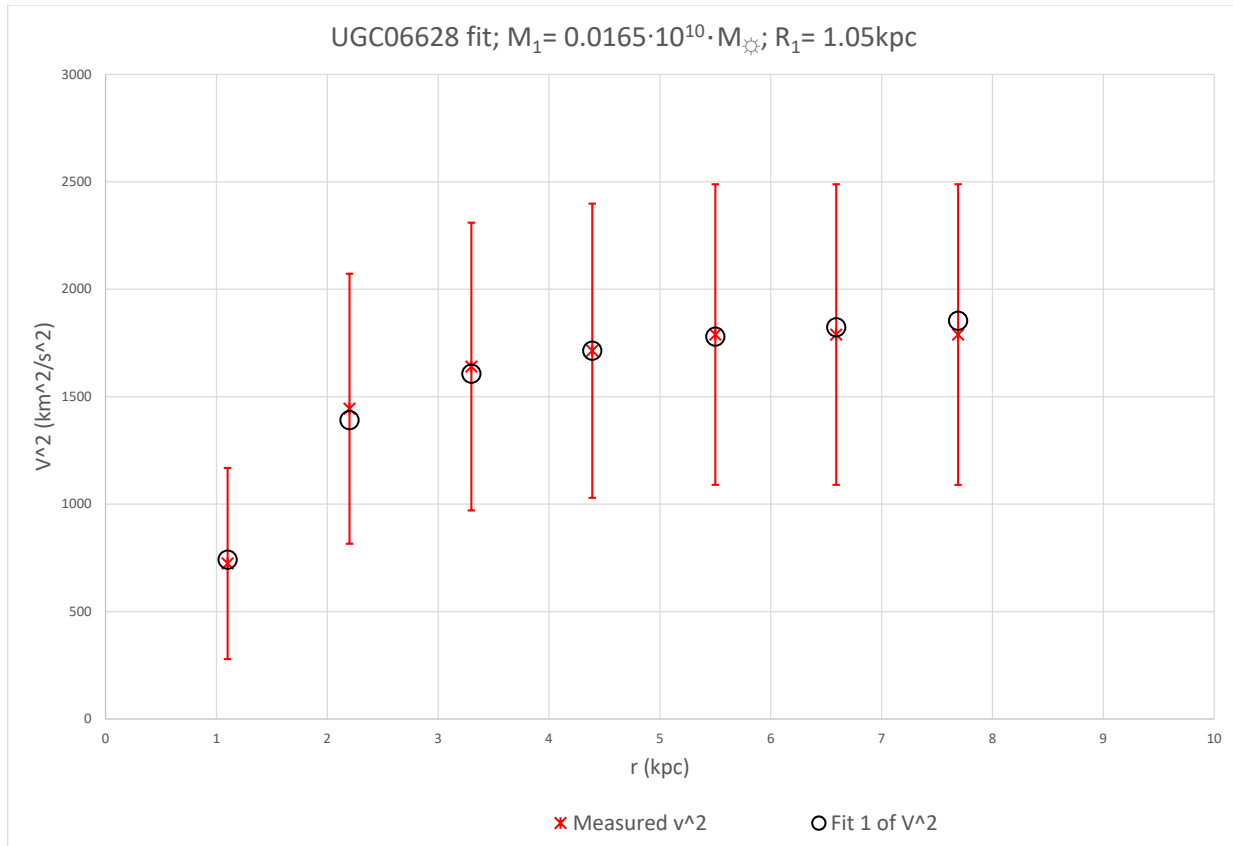
UGC06399 fit; $M_1 = 0.177 \cdot 10^{10} \cdot M_{\odot}$; $R_1 = 2.4 \text{ kpc}$;
 $M_2 = 0.043 \cdot 10^{10} \cdot M_{\odot}$; $R_2 = 1.3 \text{ kpc}$

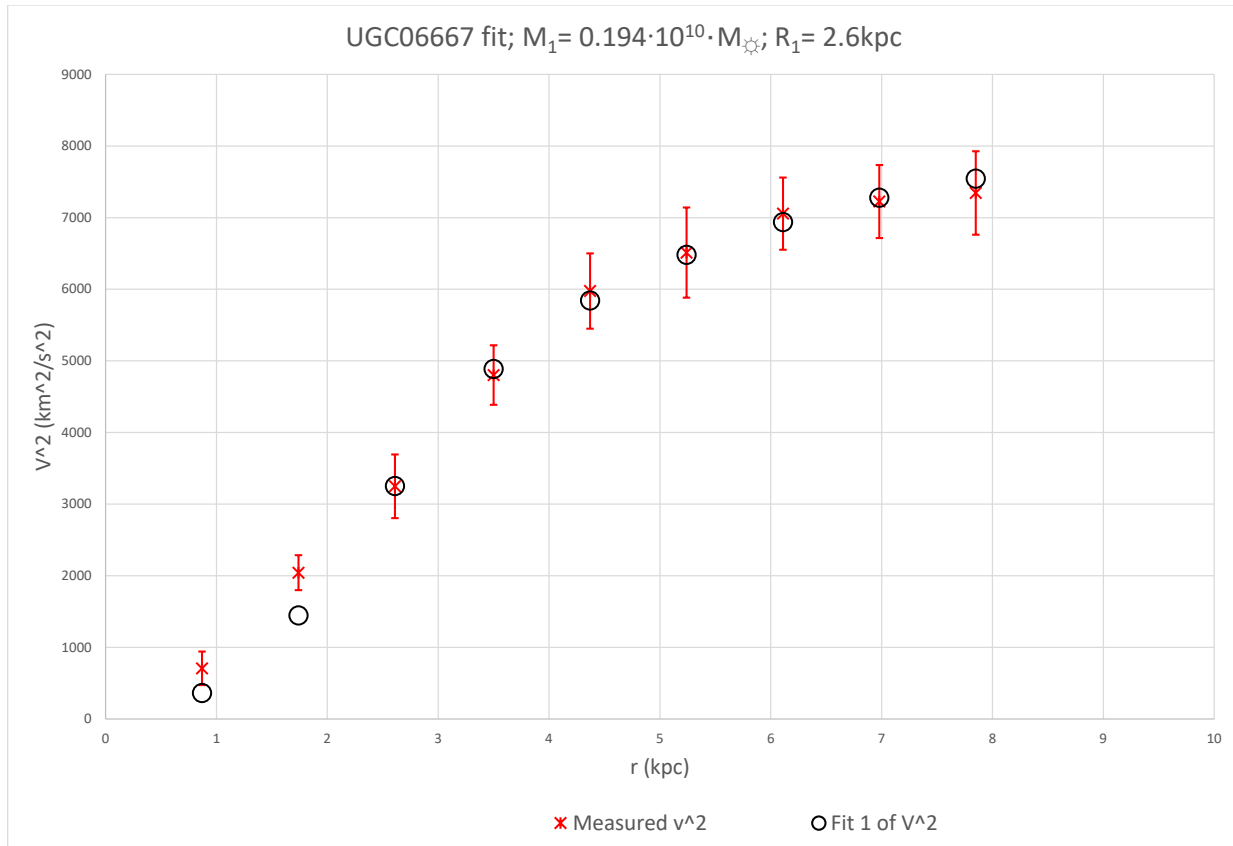


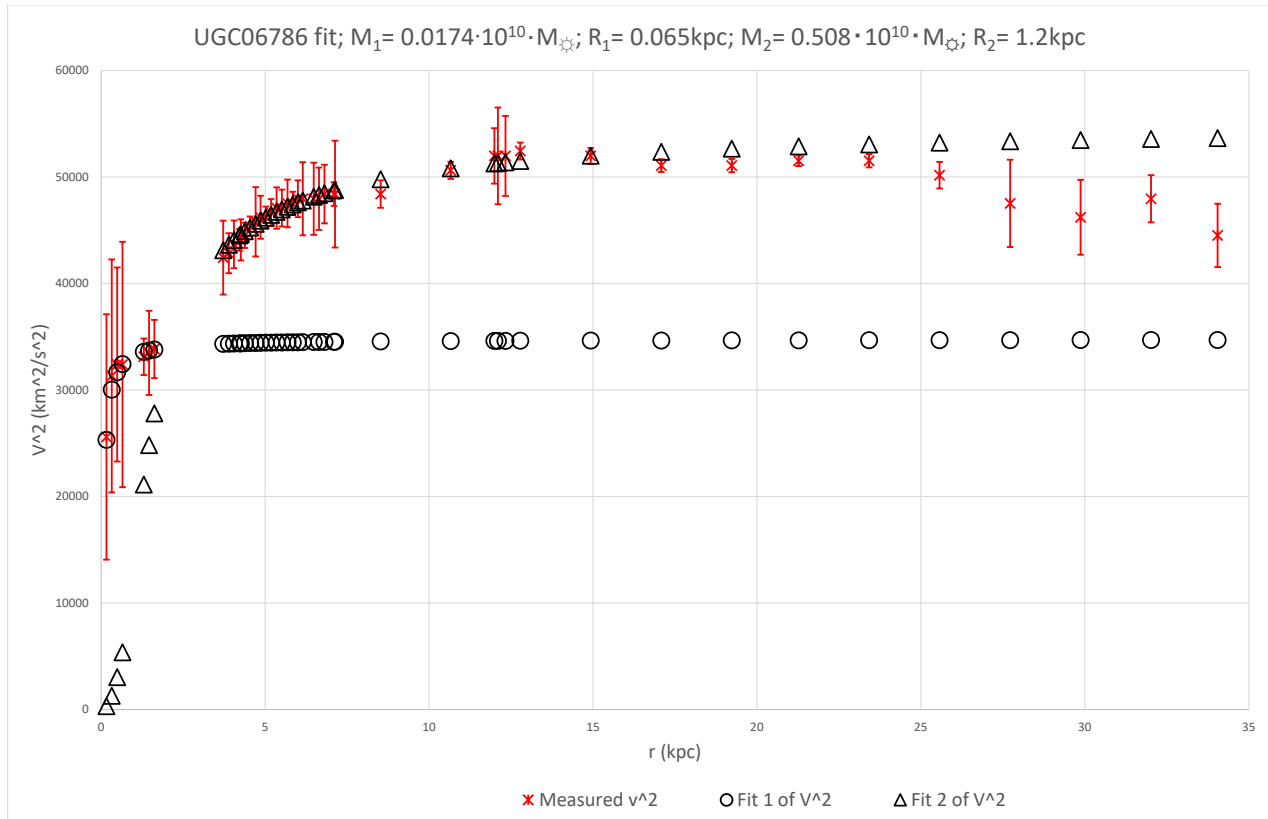
UGC06446 fit; $M_1 = 0.035 \cdot 10^{10} \cdot M_{\odot}$; $R_1 = 0.8 \text{ kpc}$;
 $M_2 = 0.0574 \cdot 10^{10} \cdot M_{\odot}$; $R_2 = 1 \text{ kpc}$

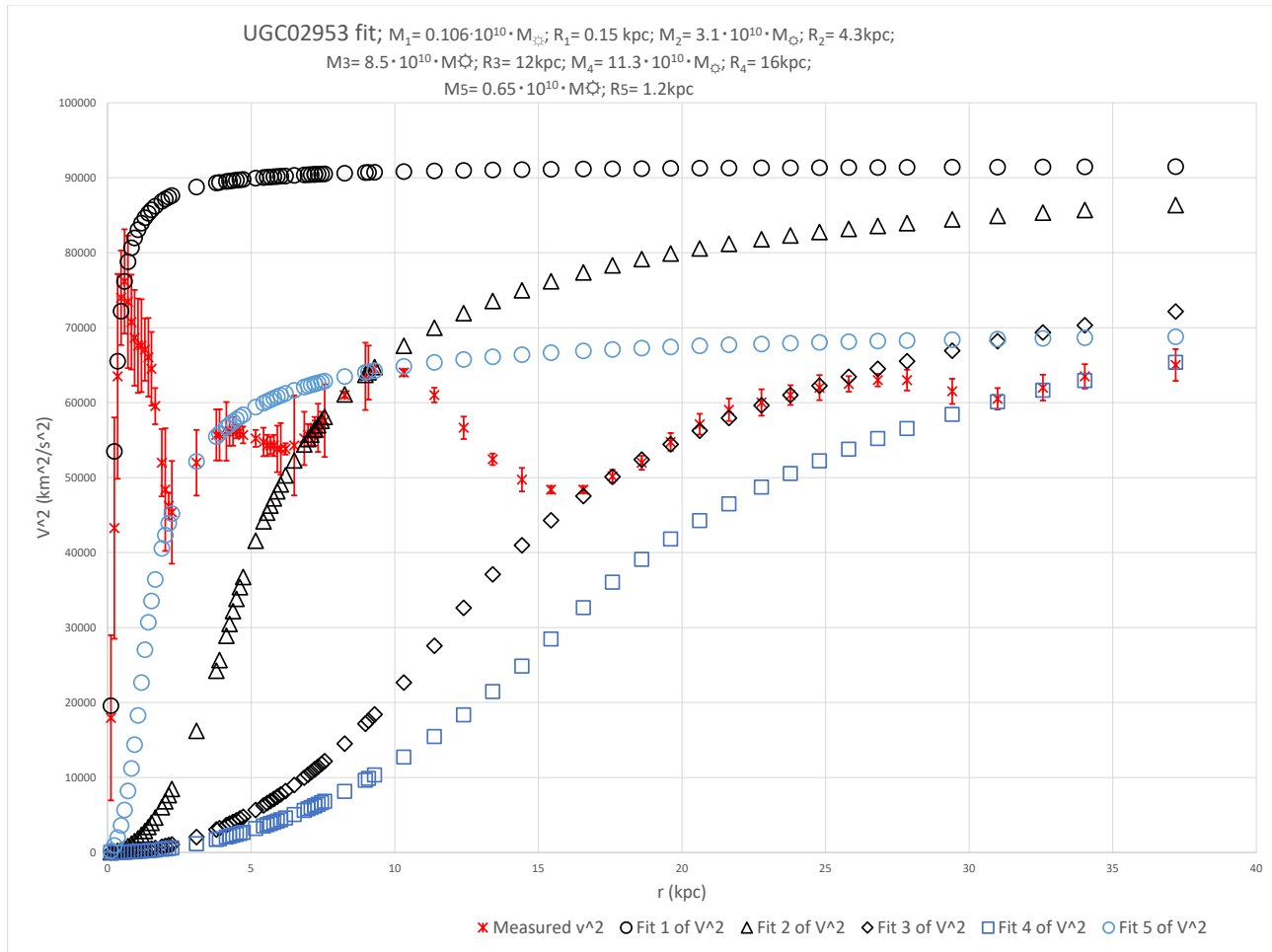


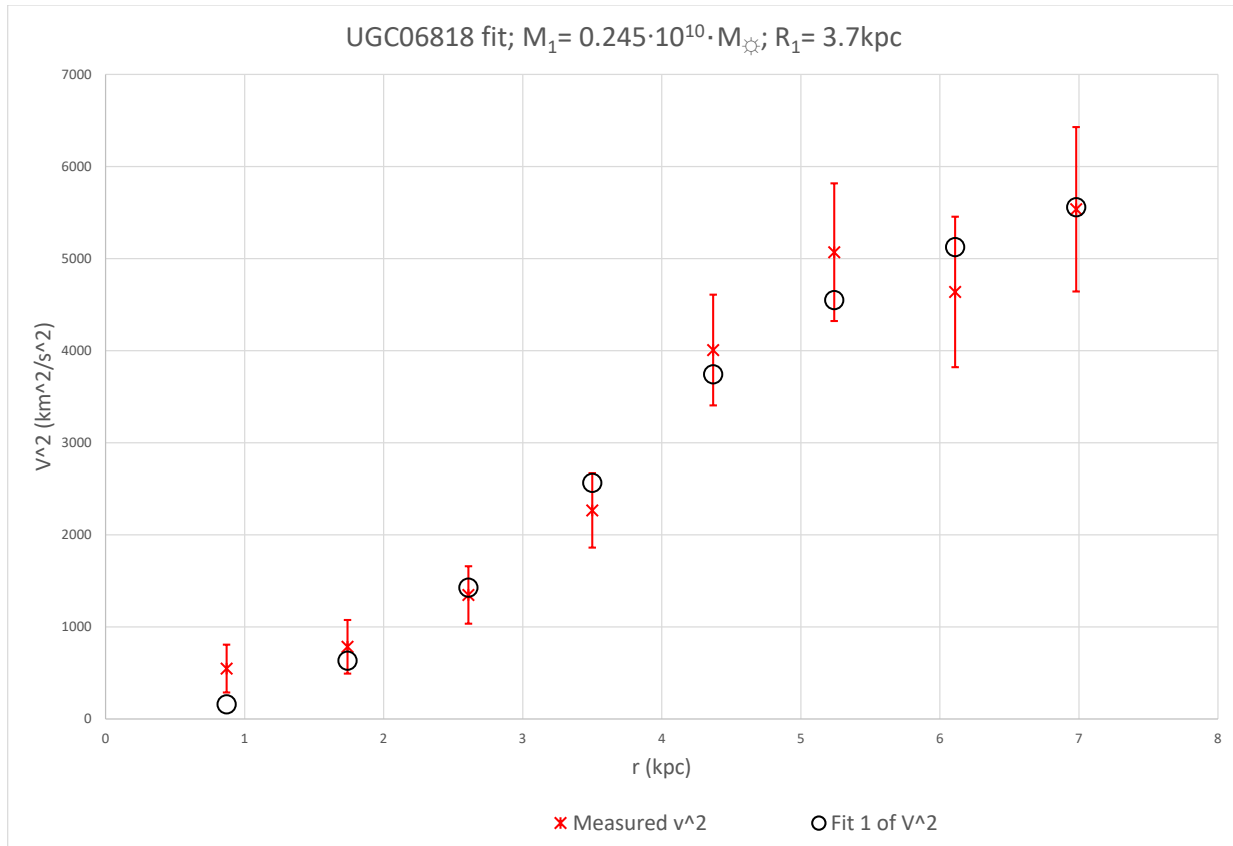


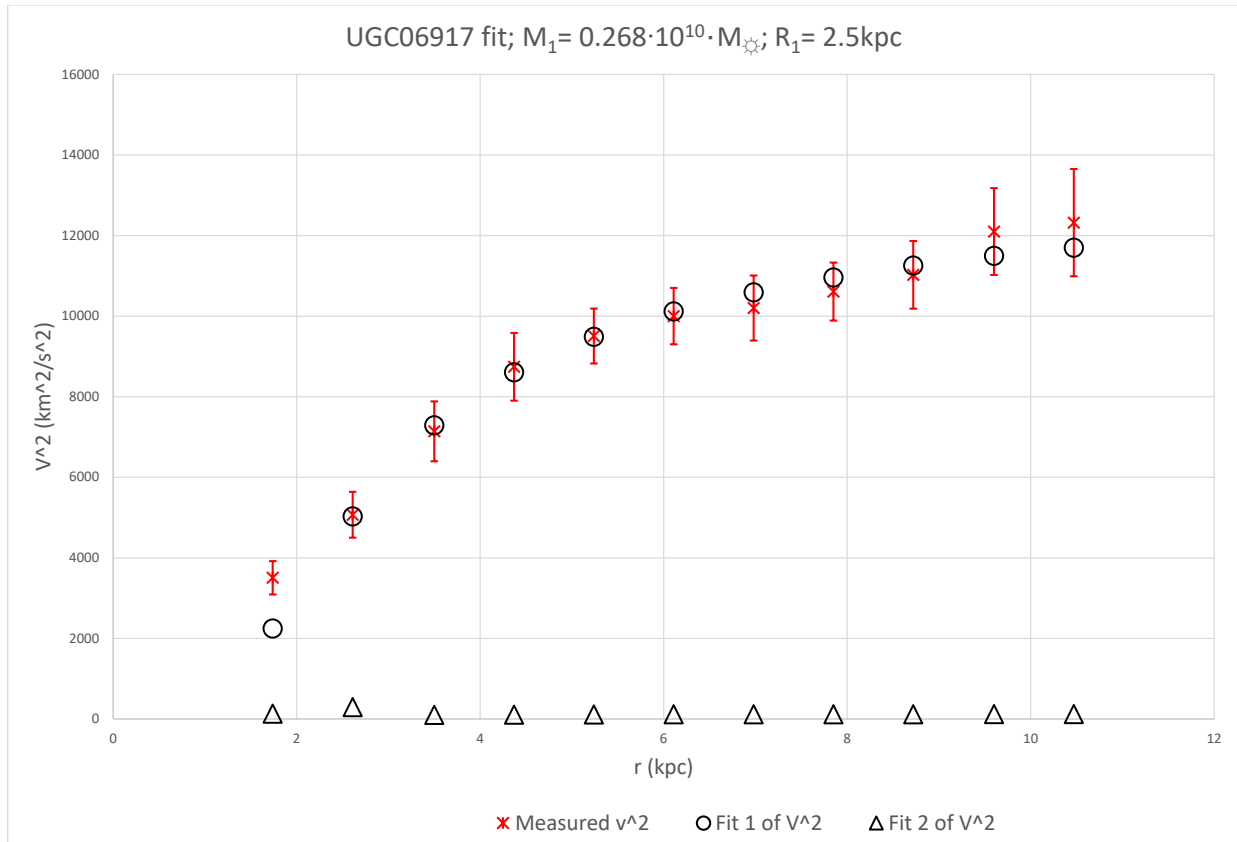


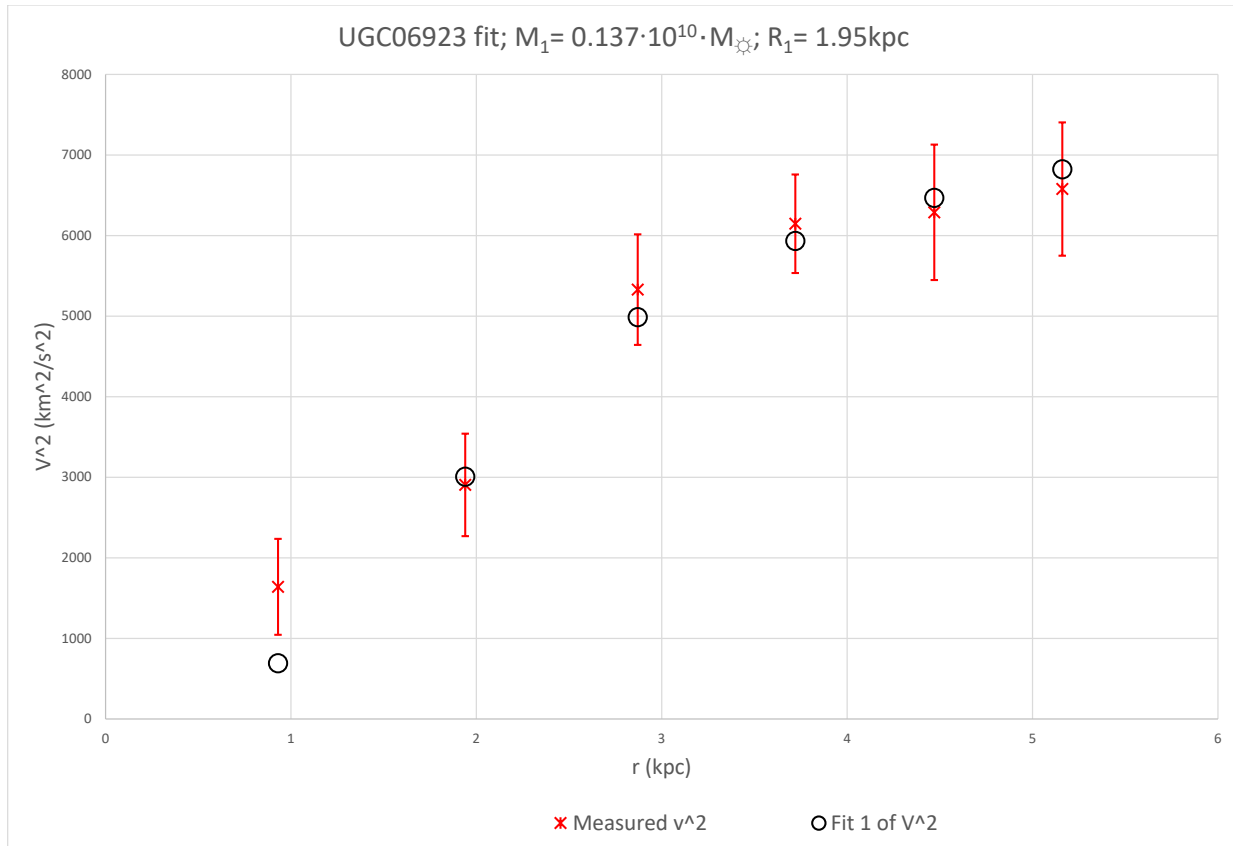


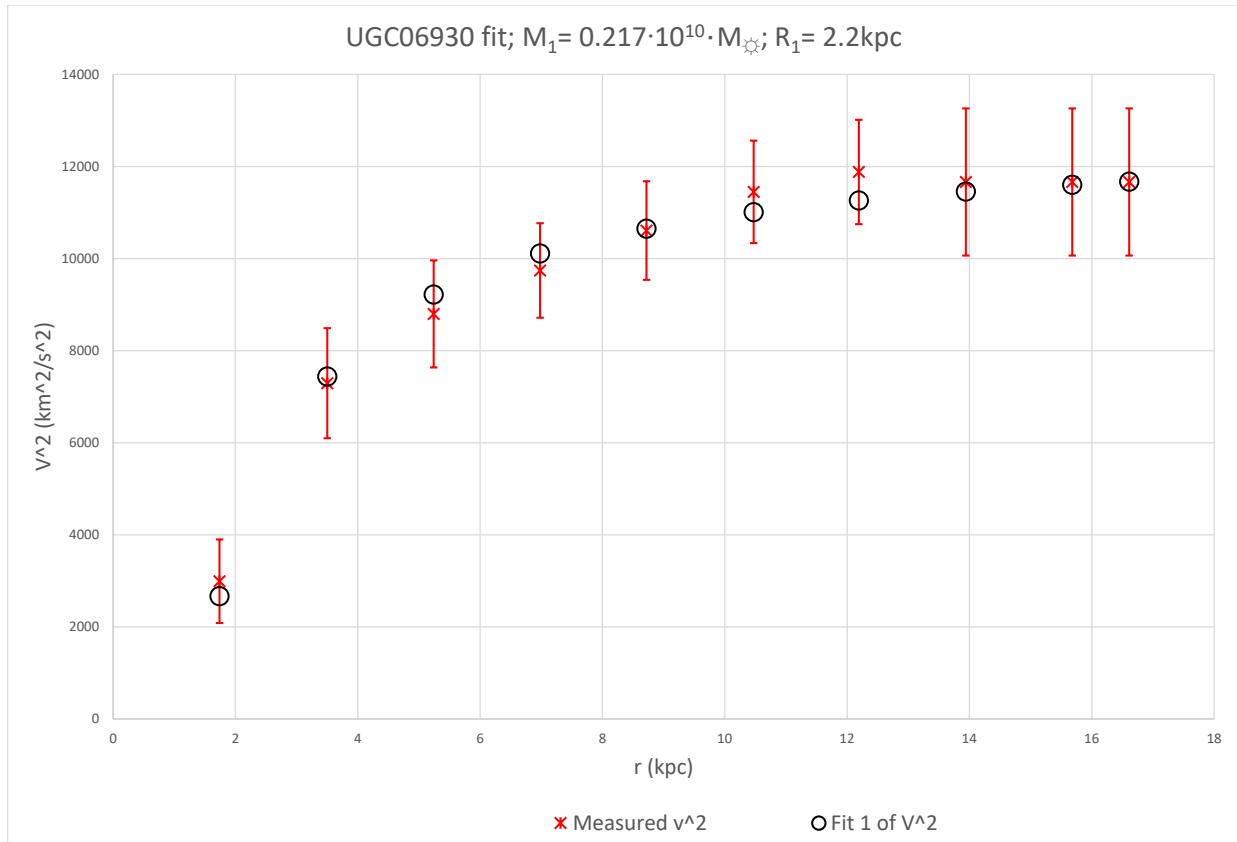




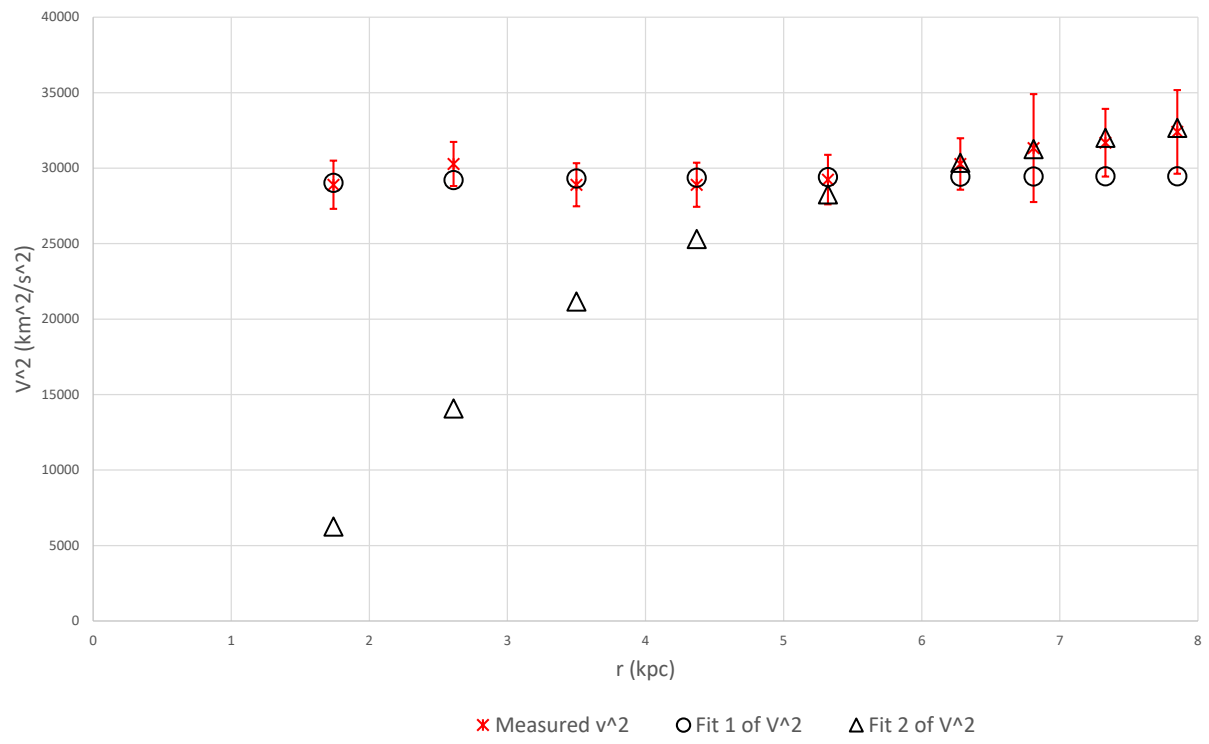


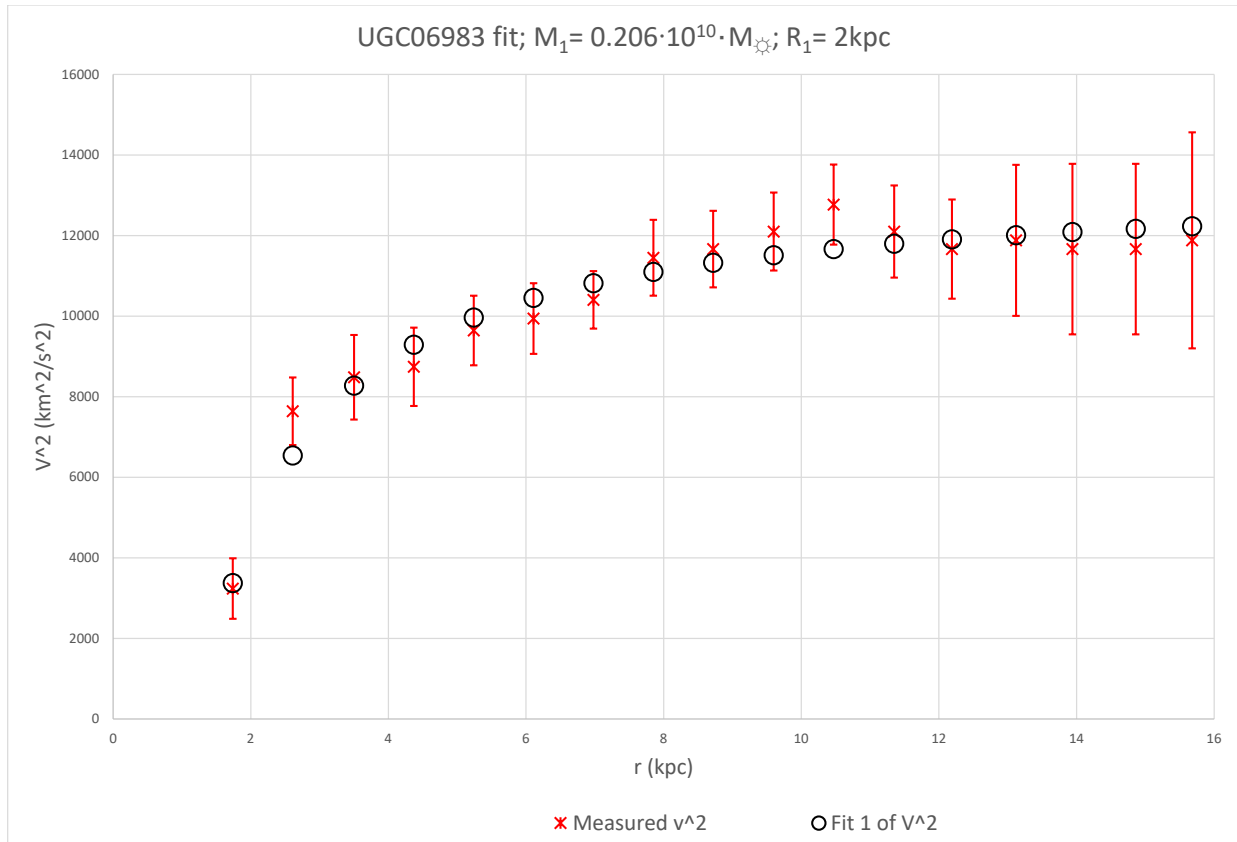




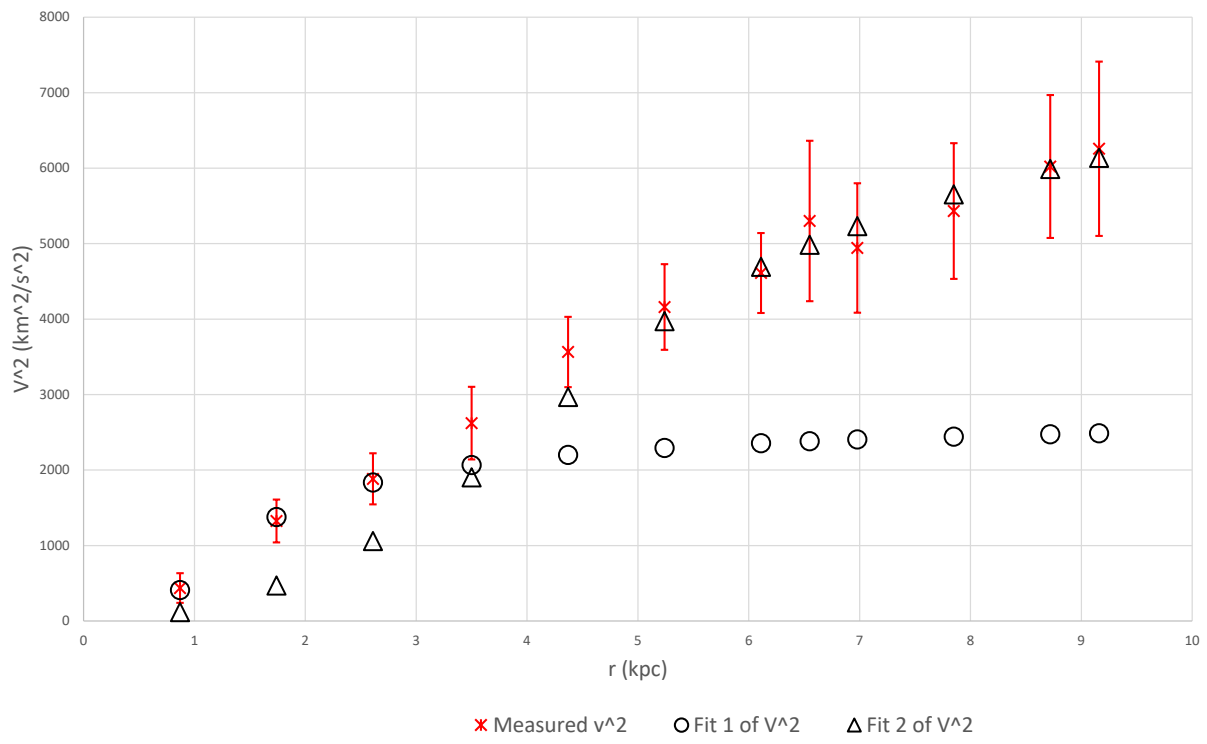


UGC06973 fit; $M_1 = 0.0114 \cdot 10^{10} \cdot M_{\odot}$; $R_1 = 0.05 \text{ kpc}$;
 $M_2 = 0.84 \cdot 10^{10} \cdot M_{\odot}$; $R_2 = 2.6 \text{ kpc}$

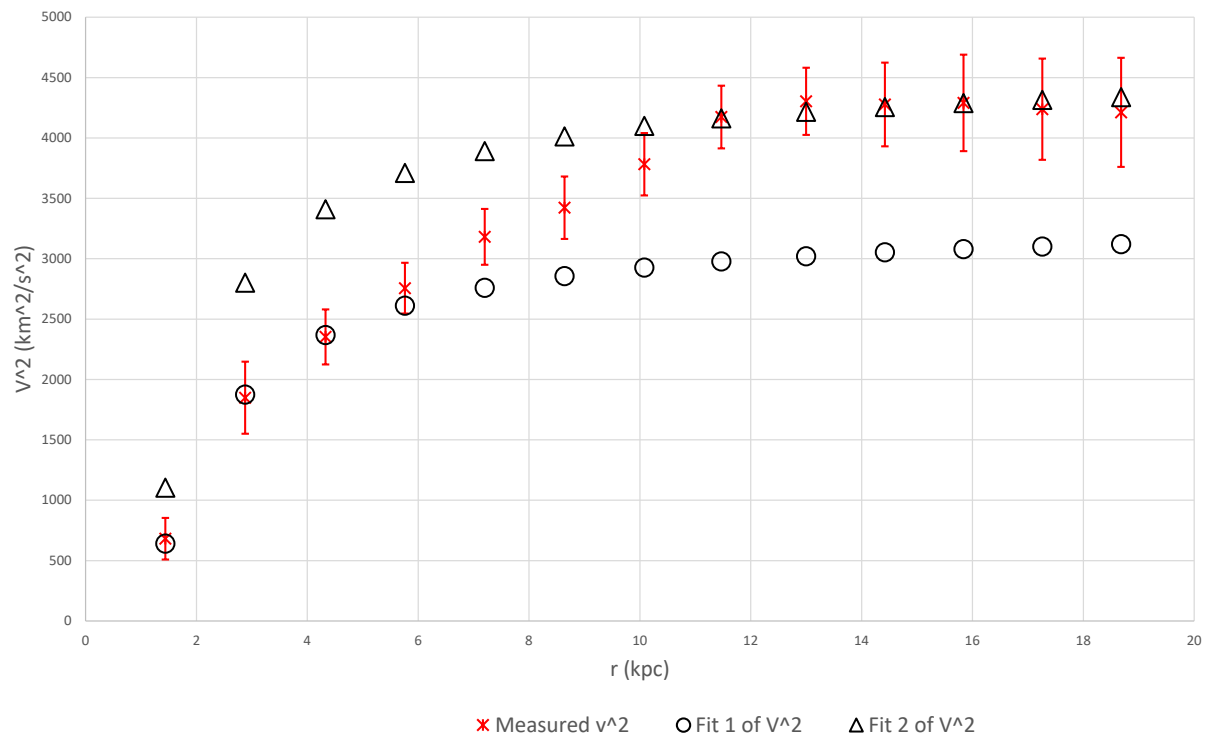


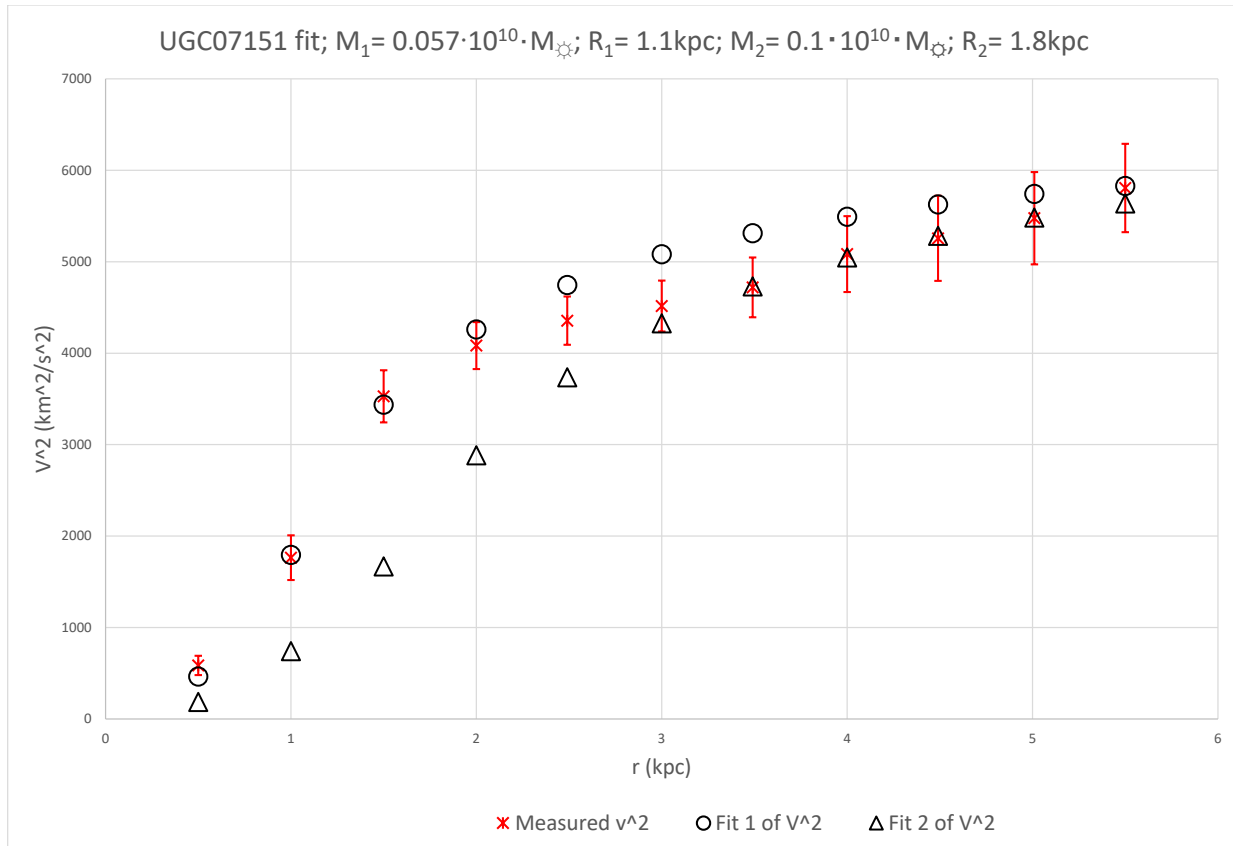


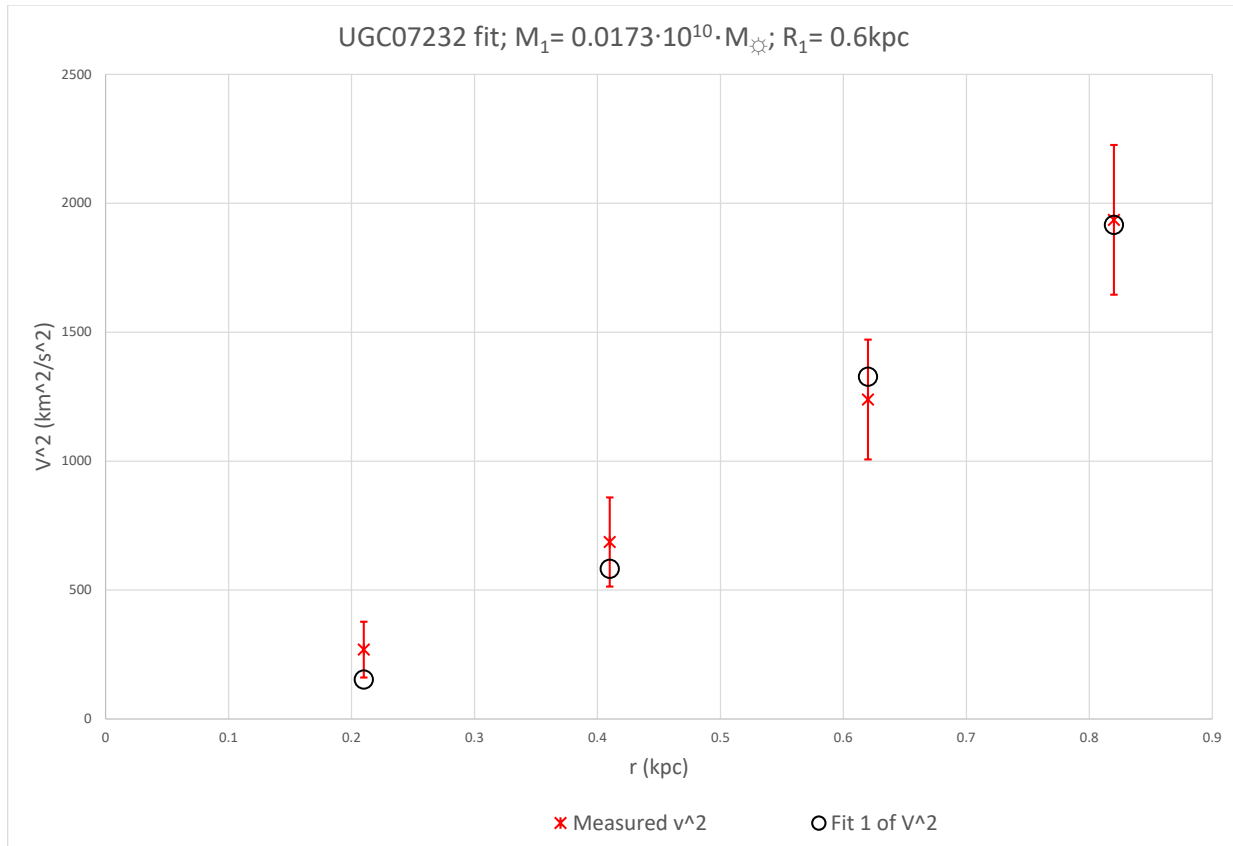
UGC07089 fit; $M_1 = 0.0275 \cdot 10^{10} \cdot M_{\odot}$; $R_1 = 1.3 \text{ kpc}$;
 $M_2 = 0.306 \cdot 10^{10} \cdot M_{\odot}$; $R_2 = 4.4 \text{ kpc}$

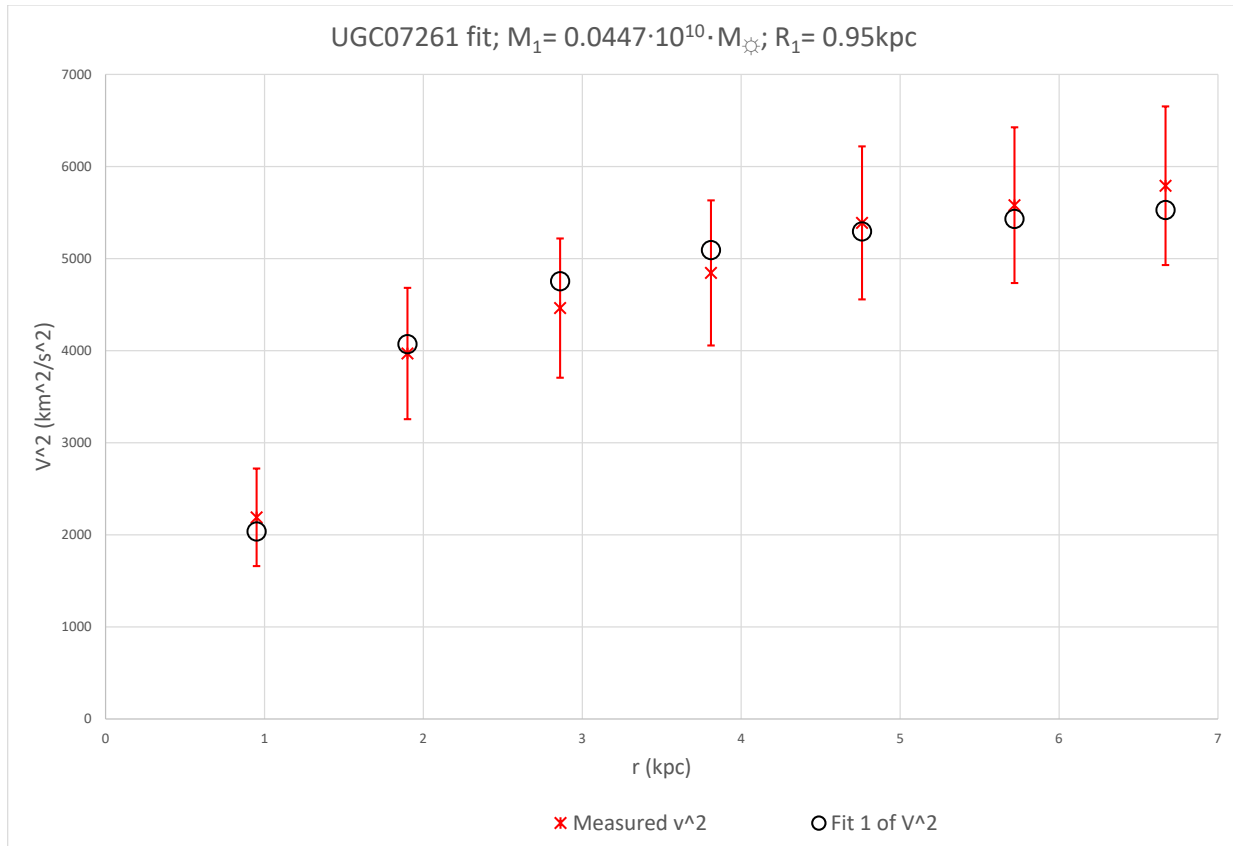


UGC07125 fit; $M_1 = 0.049 \cdot 10^{10} \cdot M_{\odot}$; $R_1 = 1.9 \text{ kpc}$;
 $M_2 = 0.0605 \cdot 10^{10} \cdot M_{\odot}$; $R_2 = 1.7 \text{ kpc}$

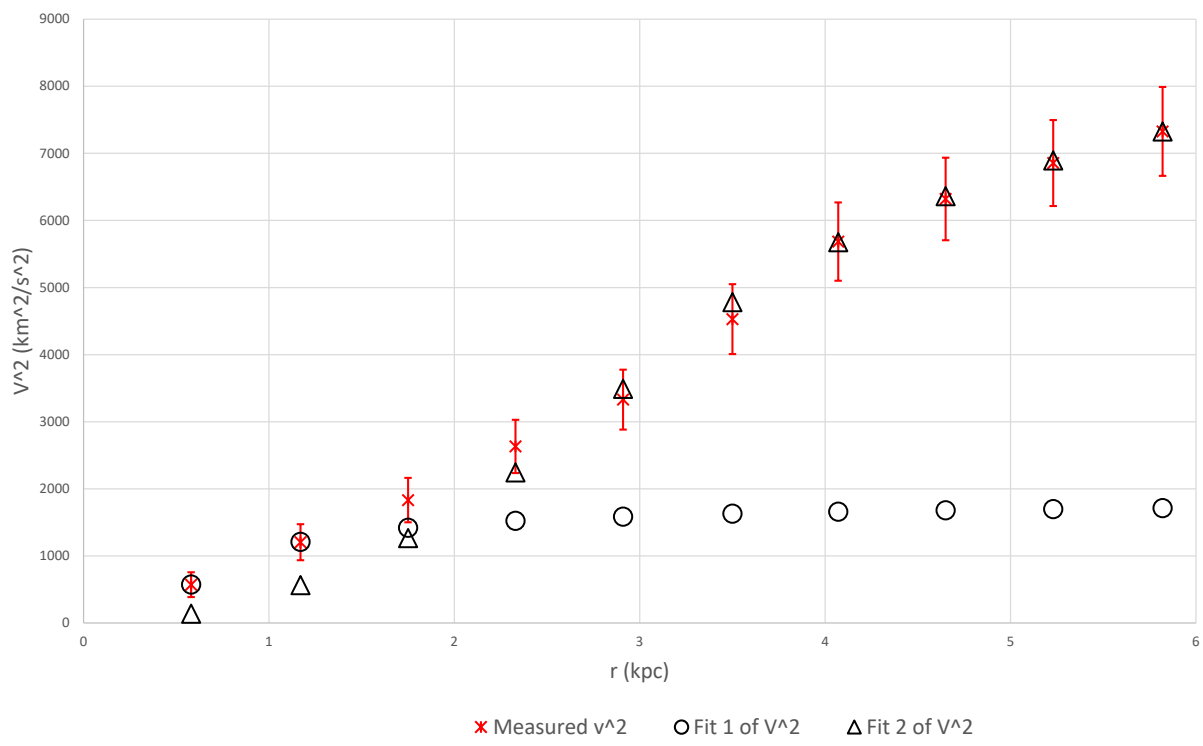




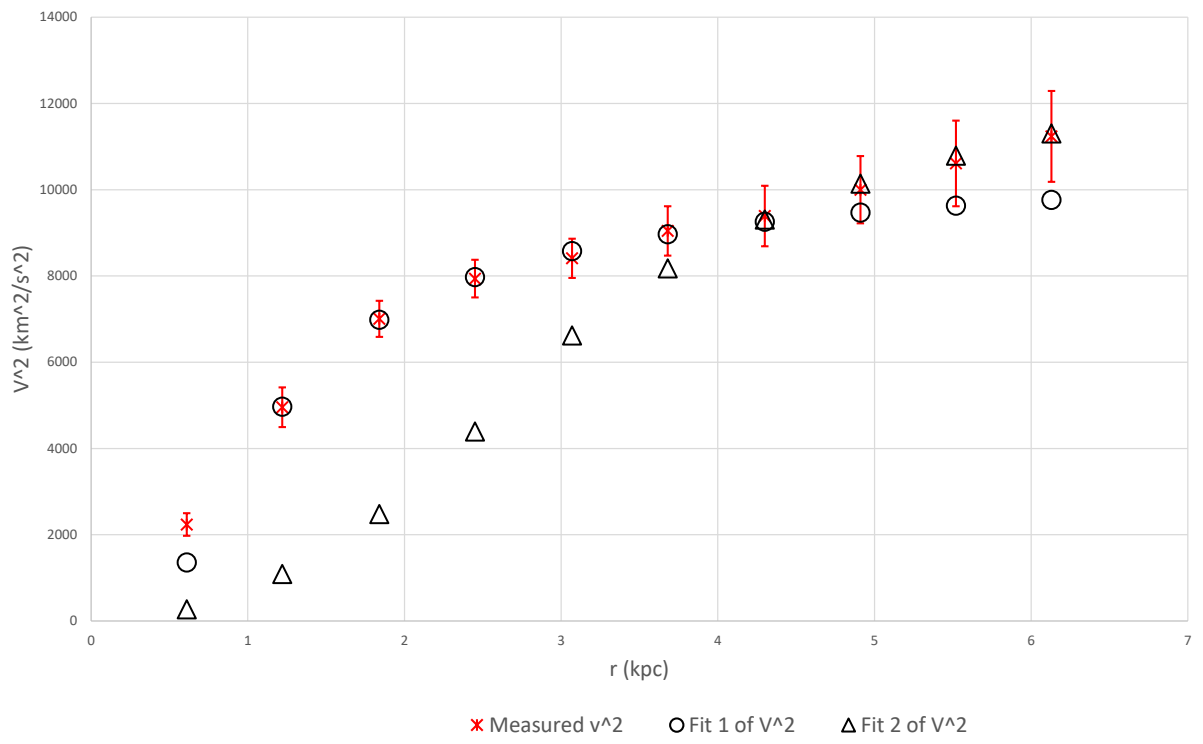




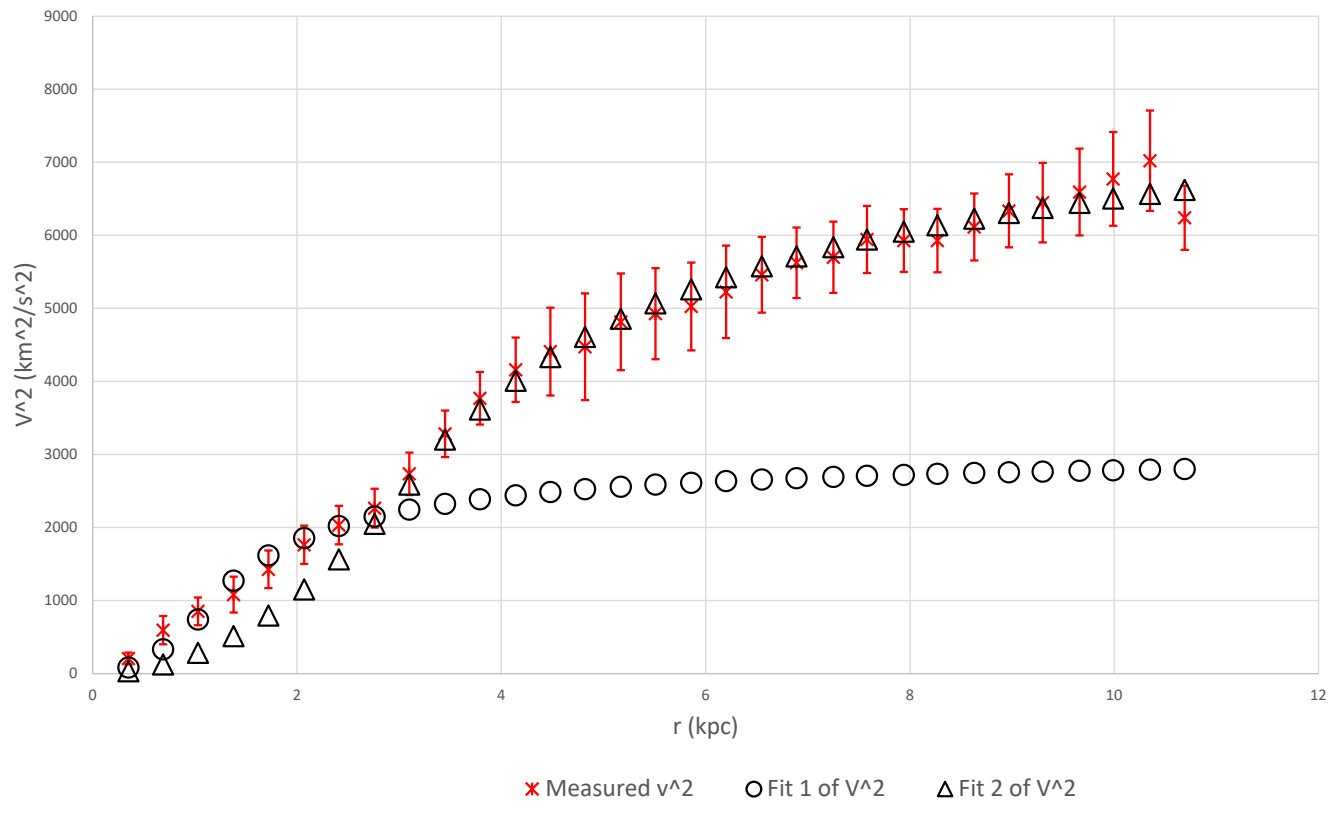
UGC07323 fit; $M_1 = 0.0085 \cdot 10^{10} \cdot M_{\odot}$; $R_1 = 0.6 \text{ kpc}$;
 $M_2 = 0.258 \cdot 10^{10} \cdot M_{\odot}$; $R_2 = 3 \text{ kpc}$

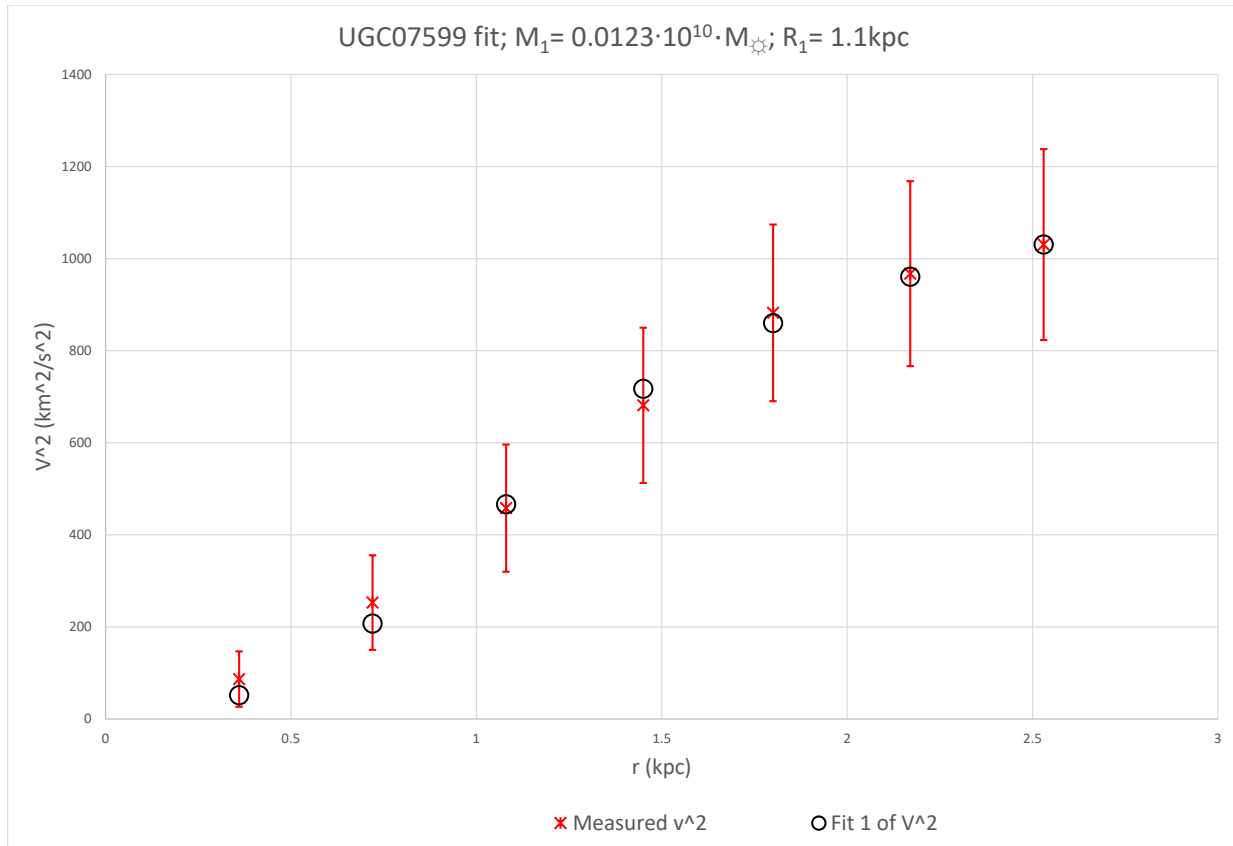


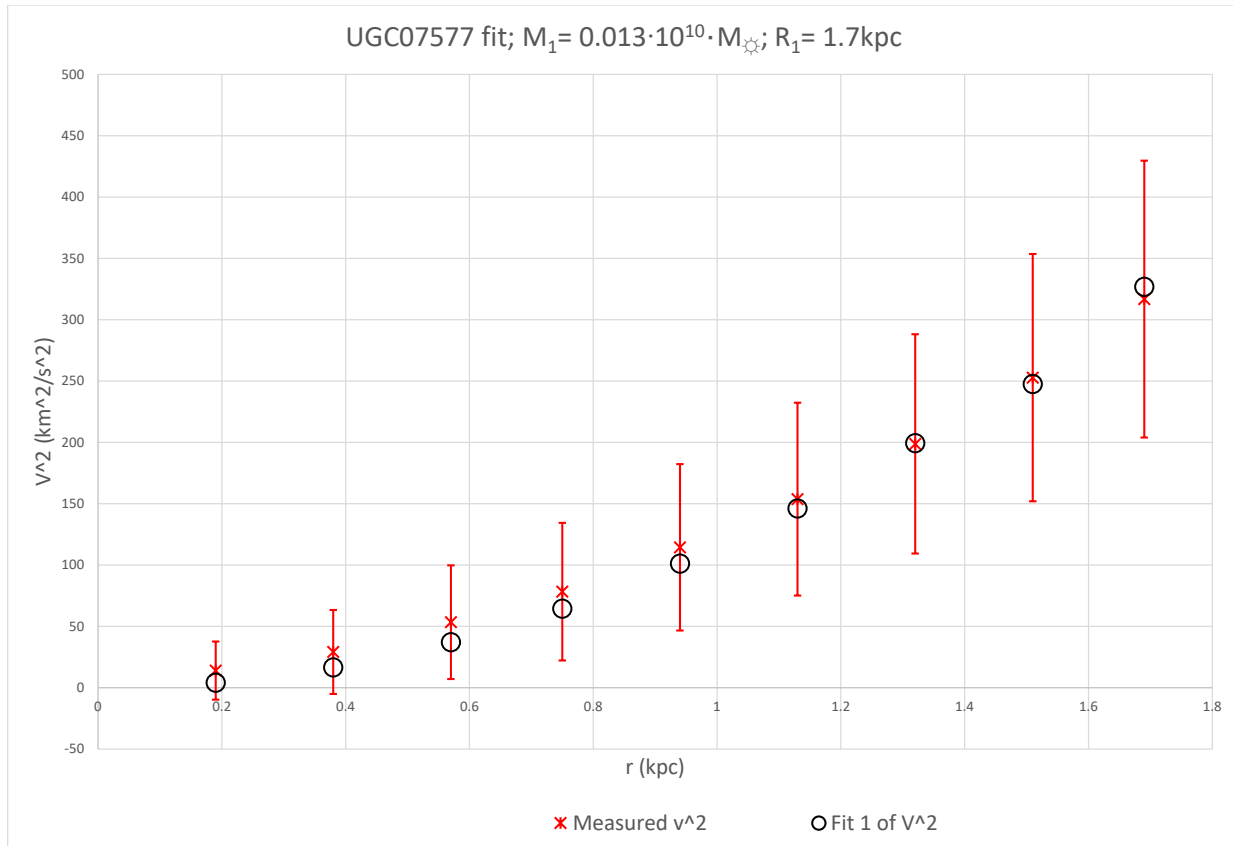
UGC07399 fit; $M_1 = 0.0844 \cdot 10^{10} \cdot M_{\odot}$; $R_1 = 1 \text{ kpc}$;
 $M_2 = 0.0333 \cdot 10^{10} \cdot M_{\odot}$; $R_2 = 2.7 \text{ kpc}$



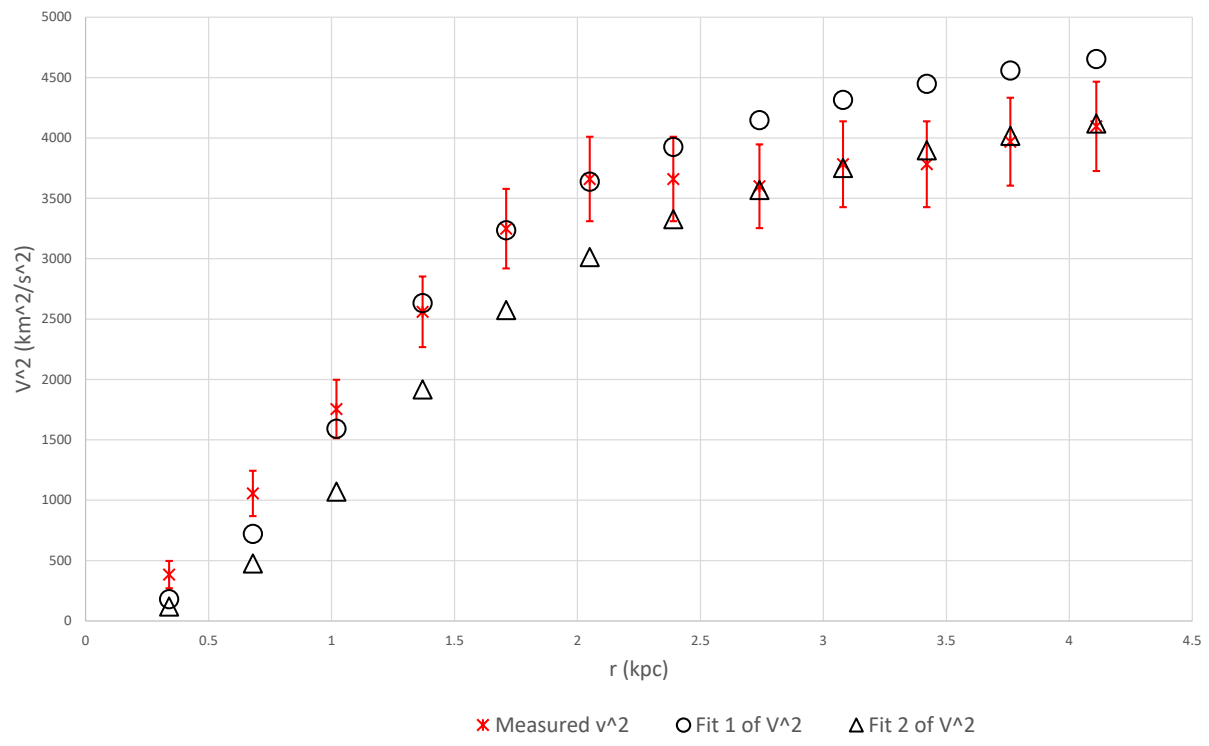
UGC07524 fit; $M_1 = 0.028 \cdot 10^{10} \cdot M_{\odot}$; $R_1 = 1.2 \text{ kpc}$;
 $M_2 = 0.204 \cdot 10^{10} \cdot M_{\odot}$; $R_2 = 3.2 \text{ kpc}$

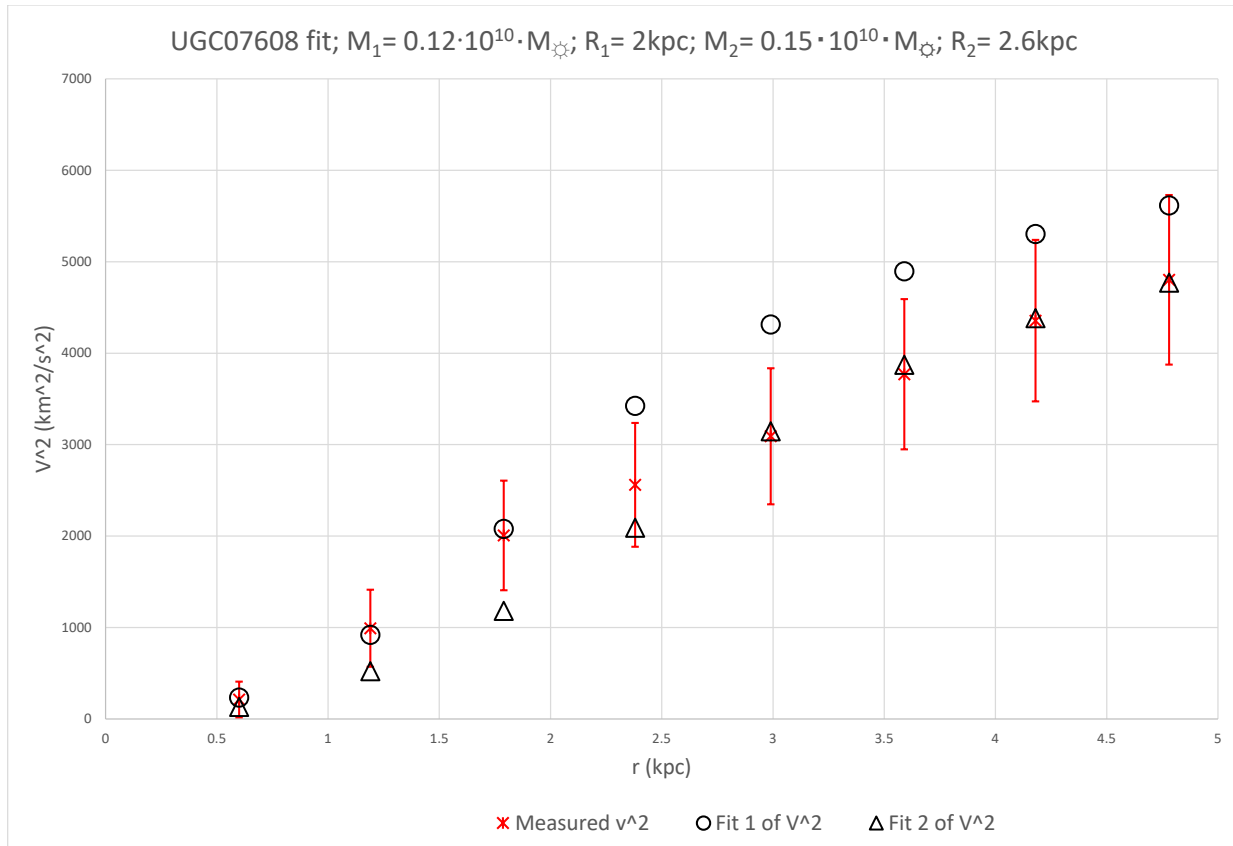




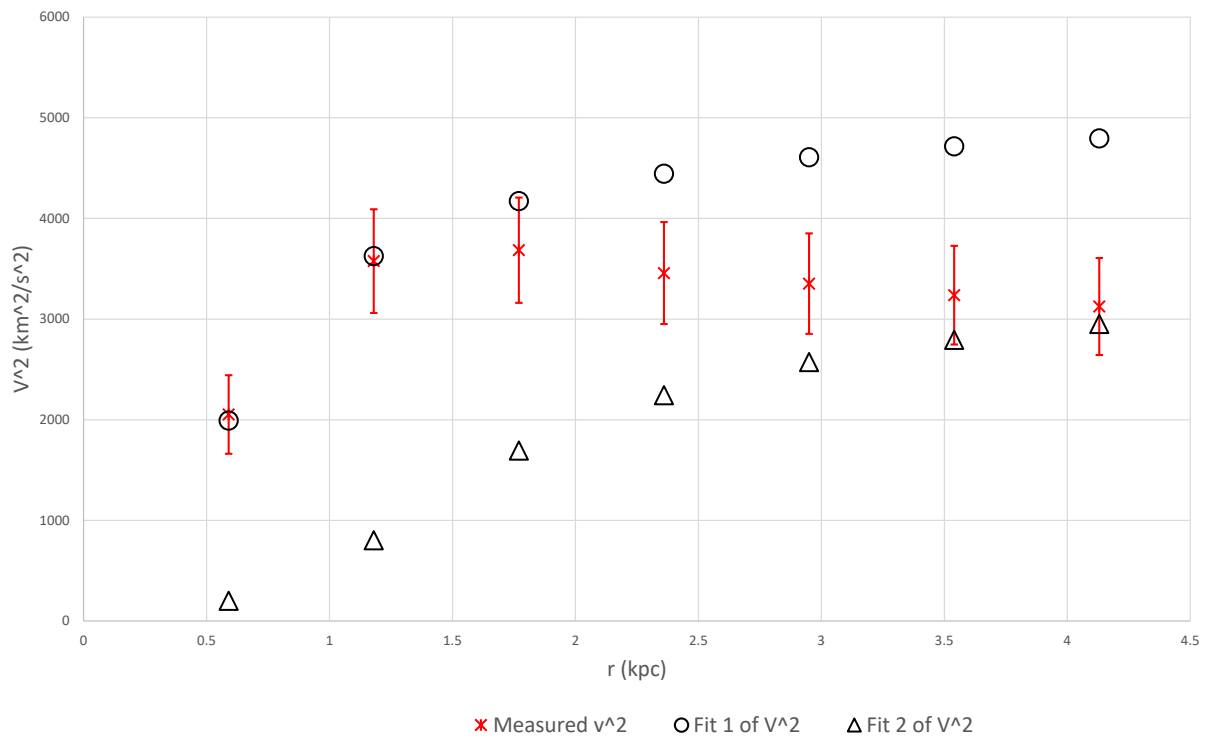


UGC07603 fit; $M_1 = 0.048 \cdot 10^{10} \cdot M_\odot$; $R_1 = 1.1 \text{ kpc}$;
 $M_2 = 0.0523 \cdot 10^{10} \cdot M_\odot$; $R_2 = 1.3 \text{ kpc}$

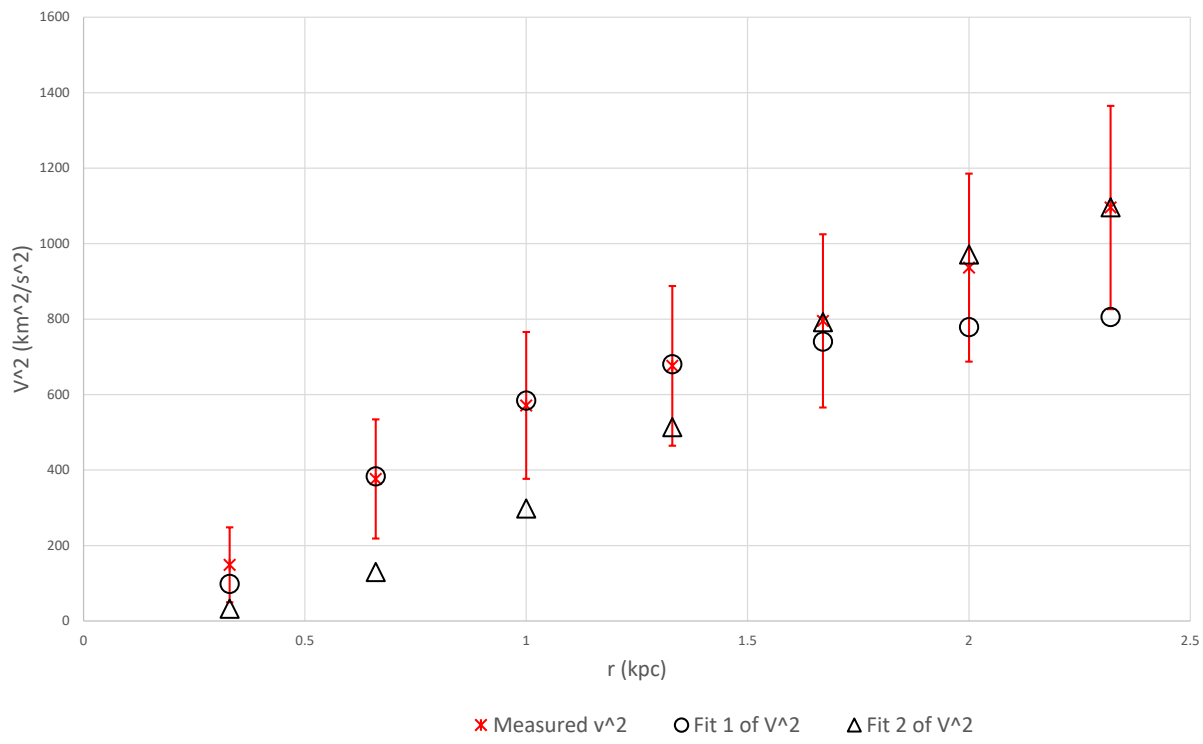


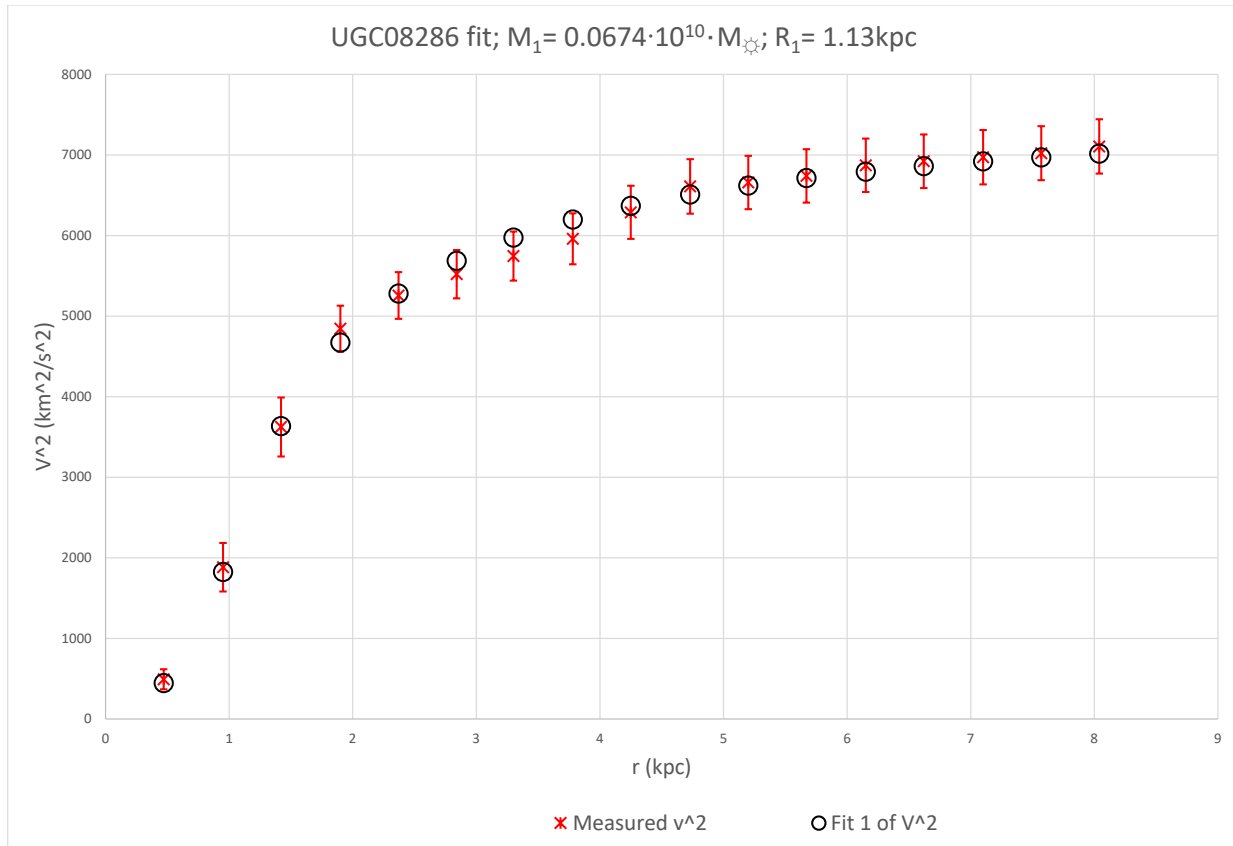


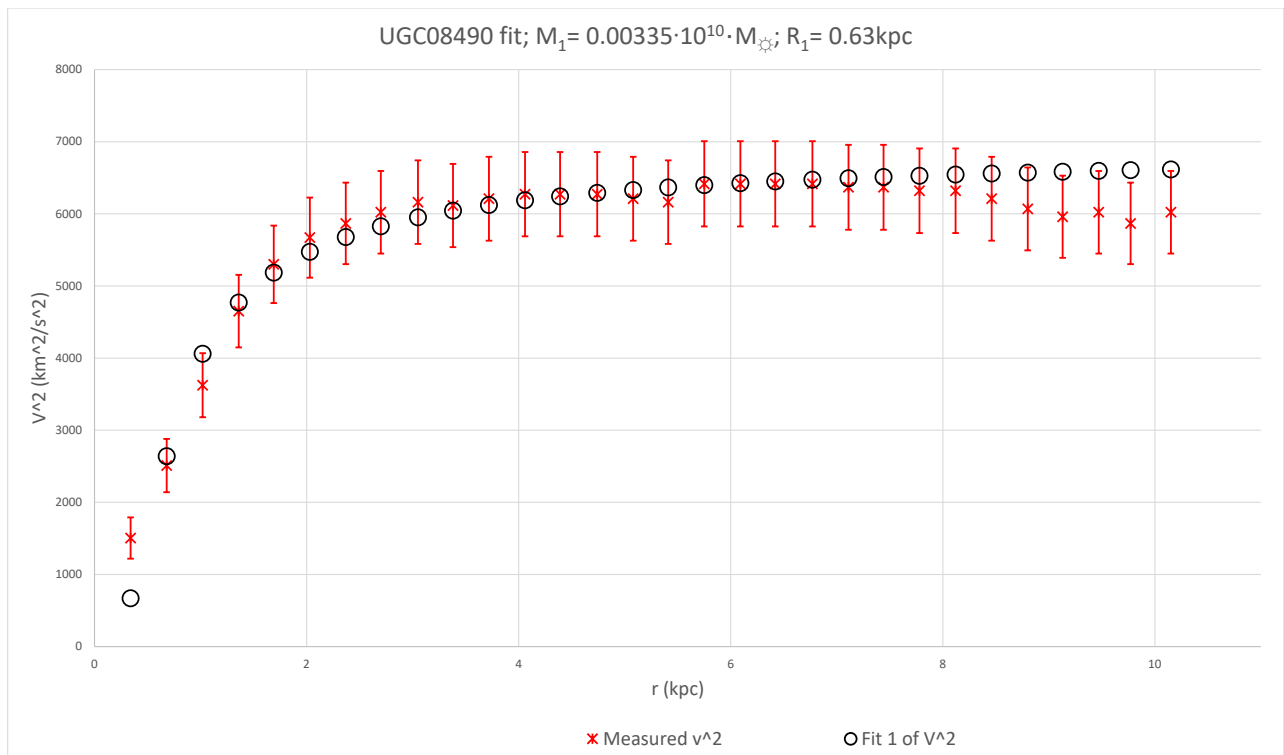
UGC07690 fit; $M_1 = 0.0223 \cdot 10^{10} \cdot M_{\odot}$; $R_1 = 0.55 \text{ kpc}$;
 $M_2 = 0.045 \cdot 10^{10} \cdot M_{\odot}$; $R_2 = 1.5 \text{ kpc}$



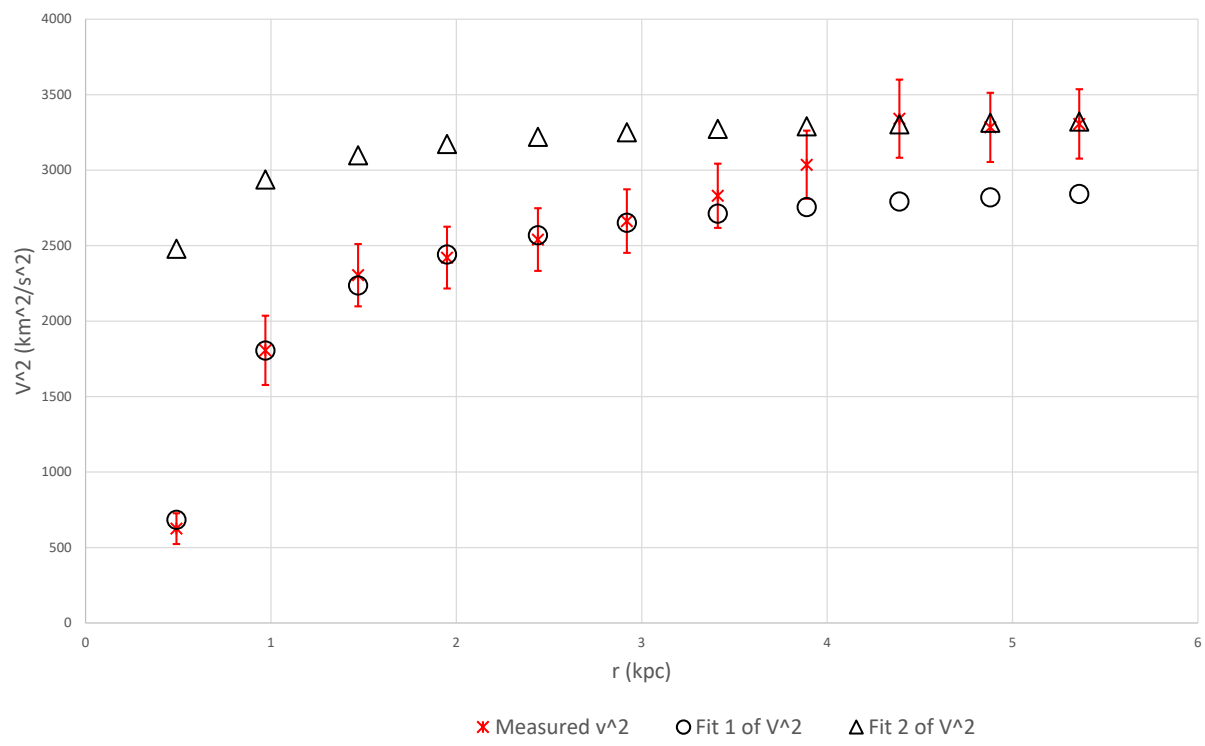
UGC07866 fit; $M_1 = 0.0045 \cdot 10^{10} \cdot M_{\odot}$; $R_1 = 0.6 \text{ kpc}$;
 $M_2 = 0.021 \cdot 10^{10} \cdot M_{\odot}$; $R_2 = 1.45 \text{ kpc}$

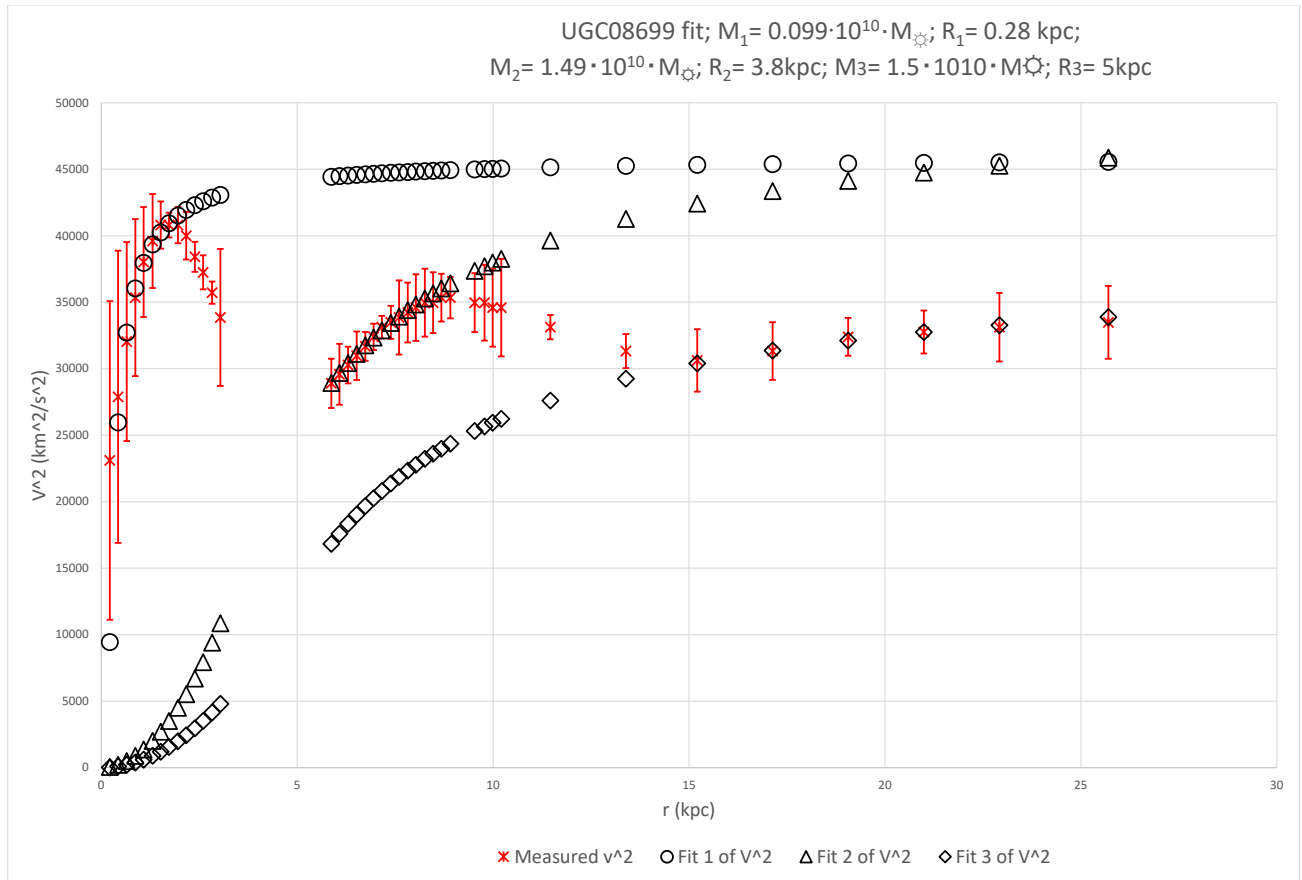


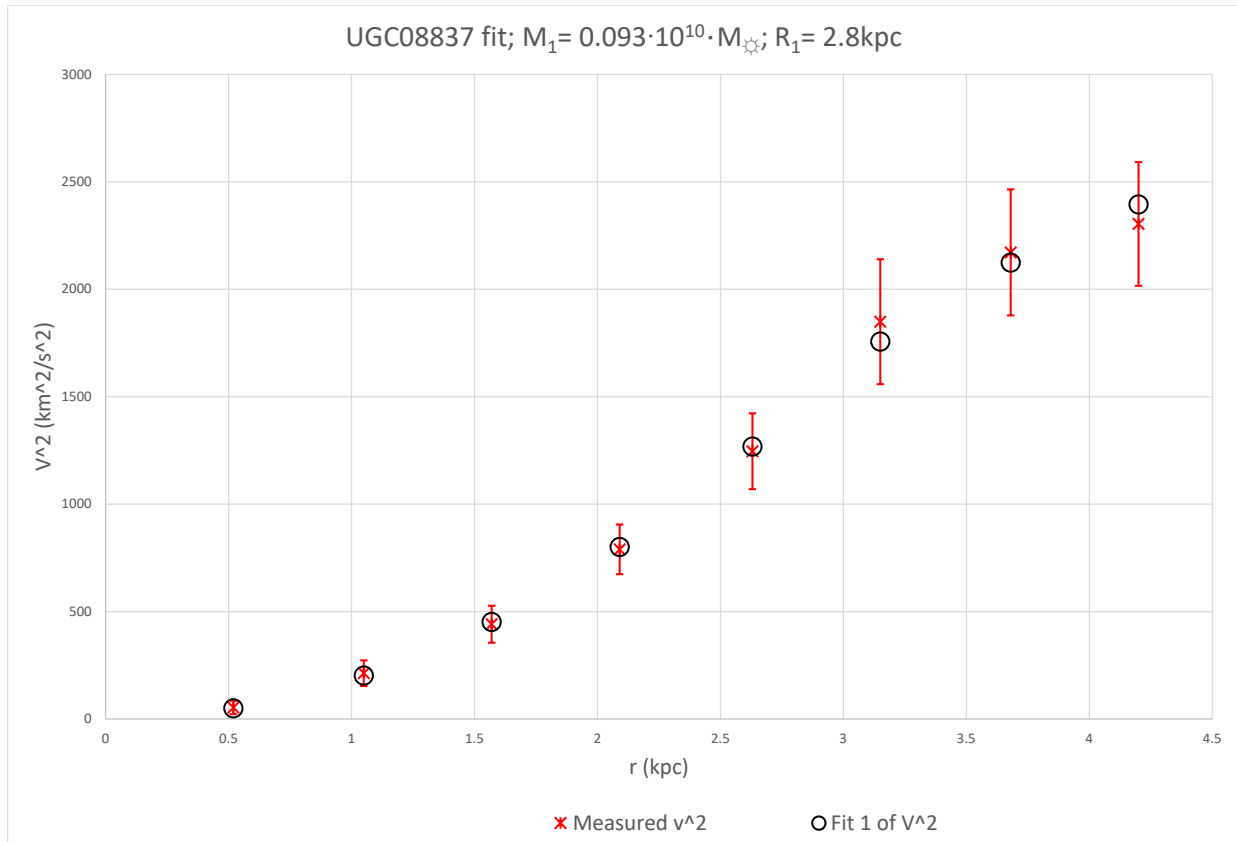


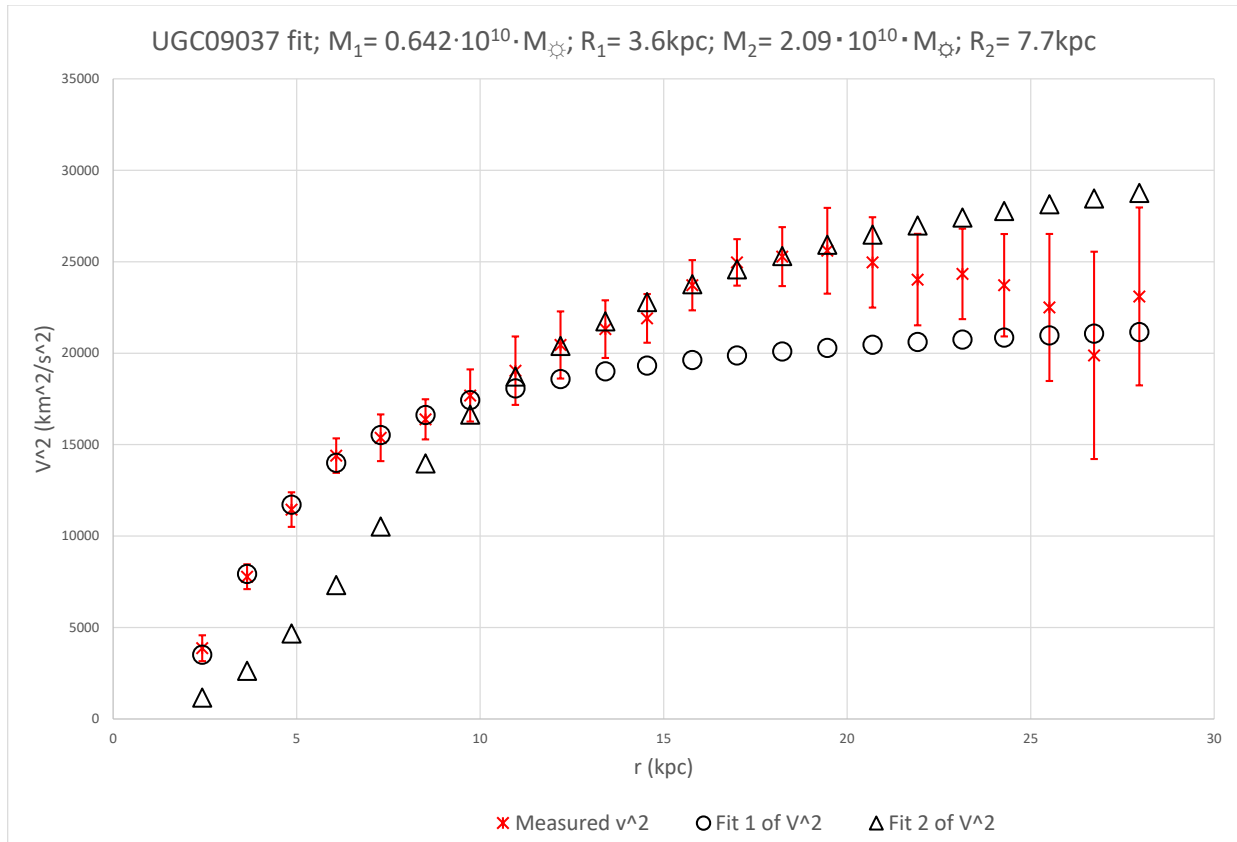


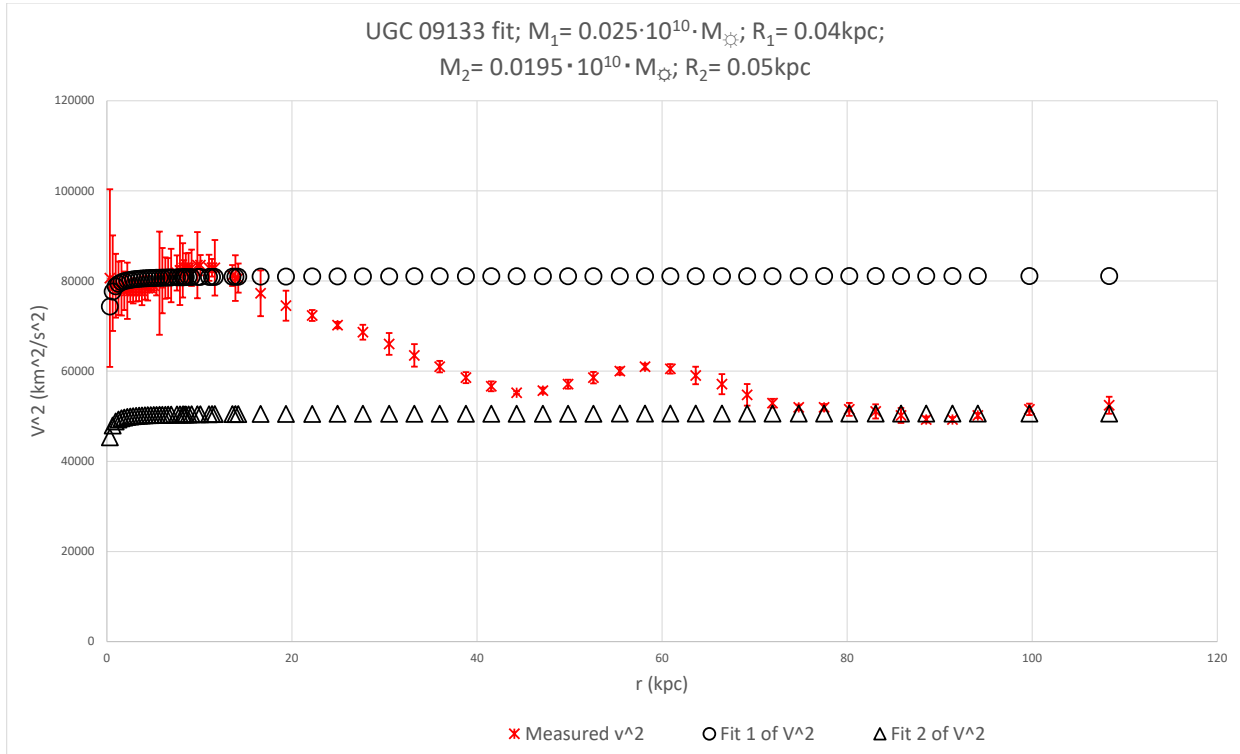
UGC08550 fit; $M_1 = 0.0142 \cdot 10^{10} \cdot M_{\odot}$; $R_1 = 0.6 \text{ kpc}$;
 $M_2 = 0.00525 \cdot 10^{10} \cdot M_{\odot}$; $R_2 = 0.2 \text{ kpc}$

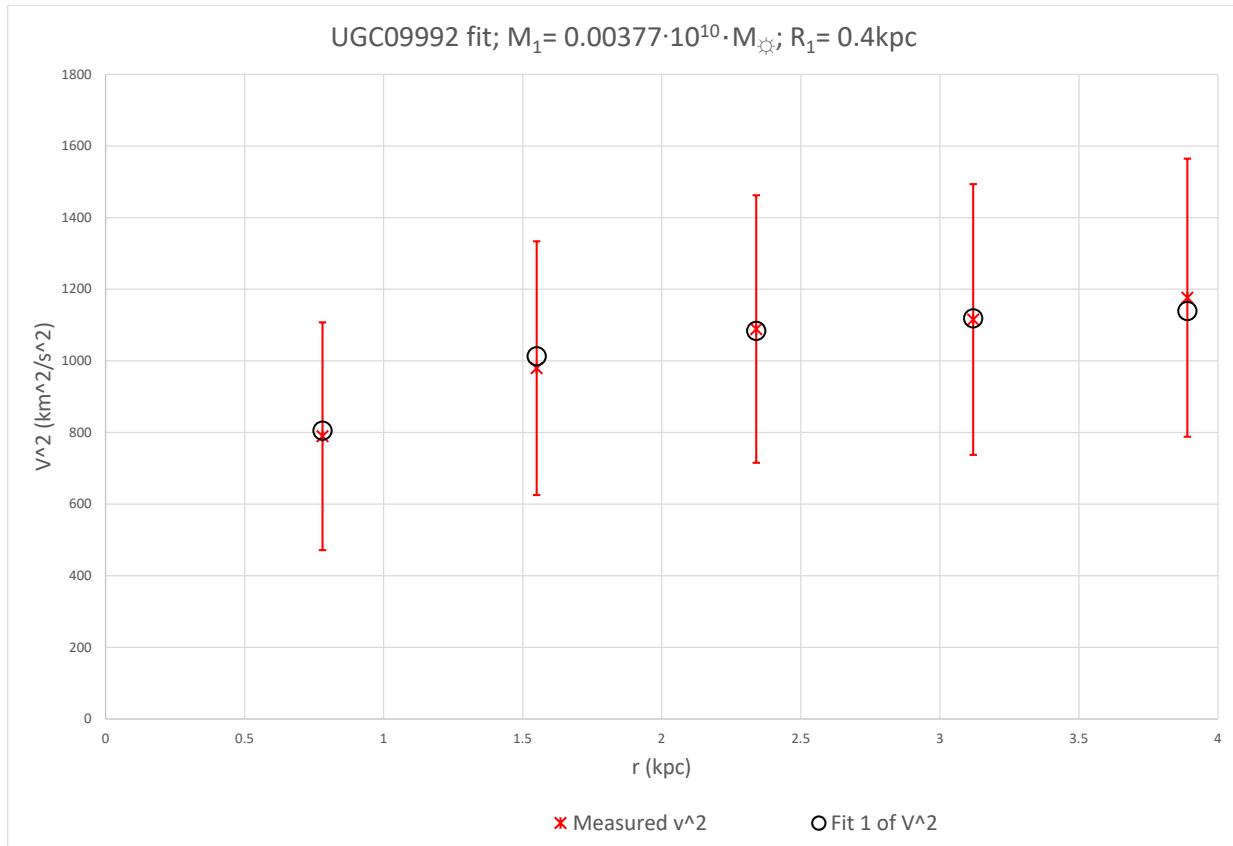


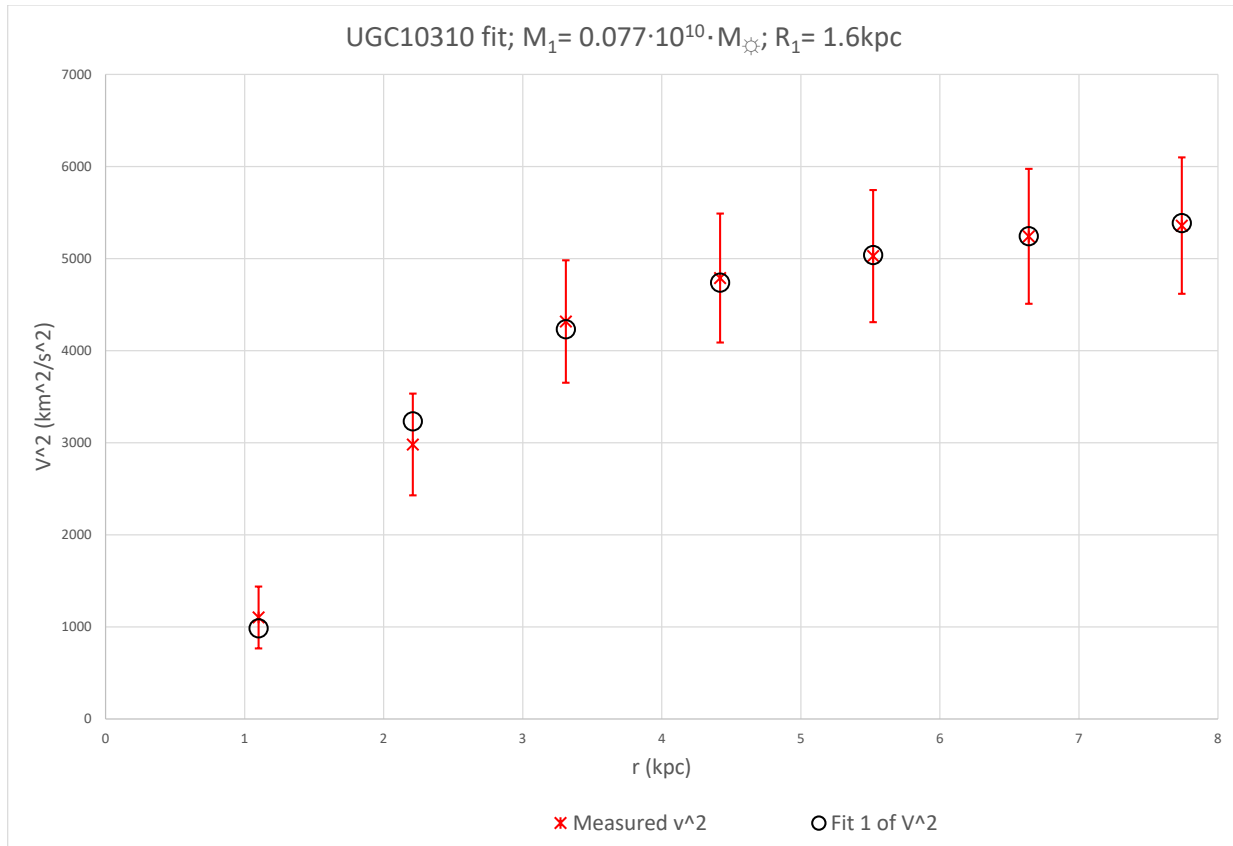


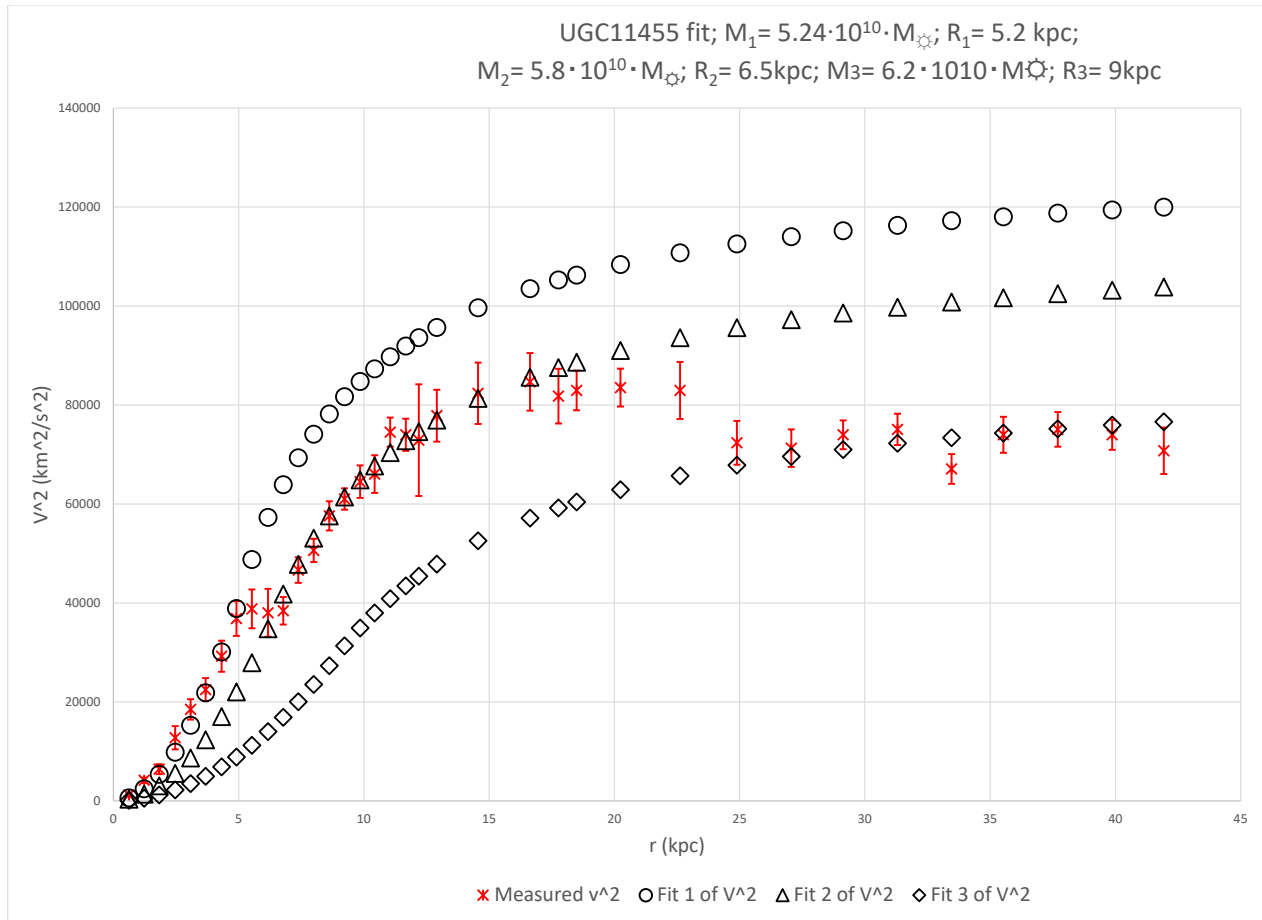


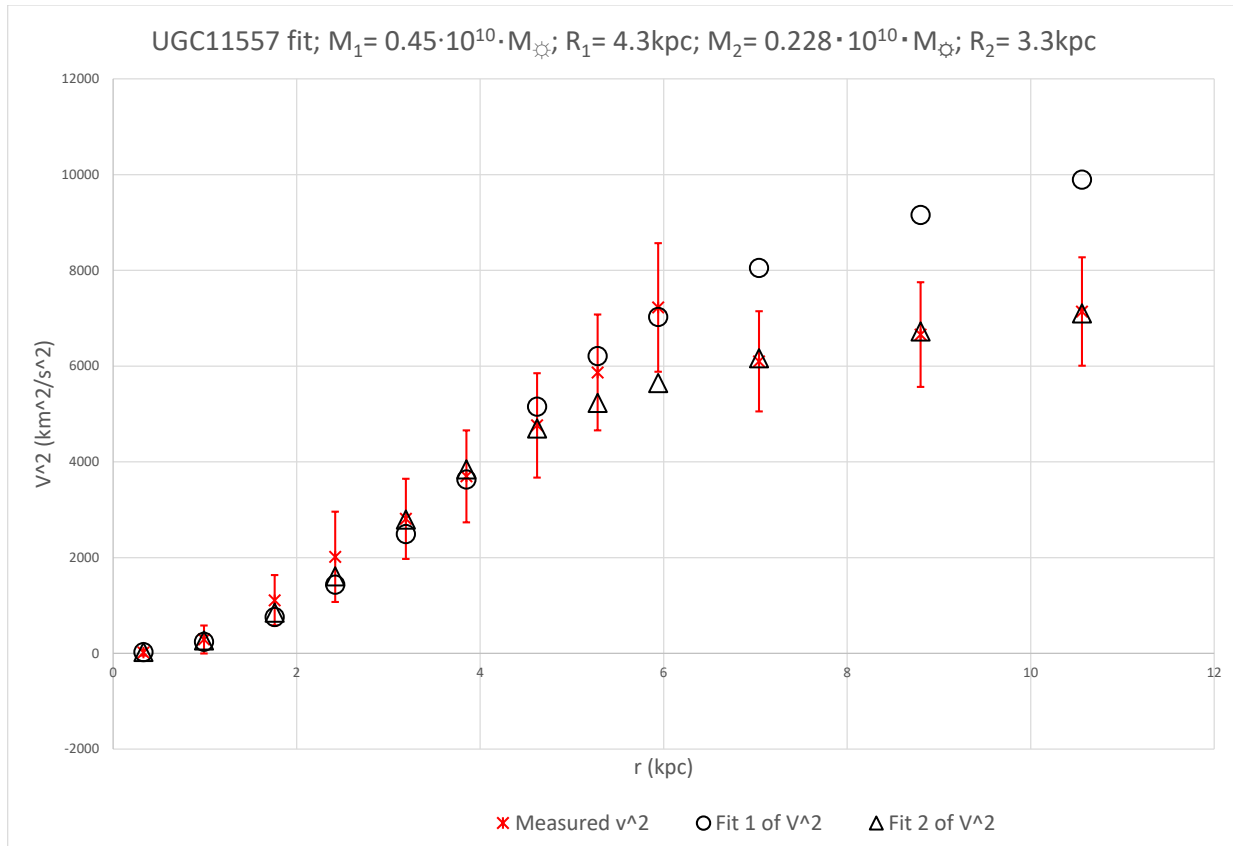




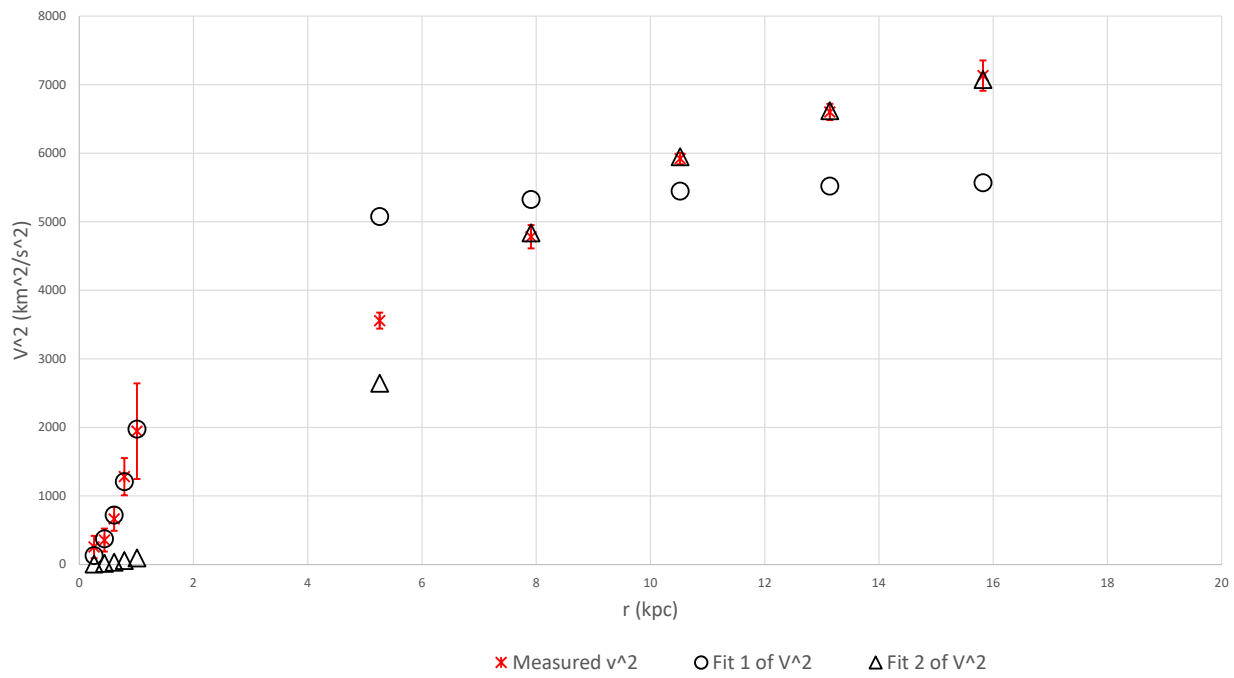




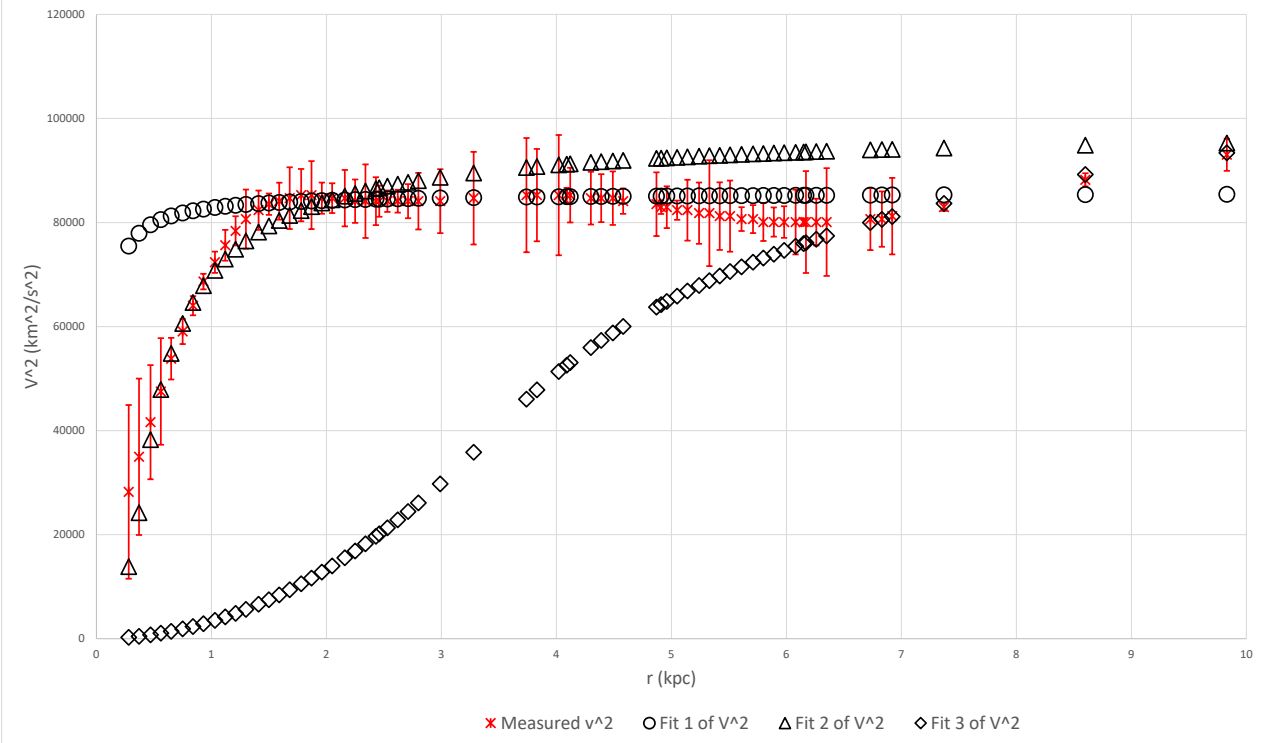


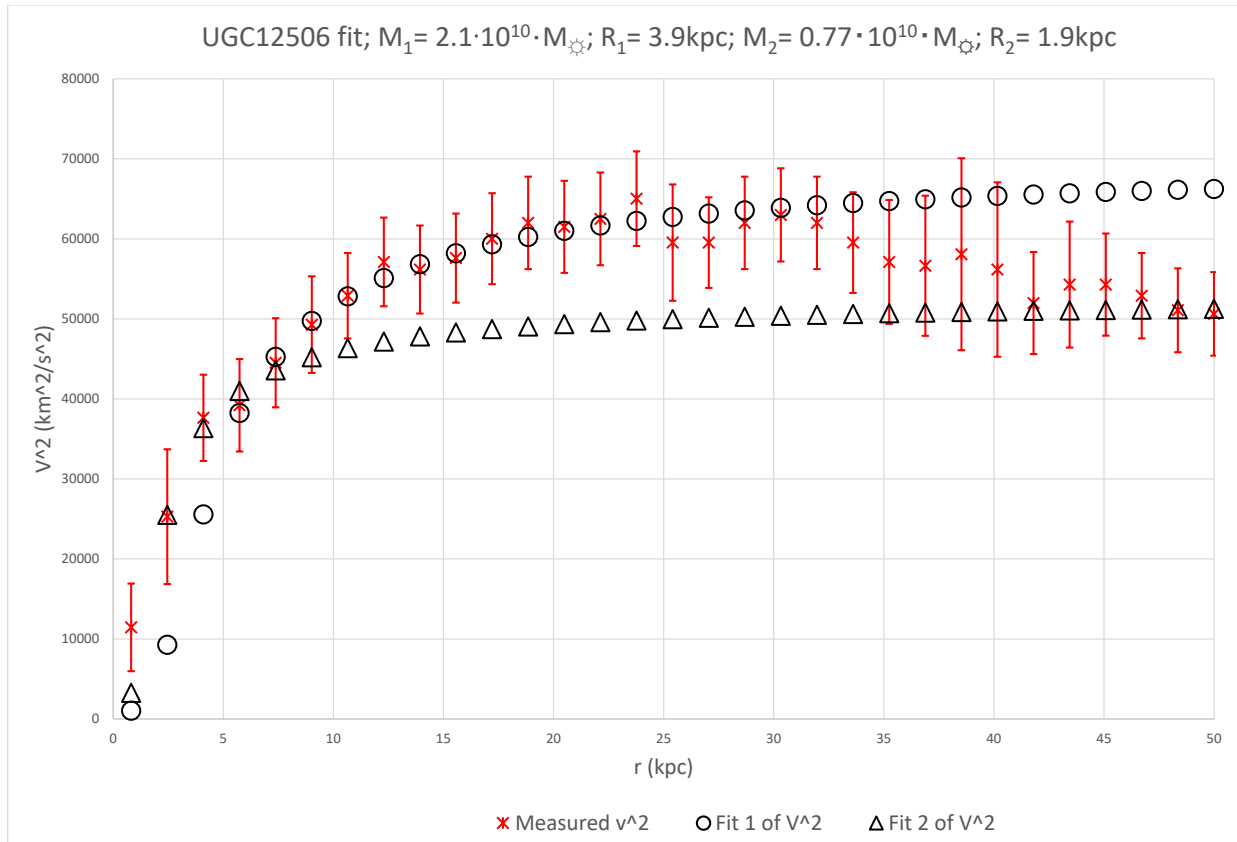


UGC11820 fit; $M_1 = 0.0448 \cdot 10^{10} \cdot M_{\odot}$; $R_1 = 1 \text{ kpc}$;
 $M_2 = 0.409 \cdot 10^{10} \cdot M_{\odot}$; $R_2 = 5.7 \text{ kpc}$

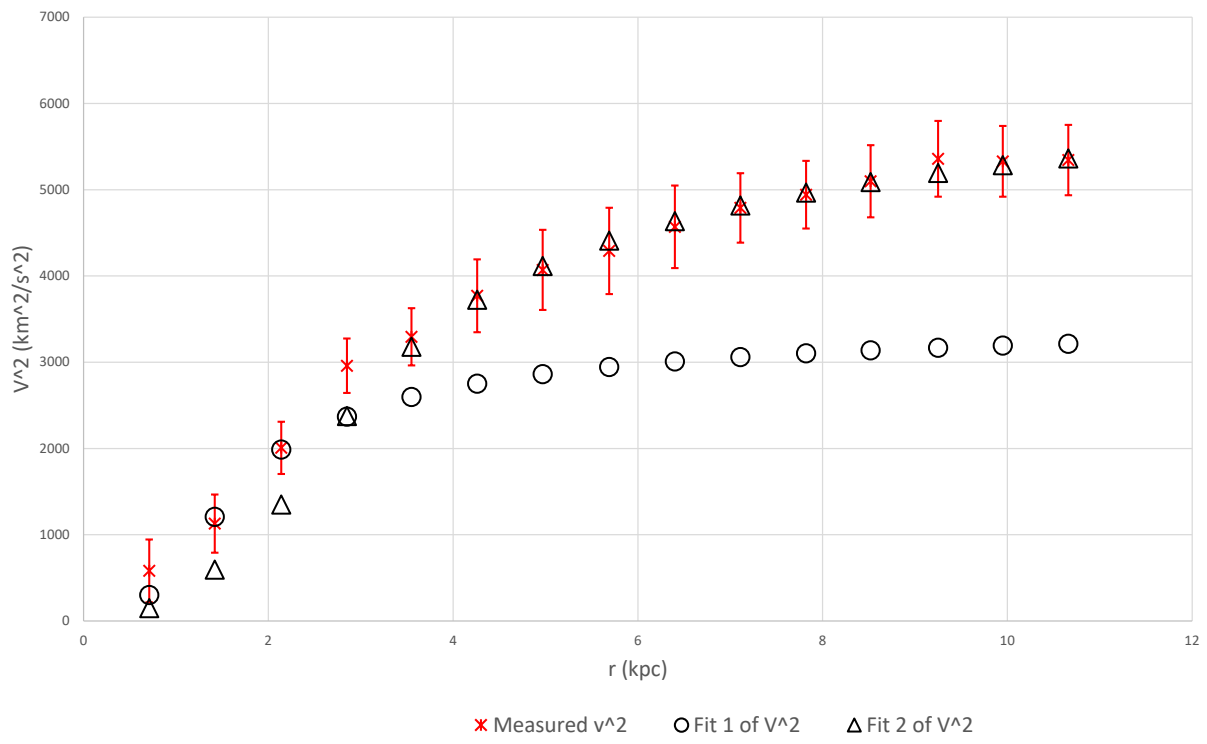


UGC11914 fit; $M_1 = 0.033 \cdot 10^{10} \cdot M_{\odot}$; $R_1 = 0.05 \text{ kpc}$;
 $M_2 = 0.325 \cdot 10^{10} \cdot M_{\odot}$; $R_2 = 0.43 \text{ kpc}$; $M_3 = 3.3 \cdot 10^{10} \cdot M_{\odot}$; $R_3 = 3.5 \text{ kpc}$





UGC12632 fit; $M_1 = 0.038 \cdot 10^{10} \cdot M_{\odot}$; $R_1 = 1.4 \text{ kpc}$;
 $M_2 = 0.1342 \cdot 10^{10} \cdot M_{\odot}$; $R_2 = 2.7 \text{ kpc}$



UGC12732 fit; $M_1 = 0.135 \cdot 10^{10} \cdot M_{\odot}$; $R_1 = 1.65 \text{ kpc}$;
 $M_2 = 0.195 \cdot 10^{10} \cdot M_{\odot}$; $R_2 = 3 \text{ kpc}$

